NCHRP

Project No. NCHRP 9-44 A

Validating an Endurance Limit for Hot-Mix Asphalt (HMA) Pavements: Laboratory Experiment and Algorithm Development

Appendix 1

Integrated Predictive Model for Healing and Fatigue Endurance Limit for Asphalt Concrete

Prepared for

NATIONAL COOPERATIVE HIGHWAY RESEARCH PROGRAM
TRANSPORTATION RESEARCH BOARD
Of
The National Academies
Submitted by:

Matthew Witczak, Project P.I.
Michael Mamlouk, Project Co-P.I.
Mena Souliman, Research Assistant
Waleed Zeiada, Research Assistant

July 2013

Table of Contents

List of Tables

Table Page

List of Figures

Figure Page

CHAPTER 1

INTRODUCTION

BACKGROUND OF FATIGUE CRACKING

Load associated fatigue cracking is one of the major distress types occurring in flexible pavements. Fatigue cracks are caused by the repeated application of wheel loads that results in fatigue failure of the asphalt surface and base courses. This type of cracking generally starts as short longitudinal cracks in the wheel path and progresses to an alligator cracking pattern (interconnected cracks).

The action of repeated loading is caused by traffic-induced tensile and shear stresses in the bound layers, which eventually leads to the loss of the structural integrity of the stabilized layer material. Fatigue initiated cracks start at points where maximum tensile strains and stresses exist. Once the crack initiates at the critical location, the action of traffic eventually causes the crack to propagate through the entire bound layer.

Over the last 3 to 4 decades, researchers have commonly assumed that fatigue cracking normally initiates at the bottom of the asphalt layer and propagates to the surface (bottom-up cracking). This is due to the bending action of the pavement layer that results in flexural stresses developing at the bottom of the bound layer. However, numerous recent studies have clearly demonstrated that fatigue cracking may also be initiated from the top of the bound layer and propagate down (top-down cracking). This type of fatigue cracking is not as well defined from a mechanistic viewpoint as the more classical "bottom-up" fatigue. In general, it is hypothesized that critical tensile or shear stresses develop at the surface at the tire edge-pavement interface, which, coupled with highly aged (stiff) thin surface layer, causes surface cracks to develop.

In order to characterize fatigue in asphalt layers, several model forms can be found in the literature. The most common model form used to predict the number of load repetitions to fatigue cracking is a function of the tensile strain and mix stiffness (modulus) (1).

BACKGROUND OF THE HOT-MIX ASPHALT (HMA) ENDURANCE LIMIT

The HMA Endurance Limit, (HMA-EL) is defined as the repeated HMA flexural strain level below which HMA damage is not cumulative. Thus, an HMA layer experiencing strain levels less than the HMA-EL should not fail due to fatigue.

Monismith postulated many years ago that there appeared to be a strain below which there is no fatigue damage to the HMA (2). This concept has been investigated by Carpenter (3) starting in 2000, and more recently by National Center for Asphalt Technology (NCAT) by conducting lengthy tests at low strain levels (4). These studies suggested that there is a definite point at which each mixture's traditional strain-N_f curve deviates from the typical log-log straight line relationship and assumes a relatively flat slope.

Depending on different mixture and testing factors, this extended plateau value can be reached at significantly different strain values. Strains below the HMA-EL will begin to show extraordinarily long fatigue lives as compared to those that would be predicted by the traditional phenomenological fatigue model shown in Equation 1. The difficulty in differentiating the mixture variables and their impact on the HMA-EL derives from the use of this simplified relationship for strain and loads to failure. Since this relationship is not fundamental, it cannot

adequately describe the mixture performance under very low strains.

The HMA-EL represents the balance point between damage and healing in HMA. For strain levels above the HMA-EL, the damage done is considerably greater than the healing potential of the HMA (4). When strains are below the HMA-EL value, the damage is equal to or less than the healing potential and the damage is small enough that it is potentially completely repaired during the load pulse in the field or the load cycle in the lab.

Previous HMA-EL studies (5) indicated that a 70 microstrain level is a conservative value that guarantees a structural design will perform in the region of extended fatigue life, providing a "no damage" performance. A design incorporating this 70 microstrain level under the most extreme conditions can be considered a perpetual pavement. If the strain remains around 70 - 100 microstrain during the pavement life, there is no accumulation of HMA fatigue damage.

Different mixtures produce different HMA-EL values. While this can be mostly attributed to binder differences, the lack of relevant binder data to date only allows a comparison with modulus, which for a specific aggregate gradation will be controlled primarily by the binder type, binder content, and air voids (5). Such data clearly indicate that for mixtures of similar design, alteration of the modulus, essentially through binder differences, produces a strong relationship between modulus and the HMA-EL. What is important for these mixtures is that there is a strong indication that as the modulus increases, the HMA-EL decreases asymptotically (5).

Some previous studies showed that the relationship between the HMA-EL and the flexural modulus also clearly indicates that there is a lower limit to the HMA-EL that appears to be well above the 70 microstrain level. Further, because healing potential increases as temperature increases, it can be expected that the HMA-EL will change with temperature, which may be indirectly indicated by this modulus relationship (5).

Utilizing HMA-EL concepts with a traditional fatigue curve is not consistent as the one incorporates healing while the other ignores it even though it is present. Load damage levels change with the volume and speed of traffic which can be represented by a rest period between each cyclic loading in beam fatigue testing. The HMA-EL also changes with temperature and binder type. Unless these factors are accounted for, the fatigue pavement design would not provide a consistent relationship between load levels, damage, and load repetitions to failure.

Because the HMA-EL is tied closely to the healing potential of the binder, at higher temperatures healing occurs more rapidly and so the strain level that can be tolerated with no damage accumulation is increased (6). To be correctly included in the pavement design the HMA-EL must vary with season, just as the modulus and the resulting strain vary with season. Further, the impact of healing in the HMA between load pulses must be considered. Rest periods heal the damage caused by load applications and are a major factor in the lab to field shift values of 40 to 400 that have been applied to make existing lab fatigue models applicable to field conditions (5).

Current design methods of flexible pavement assume that a cumulative damage occurs where each load cycle uses up a portion of the finite fatigue life of the HMA. Thus, they do not account for the finding of recent studies that HMA may exhibit an endurance limit, where properly constructed, thick HMA pavements can be exposed to a very large number of loading cycles without exhibiting fatigue (4, 5, 7).

In NCHRP Project 9-38 (7) beam fatigue testing was used to determine the HMA fatigue life. By applying a small strain level to the beam, a fatigue life in excess of 50 million cycles was achieved. NCHRP Project 9-44 (4) developed a detailed plan to validate the endurance limit concept for HMA pavements and to incorporate it into a mechanistic-empirical algorithm for bottom-initiated fatigue cracking in flexible pavements. The current NCHRP Project 9-44A project implements the plan suggested by the previous NCHRP Project 9-44. Also, the project validates the endurance limit concept, and devises effective methods for incorporating it in mechanistic-empirical pavement design methods.

PROBLEM DEFINITION

The endurance limit, as applied to HMA and flexible pavement design, is the strain level below which HMA would endure indefinite fatigue loads and the pavement will not experience bottom-up fatigue cracking. Current mechanistic-empirical fatigue criteria for HMA, including the field calibrated criterion in the Mechanistic-Empirical Pavement Design Guide (MEPDG), assume the fatigue life of HMA to be a power function of the tensile strain at the bottom of the asphalt layer. These criteria do not include the provision for an endurance limit. A concentrated research effort is needed to validate the endurance limit concept, and to devise effective methods for incorporating it in mechanistic-empirical pavement design methods.

RESEARCH OBJECTIVES

The major objectives of this research project were:

1. Verify the concept of endurance limit of HMA by carrying out laboratory experiments to identify the mixture and pavement layer design features related to endurance limit for bottom-initiated fatigue cracking of HMA,
2. Develop an integrated predictive model for healing and endurance limit for flexible pavements, and
3. Develop a methodology to incorporate the endurance limit into the MEPDG simulation process.

SCOPE OF RESEARCH

The scope of this research includes:

- **Conduct Literature Review Search**
  The goal of the literature review was to document previous HMA endurance limit studies needed to accomplish the objectives of this study. Literature review included the concept of fatigue healing, endurance limit, and the effect of introducing a rest period after loading on the fatigue life. The literature review ensured that all the essential information needed to accomplish the objectives of this study was obtained.
- **Test Program and Plan**
  A comprehensive test plan was developed to include testing typical mixtures and testing factors that might affect the endurance limit of HMA. Six main factors were selected to be evaluated in this study: binder type, binder content, air voids in the mix, testing

temperature, amount of rest period applied between each loading cycle, and number of cycles till failure for the test without rest period (N_f).

- **Materials and HMA Mix Design**
  The three binder types that were used in this study were characterized by performing conventional penetration and viscosity-graded binder tests followed by performance-graded binder tests. Aggregate gradation determination and Superpave mix design was completed for the three mixes used.
- **Specimen Preparation and Beam Fatigue Machine Calibration**
  Specimen preparation and machine calibration procedures were carried out.
- **Preliminary Quality Assurance (QA) Studies**
  Several small QA studies were performed to insure obtaining comparable results from both beam fatigue machines used in the research and to verify the testing conditions.
- **Stiffness Ratio Model Development and Endurance Limit Determination**
  An integrated stiffness ratio (SR) model of all three mixtures was developed in order to calculate the amount of HMA healing. The HMA healing was then coupled with damage produced during loading to estimate HMA-EL under different conditions.
- **Final Report**
  A final report was prepared to document the work completed. The report included the conclusions and recommendations for further research.

REPORT ORGANIZATION

This report is organized into nine chapters:

1. Introduction and Research Objectives
2. Literature Review
3. Design of Experiment
4. Materials and HMA Mix Design
5. Specimen Preparation and Beam Fatigue Machine Calibration
6. Preliminary QA Studies
7. Healing Index and Endurance Limit Determination
8. Incorporating Endurance Limit in the MEPDG
9. Conclusions and Recommendations for Further Research

Chapter 1 outlines the research background, problem definition, and objectives and scope of the research. Chapter 2 provides a literature review and theoretical background of HMA fatigue cracking phenomenon, HMA healing, and HMA endurance limit. Chapter 3 contains the experimental design of the test program. Chapter 4 contains the binder testing characterization, aggregate properties, and the Superpave mix design results. Chapter 5 includes specimen preparation and the beam fatigue testing machine calibration check procedure. Chapter 6 includes the results of the QA studies conducted before the main experiment in order to evaluate the compliance of measurement equality among beam fatigue testing machines and to refine test conditions. Chapter 7 contains the laboratory test results, healing analysis, development of the integrated predictive stiffness ratio model for healing and endurance limits under different conditions. Chapter 8 presents a methodology to incorporate the endurance limit into the

MEPDG. Chapter 9 presents the conclusions of the study and the recommendations for future research.

All supporting test data and additional graphical plots are included in the Appendixes to this report.

CHAPTER 2

LITERATURE REVIEW

FATIGUE CRACKING MECHANISMS

Fatigue cracking is treated as a long-term distress mode by most mix and pavement design and evaluation procedures. Fatigue cracks are caused by the repeated application of wheel loads that results in fatigue failure of the asphalt surface and base courses. This type of cracking generally starts as short longitudinal cracks in the wheel path and progresses to an alligator cracking pattern (interconnected cracks). Fatigue cracks occur in both wheel paths but usually initiate in the outer wheel path for relatively thin HMA surfaced pavements and in the inner wheel path for thick HMA surfaces (8).

The predominant types of fatigue cracks that occur in flexible pavements are defined by the direction of crack propagation: bottom-up and top-down. It is difficult to identify where the fatigue cracks initiate without taking cores or excavating test pits to visually observe the direction of crack propagation. Bottom-up fatigue cracking is more common than top-down cracking. However, top-down cracking is more visible and allows water and air to readily infiltrate deeper into the HMA mixture. Conversely, fatigue cracks that initiate at the bottom of the HMA layer must propagate to the surface before they become visible and allow water infiltration.

Fatigue cracks that initiate at the bottom of the HMA layer and propagate to the surface are the more classically defined alligator area cracks, as defined by the LTPP Distress Identification Manual (9). This type of fatigue cracking first shows up as short longitudinal cracks in the wheel path that quickly spread and become interconnected to form a cracking pattern generally defined as alligator cracks.

Fatigue cracks that initiate at or near the surface of the HMA layer and propagate downward through the HMA layers generally occur in thick HMA pavements. This type of fatigue cracking first shows up as relatively long longitudinal cracks adjacent to the tires. This type of cracking is characteristic of longitudinal cracks in the wheel path that are not interconnected (8).

"Bottom-Up" Fatigue Cracking–Alligator Cracking

Alligator cracking is a result of the repeated bending of the asphalt layer under traffic. Basically, the pavement deflects under wheel loads producing tensile strains and stresses at the bottom of the asphalt layer. With the continued bending, the tensile stresses and strains cause cracks to initiate at the bottom of the layer that eventually propagate to the surface.

The more bending or the higher the deflections, the greater the tensile strains and stresses and the fewer the number of repeated wheel loads to cause the cracks to initiate at the bottom of the layer and propagate to the surface. The following summarizes key reasons for higher tensile strains and stresses to occur at the bottom of the HMA layer (8).

- Relatively thin or weak HMA layers for the magnitude of the wheel loads.
- High wheel loads and tire pressures.
- Soft spots or areas in unbound aggregate base materials or in the subgrade soil.

- Weakening of aggregate base and subbase layers by an increase in their moisture content.

"Top-Down" Fatigue Cracking–Longitudinal Cracks in Wheel Path

For thick HMA layers, load-related cracks may initiate at the surface and propagate downward. There are several opinions on the mechanisms that cause this type of crack, but there are no conclusive data to suggest that one is more applicable than the other. Some of the suggested mechanisms are (8):

- Tearing of the HMA surface mixture by radial tires with high contact pressures near the edge of the tire, causing the cracks to initiate and propagate both in shear and tension.
- Severe aging of the HMA mixture near the surface resulting in high stiffness that, when combined with high contact pressures adjacent to the tire loads, causes the cracks to initiate and propagate in shear.
- Superposition or combination of wheel load induced tensile stresses and strains with the thermal stresses and strains that occur at the surface when the temperature decreases causing the cracks to initiate and propagate in tension. Aging of the HMA surface mixture accelerates this crack initiation-propagation process.

The stiffer or more brittle the surface in combination with the higher tire pressures and greater temperature changes, the larger the tensile and shear stresses and strains and the fewer the number of wheel loads needed to cause the cracks to initiate at the top of the layer.

FATIGUE LIFE MODELS AND RELATIONSHIPS

General Fatigue Model

In order to characterize the fatigue in asphalt layer, numerous model forms can be found in the literature. The commonly used mathematical relationship used for fatigue characterization is of the following form (10):

$$N_f = A_f K_1 \left(\frac{1}{\varepsilon_t}\right)^{k_2} \left(\frac{1}{E}\right)^{k_3} = A_f K_1 (\varepsilon_t)^{-k_2} (E)^{-k_3} \quad (1)$$

where:

N_f = number of repetitions to fatigue cracking
ε_t = tensile strain at the critical location
E = stiffness of the material
k_1, k_2, k_3 = laboratory calibration parameters
A_f = laboratory to field adjustment factor

Fatigue Life Relationships

It has been accepted for many years that the fatigue behavior of asphalt-aggregate mixes can be characterized by a relationship of the form:

$$N_f = a(1/\varepsilon_t)^b \quad (2)$$

where,

ε_t = initial tensile strain

a, b = experimentally determined coefficients

The above relationship is applicable to a given asphalt mix. Figure 1 shows a general plot of the fatigue relationships for asphalt-aggregate mixes. Some researchers (1) have suggested that a relationship which is more applicable to asphalt-aggregate mixes in general is the following.

$$N_f = a\left(1/\varepsilon_o\right)^b \left(1/E_0\right)^c \quad (3)$$

where,

E_o= initial mix stiffness, and

a, b, c = experimentally determined coefficients

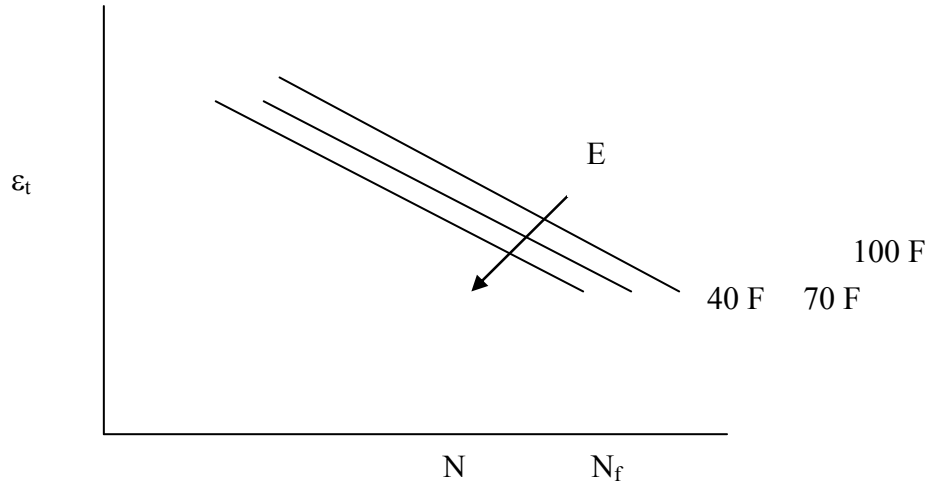

Figure 1. General fatigue relationship for asphalt mixture under controlled strain at different temperatures (logarithmic scale).

Based on the laboratory test data presented in the form of the Equation 4, several strain based models have been proposed to predict pavement fatigue life (11, 12, 13).

Other researchers (14, 15, 16, 17, 18) have used an energy approach for describing the fatigue behavior and have shown that the total, or cumulative, dissipated energy to failure is related to fatigue life as follows:

$$W_N = A(N_f)^z \quad (4)$$

where,

W_N= Cumulative dissipated energy to failure

A, z = Experimentally determined coefficients

In Equations 3 and 4, fatigue life is related to the initial test conditions, namely, the initial strain and initial mix stiffness. In Equation 5, fatigue life is related to terminal test condition, namely the cumulative dissipated energy to failure. Neither approach directly recognizes how damage to the mix actually develops as loading proceeds from the beginning to the end. The cumulative dissipated energy to failure, W_N, is related to w_i, the energy dissipated during the *i*th load cycle as follows:

$$W_N = \sum_{i}^{N_f} w_i \quad (5)$$

For a sinusoidal loading condition.

$$w_i = \pi \varepsilon_i^2 S_i \sin \phi_i \quad (6)$$

where,

w_i= Dissipated energy at load cycle i,

ε_i = Strain amplitude at load cycle i,

S_i = Mix stiffness at load cycle i,

ϕ_i = Phase shift between stress and strain at load cycle i, and

FATIGUE CRACKING PREDICTION EQUATION APPROACHES

Three methodologies or model types have been used to predict fatigue cracking:

1. Basic pavement response using tensile strain, stress, and deflection–the methodology commonly used by most of the design procedures in existence today.
2. Fracture mechanics–the methodology commonly used for predicting thermal cracks.
3. Energy or dissipated energy–the least used methodology, but believed to have good potential for accuracy.

Several models have been developed in the last few decades based on the first approach including the Shell model (12), the Asphalt Institute model (13), the University of California at Berkeley model (10, 18, 19), and the MEPDG model (20).

LABORATORY FATIGUE TESTS

Fatigue of the asphalt concrete mixture is the accumulation of damage under repeated loading.

Asphalt concrete fatigue properties are obtained by laboratory repeated-loading testing in the bending beam mode. In general two modes of loading are used in beam fatigue testing: controlled stress and controlled strain.

Results from laboratory fatigue tests are usually reported as the number of load cycles to failure as a function of the initial tensile strain, normally referred to as fatigue curves. In either controlled stress or controlled strain testing mode, different mixture responses have been related to the number of cycles to failure. These responses have included the initial tensile strain, initial tensile stress, and center-beam deflection. The initial tensile strain is the one most commonly used.

Several mathematical equations have been used to describe the results from fatigue tests by relating the mixture response to the number of loading cycles to failure. Most of the mathematical models for the fatigue curves take the generalized form of Equation 1 (1).The material properties k_1, k_2, and k_3 are obtained through fatigue beam testing in the laboratory.

Adjustment to Lab Fatigue Curves

All laboratory measured fatigue curves must be adjusted or shifted to account for the inaccuracies in simulating field conditions and crack propagation through the HMA layer. The

shifting of laboratory measured fatigue curves is defined by a shift factor and is dependent on the extent and severity level of fatigue cracking used to define failure along the roadway, as well as the type of fatigue cracks (top-down versus bottom-up). The shift factors that have been reported in the literature vary widely from 3 to over 100 depending upon the thickness of the asphalt layer, the mix properties, traffic volume and composition, environmental conditions, fatigue failure criterion, and type of fatigue test (8). Shift factors have not been developed separately for the two categories of fatigue cracks (bottom-up and top-down). The lower values of the shift factors may be more applicable to top-down cracking, while the larger values maybe more applicable to bottom-up cracking (8).

Fatigue cracking initiates at critical points within the HMA layers where the largest tensile strains occur under repeated traffic loading. Continued traffic loading eventually causes these cracks to propagate through the entire HMA layer thickness. The number of load repetitions to failure, defined in terms of a specific area and severity of fatigue cracking on the roadway, is related to the material properties of the HMA mix and the tensile strains at the critical pavement location. The laboratory relationship (Equation 7) is commonly adjusted or shifted to account for this crack propagation and extent.

$$N_{f(fatigue)} = \beta_{f(fatigue)}\left(N_{f(Lab)}\right) \quad (7)$$

where:

$N_{f(fatigue)}$ = Number of load repetitions to a specific area and severity of fatigue cracking

$\beta_{f(fatigue)}$ = Field calibration function (or shift factor) for fatigue cracking relating the laboratory fatigue curve to the area or extent and severity of cracking along the roadway

Fatigue Failure Criteria

Several methods are currently available to define failure in the flexure fatigue test for HMA. These methods may not produce the same results and their method of detecting the failure point may vary. It was important to select an accurate, standardized, and consistent method to be used in the main experiment of this study in order to maintain the integrity of the test results and provide a consistent basis for any implementation scheme.

Failure in any mode of loading is the point at which the specimen can no longer sustain a stable resistance to the damage being done by the loading sequence. When the specimen starts to fail, the damage done per load cycle should increase dramatically, regardless of the load sequence.

For controlled-stress tests, failure can be easily defined as the point when the beam fractures (21, 22, 23). Van Dijk defined failure when the initial strain had doubled (15). Other researchers have defined failure under constant stress as 90 percent reduction in the initial stiffness (24). For controlled-strain tests, failure is more arbitrary and is usually defined at a point during the test when a specified reduction of the original mixture modulus occurs, most commonly when 50 percent of the original modulus (23, 17, 19) is reached or a 50 percent reduction in the initial stress or initial force is obtained (10, 16). In either testing mode, different mixture responses have been related to the number of cycles to failure. These responses have included the initial tensile strain, initial tensile stress, and center-beam deflection. The initial tensile strain is more commonly used.

One of the main concepts used to define fatigue failure is the dissipated energy approach, which is defined as the damping energy or the energy loss per load cycle in any repeated or dynamic test as illustrated in Figure 2.

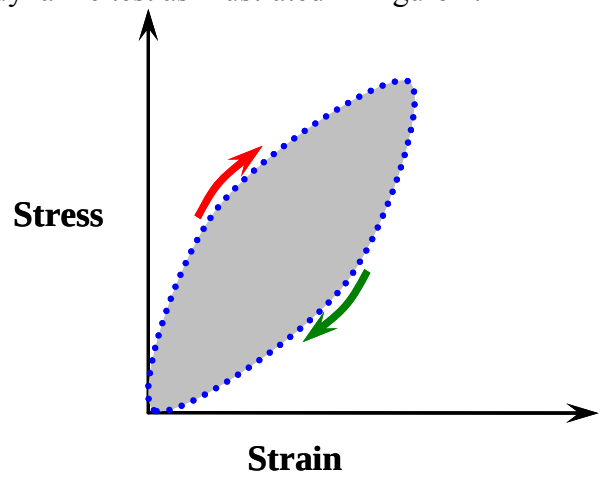

Figure 2. Dissipated energy approach.

To determine the fatigue life from dissipated energy, fatigue tests are conducted where the phase angle, mixture modulus, and dissipated energy are measured during the repeated loadings. Several mechanistic parameters are then calculated and used to relate fatigue life to dissipated energy by the following equation (25):

$$N_f = \left(\frac{W}{A}\right)^{-Z} \quad (8)$$

where:

W = Total dissipated energy.
A, Z = Mixture characteristic constants.

Flexure center and third-point beam fatigue tests are normally used when applying such a method with either controlled stress or controlled strain mode of loading. The dissipated energy per cycle for a beam specimen is computed as the area within the stress -strain hysteresis loop (Figure 3). The dissipated energy is given by the following equation:

$$\omega_i = \pi \sigma_i \varepsilon_i \sin \phi_i \quad (9)$$

where,

ω_i = Dissipated Energy at load cycle i
σ_i = Stress at the load cycle i
ε_i = Strain at the load cycle i
ϕ_i = Phase angle between stress and strain at load cycle i

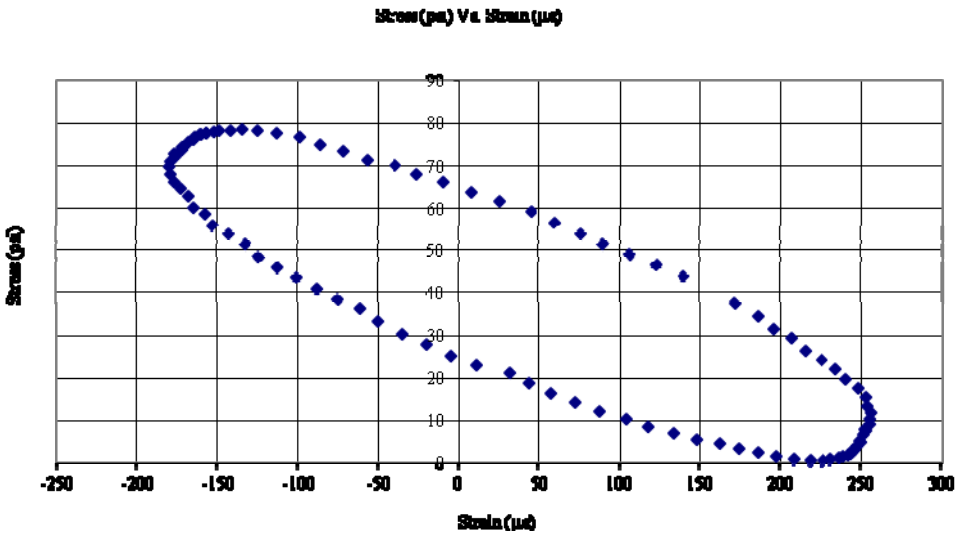

Figure 3. Stress-strain hysteresis loop for controlled-stain test (8).

This energy is then summed over load cycle increments where the lag between stress and strain response cycles is constant.

$$W_{total} = \sum_{i=1}^{n} w_i \qquad (10)$$

where:

W_{total} = Total dissipated energy

w_i = Dissipated energy in the i^{th} load cycle

While this method provides sound mechanistic relationships between stress, strain, energy, and fatigue life, and can be applied under a wide variety of environmental factors, fatigue life cannot be reliably predicted without extensive fatigue testing.

The use of dissipated energy for fatigue life prediction has been investigated over the last three decades (5, 6, 26).

A more recent fatigue failure criterion was developed at Arizona State University (ASU) based on the Rowe and Bouldin's failure definition (8). A new stiffness ratio is developed as (N_i*S_i/S_o), where N_i is the cycle number, S_i is the stiffness at cycle i, and S_o is the initial stiffness taken at cycle number 50. By plotting the stiffness degradation ratio value (N_i*S_i/S_o) versus the load cycles a peak value can be obtained. Failure is then defined as the number of load repetitions at the peak value of that curve for both controlled strain and controlled stress modes as shown in the example in Figure 4. The results also show that there is no significant difference between the two curves for controlled stress and controlled strain; the curves from constant strain testing and constant stress testing have almost the same trend. Using the ASU method, the final damage ratio was around 0.5 of the initial stiffness. The results of that study verified that 50 percent of the initial stiffness was the best value for the failure fatigue criterion used in this project.

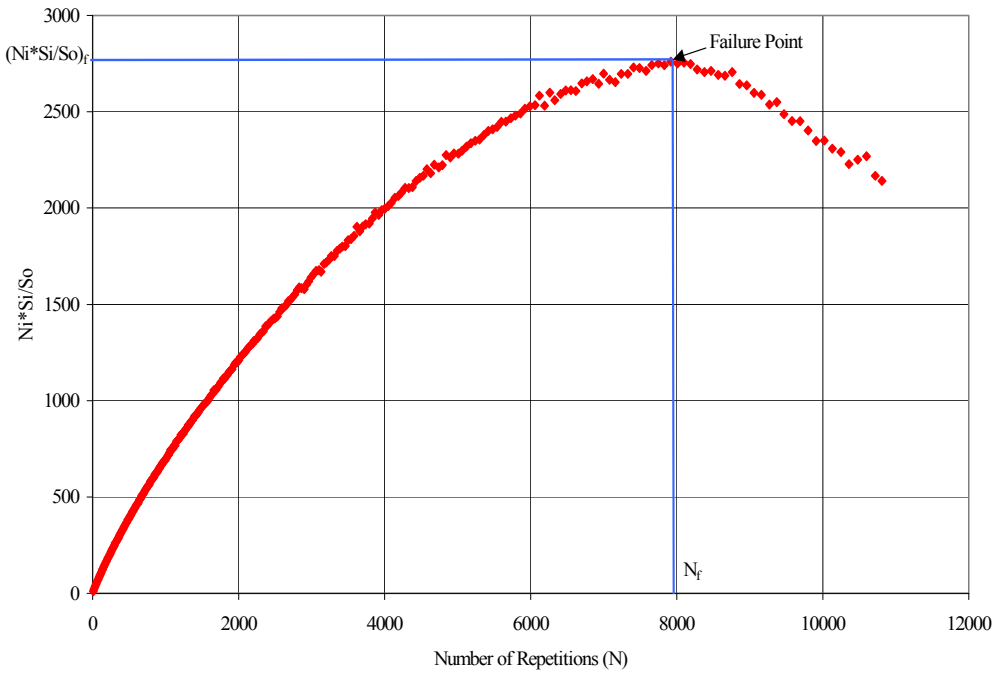

Figure 4. Example of flexural stiffness degradation ratio Ni Si/So versus number of load repetitions using ASU method (8).

Selection of the Failure Criterion

A pilot study (27) was completed in this project to select the appropriate methodology for detecting fatigue cracking cycles to failure. Beam fatigue test results conducted at ASU (8) were analyzed using different methods. The study incorporated a total of 62 beam specimens that used three binders (58-22, 64-22 and 76-16) and were tested at three temperatures (40^0F, 70^0F, and 100^0F). The study used a total of seven different methodologies to find the number of cycles to failure: Pronk's Method (26), Pronk and Hopman's Method (17), Rowe's Method (24), ASU Method (8), Carpenter's Method (3, 5, 6), 3-Stage Weibull Distribution (28, 29, 30), and Francken Models that were developed at ASU (31).

The number of cycles to failure was determined using the seven methods listed above. The results were compared and statistically analyzed. According to the ANOVA statistical analysis, the ASU, Pronk, Hopman, and Rowe methods were statistically the same when considering both the means and variances of the normalized N_f and the stiffness ratio at failure.

Finally, the ease of use to the user of each method was presented. The ease of use was based on the applicability and complexity of the calculation of the results and the implementation in a routine testing program. The ease of use comparison concluded that the ASU and Rowe methods are the easiest methods to use (27).

Another factor considered was that methods based on dissipated energy would not be applicable for testing conducted using rest periods since the HMA material relaxes during the rest period and stress and strain will be almost in-phase at the beginning of each cycle. Therefore, the dissipated energy calculated for the test with rest period is expected to be less

accurate than the case without rest period. Stiffness-based methods such as the ASU method (27) were better suited to the use of rest periods.

For the current study, Pronk's method and the ASU method were recommended, with failure defined as 50 percent of the initial stiffness.

FACTORS AFFECTING FATIGUE CRACKING RESPONSE

The most important factors affecting fatigue response of asphalt mixtures in the laboratory are:

1. Mix variables such as asphalt type and source; aggregate gradation, type, and source; air voids content; asphalt content; etc.
2. Environmental variables such as temperature, temperature gradient, moisture, etc.
3. Loading magnitude, type (strain or stress control), frequency, and existence of rest period.
4. Specimen fabrication and preparation procedure and compaction method.
5. Test conditions such as specimen shape, size, loading configuration, etc.
6. Aging of the asphalt binder.

The following sections discuss these factors.

Asphalt Content and Air Voids

Results from the SHRP A-003A project indicated that lower asphalt contents and lower air voids led to higher stiffness, while higher asphalt contents and lower air voids led to higher fatigue lives (10). Harvey and Tsai (32) produced similar results for a typical California mix. To simulate the effect of air void and asphalt content on several example overlays, the elastic layer theory was used. By using the models for stiffness and fatigue lives obtained from laboratory test results, the simulation indicated that an increase in predicted pavement fatigue life was found for higher asphalt contents and lower air voids.

Tayebali et al. (33) found that air voids have a large effect on fatigue life. As air voids increased, fatigue life decreased for both control strain and control stress. It was found that the observed effects of asphalt content on stiffness and fatigue life were small and inconsistent. It was concluded that stiffer mixes would perform better for thick pavements, while low stiffness mixes would perform better for thin pavements.

Aggregate Gradation

A study conducted by Sousa et al. (34) investigated to what extent gradation has an effect on fatigue performance of asphalt-aggregate mixes. The study concluded that fine gradations (passing through or above the restricted zone) appeared to have better fatigue performance than gradations passing below the restricted zone because of their ability to accommodate higher binder contents. Also, the use of a stiff binder may result in good fatigue performance of relatively thick pavements. The SHELL fatigue predictive equation (12) based on percent of binder volume, strain level and moduli was able to predict relatively well the actual laboratory fatigue performance of the mixes. No shift factor was needed between laboratory results and predicted values using the SHELL fatigue equation (34).

Mode of Loading

The constant stress type of loading is applicable to pavement layers usually more the 8 inches (8) thick. For this type of structure, the thick asphalt layer is the main load-carrying component and the strain increases as the material gets weaker under repeated loading. However, with the reduction in the stiffness because of the thickness, changes in the stress are not significant and this fact leads to a constant stress situation.

In the controlled stress mode of loading, the stress amplitude is maintained at the same level as the initial force. Because of repetitive application of this stress, the strain amplitude increases until it reaches twice the initial amplitude, when the flexural stiffness is reduced to half the initial flexural stiffness, which constitutes failure according to Button et al. (35). On the other hand, the constant strain type of loading is applicable to thin pavement layers since the pavement layer is not the main load-carrying component (8). The strain in the asphalt layer is governed by the underlying layers and is not affected by the decrease in the asphalt layer stiffness. This situation is conceptually more related to the category of constant strain. However, for intermediate thickness layers, fatigue life is generally governed by a situation that is a combination of constant stress and constant strain.

In the controlled strain test, the strain amplitude is maintained at a constant value and the force required to maintain the initial strain level decreases gradually after crack initiation, as the flexural stiffness of the mix is effectively decreased. The failure, or termination point, is arbitrarily selected as a certain reduction in the initial stiffness from that at the commencement of the test, generally 50-percent, as there is no well-defined fracture of the specimen. In addition, the controlled strain mode of loading simulates conditions in thin asphalt pavement layers usually less than 2 inches. The pavement layer is not the main load carrying component. The strain in the asphalt layer is governed by the underlying layers and is not greatly affected by the change in the asphalt layer stiffness. This situation is conceptually more related to the category of constant strain. Also, the strain mode of loading accounts for both crack initiation and propagation while the stress-strain mode of loading does not account for both crack initiation and propagation, because the number of cycles to crack propagation is small compared to the number of cycles to failure which is defined by the fracture of the sample (36). Therefore, fatigue life is usually greater in control strain than control stress (in general approximately 2.4 times greater) (33).

Mixes of higher stiffness, whether due to temperature or asphalt type, tend to perform better under controlled stress than controlled strain. Stiffer mixes generally have higher fatigue life under controlled stress, whereas stiffer mixes have lower fatigue life under controlled strain. Thus, stiffer layers are preferred for thick pavements and less stiff layers are preferred for thin pavements. It was concluded that controlled stress and controlled strain testing might yield similar mix ranking when test results are interpreted in terms of performance expected of the pavement types in which they are placed (33, 10).

The mode of loading analysis was evaluated with a least square calibration of models of the following type (10).

$$N_f = a \exp^{b*MF} \exp^{c*Vo} (\varepsilon_o \text{ or } \sigma_o)^d (S_0)^e \quad (11)$$

where,

MF = Mode factor assuming a value of 1 for controlled strain and -1 for controlled stress,
a, b, c, d, e = Regression constants

The controlled-strain and controlled-stress combined model was as follows:

$$N_f = 0.9500 \exp^{0.4472\,MF} \exp^{-0.2566 Vo} (\varepsilon_o)^{-3.3669} (S_0)^{-1.1633} \quad (12)$$

It was suggested in SHRP Project A-003A that the evaluation of mix performance might well be independent of laboratory mode of loading. Controlled stress and controlled strain testing may yield a similar mix ranking. The effect of mix stiffness on fatigue life is generally reversed for the two modes of loading (10).

In conclusion, Table 1 shows the difference between controlled stress and controlled strain fatigue testing and their influence on the measured characteristics of HMA specimens.

Table 1. Difference between Controlled Stress and Controlled Strain Fatigue Testing (37).

Variables	Stress Controlled	Strain Controlled
Thickness of asphalt layer	Comparatively thick asphalt bound layers	Thin asphalt-bound layer; < 3 inches
Definition of failure, number of cycles	Well-defined since specimen fractures	Arbitrary in the sense that the test is discontinued when the load level has been reduced to some proportion of its initial value; for example, to 50 percent of the initial level
Scatter in fatigue test data	lass scatter	More scatter
Required number of specimens	Smaller	Larger
Simulation of long-term influences	Long-term influences such as aging lead to increased stiffness and presumably increased fatigue life	Long-term influences leading to stiffness increase will lead to reduced fatigue life
magnitude of fatigue life, N	Generally shorter life	Generally longer life
Effect of mixture variables	More sensitive	Less sensitive
Rate of energy dissipation	Faster	Slower
Rate of crack propagation	Faster than occurs in-situ	More representative of in-situ conditions
Beneficial effects of rest periods	Greater beneficial effects	Lesser beneficial effect

Rest Period

It is known that asphalt mixes recover to some extent after a loading cycle as the result of asphalt relaxation. In practice, intermittent loading has a less damaging effect than continuous loading because of the asphalt healing process. The effect of discontinuous loading on fatigue properties has been investigated in several studies. Notably, Van Dijk and Visser (16) investigated the effect of rest period on the fatigue life of a rolled asphalt base course mix. It was found that increased rest periods can increase fatigue life by a factor of 1 to 10 times.

Over the last four decades, several researchers have studied the significance of rest periods between load applications during the fatigue testing of HMA. Different findings have been presented in the literature showing diverse opinion on the effect of rest period. Some researchers think that rest period only leads to a temporary modulus recovery without actually extending the fatigue life, while others found that the modulus recovery did extend fatigue life by a certain amount. These different conclusions were mainly based on a large variety of tested mixtures, laboratory testing setup, and research approaches.

Depending on the way the material is allowed to rest, there are two different ways of introducing rest periods into fatigue testing:

- With rest intervals: this is a classic fatigue test with continuous loading cycles where rest intervals (storage periods) are introduced after a certain number of continuous loading cycles. At the end of each rest interval, the test is continued until the next rest interval.
- With intermittent loads: Each loading cycle is followed by a rest period.

The second method with intermittent loading more closely resembles the sequence of traffic pulses in the field, although both testing methods have been applied by researchers for studying the effect of rest period and healing in HMA fatigue behavior.

Monismith, et al. (38) assessed the effect of rest period by conducting repeated flexure tests on beam specimens supported by a spring base. The loading cycles consisted of 1 sec. of load and 1, 3, or 19 sec. of rest period. The tests were performed at 77ºF and 3, 15, and 30 load applications per minute. The test results indicated that increasing the rest period from 1 to 19 seconds had no effect on fatigue performance. This conclusion is different from many other later research results that showed an enhancement of the fatigue life due to rest periods.

Raithby and Sterling (39) performed uniaxial tensile cyclic tests on beam samples sawed from a rolled layer of asphalt concrete to dimensions of 75mm× 75mm × 225mm. The tests were conducted under controlled stress mode at two loading frequencies (2.5Hz and 25Hz) and two temperatures (10ºC and 25ºC), with sinusoidal load pulse, which has equal tensile and compressive stresses in each cycle. Pulsed loading without and with rest periods varying from 40μs to 800μs was applied until failure occurred. In the tests when rest periods were introduced, the specimens were rested at zero stress. It was observed that the strain recovery during the rest periods resulted in a longer fatigue life by a factor of five or more than the fatigue life under continuous loading.

McElvane and Pell (40) performed rotating bending fatigue tests on a typical British base course mix at 10ºC using a 16.7 Hz frequency. The specimens were subjected to multi-level loading with random duration of rest periods. It was concluded that rest periods have a beneficial effect on the fatigue life depending on the damage accumulated during loading periods. No evidence was found for a limiting value of the fatigue life extension.

Verstraeten et al. (41) performed dynamic two-point bending beam tests in a constant-stress mode (frequency of 54 Hz, temperatures of -5ºC and 15ºC). The loading conditions were maintained either until failure or an 80 % stiffness reduction. The specimens were then stored

for periods varying from 3 to 21 hours at temperatures from -5ºC to 35ºC. The authors concluded that the longer the storage periods and the higher the temperatures, the greater the beneficial effect, although their effects on the susceptibility of mixtures to fatigue couldn't be quantified.

Franken (42) carried out experiments on a typical Belgian mix using a two-point bending beam apparatus. The test was run in constant stress mode of loading at 55.6 Hz frequency. The test results showed an increase in service life when rest periods were incorporated in the fatigue tests. From the test results, an empirical relationship between the cumulative cycle damage ratio in Miner's law (N_i/N_c) and the loading ration (n_r/n_l) that accounts for the effect of rest period was derived:

$$\frac{N_i}{N_c} = 1 + 2.8(\frac{n_r}{n_1})^{0.44} \quad (13)$$

where,

n_r = number of rest periods

n_l = number of loading cycles

Hsu and Tseng (43) conducted a repeated load fatigue test on beam specimens using a haversine waveform with a loading duration of 0.1 sec. To study the effect of the rest period on the fatigue response of asphalt concrete mixtures, loading ratios of 1, 4, and 8, which represent the ratio of the duration of the rest period to that of loading, were applied. During the test, approximately 10% of the applied load was pulled upward on the specimen for each loading to simulate the rebound of the pavement after each vehicle passage. The test results of the controlled stress test showed that asphalt concrete mixtures with higher loading ratios and asphalt content 0.5% more than optimum exhibited longer fatigue life.

Breysse, et al. (44) performed the two-point bending fatigue test on trapezoidal specimens, clamped at the lower base and submitted to a cyclic loading at their free end, to study the balance between damage and recovery in HMA. A controlled displacement test was performed at 20°C and a 40 Hz loading frequency. Specimens were continuously loaded until the overall stiffness reduction reached a given ratio of α%. The stiffness recovery during the rest periods was then monitored by applying a low magnitude loading (supposed not to create any damage) until the response was stabilized. This process was repeated iteratively as many times as wanted, for the same α% ratio. The tests were conducted for α values between 10 and 50% to study the effect of low and severe damage histories on the stiffness recovery values. The results showed that the maximum magnitude of recovery depended on the previous number of applied fatigue cycles. It was noted that part of the recovery observed due to the interrupted loading sequence is a temporary stiffness recovery rather than a true healing. This is why material will return to its original status (damaged status) very quickly after reloading.

Castro, et al. (45) conducted flexural beam fatigue tests with and without rest periods; a constant rest period of 1 second following every 0.1 second loading was applied. The fatigue curves were evaluated by means of discriminant analysis so as to rigorously confirm that they were different. It was concluded that the rest period could increase the fatigue life of an AC specimen up to 10 times, compared to tests without rest periods.

Thus, introducing a rest period in the loading waveform increases fatigue life, and increasing the duration of the rest period also increases the fatigue life up to a certain value, above which the increase in fatigue life is minimal. Since increasing the duration of the rest period increases the testing time, it is important to determine an "optimum" value of the rest

period such that its increase would not cause a significant increase in fatigue life and an excessive duration of the test.

In an attempt to investigate a rational value of the optimum rest period, Raithby and Sterling (46) applied a range of rest periods between none and 25 times the loading time (i.e., 0.1 sec. loading time and 2.5 sec. rest period) on a rolled asphalt base course using a dynamic push-pull test. A constant stress mode producing different waveforms (sine, triangle, and square) was used. It was found that fatigue life does not increase significantly for rest periods greater than ten times the loading time (or 1 sec. rest period) and waveform was less important than the duration of rest periods.

Van Dijk and Visser (16) had tested a rolled asphalt base course mixture in a three-point bending beam apparatus in a constant strain mode (frequency 40 Hz, temperature 20 ºC) with loading ratios varying from 1 to 25 (0.025 sec. loading time and up to 0.625 sec. rest period). Their results showed an increasing fatigue life with increasing rest periods. The maximum beneficial effect of a rest period on the fatigue life (life ratio of about 10) was determined by extrapolation to be achieved at a loading ratio of about 50.

Bonnaure, et al. (47) conducted a three point bending beam fatigue test on rectangular beams with dimensions of 230mm× 30mm× 20mm in order to study the effect of rest periods. An intermittent loading with rest periods of 0 and 3, 5, 10, and 25 times the length of the loading cycle (0, 0.075, 0.125, 0.25 and 0.625 sec.) was applied. The tests were done under both constant stress and constant strain modes of loading at three temperatures (5ºC, 20ºC, and 25ºC) and a 40Hz frequency. The authors concluded that:

1. Increasing the rest period between the loading cycles increases fatigue life. The maximum beneficial effect of rest periods on the fatigue life was at a rest period equal to 25 times the loading cycle (0.625 sec.).
2. Higher fatigue life occurs at higher temperatures.
3. Softer binders increase fatigue life.

The authors also concluded that the stress and strain levels seemed to have no effect on the increase of the fatigue life due to rest periods. In addition, the constant-stress mode resulted in a greater increase in fatigue life as compared to the constant-strain mode.

It was also concluded that the optimum rest period would be different according to mixture properties (aggregate gradation, binder content, binder grade, mixture volumetric), test type (flexure beam fatigue, direct tension, tension-compression, etc.) and test conditions including mode of loading, temperature, frequency, stress or strain levels, etc.

FATIGUE TEST TYPES

Since the 1960s, many beam fatigue tests have been conducted in the pavement community and reported in the literature. A great deal of this fatigue testing of has been conducted at the University of California at Berkeley as well as the University of Nottingham, England. The predictive quality of the fatigue life obtained by any of these test methods depends on how accurately the method simulates the condition of loading, support, stress state and environment which the material is subjected in the pavement. Moreover, selecting any of these test methods will depend on the simplicity and feasibility of the method.

Brief descriptions of selected test methods along with their advantages, disadvantages and limitations can be found in SHRP's "Summary Report on Fatigue Response of Asphalt Mixes" (25). The following is a summary of the most popular fatigue test types.

Flexure Beam Test

One of the principal objectives of SHRP Project A-003A (48) was to develop a proposed test method and associated equipments for testing and evaluation of fatigue properties of asphalt mixes using repetitive flexural bending of beam specimens (10). SHRP Project A-003A also developed surrogate fatigue equations to model the behavior of asphalt mixtures under controlled stress and controlled strain conditions.

Flexural beam tests were used as a means of accelerated testing of asphalt concrete mixture for both fatigue life and flexural stiffness under controlled conditions with the aid of computerized control and data acquisition. A comprehensive methodology to predict asphalt pavement fatigue life was formulated. Using the third-point bending beam apparatus for this test, a load is applied, under either controlled strain or controlled stress loading, on the beam specimen until failure. The beam test specimen generally has a standard rectangular cross section of 2.5 in. (63.5 mm) wide, 2.0 in. (50.8 mm) high, and 15 in. (381 mm) long. Failure is arbitrarily defined by a certain percent reduction in the initial stiffness. In general, a 50 percent of the initial stiffness under controlled strain or complete fracture of the beam specimen (under controlled stress) is used.

Two major improvements were made during SHRP Project A-003A (18) to minimize the setup and testing time and improve the reliability of the test results These improvements were:

1. Increasing the size of beam test specimen from 1.5 in. (38.1 mm) wide, 1.5 in. (38.1 mm) high, and 15 in. (381 mm) long to 2.5 in. (63.5 mm) wide, 2.0 in. (50.8 mm) high, and 15 in. (381 mm) long.
2. Building and designing a new beam fatigue module as a stand-alone device. Software was developed to automatically perform what is now AASHTO Standard Method of Test T 321. The latest software allows for both controlled strain and controlled stress loadings.

Cantilever Beam Rotating Test

At the University of Nottingham, Pell and Hanson (49) used a rotating cantilever machine where specimen is mounted vertically on a rotating cantilever shaft. A load is applied at the top of the specimen to induce a bending stress of constant amplitude through the specimen. The tests were usually conducted at 10°C and a speed of 1,000 rpm. The dynamic stiffness was measured by applying constant sinusoidal amplitude deformations.

Pell also carried out this test using a controlled-strain torsional fatigue machine where the sample is clamped vertically on a shaft. The bottom of the sample is clamped to the bottom of the machine and the loading arrangement gives a sinusoidal varying shear strain of constant amplitude into the specimen.

Trapezoidal Cantilever Beam Test

The trapezoidal cantilever beam test has been popular in Europe. Tests on trapezoidal specimens have been conducted by Shell researchers (15) and LCPC (50). The larger dimension of the trapezoidal specimen is fixed and the smaller end is subjected to either a sinusoidal applied strain or stress. The trapezoid shape of the specimens yields failure at about mid height where the bending stress is largest rather than at the base where boundary conditions might adversely affect interpretation of test results. As an example, specimens tested by van Dijk (15) had a base cross section of 2.2 in by 0.8 in (55 mm by 20 mm), a top cross section of 0.8 in by 0.8 in (20 mm by 20 mm), and a height of 10 in (250 mm).

Supported Flexure Test

A supported flexure test was used to better simulate stress state and mode of loading in the field. Majidzadeh (51) and others used circular samples supported on a rubber mat and subjected to a circular shaped repeated load applied to the center of the slab, resulting in a stress state in the slab which is very similar to that occurring in the pavement structure. Barksdale (52) used asphalt concrete beams placed upon 4 inch thickness of rubber mate supporting the beam and subjected to a haversine load pulse with a 0.06 second duration and frequency of 45 rpm. The fatigue specimen and rubber support were enclosed in a temperature control chamber maintained at 80°F (27°C).

This test method can reduce the scatter of test results by better duplicating field conditions. On the other hand, the test is expensive and time consuming, and requires a large sample size and complicated test machines.

Triaxial Test

The University of Nottingham (22) and the University of California, Berkeley (53) developed this type of device to best represent the in-situ state of stress. Pell and Cooper tested cylindrical specimens with a diameter of 4 in (100 mm) and a height of 8 in (200 mm). The specimen was bonded to end caps with epoxy resin and was mounted in the rig. Specimens enclosed in a Perspex triaxial cell were subjected to a sinusoidally varying axial stress. The only concern about this kind of test is that the shear strains must be well controlled; otherwise the predicted fatigue lives could be considerably different than the field results.

Sousa (53) developed equipment which is capable of applying shear strains by torsion (repeated or constant) together with radial tensile stress using specimens fabricated as hollow cylinders. To date, only shear fatigue (torsional) tests have been conducted. This equipment can be further developed to apply repeated radial tensile stresses through the pulsating fluid within the hollow cylinder, thus simulating the necessary conditions including shear stresses (through torsion) and vertical stresses.

Triaxial tests simulate the field loading condition in which compression is followed by tension and the results can be used for mixture design and, with field correlation factors, for structural design. This type of test is costly, requires specialized equipment, and is time consuming.

Direct Tension Test

The Transport and Road Research Laboratory (TRRL) of the United Kingdom (54) (now the Transport Research Laboratory (TRL)) performed uniaxial tensile tests without stress reversal using a loading frequency of 25 Hz, duration of 40 milliseconds, and rest periods varying from 0 to 1 sec. These tests were conducted in the controlled-stress mode. Direct tension tests were performed in the Netherlands (55) at frequencies of 1 and 0.1 Hz using haversine loading in the controlled-strain mode. Most recently, this test has been used in the United States at Texas A&M University and North Carolina State University to characterize microdamage healing in asphalt binder and asphalt concrete using viscoelastic continuum damage, fracture micromechanics, and dissipated energy approaches.

One advantage of the direct tension test is the test specimen may be circular as well as rectangular in cross section. In addition, the direct tension test is less costly as testing time is shorter because fewer loading cycles can be sustained before failure. The primary disadvantages of this test are that (1) the loading condition does not necessarily represent field conditions and (2) the test requires extensive specimen and setup preparation.

Tension/Compression Test

The tension/compression fatigue test was developed at the Transport and Road Research Laboratory (TRRL) (54). Axial tensile and compressive loadings were applied using in a servo-controlled electro-hydraulic machine. Specimens were prismoidal, with 3 in (75 mm) square cross sections and 9 in (225 mm) lengths. Loading frequencies were 16.7 and 25 Hz, and the effects of rest period, waveform shape, and load application sequence (compression/tension, tension/compression, compression only, and tension only) were evaluated.

Except for its ability to simulate the loading pulse observed in the field, this test does not represent field conditions well, requires long testing times, is costly, and requires specialized equipment.

Diametral Test

The diametral fatigue test is an indirect tensile (IDT) test conducted by repetitively loading a cylindrical specimen with a compressive load which acts parallel to and along the vertical diametral plane. This loading configuration develops a reasonably uniform tensile stress in the specimen perpendicular to the direction of the applied load. Test specimens are usually 4 or 6 in. in diameter and 2.5 to 3.0 in. high. Load is transmitted to the sides of the cylinder through a 0.5 in wide loading strip. Usually a haversine or sine load pulse is applied. The load frequency most commonly used is from 20 to 120 cycles per minute.

Repeated-load indirect tensile tests have been extensively conducted at the Center for Highway Research at the University of Texas at Austin (57, 57, 58, 59). The diametral test offers a biaxial state of stress, which is possibly of a type that better represents field conditions. A key problem with this method is that it will significantly underestimate fatigue life if the principal tensile stress is used as the damage determinant.

Wheel-Track Test

In order to better simulate the effects of a rolling wheel on the pavement and to better understand the pattern of crack initiation and propagation, a wheel-track test was developed to study fatigue characteristics of asphalt pavements. The wheel-track test can be conducted in the laboratory or in a full scale pavement section.

For a laboratory wheel-track test, Van Dijk (15) developed a loaded wheel with a pneumatic tire that rolled back and forth over a slab of asphalt concrete. The diameter of the wheel was 0.25 m and its path was 0.60 m long with a width in the range of 0.05 to 0.07 m, with the slab supported by a rubber mat. Strains were measured at the bottom of slab, and crack initiation and propagation were detected. Results can be expressed in terms of three fatigue stages associated with the development of hairline cracks, real cracks, and slab failure. Based on the test results, Van Dijk suggested that controlled-strain data may be more appropriate to define pavement cracking than controlled-stress data.

The main limitation of the laboratory wheel-track test is the speed of the rolling wheel. In addition, the test is time consuming and does not measure a fundamental mixture property. Moreover, for mixes of low stiffness, rutting becomes significant and may affect fatigue measurements.

Full-scale wheel-track test facilities have been built in several countries around the world. Well-known examples include the circular tracks located at Nantes in France, at Pullman, near the Washington State University campus, the Federal Highway Administration's ALF (Accelerated Loading Facility), and in Australia (ARRB), New Zealand (Canterbury), Denmark, and the United Kingdom (TRRL). The tracks are often divided into sections, each with a different pavement structure, and loads are applied by several sets of dual truck tires.

With full-scale testing facilities, it is possible to examine the effect of changes in the pavement structural section on pavement performance and other forms of pavement distress in addition to fatigue can be studied as well. High initial costs and annual operation and maintenance costs are the main disadvantages. Also, a parallel, supplementary laboratory testing program is still needed, since the field track tests do not directly measure fundamental mixture properties.

HEALING OF HMA

Healing Mechanism

Healing phenomena have been investigated in the literature for many years. Healing is generally considered as the capability of a material to self-recover its mechanical properties (stiffness or strength) to some extent upon resting due to the closure of cracks. In fact, various metallic and non-metallic engineering materials have this ability.

For metallic materials such as steel, aluminum, etc., Suresh (60) categorized the various mechanisms of fatigue crack closure or healing that are induced by a variety of mechanical, microstructural, and environmental factors based on his own results and of the work of other researchers. These mechanisms of crack closure include the followings:

1. Residual plastic stretch at crack wake (plasticity-induced crack closure),
2. Corrosion layers formed within a fatigue crack (oxide-induced crack closure),
3. Microscopic roughness of the fatigue fracture surfaces (roughness-induced crack closure),

4. Viscous fluids penetrated inside the crack (viscous fluid-induced crack closure), and
5. Stress- or strain- induced phase transformations at the crack tip (transformation-induced crack closure).

For non-metallic materials and composites such as glass, polymers, Portland cement concrete, and asphalt concrete mixtures, there are several mechanisms which hinder the growth of fatigue cracks and induce crack healing, which can be summarized as follow (60):

1. Crack deflection;
2. Crack-bridging or trapping; and
3. Crack-shielding due to microcracking, phase transformations, or dislocations.

Effect of Healing on Fatigue Life

A significant amount of work has documented the effect of rest periods on the fatigue life of asphalt mixtures, but little research has focused on the mechanism of healing.

Phillips (61) proposed that the healing of asphalt binders is a three-step process consisting of:

1. The closure of microcracks due to wetting (adhesion of two crack surfaces driven by surface energy);
2. The closure of macrocracks due to consolidating stresses and binder flow; and
3. The complete recovery of mechanical properties due to diffusion of asphaltene structures.

Step 1 is supposed to be the fastest, resulting only in the recovery of stiffness, while steps 2 and 3 are thought to occur much slower but improve both the stiffness and strength of the material similar to the virgin material.

Jacobs, (62) studied the fatigue properties of asphalt mixes under sinusoidal loading, and found that the introduction of rest periods has a beneficial effect on the fatigue resistance of the mixes. He proposed that this healing effect is caused by diffusion of maltenes (low molecular weight bitumen component) through the microcracks, re-establishing the chemical bonds in the cracked area. The maltenes are the most mobile components of the bitumen, although higher molecular weight molecules could also diffuse during longer rest periods, resulting in completely restored material properties.

Lytton (63) used the "dissipated pseudo strain energy concept" to explain the fracture and healing process. The fracture or healing of an asphalt mixture is related to two mechanisms: the surface energy storage or the surface energy release. Which one dominates is related to the polar or non-polar characteristic of the binder. The energy stored on or near the newly created crack faces governs the energy available to make the crack grow. This surface energy depends mainly on the chemical composition of the binder. The micro-fracture and healing of the asphalt-aggregate mixture is governed by the energy balance per unit of crack area between the "dissipated pseudo-strain energy" released and the energy that is stored on the surface of the crack.

When considering healing, there is disagreement whether it happens only during rest periods, during all the loading and unloading periods, or just under certain conditions such as certain temperature and material damage level. These different conclusions are mainly based on a large variety of laboratory testing setup and research approaches.

Although healing has received little attention by pavement engineers, it is a well-known subject in polymer engineering. A considerable volume of work has been done to study the healing phenomenon of polymeric materials. Prager and Tirrell (64) described the healing phenomenon:

"When two pieces of the same amorphous polymeric material are brought into contact at a temperature above the glass transition, the junction surface gradually develops increasing mechanical strength until, at long enough contact times, the full fracture strength of the virgin material is reached. At this point the junction surface has in all respects become indistinguishable from any other surface that might be located within the bulk material: we say the junction has healed."

In asphalt concrete pavements, healing is the process of structural changes that occurs during rest periods, and leads to a structural regain, enhancement, or beneficiation. According to Peterson (65), the association force (secondary bond) is the main factor controlling the physical properties of asphalt cement. That is, the higher the polarity, the stronger the association force, and the more viscous the fraction even if molecular weights are relatively low. Ensley et al. (66) subscribe to the view that asphalt cement consists of aggregations of micelles. These micelles consists of two or more molecules of asphaltenes and associated (if present) peptizing materials of lower molecular weight. The interactions of these micelles among themselves and with aggregates largely determine cohesion and bond strengths, respectively.

A significant breakthrough in understanding the effect of asphalt composition on the healing of asphalt cement was made by Kim et al. (67). They observed that healing was directly proportional to the amounts of longer-chained aliphatic molecules in the saturates and long-chained aliphatic side chains in the naphthene aromatics, polar aromatics, and asphaltenes generic fractions. They proposed methylene to methyl ratio (MMHC) as a quantifier of the nature of the long-chained aliphatic molecules and side chains. MMHC is defined as the ratio of the number of methyl and methylene carbon atoms in independent aliphatic molecules or aliphatic chains attached to cycloalkanes or aromatic centers. While the effects of rest periods on the fatigue life of asphalt mixes have been intensely studied, only limited research in the area of asphalt concrete healing has been reported (68, 69, 70, 71). In recent years, a mechanical approach in identifying the healing potential of asphalt concrete was used by Kim and Little (69). They performed cyclic loading tests with varying rest periods on notched beam specimens of sand asphalt. They obtained a consensus that the rest periods enhance the fatigue life through healing and relaxation mechanisms. They proposed a concept called the healing index and found it to be highly sensitive to the binder used in the tests. Schapery's elastic-viscoelastic correspondence principle (72) was applied in their study to separate viscoelastic relaxation from chemical healing. After separating the relaxation from the healing, the magnitudes of pseudo energy density before and after rest periods were used to calculate the healing index.

Schapery (73) proposed the mechanics of quasi-static crack closing and bonding of the same or different linear viscoelastic materials. He developed equations for predicting crack length or contact size as a function of time for relatively general geometries using continuum mechanics. Atomic and molecular processes associated with the healing or bonding process are taken into account using a crack tip idealization. Using his correspondence principle, an expression was derived for the rate of the edge of the bonded area that is a function of a pseudo stress intensity factor. He found that both the bonding-zone length and speed increase with this pseudo stress intensity factor decreases.

Field Tests

A field study on fatigue damage growth and microdamage healing during rest periods was performed by Kim and Kim (71). The stress wave test technique and dispersion analysis method based on Short Kernel Method employed in their study effectively assessed the changes in elastic modulus due to fatigue damage growth and microdamage healing in an asphalt surface layer. It was found that the elastic modulus decreases following a characteristic S-shape curve when plotted against the number of loading cycles. The major reduction in the elastic modulus occurred during the early stage of fatigue life when there were no visible cracks on the pavement surface. This reduction was concluded to be related to microcrack initiation, propagation, and densification. Introduction of a rest period between loading cycles shifts the curve upward, resulting in a longer fatigue life.

HMA ENDURANCE LIMIT

Historical Background

Pavements have been primarily designed to resist rutting of the subgrade and bottom-up fatigue cracking. In classical pavement design, as design load applications increase, pavement thickness must also increase. There is a growing belief that for thick pavements bottom-up fatigue cracking does not occur. The concept of an endurance limit has been developed to provide a theoretical basis for this belief. This concept assumes that there is a strain level below which no fatigue damage occurs. This strain level is referred to as the endurance limit. Therefore, additional pavement thickness, greater than that required to keep strains below the endurance limit, would not provide additional life. This concept has significant design and economic implications.

The fatigue endurance limit concept was first proposed by Wöhler (74) for metallic materials. The classical Wöhler S/N curve was found to approximate a hyperbola (75), as shown in Figure 5. The asymptote of this line parallels the time (load cycle) axis indicating there is a load level below which the number of cycles to failure does not proportionally increase with decreasing load; thus, the material tends to have unlimited fatigue life. This asymptote represents the fatigue endurance limit (FEL).

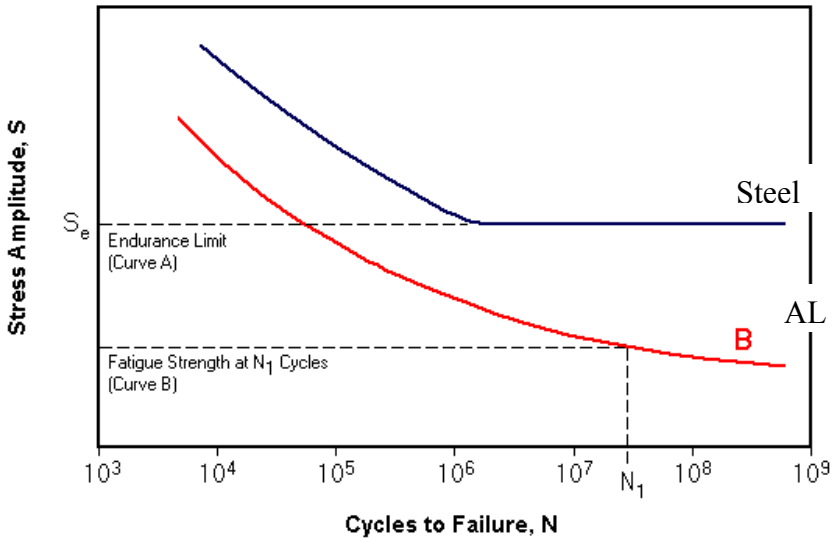

Figure 5. Fatigue Endurance Limit concept (from Wöhler curve).

Wöhler's fatigue endurance limit concept was later applied to adhesive joints by Lagace and Allen et al. (76) and explained as: "If a stress exists below which the life of a joint is not dependent upon the loading but only on the ability of the adhesive to resist oxidation or other environmental degradation, then joints could be designed to have a safe working life determined only by the chemical stability of the adhesive." Although the "endurance limit" concept has been widely studied and defined in metal and other materials, relatively less work has been done for viscoelastic HMA materials.

Endurance Limit Studies

Monismith and McLean (77) first proposed an endurance limit of 70 microstrain for asphalt pavements. It was observed that the log-log relationship between strain and bending cycles converged at approximately 70 microstrain at approximately 5 million cycles. Maupin and Freeman (78) noted a similar convergence.

In the field, Nunn (79) in the United Kingdom (UK) and Nishizawa et al. (6) in Japan proposed concepts for long-life pavements for which classical bottom-up fatigue cracking would not occur. Nunn (79) defines long-life pavements as those that last at least 40 years without structural strengthening. The UK's pavement design system was based on experimental roads which had carried up to 20 million 18-Kips standard axles. When this study was conducted, these relationships were being extrapolated to more than 200 million standard axles. Nunn (79) evaluated the most heavily traveled pavements in the UK, most of which had carried in excess of 100 million standard axles to evaluate the then current design system. Nunn (79) concluded:

- For pavements in excess of 180 mm thick, rutting tended to occur in the HMA layers, not in the underlying structure.
- Surface initiated cracking was common in high traffic pavements, but there was little evidence of bottom-up fatigue. Surface initiated cracks tended to stop at a depth of 100 mm.
- It was observed that the stiffness of thick pavements increased with time, most likely due

to binder aging. This would not tend to occur if the pavement was weakening due to accumulated damage.

- A minimum thickness for a long-life pavement was recommended as 7.9 inches with a maximum thickness of 15.4 inches. The range is based on a variety of factors such as binder stiffness.

Nishizawa (80) reported an endurance limit of 200 microstrain based on the analysis of in-service pavements in Japan. Similarly, strain levels at the bottom of the asphalt layer of between 96 and 158 microstrain were calculated based on back-calculated stiffness data from the falling-weight deflectometer for a long-life pavement in Kansas (81). Other studies (82, 83) report similar findings, particularly the absence of bottom-up fatigue cracking in thick pavements and the common occurrence of top-down cracking.

Monismith et al. (38) found that when performing laboratory testing, if the bending deformations were very low (of the order of 100 microstrain) the beams were able to carry a large number of repetitions (approximately 106 load repetitions) without fracture. He and other researchers (84, 85) further proposed that limiting tensile strain at the bottom of the asphalt layers to no greater than 70 microstrain can extensively increase pavement fatigue life. A similar convergence was noted by Maupin and Freeman (78).

Another study that was performed by Von Quintus (86, 87) suggested that the endurance limit is a valid design premise and an HMA mixture property; he concluded that as the modulus decreases, the endurance limit increases.

Carpenter supported the idea of the existence of a fatigue endurance limit (88). He concluded that the endurance limit is most dependent on binder type and is not readily connected with mix composition. The magnitude of an endurance limit for all mixtures is never lower than 70 microstrain, and for some mixtures it goes up to 100 microstrain, with polymer modified mixtures showing HMA-EL values approaching 300 microstrain. This provides a valid design concept for extended life HMA pavements.

Only limited HMA fatigue research was conducted at low strain levels until recently when the Asphalt Pavement Alliance began promoting the concept of perpetual pavement design (89). A perpetual pavement is an asphalt pavement that provides a very long life without structural failure and only requires periodic replacement of the surface. A key element of perpetual pavement design is to eliminate fatigue cracking that initiates at the bottom of the HMA base due to repeated flexure under traffic loading and to confine distresses to the surface of the pavement, which can easily be renewed by milling and resurfacing.

In response to increasing interest in perpetual pavements, a substantial amount of laboratory fatigue testing has recently been performed in the United States in an effort to demonstrate that HMA does exhibit an endurance limit. Most of this work has been performed at the University of Illinois (3, 5) and the NCAT (7). These studies provide clear evidence that the fatigue behavior of HMA is much different in low strain level tests compared to normal strain level tests. Figure 6 shows a consolidated plot of the University of Illinois fatigue data including low and normal strain level test data. Below approximately 100 microstrain, the fatigue life is significantly longer than estimated from extrapolation of normal strain level test data. Healing of microdamage has been proposed as the primary reason for the increased fatigue life at low strain levels (90, 6, 91). For cyclic tests at low strain levels, it appears that the damage that is caused by loading is offset by healing that occurs during unloading, resulting in an essentially infinite fatigue life.

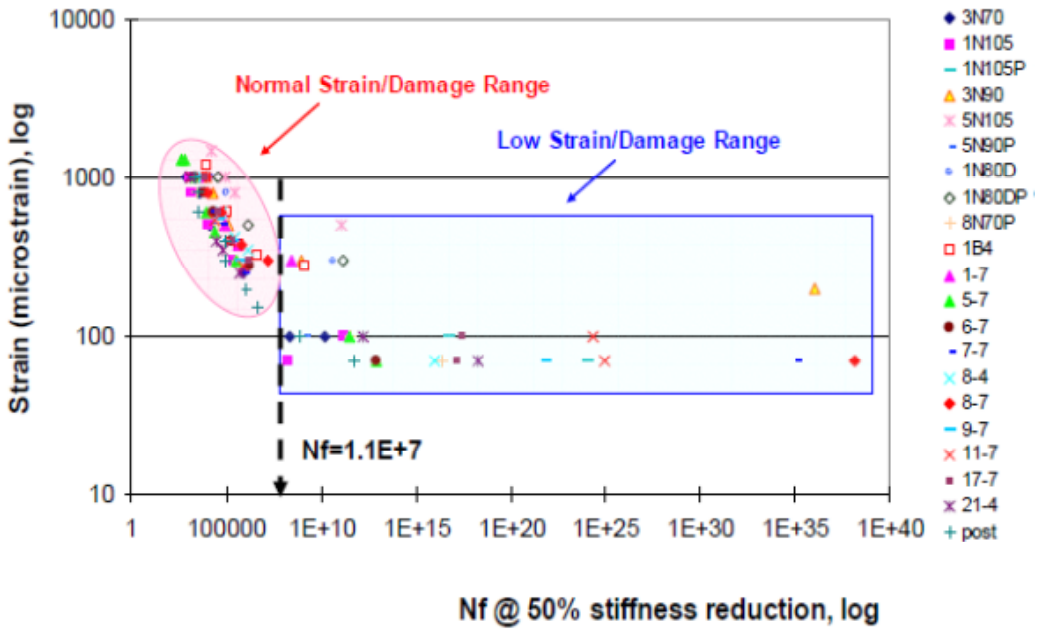

Figure 6. Results of flexural fatigue tests by Carpenter et al. (3) including extrapolated results at low strain levels.

Kansas Department of Transportation conducted a field trial to investigate the suitability of the perpetual pavement concept for Kansas highway pavements (92). The experiment involved the construction of four thick flexible pavement structures on a new alignment on US 75 near Sabetha, Kansas. The four pavements were instrumented with gauges for measuring the strains at the bottom of the asphalt base layers. Seven sessions of pavement response measurements under known vehicle load, consisting of multiple runs of a single-axle dump truck at three speeds, were performed between, before, and after the pavement sections were opened to traffic. The analysis of the measured strain data led to the following major conclusions:

- With few exceptions, the longitudinal and transverse strains were lower than 70 microstrain which is matching the endurance strain limit recommended in the literature for asphalt concrete.
- The pavement response was affected significantly by the temperature in the asphalt layers and by the speed of the loading vehicle. The strains recorded for a truck speed of 20 mph were almost double the strains recorded for a speed of 60 mph.

Bhattacharjee et al. (93) presented an improved method to determine the fatigue endurance limit of asphalt concrete without the need for long-term fatigue tests. The recommended approach employs the elastic–viscoelastic correspondence principle and identifies the strain level at which hysteresis loops form in a stress-pseudo strain relationship, indicating that damage is occurring. The approach requires the linear viscoelastic characterization of the mixture through dynamic modulus testing. This was followed by an increasing amplitude fatigue test to determine the strain level above which damage occurs in the mix. This method was recommended as an alternative method of determining the fatigue endurance limit of HMA. The endurance limit values obtained through uniaxial testing ranged from 115 to 250 microstrain which showed comparable magnitudes as those obtained from beam fatigue tests (93).

Detailed investigation of four heavily trafficked pavements in the United Kingdom support the perpetual pavement concept and the likelihood of an endurance limit for HMA. This

comprehensive study found no evidence of fatigue damage at the bottom of properly constructed thick flexible pavements with total HMA thickness ranging from 230 to 350 mm (94). Cracks in these pavements were found to have initiated at the surface and deflections monitored over a number of years generally showed steady or decreasing deflection with increasing cumulative traffic, indicating that fatigue damage to the bottom of the HMA was not occurring. Similar conclusions concerning the absence of cracking at the bottom of thick HMA pavements have been reported by others (95, 81, 96). In summary, there is mounting evidence that an endurance limit for HMA does exist. It has been observed in laboratory studies of fatigue at low strain levels, and several documented case studies indicate that bottom-initiated fatigue cracking is almost non-existent in properly constructed, thick HMA pavements. The HMA endurance limit, however, does not reflect an absence of load induced damage in the HMA. It is the result of a balance of damage caused by loading and healing or damage recovery that occurs during rest periods (5). The endurance limit for HMA is, therefore, not a single value, but will change depending on the loading and environmental conditions applied to the HMA. Considering an endurance limit in flexible pavement design requires considering the effects of loading, environment, and material properties on both damage accumulation and healing. These findings concerning the endurance limit for HMA served as the research hypothesis upon which the HMA Endurance Limit Validation Study Research Plan (4) was formulated. In conclusion, the literature demonstrates endurance limits at certain conditions but there is no general model is currently available to estimate endurance limit values under different conditions.

CHAPTER 3

STATISTICAL DESIGN OF EXPERIMENT

BACKGROUND

The main objective of this chapter is to present the proposed statistical experimental plan, originally developed in a previous study (NCHRP 9-44) and substantially refined in NHCRP Project 9-44A.

NCHRP PROJECT 9-44 PROPOSED DESIGN

The work plan proposed by the NCHRP Project 9-44 (4) consisted of the five separate experiments summarized in Table 2. The plan shows that 10 factors can possibly influence the fatigue endurance limit. Using a full factorial design would lead to an enormous amount of testing to evaluate their effects.

It was clear that some type of reduced statistical plan is needed to address all variables and. Therefore, the NCHRP 9-44 proposal breaks down the study into five (sequential) study experiments, each of which is based upon the results of the preceding experiment and with 2 or 3 more variables evaluated in the succeeding experiment. For example, Experiment 1 was intended to identify mixture compositional factors that affect healing. Experiments 2-5 use the significant factors identified in Experiment 1 and determine the effects of other factors separately. Although this approach reduces the required number of tests, it might not produce accurate and meaningful results as discussed below.

Table 2. Summary of Laboratory Experiments Proposed by the NCHRP Project 9-44 (4).

Experiment	Topic	Factors
1	Mixture Compositional factors affecting healing in HMA	• Binder type • Binder age • Effective binder conent • Air voids • Design compaction • Gradation • Filler content
2	Effect of Applied strain on healing	• Strain level • Healing from experiment 1
3	Effect of temperature and rest perod duration on healing	• Temperature • Rest period from experiment 1
4	Development of testing and analysis procedures to determine allowable strain levels	• Healing rate from experiment 1 • Mixtures from NCHRP 9-38

5	Estimation of allowable strain levels from mixture composition	• Mix compositional factors affecting damage accummulation • Significant factors from experiment 1 • Temperature • Rest period duration

In Experiment 1, a fractional factorial experiment has been proposed using 7 factors and 2 levels for each factor. However, all tests are performed at 20°C, resulting in 16 tests. This experimental design has some shortcomings that may produce inaccurate results. For example, different temperatures may produce different results. Factors that are not significant at 20°C might be significant at lower or higher temperatures. Also, the proposed plan uses the Plackett-Burman design approach (97), which considers the main effects of the different factors involved, but assumes that there is no interaction among the different factors. For example, an interaction between binder type, binder content, and strain level could have a significant effect on healing, while individual factors such as the strain level only might not be significant. Another well-established interaction in fatigue practice is that the N_f (failure repetitions) of any specimen has been conclusively shown to interact with the V_{fb}, V_{beff} and AV%.

Another limitation of the proposed NCHRP 9-44 plan was its recommendation to use two replicates for each testing condition, which represents the lowest number required to compute the standard deviation of any variable. One should recognize that fatigue is indeed a highly variable phenomenon, and the variance of any computed healing index value would be the sum of the variances associated with the stiffness with and without rest period. In other words, one should logically expect that the variance of the Healing Index (HI) parameter may be very large. This leads to the possible unfortunate consequence that an ANOVA assessment of the significance of the variance components would be hard to prove since the statistical F-ratios of the variances would be large.

A third limitation of the proposed NCHRP 9-44 plan is related to the spreading of the variables among five experiments rather than considering all variables in one experiment. The following sections discuss some of the factors proposed in the NCHRP 9-44 plan and their limitations as related to the plan ultimately used in this research.

Asphalt Binder Type

For all practical purposes, the proposed NCHRP 9-44 plan simply eliminates properties of the asphalt binder as a primary variable. This experimental design cannot produce global conclusions related to the effect of the asphalt binder type. What is missing in the plan is an assessment whether there are any quantifiable differences in healing between the asphalt binder performance grades (shear stiffness). It is imperative to assess what properties of a given performance grade (as well as perhaps any interactions of this property with other variables) may alter the healing index and fatigue endurance limit of the mix.

Binder Aging

The proposed NCHRP 9-44 plan called for the analysis of 2 levels of aging. While it is not denied that aging is likely a factor in fatigue endurance, it appears that the first order effect of aging can be viewed as an increase in stiffness of the binder. As such, the use of a wider range of asphalt binder performance grades should allow a first order assessment of the influence of aging.

Compaction Level

The use of the design compaction level controlled by the number of compaction gyrations is a major variable in the NCHRP Project 9-44 plan. The design level of gyrations directly impacts the actual target air voids and design asphalt content. Therefore, it is better to use the, volume of effective bitumen percent, V_{beff}%, to quantify the amount of asphalt in a given mix. If the AV% and V_{beff}% are used as two prime mix volumetric variables, the impact of mix volumetrics should already be included in any mathematical algorithm used in the overall study. Thus, the use of design compaction would be redundant.

Gradation and Filler Content

In the NCHRP Project 9-44 plan, gradation and filler content are treated as main factors. Again, these variables must be viewed as factors that possibly may have a potential impact upon the fatigue endurance limit. However, gradation specifications for asphalt concrete base layers do not vary significantly among the state DOT. The research team felt that highway agencies typically use standard base gradations and filler contents based on their previous experience. These standard gradations and filler contents have been selected to optimize the properties of their mixes and any changes in these factors might result in poor performance. Thus, the selection of a typical gradation for the mixtures used in this experiment should suffice until more results are obtained from this and other studies.

In summary, notwithstanding the excellent work accomplished in NCHRP Project 9-44, changes were needed to the original NCHRP Project 9-44 to enhance the probability of its success in NCHRP Project 9-44A. The following section discusses the specific experimental plan used in the current study.

NCHRP PROJECT 9-44A DESIGN

A revised experimental design approach is proposed that produces a more comprehensive solution to mathematically define the fatigue endurance algorithm. The design approach is based on studying all major factors and levels together in one main experiment rather than dealing with incomplete, separate, sequential experiments. The experiment considers more important factors than those proposed in the NCHRP Project 9-44 study and ignores less important factors. As results on main portions of the experimental plan were accomplished; necessary changes and modifications to the initial plan were made to ensure that the latest experimental results were used to increase the efficiency of the remaining portions of the work plan.

This study considers the following factors.

1. Binder type (3 levels: PG 58-28, PG 64-22, PG 76-16)

2. Binder content (2 levels: optimum ± 0.5 %)
3. Air voids (2 levels: 4.5, 9.5 %)
4. N_f as controlled by the strain level (2 levels: L, H)
5. Temperature (3 levels: 40, 70, 100°F)
6. Rest period (2 levels: 0, 5 sec.)

It was initially planned to start the experiment using three replicates for each factor combination. As results were obtained and evaluated; an analysis was conducted to re-evaluate the efficiency and accuracy of the use of three replicate specimens and to find ways to reduce the number of tests instead of using a full factorial design.

Two possible factorial design approaches were evaluated to study the effect of the six main factors. The six-factor design approach considers all six factors together in one experiment. The five-factor design approach uses the first five factors stated above for each rest period separately. In other words, the effect of the first five factors would be evaluated with and without a 5-second rest period. The two design approaches are discussed below.

Six-Factor Design

In this design, all six factors stated above would be evaluated. The SR will be obtained from the fatigue test results,. Using a statistical program (98), a model will be developed to estimate the SR as a function of all six factors as shown in the following equation.

$$SR = f(BT, AC, V_a, SL, T, RP) \quad (14)$$

Where BT is the binder type, AC is the binder content, AV is the air voids, SL is the strain level, T is the temperature, and RP is the rest period. Substituting values of 0 and 5 seconds in the model produces the corresponding stiffness values at failure. Figure 7 shows stiffness ratio versus number of loading cycles for the cases with and without rest period. Healing Index (HI) can be defined as the difference between the stiffness ratios for the tests with and without rest period at N_f w/o RP (number of cycles to failure for the test without rest period) as shown in Figure 7.

$$HI = [SR_{w/\ RP} - SR_{w/o\ RP}]_{at\ Nf\ w/o\ RP} \quad (15)$$

where,

$SR_{w/\ RP}$ = Stiffness ratio with rest period
$SR_{w/o\ RP}$ = Stiffness ratio without rest period

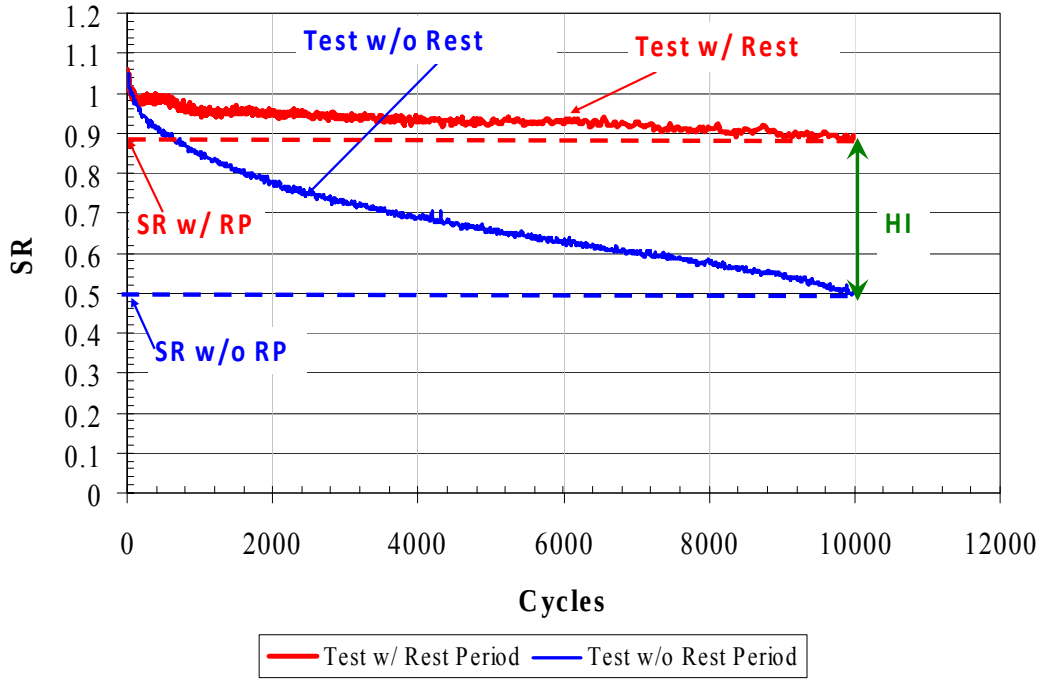

Figure 7. Example of stiffness versus number of loading cycles with and without rest period.

According to this definition of HI, SR needs to be recorded for both tests with and without rest period at N_f w/o RP as shown in Figure 7. Also, extrapolation was used to predict the SR for the test with rest period at N_f w/o RP since it was decided to run all tests with a rest period up to 20,000 cycles only. Figure 8 shows the extrapolation process to determine SR for the tests with rest period at N_f w/o RP.

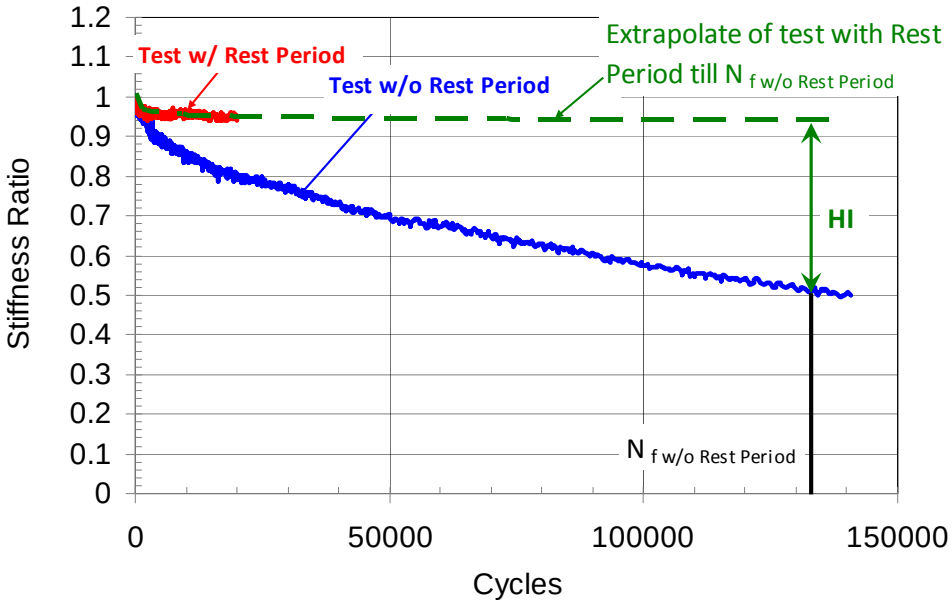

Figure 8. Extrapolation process to estimate SR (with rest period) at $N_{f\ w/o\ RP}$ (PG 64-22, 40F, 4.2 AC%, 4.5 V_a%, 200 microstrain).

Six-Factor Full Factorial Design

Table 3 shows the full factorial design in which all factor combinations are tested. The full factorial design will require 3 x 2 x 2 x 2 x 3 x 2 x 3 replicates = 432 tests. This full factorial design would allow a full analysis of all possible interactions of all main variables.

Table 3. Six-Factor Full Factorial Design.

Binder Type			PG 76-16				PG 64-22				PG 58-28			
Binder Content			4.2		5.2		4.2		5.2		4.2		5.2	
Air Voids (%)			4.5	9.5	4.5	9.5	4.5	9.5	4.5	9.5	4.5	9.5	4.5	9.5
Temp	N_f w/o RP	Rest Period (sec)												
L	L	0												
		5												
	H	0												
		5												
M	L	0												
		5												
	H	0												
		5												
H	L	0												
		5												
	H	0												
		5												

In an effort to reduce the number of tests and still produce accurate results, a fractional factorial design approach was considered. The fractional factorial approach was designed in such a way as to produce the main effects, as well as all salient 2-factor and 3-factor interactions (99). The only drawback of the fractional factorial design is that all 4-factor and higher interactions would be ignored. However, from a practical viewpoint, 4-factor and higher interactions are of little or no consequence to the final accuracy of the experiment. Two fractional factorial designs were studied further. One was considered a complete randomization and the other viewed as a partial randomization. These are discussed in the following paragraphs.

Six-Factor Fractional Factorial Design with Complete Randomization

This statistical fractional factorial design considers all six factors with all levels previously listed. There are many design optimality criteria and the most popular criterion is called D-optimality (99). The D-optimality design minimizes the volume of the joint confidence region on the vector of regression coefficient. A computer generated design is used to reduce the number of runs using the JMP software (98). Table 4 shows the factor combinations at which the tests would be performed. The table shows that 96 combinations would be tested with 3 replicates for each combination. This design would require a total of 288 tests instead of the 432 tests required for the 6-factor full factorial design. This would save 144 tests as compared to the full factorial design.

Table 4. Factor Combinations at Which the Test Will be Performed for the 6-Factor Fractional Factorial Completely Randomized Design.

Binder Type			PG 76-16				PG 64-22				PG 58-28			
Binder Content			4.2		5.2		4.2		5.2		4.2		5.2	
Air Voids (%)			4.5	9.5	4.5	9.5	4.5	9.5	4.5	9.5	4.5	9.5	4.5	9.5
Temp	N_f w/o RP	Rest Period (sec)												
L	L	0	■			■		■	■		■	■	■	■
		5		■	■		■			■	■	■	■	■
	H	0		■	■		■	■		■	■	■	■	■
		5	■			■		■	■		■	■		■
M	L	0		■	■		■	■	■	■	■			■
		5	■			■	■	■	■	■		■	■	
	H	0	■			■	■	■	■	■		■	■	
		5		■	■		■	■	■	■	■			■
H	L	0	■	■	■	■	■			■		■	■	
		5	■	■	■	■		■	■		■			■
	H	0	■	■	■	■		■	■		■			■
		5	■	■	■	■	■			■		■	■	

Table 5 shows the main and two and three-factor interaction terms that can be estimated from this experimental design. It is obvious that all of the major three-factor interactions are accounted for in the fractional design and a model with up to 41 variable parameters can be developed.

Table 5. Factors and Factor Interactions Estimated from the Experiment.

All main effect	Two-factor interactions	Three-factor interactions
Binder Content	Binder Content*Air Voids	Binder Content*Air Voids* Damage Level
Air Voids	Binder Content* Damage Level	Binder Content*Air Voids*Rest Period
Damage Level	Binder Content*Rest Period	Binder Content*Air Voids*Temperature
Rest Period	Binder Content*Temperature	Binder Content* Damage Level*Rest Period
Temperature	Air Voids* Damage Level	Binder Content* Damage Level*Temperature
	Air Voids*Rest Period	Binder Content* Rest Period*Temperature
	Air Voids*Temperature	Air Voids* Damage Level*Rest Period
	Damage Level*Rest Period	Air Voids* Damage Level*Temperature
	Damage Level*Temperature	Air Voids*Rest Period*Temperature
	Rest Period*Temperature	Damage Level*Rest Period*Temperature

Six-Factor Fractional Factorial Design with Partial Randomization

It is important to randomize the tests in the lab in order to reduce the effect of errors. For example, if a machine error occurs on a certain day, randomization would distribute the error among different factor combinations instead of concentrating the error on a few factor combinations. However, complete randomization may not always be practical. For example, complete randomization would require testing a specimen with a certain factor combination

followed by a specimen with a completely different factor combination, etc. This would reduce the efficiency of the specimen preparation and testing program.

In the experiment involving Partial Randomization; a split-plot design is used in which the factors are divided into two groups: whole plot and subplot (99). The whole plot includes factors whose levels are hard to randomize, while the subplot includes factors whose levels are easy to randomize. In this experiment, the whole plot factor is the binder type, while the subplot includes the rest of the factors. This means that all tests of the first binder are completed first, followed by the second binder tests and then the third binder tests. Within each set of binder tests, all other factors are randomized. This order of testing is more practical than completely randomizing all tests. The results are analyzed according to the split-plot design procedure (98). This statistical design method does not affect the required number of tests for the fractional factorial design.

This approach, in reality, is a practical necessity in the laboratory as specimen preparation can be easily accomplished for each specific binder type used in the study. Use of a completely randomized design would incredibly complicate and slow the specimen production process by requiring random use of the various binder types.

Table 6 shows the factor combinations at which the tests would be performed. The table shows that 96 combinations are tested with 3 replicates for each combination with a total of 288 tests. Similar to the completely randomized experiment, all main and two and three-factor interaction terms are estimated as shown in Table 4.

Table 6. Factor Combinations at Which the Test Will Be Performed For the 6-Factor Fractional Factorial Split-Plot Design.

Binder Type			PG 76-16				PG 64-22				PG 58-28			
Binder Content			4.2		5.2		4.2		5.2		4.2		5.2	
Air Voids (%)			4.5	9.5	4.5	9.5	4.5	9.5	4.5	9.5	4.5	9.5	4.5	9.5
Temp	N_f w/o RP	Rest Period (sec)												
L	L	0		■	■		■	■		■	■			■
		5	■			■	■		■	■		■	■	
	H	0	■			■	■		■	■		■	■	
		5	■	■	■			■	■	■	■			■
M	L	0		■	■			■	■		■			■
		5	■		■	■	■	■		■		■	■	■
	H	0	■		■	■	■	■		■		■	■	■
		5		■	■		■		■	■	■	■	■	
H	L	0	■			■	■			■		■	■	
		5	■	■	■	■		■	■		■		■	■
	H	0		■	■	■		■	■		■		■	■
		5	■	■	■	■	■	■		■	■	■	■	■

Five-Factor Design

Since the healing index requires testing with and without rest period, another possible experimental design would be to remove the factor of rest period from the statistical model and use the remaining 5 factors only. This method would require developing two 5-factor models, with and without rest period. The number of cycles to failure are compared the same way as the case of the 6-factor design to determine the healing index.

From the fatigue test results, the SR is obtained. Using the statistical program (98), a model is developed to estimate SR as a function of all 5 factors for each case of rest period as shown in Equation 16.

$$SR = f(BT, AC, AV, SL, T) \quad (16)$$

Comparing the SR for the case without rest period with the number of cycles for a 5-second rest period, the healing potential of the material can be estimated by determining the Healing Index (HI) as shown in Equation 15.

Five-Factor Full Factorial Design

Table 7 shows the full factorial design in which all factor combinations are tested. The full factorial design would require 3 x 2 x 2 x 2 x 3 x 3 = 216 tests. If two rest periods are used (0 and 5 seconds), the total number of tests would be 216 x 2 = 432 tests.

Table 7. Five-Factor Full Factorial Design For Each Rest Period.

Binder Type		PG 76-16				PG 64-22				PG 58-28			
Binder Content		4.2		5.2		4.2		5.2		4.2		5.2	
Air Voids (%)		4.5	9.5	4.5	9.5	4.5	9.5	4.5	9.5	4.5	9.5	4.5	9.5
Temp	N_f w/o RP												
L	L												
	H												
M	L												
	H												
H	L												
	H												

Five-Factor Fractional Factorial Design with Complete Randomization

Using the D-optimality design previously mentioned, Table 8 shows the factor combinations at which the fractional factorial test is performed. This design would require a total of 156 tests for each case of rest period, or 312 tests for the two cases.

Table 8. Factor Combinations at Which the Test Will Be Performed For the 5-Factor Fractional Factorial Completely Randomized Design For Each Case of Rest Period.

Binder Type		PG 76-16				PG 64-22				PG 58-28			
Binder Content		4.2		5.2		4.2		5.2		4.2		5.2	
Air Voids (%)		4.5	9.5	4.5	9.5	4.5	9.5	4.5	9.5	4.5	9.5	4.5	9.5
Temp	N_f w/o RP												
L	L												
	H												
M	L												
	H												
H	L												
	H												

Five-Factor Fractional Factorial Design with Partial Randomization

Using the split-plot design mentioned above, Table 9 shows the factor combinations at which the test is performed with partial randomization. This design would require a total of 156 tests for each case of rest period, or 312 tests for the two cases. Note that there are 52 runs, where each run consists of 3 replicates to be performed together without randomization.

Table 9. Factor Combinations at Which The Test Will Be Performed For The Five-Factor Fractional Factorial Split-Plot Design For Each Case of Rest Period.

Binder Type		PG 76-16				PG 64-22				PG 58-28			
Binder Content		4.2		5.2		4.2		5.2		4.2		5.2	
Air Voids (%)		4.5	9.5	4.5	9.5	4.5	9.5	4.5	9.5	4.5	9.5	4.5	9.5
Temp	N_f w/o RP												
L	L												
	H												
M	L												
	H												
H	L												
	H												

Comparing Six-Factor and Five-Factor Factorial Designs

Considering all six experimental designs discussed above, the six-factor design is preferred over the five-factor design because it would provide more accurate results and require less number of tests. The six-factor design can capture and evaluate the significance of the rest period factor on the fatigue results, whereas the five-factor design does not consider this factor effect. If the results show that the rest period and its interaction terms are significant, they will be added to the general model of estimating the fatigue. Thus, the model produced by the six-factor design allows the user to input different values of rest period (such as 1 or 3 seconds) and estimate the fatigue results. On the other hand, the results of the five-factor design rely on only the calculation of 0 and 5 second rest periods. That is, it cannot estimate the fatigue results of the other rest periods.

Comparing all three possible six-factor designs, the six-factor fractional factorial design with partial randomization was recommended for this study. The complete randomization condition cannot be satisfied in this experiment due to the constraints of the production process and testing. Thus, it is most appropriate to do the experiment using partial randomization to

accommodate the study constraints. This design also reduces the number of tests from 432 (full factorial design) to 288 (fractional factorial design with partial randomization).

Other Detailed Experiments

Based in the outcomes of the previous study, other detailed experiments were performed to study certain factors in more details. For example, other rest periods and strain levels might be tested with a smaller number of other factors. The details of these experiments are discussed below.

Final Design

The final design approach is based on studying all factors together in one main experiment rather than dealing with incomplete, separate experiments. The study considers the factors of binder type, binder content, air voids, N_f level, temperature, and rest period.

The 6-factor fractional factorial design with partial randomization was chosen since it would provide better results and requires less number of tests. A total of 288 tests are required as shown in Table 9 with 3 replicates for each factor combination.

CHAPTER 4

MATERIALS AND MIX DESIGN

BACKGROUND

This chapter reports and discusses the testing undertaken by ASU, Tempe, Arizona, and MACTEC (Phoenix, Arizona) in support of the fatigue testing described in Chapters 5 and 6. MACTEC undertook (1) determination of the range of compaction and mixing temperatures, (2) asphalt binder characterization using the Superpave binder tests including the Dynamic Shear Rheometer (DSR) and the Bending Beam Rheometer (BBR), and (3) mixture design. ASU conducted a comprehensive characterization study of the rheological properties of asphalt binder, using one performance-graded asphalt binder test (Brookfield viscometer) and two penetration-graded asphalt binder tests (penetration and softening point) at a wide range of temperatures.

MATERIALS

Three asphalt binder types were provided by Holly Asphalt Company, Phoenix, Arizona, and used by MACTEC and ASU for the mix design and binder characterization tests. They are all unmodified and classified as PG 58-28, PG 64-22, and PG 76-16. Mineral aggregates were supplied by CEMEX Plant #1386, Phoenix, Arizona, and were used by MACTEC for the mix design.

BINDER AGING METHODS

For the binder characterization tests, samples of the three asphalt binder types were aged by the short-term (rolling thin-film oven, RTFO) and long-term (pressure aging vessel, PAV) conditioning protocols in accordance with AASHTO T 240 and AASHTO R 28, respectively.

For the RTFO test (Figure 9), unaged asphalt binder is placed in a cylindrical jar, which is then placed in a carousel inside a specially designed oven. The oven is heated to 325°F (163°C) and the carousel is rotated at 15 rpm for 85 minutes. The carousel rotation continuously exposes new asphalt binder to the heat and air flow and slowly mixes each sample.

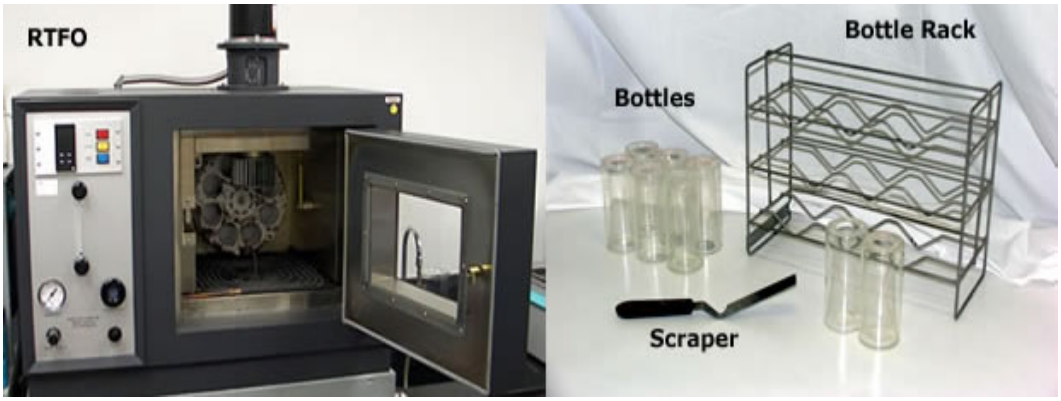

Figure 9. RTFO test setup.

In the PAV test, the RTFO aged asphalt binder is placed in an unpressurized PAV preheated to the test temperature. When the PAV reaches the test temperature it is pressurized to 300 psi (2.07 MPa). After 20 hours of treatment the samples are removed, degassed and stored for future testing. Figure 10 shows the PAV apparatus.

Figure 10. PAV apparatus.

ASPHALT BINDER TEST RESULTS

Viscosity—Temperature Curves

The laboratory mixing and compaction temperatures for the mix design were determined using the viscosity–temperature relationship. The temperatures were selected corresponding with binder viscosity values of 0.17±0.02 Pa·s for mixing and 0.28±0.03 Pa s for compaction. Viscosity values were determined using a Brookfield Rheometer (ASTM D4402). To develop the viscosity—temperature curves, viscosity values were measured at temperatures of 275, 311, and 347°F (135, 155, and 175°C) for the PG 58-28 and PG 64-22 binders, while viscosity values were measured at temperatures of 275 and 347°F (135 and 175°C) for the PG 76-16 binder. Table 10 summarizes the lab mixing and compaction temperatures determined.

Table 10. Summary of Laboratory Mixing and Compaction Temperatures for Mix Design, °F (°C) Provided by MACTEC.

	Temperature, °F (°C)	Binder Type		
		PG 58-28	PG 64-22	PG 76-16
Mixing	Min	295 (146)	308 (153)	329 (165)

	Max	305 (152)	320 (160)	340 (171)
Compaction	Min	275 (135)	287 (142)	310 (154)
	Max	284 (140)	296 (147)	318 (159)

Performance-Graded Binder Characterization Tests

The Dynamic Shear Rheometer (DSR) and Bending Beam Rheometer (BBR) tests were performed to characterize the three asphalt binders used for the mix design and to confirm that the binders meets the performance-graded binder specifications.

For the characterization of binder at intermediate and high temperatures, the DSR test was conducted at 15, 30, 45, 70, 95, and 115°C. The complex shear modulus (G*) and phase angle was measured at a constant frequency (10 rad/sec). For the low temperature binder response, the BBR test was conducted and the flexural creep stiffness (S) at 60s at a specified temperature and slope (m-value) were measured. The temperatures used to measure the flexural creep stiffness were -18, -12, and -6°C for PG 58-28, PG 64-22, and PG 76-16, respectively. Table 11 summarizes the test methods and their properties and test conditions. It should be noted that the DSR test was separately conducted for each aging condition: Neat or Tank, RTFO, and RTFO+PAV, while the BBR test was conducted only for the PAV condition.

Table 11. Performance-Graded Binder Characterization Tests Conducted by MACTEC.

Test	Property	Method	Conditions
Dynamic Shear Rheometer	Complex Shear Modulus (G*) and Phase Angle (δ)	AASHTO T315	10 rad/sec 59, 86, 113, 158, 203, and 239°F (15, 30, 45, 70, 95, and 115°C)
Bending Beam Rheometer	Creep Stiffness (S) and Slope (m-value)	AASHTO T313	60 sec -0.4, 10.4, and 21.2 °F, (-18, -12, and -6°C)

A viscosity–temperature relationship was developed using the DSR test results (i.e., G* and phase angle) at three aging conditions (Figures 11, 12, and 13). It is obvious from the plots that, as expected, the binder becomes more viscous as it is aged. Note that the viscosity values in each plot were obtained from the G* and phase angle values at the specified test temperatures by converting them into viscosity by the Cox-Merz equation.

$$\eta = \frac{G^*}{10}\left(\frac{1}{\sin\delta}\right)^{4.8628} \times 1000 \qquad (17)$$

where,

η = viscosity, cP
G* = complex shear modulus, Pa
δ = phase angle, degree

The creep stiffness results from the BBR test were found to meet the requirements of AASHTO M 320. Table 12 shows the test results for each binder type indicating that they met the specifications.

Table 12. Summary of BBR Test Results (S and m-Value).

Property	Binder Type			AASHTO M 320 Specification Limits
	PG 58-28	PG 64-22	PG 76-16	
Creep Stiffness, S (MPa)	232	191	138	300 max
Slope, m-value (unit less)	0.323	0.316	0.337	0.300 min

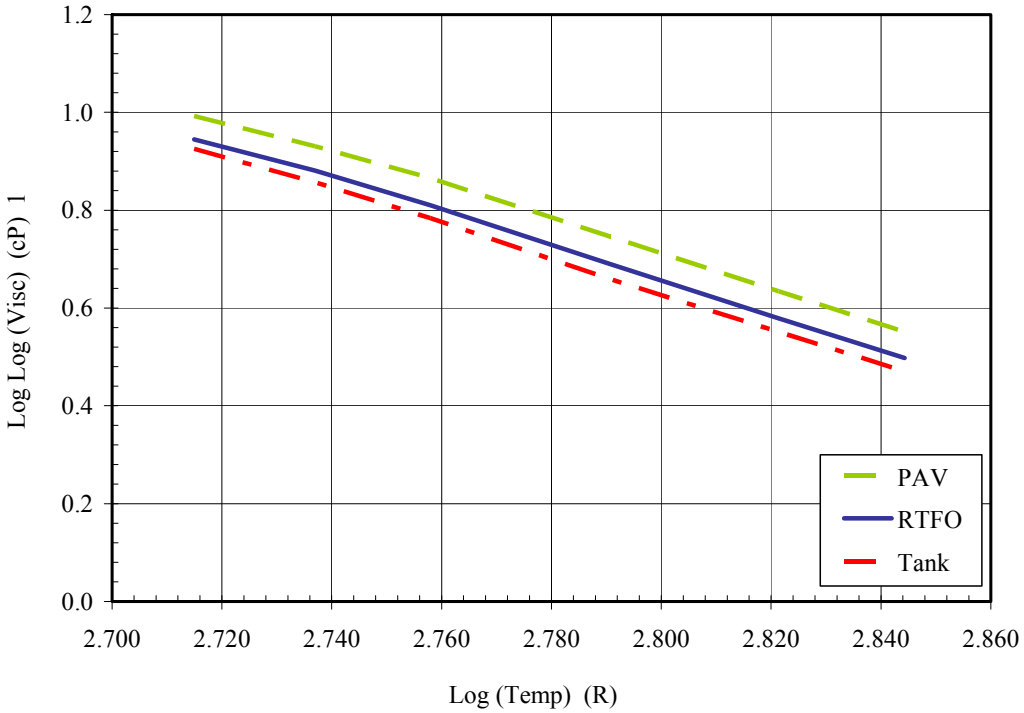

Figure 11. Temperature-viscosity relationship from DSR results, (PG 58-28).

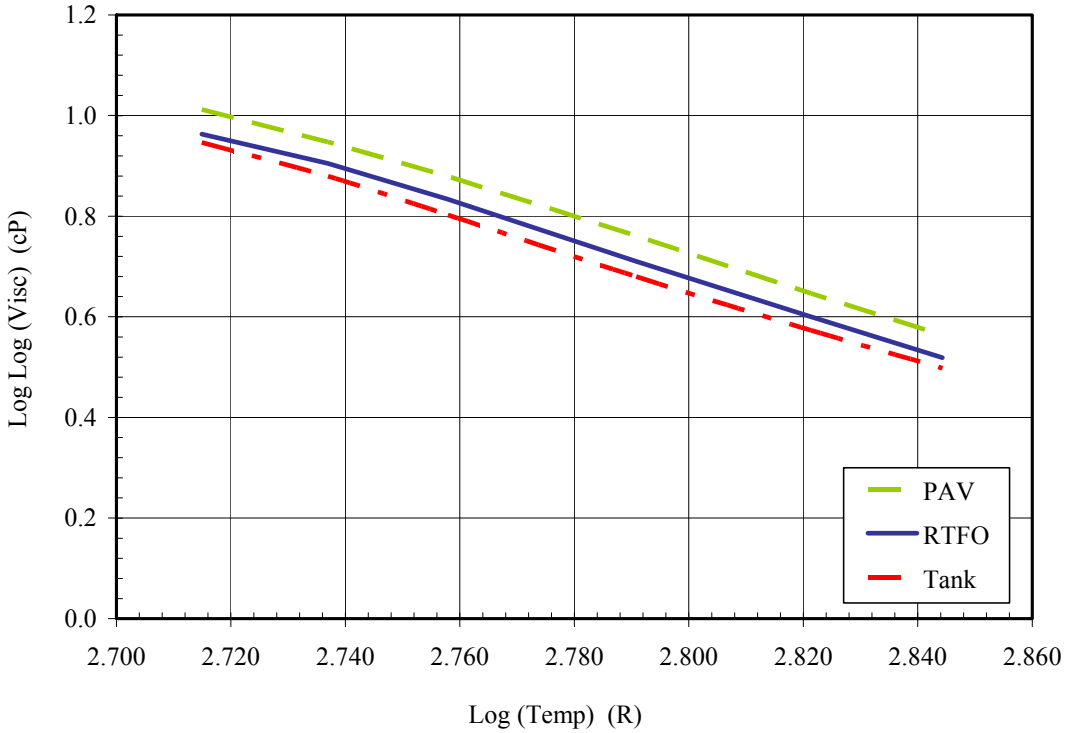

Figure 12. Temperature-viscosity relationship from DSR results, (PG 64-22).

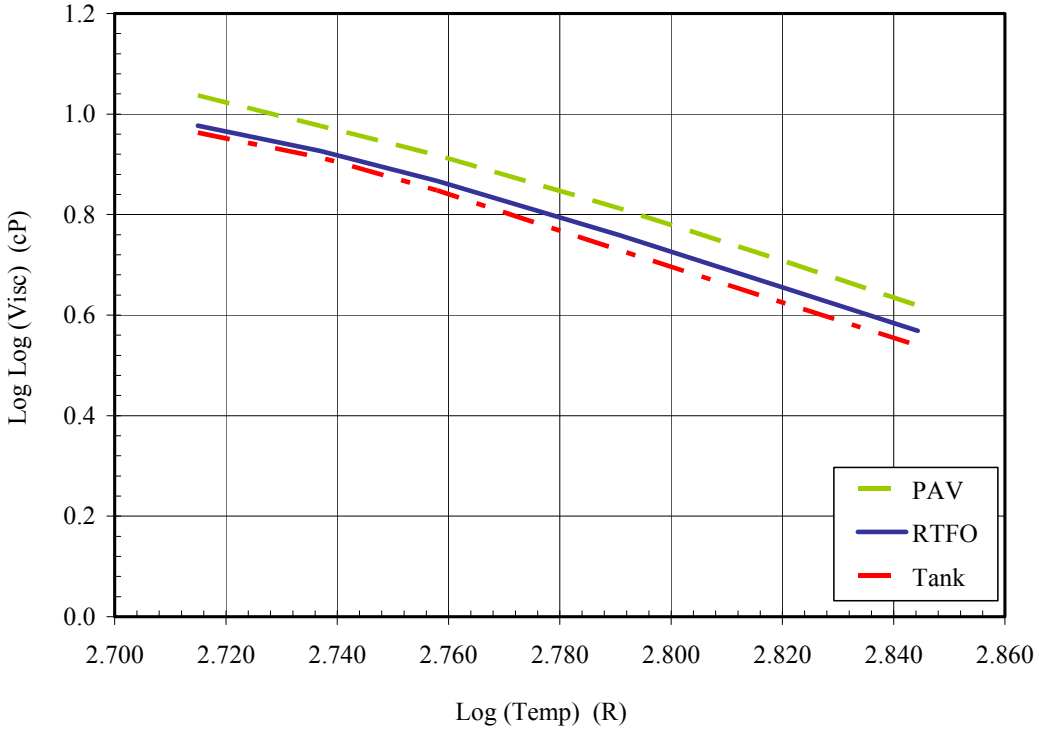

Figure 13. Temperature-viscosity relationship from DSR results, (PG 76-16).

ASPHALT BINDER CHARACTERIZATION TO DEVELOP AN A_i-VTS_i RELATIONSHIP

A comprehensive characterization study of the rheological properties of the three binder types (PG 58-28, PG 64-22, and PG 76-16) was conducted using one performance-graded binder test and two conventional (i.e., penetration- and viscosity-graded) binder tests (27). The objective of this work was to characterize the asphalt binder used in this project over a wide range of temperatures and subsequently to develop a linear relationship (i.e., A_i-VTS_i relationship) between temperature and viscosity. All binder tests were performed for three aging conditions: neat (tank) or original, short-term aged (RTFO), and long-term aged (RTFO + PAV). The conventional binder tests used in this study included the penetration test and softening point (ring and ball) test. The performance-graded binder test was the rotational viscometer (Brookfield) test.

Each of the three binder types was obtained from two sample cans (Sample 1 and 2) and each can was duplicated (Replicates A and B). This scheme applies to each aging condition. Thus, for one PG binder at a given aging condition, four specimens (2 cans * 2 duplicates) were tested for the three binder types. These four specimens were called a set and a unique number was assigned for each set as a set number. Table 13 shows an example of this set numbering scheme.

Table 13. Example of Binder Sample Preparation Scheme.

Binder Type	Aging Condition	Sample Can	Replicate	Set Number
PG 58-28	Tank Condition	1	A	10
			B	12
		2	A	11
			B	13

Table 14 summarizes the properties measured, the test standard, and the test condition for each test.

Table 14. Penetration- and Performance-Graded Binder Characterization Tests.

	Property	Method	Conditions
Conventional Test	Penetration	AASHTO T49	100 g, 5 sec, 40, 55, 77, and 90°F (4, 12.8, 25, and 32°C)
	Softening Point	AASHTO T53	Measured Temperature
Superpave Test	Brookfield Viscosity	AASHTO T316	200, 250, 300, 350°F (93, 121, 149, 177°C)

Data Analysis

A combination of nine viscosity–temperature data points (four penetration values, one softening point value, and four Brookfield values) are plotted together in a viscosity–temperature graph (Figures 14-16), in order to characterize the viscosity-temperature susceptibility

relationship over a wide range of temperature. The linear relationship can be established based upon the following equation:

$$\log \log \eta = A + VTS \log T_R \quad (18)$$

where,

η = viscosity, cP
T_R = temperature, °Rankine
A = regression intercept
VTS = regression slope of viscosity-temperature susceptibility

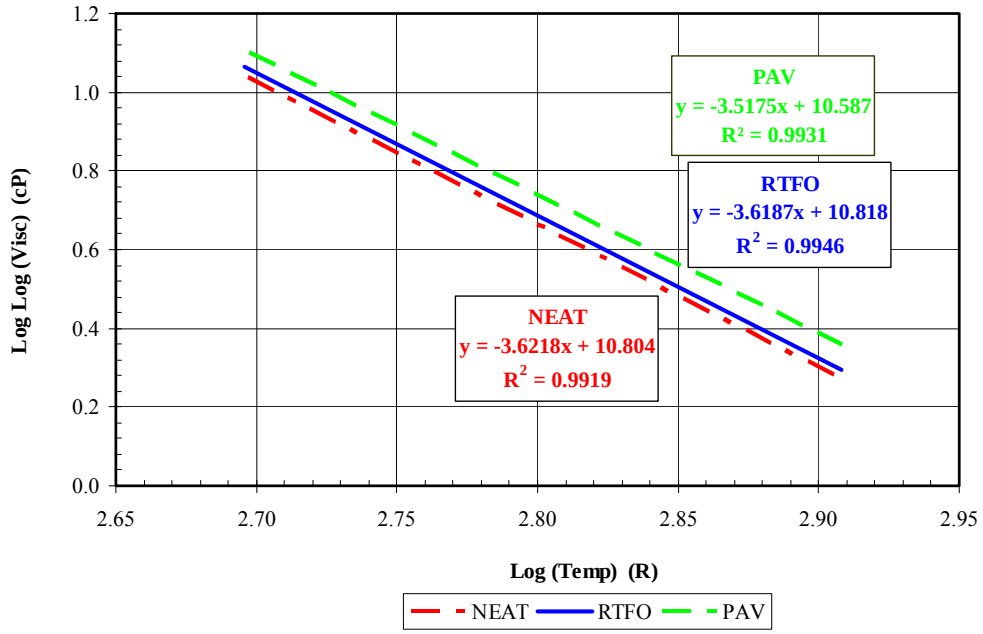

Figure 14. Viscosity – temperature relationship for PG 58-28 binder.

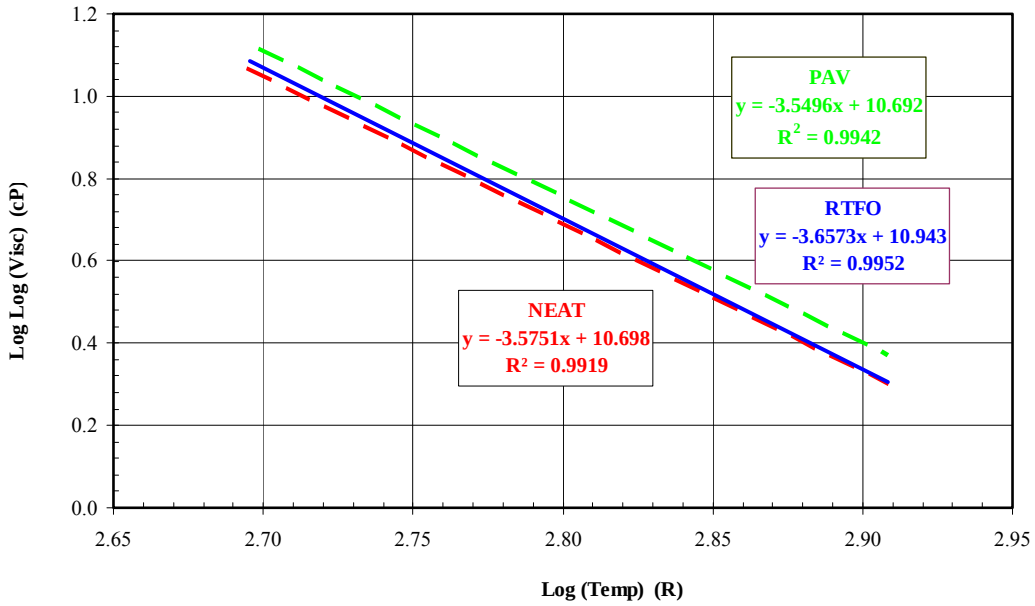

Figure 15. Viscosity – temperature relationship for PG 64-22 binder.

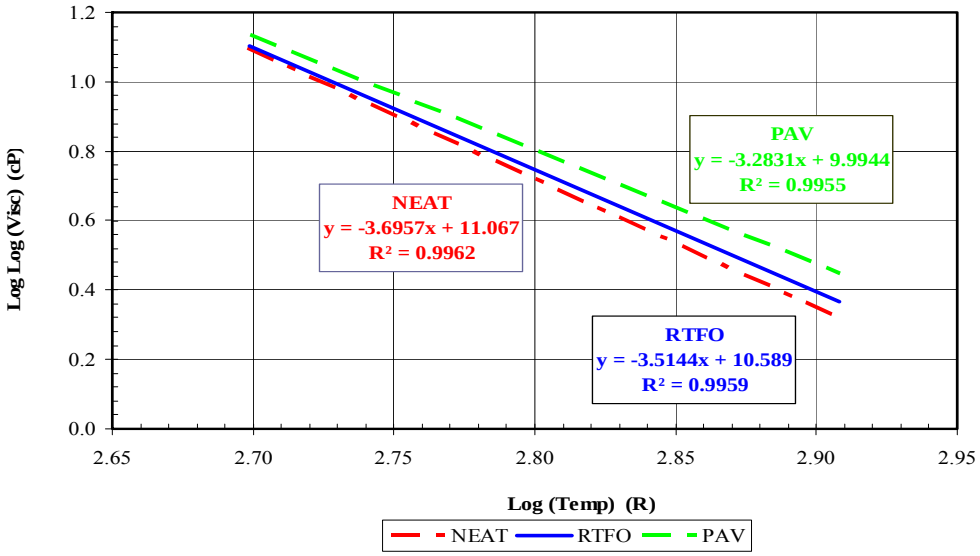

Figure 16. Viscosity – temperature relationship for PG 76-16 binder.

MIX DESIGN AND AGGREGATE BLEND RESULTS

The 19mm Superpave mix design was prepared according to the requirements of the Arizona Uniform Standard Specifications for Public Works Construction Section 710 (100). The Superpave mix design prepared herein is to provide typical paving materials used for paving arterial roads. While three different asphalt mixes were designed, each of which used a particular binder type: PG 58-28, PG 64-22, and PG 76-16, the same aggregate gradation was used for all mix designs. Table 15 shows the design aggregate gradation along with the minimum and maximum design specifications. Figure 17 illustrates the design aggregate

gradation distribution curve. Table 16 includes the composite aggregate properties. The summary of the key volumetric properties from the mix design using the three binders are presented in Table 17.

Table 15. Design Aggregate Gradation and Specification Limits.

Sieve Size	%Passing		
	Design	Minimum	Maximum
1 in.	100.0	100.0	100.0
¾ in.	95.0	90.0	100.0
½ in.	80.0	43.0	89.0
3/8 in.	59.0		
No. 4	39.0		
No. 8	29.0	24.0	36.0
No. 16	23.0		
No. 30	17.0		
No. 50	10.0		
No. 100	5.0		
No. 200	3.3	2.0	6.0

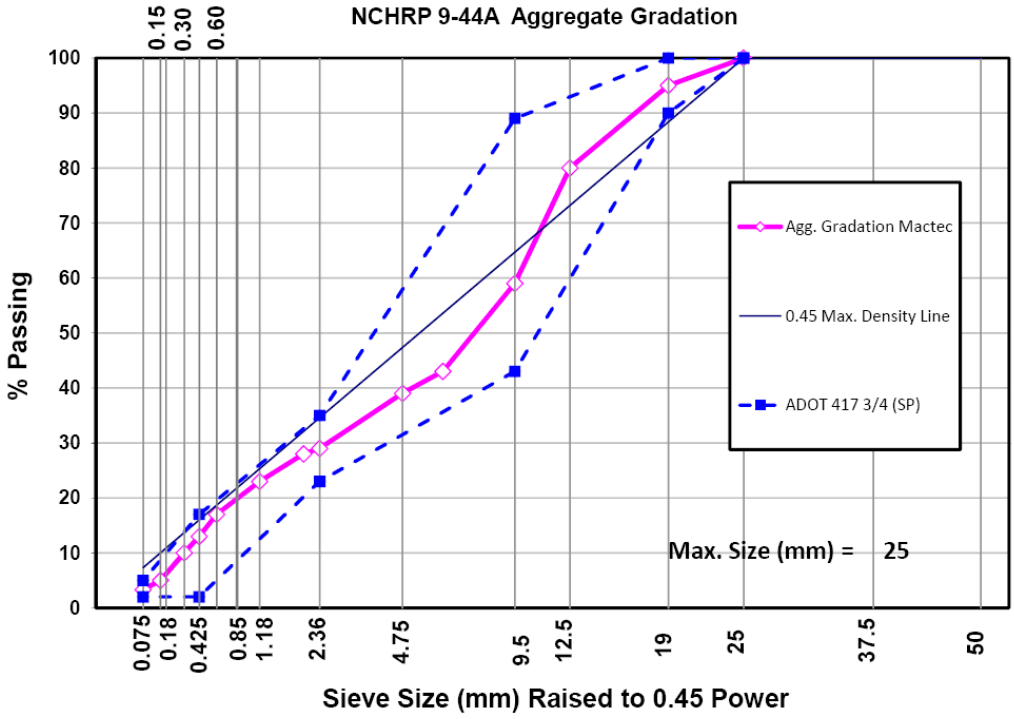

Figure 17. Designed aggregate gradation distribution curve Provided by MACTEC (27).

Table 16. Composite Aggregate Properties

Property	Value	Specifications
Bulk (Dry) Specific Gravity	2.614	(2.35-2.85)
SSD Sp. Gravity	2.638	
Apparent Specific Gravity	2.677	
Water absorption (%)	0.90	(0-2.5)
Sand Equivalent Value	71	Min 50
Fractured Face One (%)	99	Min 85
Fractured Face Two (%)	96	Min 80
Flat & Elongation (%)	1.0	Max 10
Uncompacted Voids (%)	46.8	Min 45
L.A. Abrasion @ 500 Rev.	16	Max 40

Table 17. Volumetric Mix Design for Different Binder Types Provided by MACTEC.

Volumetric Property	Binder Type			Spec.
	PG 58-28	PG 64-22	PG 76-16	
Target Asphalt Content (%)	4.8	4.5	4.7	4.5 ~ 5.5
Bulk Specific Gravity (G_{mb})	2.365	2.367	2.351	N/A
Theoretical Maximum Specific Gravity (G_{mm})	2.461	2.467	2.454	N/A
Design Air Voids (%)	3.9	4.1	4.2	3.8 ~ 4.2
VMA (%)	13.9	13.5	14.3	Min. 13
VFA (%)	71.9	69.9	70.8	N/A
Asphalt Specific Gravity (G_b)	1.024	1.024	1.042	N/A

CHAPTER 5

SPECIMEN PREPARATION AND TESTING MACHINE CALIBRATION

This chapter provides a generalized methodology to manufacture testable HMA beams using the Instron compaction machine in the Advanced Pavements Laboratory at ASU. The chapter also illustrates the beam fatigue apparatus and the calibration procedure used to insure that all beam fatigue testing machines produce accurate and comparable testing results.

MOLD ASSEMBLY AND SPECIMEN PREPARATION

Mold Assembly

The AASHTO T 321 (101) (originally published as SHRP M-009 (102)) flexural fatigue testing protocol requires a beam of asphalt concrete for testing. The AASHTO T 321 procedure requires preparation of oversize beams that are sawed to the required dimensions. The final required dimensions are 15±1/4 in. (380±6 mm) in length, 2±1/4 in. (50±6 mm) in height, and 2.5±1/4 in. (63±6 mm) in width. The procedure does not specify a specific method to prepare the beam specimen. Several methods have been used to prepare beams in the laboratory including full scale rolling wheel compaction, miniature rolling wheel compaction, and vibratory loading (103,10).

In this study beams were prepared using vibratory loading applied by a servo-hydraulic loading machine. A beam mold was manufactured from structural steel. The mold consists of a cradle and two side plates as shown in Figure 18. The inside dimensions of the mold are 1/2 inch (12 mm) larger than the required dimensions of the beam after sawing in each direction to allow for a 1/4 inch (6 mm) sawing from each face.

A top platen made of a series of steel plates welded at the two ends was used to compact the specimen (Figure 19) (8). The loading shaft is connected to the upper steel plate rather than extending it to the bottom plate so that an arch effect is introduced that would assist in distributing the load more uniformly. In addition, the bottom surface of the bottom plate is machined to be slightly concave upward in order to counter balance any bending that might occur during compaction and produce more uniform air void distribution.

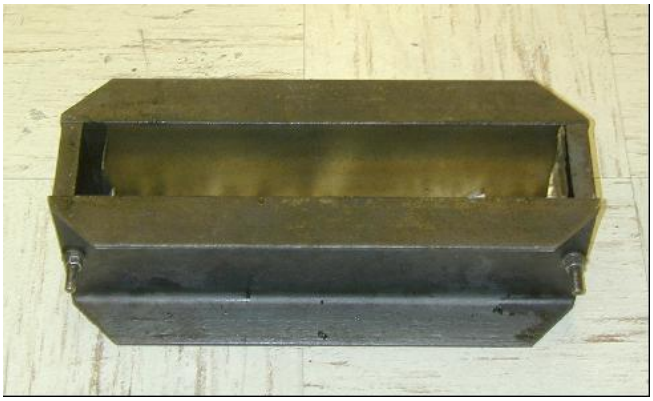

Figure 18. Major components of the mold.

Figure 19. Rigid top loading platen.

Specimen Preparation

Aggregate Batching

Aggregates were pre-sieved into different sieve sizes and were stored in labeled, covered 5-gallon plastic buckets until needed. Batches were made using empty, clean 1 -gallon metal paint cans. Paint cans were precisely filled with the calculated weights from each aggregate size per the mix design gradation in order to create individual specimens.

Binder Preparation

All binders received at the ASU Advanced Pavement Laboratory arrived in a sealed metal 5-gallon buckets with crimped lid. As a 5-gallon bucket was needed, it was first gently heated at 110^{o}C for 30 minutes to slightly liquefy the binder. The binder was then carefully poured into new, clean pint-sized metal paint cans. As the pint cans were filled, they were capped with a lid to cool for the day and the container identified with a description of the binder type, date of preparation, and appropriate ID number.

HMA Mixing

Prior to the specimen mix manufacturing process; batched aggregate cans were placed in a heated oven (295^{o}F) overnight to insure that no moisture was present in the aggregate. On the day of the specimen mixing, a pint sized can of binder was placed in a heated oven (295^{o}F) for approximately 30-45 minutes to gently bring the temperature of the binder up to the desired mixing temperature. Once the binder had reached the mixing temperature, the heated aggregates were poured into a preheated mixing bucket, and a well was created in the middle of the aggregates with a heated metal spoon. The heated bucket with aggregates was then moved on top of the swing arm balance and the balance was zeroed out. The lid was then removed from the pint can of heated binder and the heated binder was carefully poured into the well created

within the pile of aggregates. The binder was poured until the weight reached the amount necessary to achieve the precise percent binder required. The bucket was then immediately placed into the mixing machine and a heated mixing paddle was attached. The mixer was then engaged and mixing was conducted for 120 seconds.

Short-Term Aging

The properly mixed HMA was then emptied into a heated metal tray, approximately 2' x 2' and 3" deep in size, evenly spread about 1 inch thick, and placed uncovered into a preheated 135^{o}C convection oven for short-term aging per the AASHTO R 30 (104) procedure for mixture performance testing. The HMA was left uncovered in the oven for a 1 hour period, and then the door opened and the HMA hand mixed and turned over multiple times within the tray with a heated spoon for 15-20 seconds. The door was then shut and the HMA was left to age another hour. After the second hour, the hot, aged mix was mixed with the heated spoon again and mix sufficient to compact a specimen to a pre-determined AV% was immediately scooped into the beam mold, with the HMA placed in the mold in two equal weighing lifts. Once the mold was filled, it was returned to an oven for about 15 minutes to achieve the proper temperature for compaction.

Obtaining Maximum Theoretical Specific Gravity (G_{mm})

To begin the manufacturing of testable specimens meeting the required volumetric properties for a given HMA mixture, the first step was to make a HMA specimen that was heated and mixed within the laboratory, as per the standard mixing protocol, but poured loose on a table to cool overnight. The next day, the cooled HMA was crumbled and separated by hand and the theoretical maximum specific gravity (G_{mm}) was determined by the AASHTO T 209 (105) pycnometer method. This G_{mm} of the specific HMA was used to calculate the percent air voids (AV%) of all specimens prepared from the same mix. It was critically important that the G_{mm} measured on replicate samples meet the repeatability and reproducibility limits in the precision statement for AASHTO T 209.

Compacting HMA Beams

The heated, filled beam mold was placed on the bottom plate of the loading machine and the top plate was lowered just until contact was made with the top of the mixture layer. A pressure of 0.2 psi (1.4 kPa) was applied to seat the specimen. Then a stress-controlled sinusoidal load was applied with a frequency of 2 Hz and a peak-to-peak stress of 400 psi (2.8 MPa) for the compaction process.

All beam specimens were made with 4600 grams of HMA, out of the 5000 gram aggregate batch that was mixed with the binder to achieve the design binder content. The time of compaction of this standardized weight was used, and varied, in order to determine and achieve different compaction density and AV% of testable specimens after being cut and dried.

After compaction, specimens were left to cool to ambient temperature. The specimens were brought to the required dimensions for fatigue testing by sawing 1/4 inch (6 mm) from each side as shown in Figure 20. The specimens were cut using water cooled saw to the standard

dimension of 2.5 in. (63.5 mm) wide, 2.0 in. (50.8 mm) high, and 15 in. (381 mm) long. Finally, AV% was measured by using the saturated surface-dry procedure in AASHTO T 166 (106).

Figure 20. Specimen sawing.

Specimens were dried before testing. Exact specimen dimensions were obtained by obtaining three height and three width measurements and recording them in the laboratory data sheets. Each specimen was clearly identified with its ID number (both on specimen and on data sheets) and wrapped in a plastic sheet to eliminate any skin aging during storage until testing.

Determining Desired Air Voids

To determine how to produce beam specimens at a target value of 7% air voids, (or at any other air void range desired for the study), three beam specimens were compacted using 0.5 minutes, 3 minutes and 5.5 minutes of compaction time. (Note that the specific time used in the laboratory is determined by the type of compaction device used.) The three specimens were then cut and dried and the air voids of each specimen were obtained using AASHTO T 166 (106). The necessary compaction time was determined using a plot of the compaction time versus the AV% for each specimen as shown in Figure 21. Once the compaction time was established and confirmed to yield a 7% air voids beam (or the desired target AV%), multiple specimens were compacted using the appropriate compaction time determined for each mix.

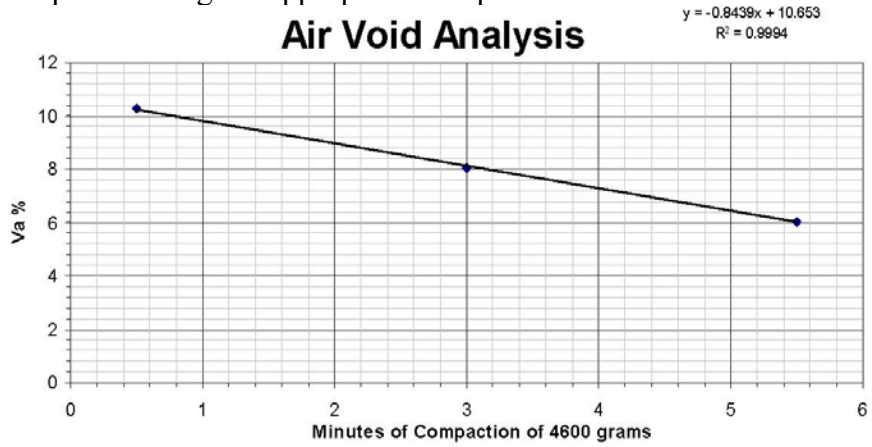

Figure 21. Comparison of compaction time of 4600 gram beam specimens vs. air void

(Va%) of trimmed specimens.

FLEXURAL BEAM FATIGUE APPARATUS

Flexural fatigue tests were performed according to the AASHTO T 321 (101). Figure 22 shows the flexural fatigue apparatus. The device was typically placed inside an environmental chamber to control the temperature during the test.

The cradle mechanism allows for free translation and rotation of the clamps and provides loading at the third points as shown in Figure 23. Pneumatic actuators at the ends of the beam center it laterally and clamp it. Servomotor driven clamps secure the beam at four points with a pre-determined clamping force. Haversine or sinusoidal loading may be applied to the beam via the built-in digital servo-controlled pneumatic actuator. The innovative floating on-specimen transducer measures and controls the true beam deflection irrespective of loading frame compliance.

Figure 22. Flexural fatigue apparatus.

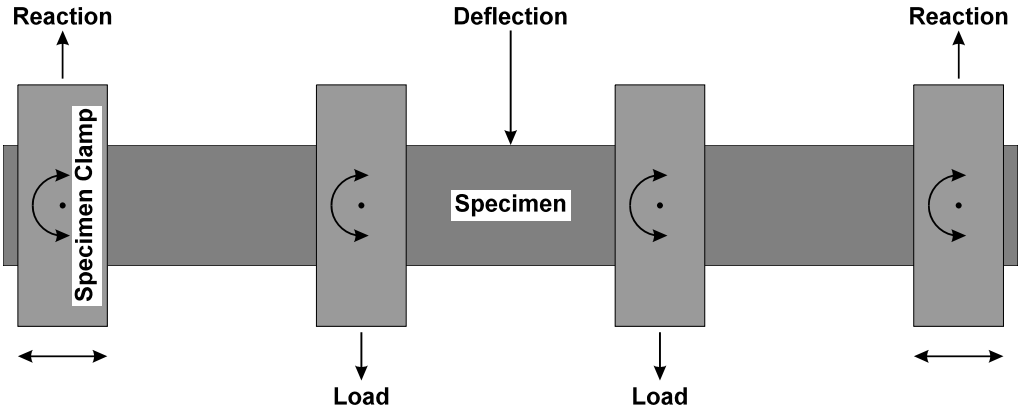

Figure 23. Loading characteristics of the flexural fatigue apparatus.

TEST PROCEDURE AND CALCULATIONS

In the fatigue test, repeated third-point loading cycles were applied as demonstrated in Figure 22 and Figure 23. A controlled-strain sinusoidal loading was applied at a frequency of 10 Hz. The maximum tensile stress and maximum tensile strain are calculated as:

$$\sigma_t = 3\ a\ P / b\ h^2 \quad (19)$$

$$\varepsilon_t = 12\ \delta\ h / (3\ L^2 - 4\ a^2) \quad (20)$$

where,

σ_t = Maximum tensile stress, Pa
ε_t = Maximum tensile strain, m/m
P = Applied load, N
b = Average specimen width, m
h = Average specimen height, m
δ = Maximum deflection at the center of the beam, m
a = Space between inside clamps, 0.357/3 m (0.119 m)
L = Length of beam between outside clamps, 0.357 m

The flexural stiffness was calculated as follow:

$$S = \sigma_t / \varepsilon_t \quad (21)$$

where,

S = Flexural stiffness, Pa

The phase angle (ϕ) in degrees was determined as follow:

$$\phi = 360\ f\ s \quad (22)$$

where,

f = Load frequency, Hz
s = Time lag between P_{max} and δ_{max}, seconds

BEAM FATIGUE APPARATUS CALIBRATION

A standard procedure was established to calibrate the testing machines to ensure accurate test results. The following is a brief calibration procedure that was implemented during the project. Calibration was performed every two months or when a problem arose indicating that the device was out of calibration.

LVDT Calibration Procedure

1. Mount the LVDT into the LVDT calibrator assembly as shown in Figure 24.
2. Adjust the calibrator to the midpoint position.
3. Open the levels screen on IPC computer display.
4. Move the LVDT so that the computer readout is close to zero volts.
5. Fine tune the zero volts reading by adjusting the calibrator. Note the initial reading on the calibrator.
6. Move the calibrator in even increments and record the computer readout onto the attached calibration sheet.
7. Determine if the calibration check was within tolerance. If not, adjust the calibration gain to bring the calibration within the acceptable tolerance.
8. A sequential listing of all activities completed to achieve compliance to calibration tolerance is recorded.

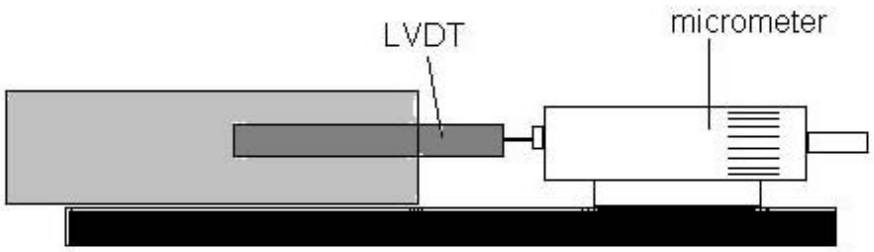

Figure 24. LVDT Calibration set up.

Load Cell Calibration Procedure

1. Open the levels screen on IPC computer display.
2. Mount the proving ring onto the top of the Beam Fatigue Apparatus assembly as shown in Figure 25. Zero the dial gauge reading on the proving ring.
3. Apply an offset so that the engineering outputs value is zeroed.
4. Using the large range laboratory scale, record the weight of the dead weights to be used in the calibration verification check.
5. Carefully apply the dead load weights to the machine and proving ring assembly. Record the readouts on the calibration sheet.
6. Determine if the calibration check was within tolerance. If not, adjust the calibration gain to bring the calibration within the acceptable tolerance
7. A sequential listing of all activities completed to achieve compliance to calibration tolerance is recorded.

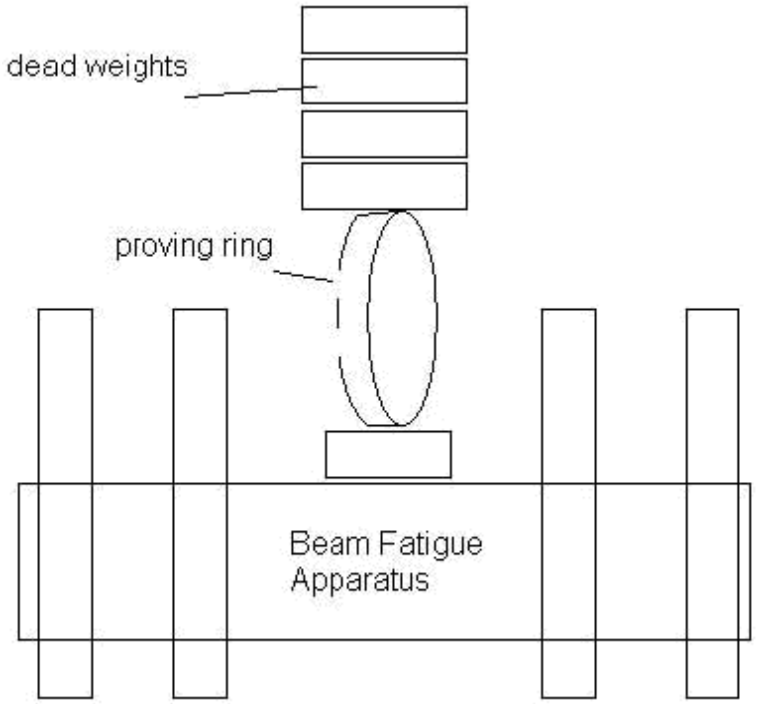

Figure 25. Calibration set up.

Temperature Calibration Procedure

1. Adjust the set point temperature on the control unit to a temperature of 4, 20, or 37°C, as needed.
2. Allow enough time for the chamber to come to equilibrium at each temperature.
3. Record the readings for the temperature controller, the computer display (if available), and the temperature calibration meter.
4. Prepare a corrected temperature chart in order to establish the controller set point reading that needs to be selected in order to achieve the three temperature settings required.
5. If the temperature reading is outside of acceptable tolerance, contact either the Laboratory Manager or Laboratory Coordinator in order to coordinate servicing of the temperature chamber(s) by the Facilities Management department.
6. A sequential listing of all activities completed to achieve compliance to calibration tolerances is recorded.

CHAPTER 6

PRELIMINARY QUALITY CONTROL/QUALITY ASSURANCE STUDIES

Two IPC beam fatigue devices (IPC-1 and IPC-2) were used in this study. It was important to insure that both devices measure statistically identical responses during the experimental testing program. In order to accomplish this goal, preliminary statistical ANOVA experiments were designed and implemented to verify this hypothesis. It was further necessary to insure that the machines apply the correct wave form in the bending beam test.

EVALUATION OF EQUALITY AMONG MACHINES USING SYNTHETIC BEAMS WITH NO REST PERIOD

Before starting the main experiment, it was prudent to compare both machines to verify the assumption that both machines operate in the same way and produce statistically comparable results. The first evaluation experiment was accomplished with three types of synthetic beams with flexural stiffness ranging from 90 ksi to 350 ksi. An experiment was conducted to statistically test this assumption. The primary variable used to measure the equality of the beam measurements was the flexural stiffness at 10,000 repetitions with a zero dwell (rest) time between pulses.

Experimental Conditions

The following experimental conditions were used.

1. Two IPC machines.
2. Three synthetic beams with three levels of stiffness: low, medium, and high.
3. Beams were tested using haversine loads at 10 Hz frequency for 10,000 cycles. The use of a haversine load implies a rest time of 0 seconds.
4. Two strain levels: low (400 microstrain) and high (800 microstrain)
5. One test temperature: 20°C.
6. A full factorial design was used with a total of 24 tests (2 machines x 3 beams x 2 strain levels x 2 replicates).

Experimental Results

Table 18 shows the flexural stiffness of the three beams under different test conditions.

Table 1816. Stiffness of Synthetic Beams (in psi).

Machine Type	Beam Stiffness					
	Low		Medium		High	
	Low Strain Level	High Strain Level	Low Strain Level	High Strain Level	Low Strain Level	High Strain Level
IPC 1	99946	96794	166500	163808	356391	350240
	93030	93330	168694	165120	361653	358960
Average	96488.0	95062.0	167597.0	164464.0	359022.0	354600.0
Standard Deviation	4890.4	2449.4	1551.4	927.7	3720.8	6166.0
Coefficient of variation, %	5.1	2.6	0.9	0.6	1.0	1.7
IPC 2	99957	93709	173738	166747	368045	368929
	102855	95107	174970	169706	381828	377047
Average	101406.0	94408.0	174354.0	168226.5	374936.5	372988.0
Standard Deviation	2049.2	988.5	871.2	2092.3	9746.1	5740.3
Coefficient of variation, %	2.0	1.0	0.5	1.2	2.6	1.5

Testing the Adequacy of the Statistical Model

The model adequacy was determined by residual analysis (107). Several assumptions were examined:

1. A normal probability plot of the residuals was constructed to determine whether the data depart from the normal assumption or not. If the normal probability plot lies along a straight line, it indicates that the data follow the normal distribution.
2. A second trend was evaluated by plotting the residuals versus the run number. This was constructed to detect any correlations between the residuals. There was no pattern or tendency for positive or negative runs of residuals. Thus, the independence assumption on the error is satisfied.
3. Finally, a report of residuals versus the predicted stiffness was constructed to detemine the homogeneity of variances. There was no pattern of residuals. Thus, the assumption of nonconstant variance was satisfied.

Comparison of IPC1 and IPC2 Machines

The adequacy of the model was checked and the analysis of variance on the IPC1 and IPC2 data are summarized as shown in Table 19. The equality of the IPC1 and IPC2 machines hypotheses were:

H_0: $\tau_{IPC1} = \tau_{IPC2} = 0$

H_1: at least one $\tau_i \neq 0$

The p-value of the machine type (Factor A) was 0.0014, which is less than 0.05 (significant level of alpha). Therefore, the null hypothesis was rejected and it was concluded that there was significant difference between IPC1 and IPC2 machines.

Table 19. Analysis of Variance for the Logarithm Transformed IPC1 and IPC2 Data.

Source	Sum of Squares	DF	Mean Square	F Value	Prob > F
Model	1.34	4	0.34	3769.02	< 0.0001 significant
Machine Type	1.25E-03	1	1.25E-03	14.01	0.0014
Beam Type	1.34	2	0.67	7526.64	< 0.0001
Strain Level	7.85E-04	1	7.85E-04	8.8	0.0079
Residual	1.70E-03	19	8.92E-05		
Lack of Fit	6.81E-04	7	9.73E-05	1.15	0.395 not significant
Pure Error	1.01E-03	12	8.45E-05		
Correlation Total	1.35	23			
Std. Dev.	9.45E-03		R-Squared	0.9987	
Mean	5.26		Adj R-Squared	0.9985	
C.V.	0.18		Pred R-Squared	0.998	

Because of the significant difference results obtained in the first experiment, it was necessary to re-calibrate the machines and carefully tune them.

Experimental Results after Recalibration and Tuning

The two IPC machines were re-calibrated and the clamps were tightened. Upon tuning each machine, the entire experiment was repeated. Additionally, the PID settings were set to a similar level for the two machines. In this second experiment 24 tests were performed (2 machines x 3 beams x 2 strain levels x 2 replicates). Table 20 summarizes the results of the second experiment.

Table 20. Stiffness Results (in psi) of the Repeated Experiment After Recalibration.

Machine Type	Beam Stiffness					
	Low		Medium		High	
	Low Strain Level	High Strain Level	Low Strain Level	High Strain Level	Low Strain Level	High Strain Level
IPC 1	99946	96794	166500	163808	356391	350240
	93030	93330	168694	165120	361653	358960
Average	96488.0	95062.0	167597.0	164464.0	359022.0	354600.0
Standard Deviation	4890.4	2449.4	1551.4	927.7	3720.8	6166.0
Coefficient of variation, %	5.1	2.6	0.9	0.6	1.0	1.7
IPC 2	99391	98190	168211	164207	357373	354662
	101535	95032	173583	163663	360103	361799
Average	100463.0	96611.0	170897.0	163935.0	358738.0	358230.5
Standard Deviation	1516.0	2233.0	3798.6	384.7	1930.4	5046.6
Coefficient of variation, %	1.5	2.3	2.2	0.2	0.5	1.4

The analysis of variance on the IPC1 and IPC2 data are summarized in Table 21. Similar to the previous analyses, the hypotheses were:

H_0: $\tau_{IPC1} = \tau_{IPC2} = 0$

H_1: at least one $\tau_i \neq 0$

The null hypothesis failed to be rejected and it was concluded that there was no significant difference between IPC1 and IPC2 machines.

Table 21. Analysis of Variance for The IPC1 and IPC2 Data.

Source	Sum of Squares	DF	Mean Square	F Value	Prob > F
Model	2.91E+11	4	7.28E+10	8408.07	< 0.0001 significant
Machine Type	2.26E+07	1	2.26E+07	2.61	0.1227
Beam Type	2.91E+11	2	1.46E+11	16810.9	< 0.0001
Strain Level	6.87E+07	1	6.87E+07	7.94	0.011
Residual	1.65E+08	19	8.66E+06		
Lack of Fit	2.84E+07	7	4.05E+06	0.36	0.9102 not significant
Pure Error	1.36E+08	12	1.13E+07		
Cor Total	2.91E+11	23			
Std. Dev.	2942.26		R-Squared	0.9994	
Mean	2.07E+05		Adj R-Squared	0.9993	

Findings from the Experimental Results

A statistical experiment was performed using synthetic beams to verify an assumption that all machines operate in the same way and produce "Statistically Identical" results. The first trial experiment showed differences in test results among the two machines. The machines were then re-calibrated and tuned and the experiment was repeated. The second experiment showed that there were no significant differences among the results of the two machines. This means that both machines can be used in the study interchangeably.

EVALUATION OF EQUALITY AMONG MACHINES USING HMA BEAMS

Another comparative study was performed to verify the assumption that both machines operate in the same way and produce statistically comparable results. This experiment was accomplished using HMA beams similar to the testable HMA samples that are used in the main experiment. The primary variable used to measure the equality of the beam measurements was the initial flexural stiffness with a zero dwell (rest) time between pulses.

Experimental Conditions

The following experimental conditions were used.

1. Two IPC machines.
2. Beams were tested using haversine loads at 10 Hz frequency for 15,000 cycles. The use of a haversine load implies a rest time of 0 seconds.
3. Two strain levels: low (500 microstrain) and high (700 microstrain)
4. Three test temperatures of 40, 70 and 100^{o}F.

5. A full factorial design was used with a total of 24 HMA specimens (2 machines x 3 temperatures x 2 strain levels x 2 replicates).

Experiment Results

Table 22 shows the flexural stiffness of the three beams under different test conditions.

Table 22. Stiffness of HMA Beams (in psi).

Machine Type	Test Temperature					
	40 F		70 F		100 F	
	Low Strain Level	High Strain Level	Low Strain Level	High Strain Level	Low Strain Level	High Strain Level
IPC 1	1713850	1685934	603145	647078	154210	188782
	1496119	1319385	637156	776303	158065	156016
Average	1604984	1502660	620151	711691	156138	172399
Standard Deviation	153959	259189	24049	91376	2726.03	23168.8
Coefficient of variation, %	9.59	17.25	3.88	12.84	1.75	13.44
IPC 2	1529680	1561575	599774	718700	152757	173428
	1672471	1375957	800803	573901	158557	155748
Average	1601076	1468766	700289	646301	155657	164588
Standard Deviation	100969	131252	142149	102388	4100.69	12501.5
Coefficient of variation, %	6.31	8.94	20.30	15.84	2.63	7.60

Comparison of IPC1 and IPC2 Machines

The adequacy of the model was checked and the analysis of variance on the IPC1 and IPC2 data are summarized as shown in Table 23. The hypotheses were:

H_0: $\tau_{IPC1} = \tau_{IPC2} = 0$

H_1: at least one $\tau_i \neq 0$

The null hypothesis failed to be rejected and it was concluded that there was no significant difference between IPC1 and IPC2 machines.

Table 23. Analysis of Variance betwwen IPC1 and IPC2 using HMA specimens.

Source	Sum of Squares	DF	Mean Square	F Value	Prob > F
Temperature	8.22556E+12	2	4.11278E+12	443.08	< 0.0001 significant
Strain Level	261102663	1	261102663	0.03	0.869 not significant
Machine	1698938055	1	1698938055	0.18	0.674 not significant
Error	1.76364E+11	19	9282340905		
Correlation Total	1.76364E+11	23			
R-Squared	0.9790				
Adj R-Squared	0.9746				

REFINEMENT OF BEAM FATIGUE TEST PARAMETERS

Several pilot studies were conducted by running HMA fatigue beam tests to evaluate the different parameters to be used in the main study such as wave form type (haversine vs. sinusoidal) and control mode type (strain control vs. stress control). Another purpose of these pilot studies was to resolve any testing problems that might be encountered before starting the main experiment. All tests were performed on a Salt River Base mix with a PG 64-22 binder, which is the same mix used in the main study as shown in Chapter 4.

The literature indicates that most previous researchers conducted the beam fatigue test without rest period under either a controlled strain or a controlled stress mode. Also, most researchers, especially in the United States, applied haversine strain or stresse wave forms. In this pilot study, both haversine and sinusoidal strain and stress-controlled tests were conducted with and without rest period. The results led to solutions to several potentially significant problems and questions.

The beam fatigue test can be performed under these four modes:

1. Haversine controlled strain (108)
2. Haversine controlled stress
3. Sinusoidal controlled strain (101)
4. Sinusoidal controlled stress

Figure 26 shows the haversine and sinusoidal wave forms. The haversine form changes from 0 to 2ε (or 2σ), whereas the sinusoidal form changes between $\pm\varepsilon$ ($\pm\sigma$). This implies that the haversine wave form bends the beam in one direction, while the sinusoidal form bends the beam in both directions. Of course, each test mode can be performed without or with rest period.

Most of the tests described in the literature have been performed without rest period. In the last several years, researchers started running tests with rest period to evaluate the healing effect. Note that the haversine stress-controlled test is not typically conducted since the specimen fails very quickly because of the rapid accumulation of permanent deformation.

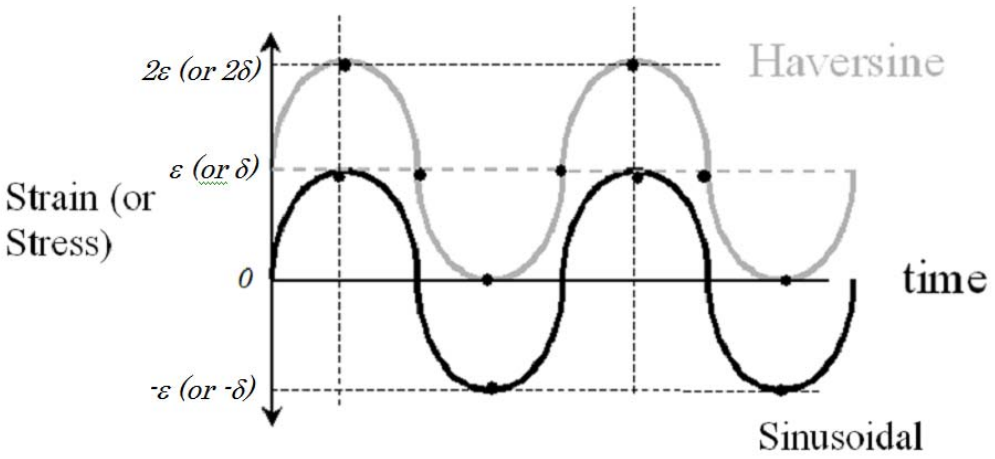

Figure 26. Haversine and sinusoidal wave forms (109).

Haversine Pulse Tests

In this part of the study, haversine strain-controlled flexure fatigue tests were performed according to ASTM D7460. In this test haversine strain-controlled cycles were applied with 0.1 second strain periods for 25,000 repetitions. The following conditions were used.

1. Three test temperatures: 40°F, 70°F, and 100°F
2. Two strain levels: 400 and 800 microstrain (μs)
3. Two rest periods: 0 and 10 seconds

This pilot study revealed some issues that needed careful study before continuing on with the work plan. The results of this pilot study are discussed below.

Figure 27**Figure 27** shows that the test with rest period in some cases resulted in faster damage and lower fatigue life than the test without rest period. This, of course, was completely opposite to the major hypothesis of the endurance limit study, which is based upon the premise that it is the rest period that "heals" the damage in the asphalt and extends the fatigue life of the material. In other cases, beams subjected to rest period failed in the middle of the test as shown in Figure 28 and Figure 29. The fatigue machines were re-calibrated and many tests were repeated several times, but the problems were not solved completely.

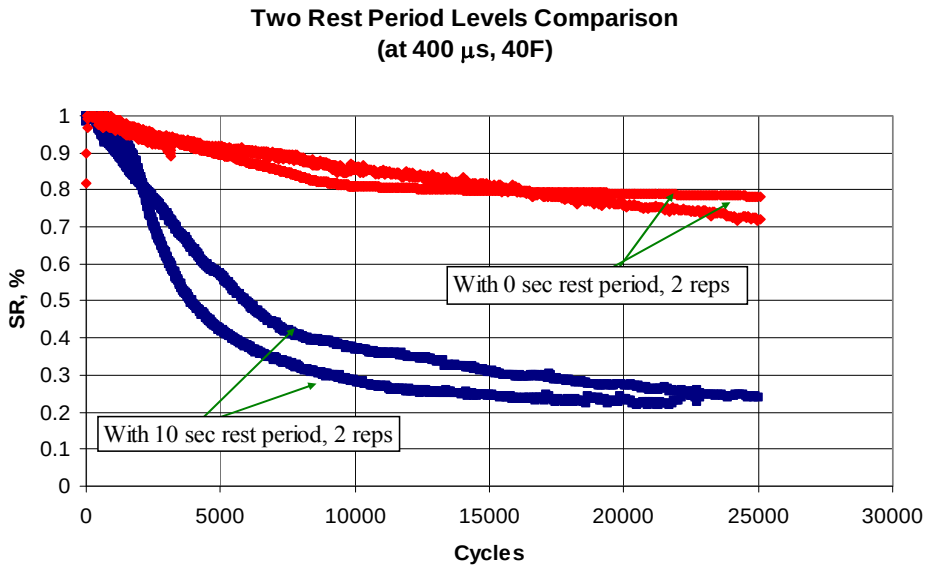

Figure 27. Stiffness ratio versus loading cycles with and without rest periods (haversine strain controlled test, 400 microstrain, 40°F).

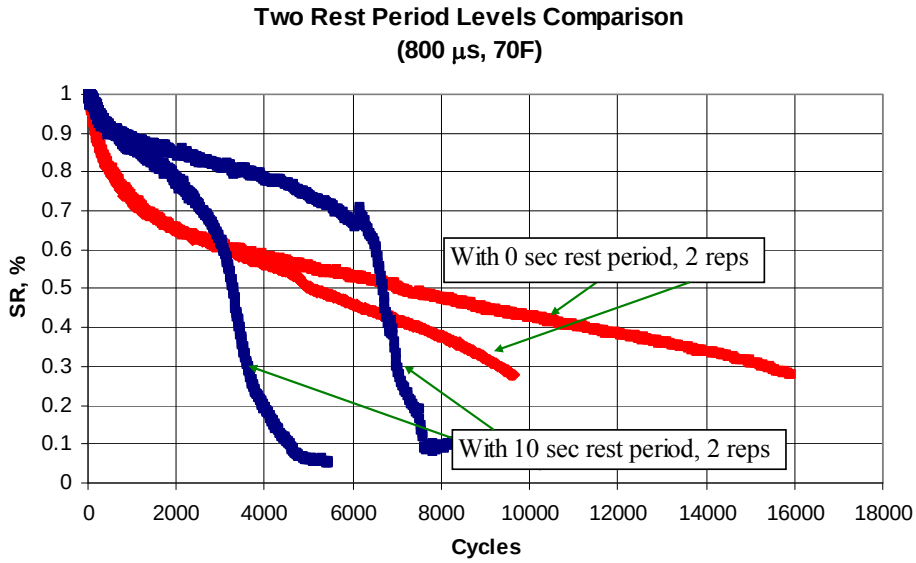

Figure 28. Stiffness ratio versus loading cycles with and without rest periods (haversine strain controlled test, 800 microstrain, 70°F).

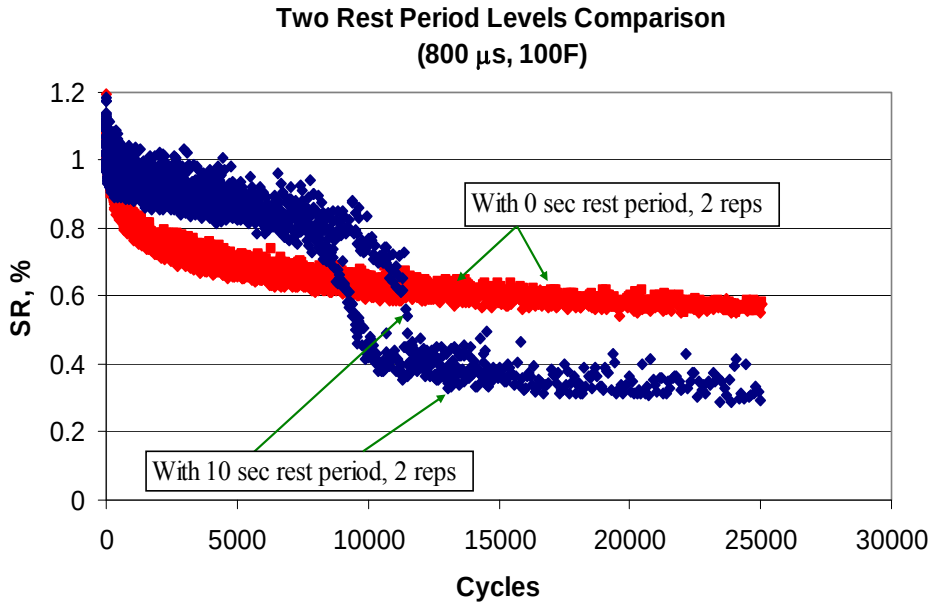

Figure 29. Stiffness ratio versus loading cycles with and without rest periods (haversine strain controlled test, 800 microstrain, 100°F).

The shape of the deflection and force pulses were examined in more detail in order to find out the reasons for these results. In the strain controlled haversine tests without rest period, it was observed that the resulting load pulses started as haversine. After only a few cycles, the load pulses transformed to sinusoidal loads, which transferred approximately half the load in one direction and the other half in the other direction as shown in Figure 30. This means that although we were trying to bend the beam in one direction, the beam actually bent in both directions.

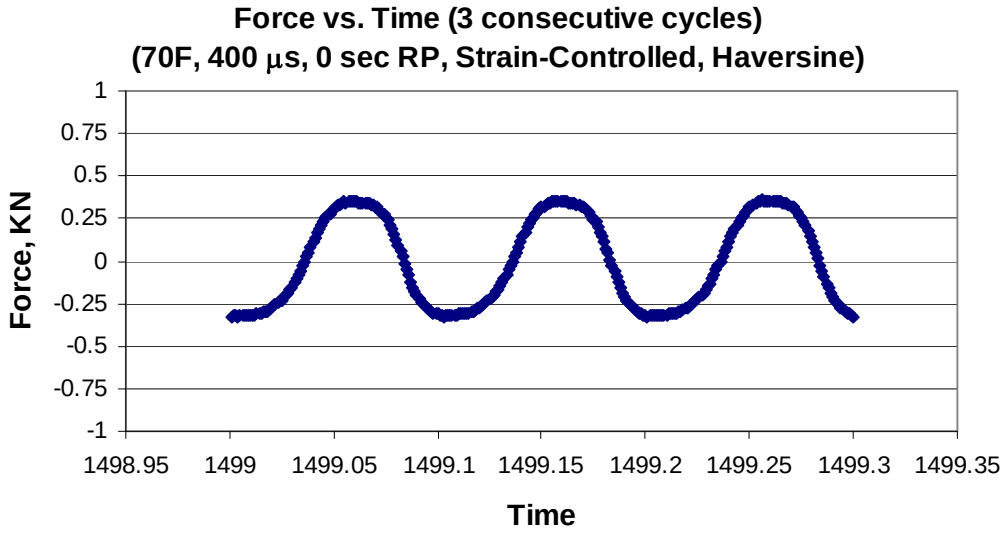

Figure 30. Force vs. time for a strain controlled test with haversine pulse without rest period.

This phenomenon was explained by Pronk et al. (109, 111). Due to the viscous character of the material, creep (permanent deformation) occurs in the beam. At the end of the first cycle the beam will go back to the original shape, but the neutral axis will be shifted as shown in Figure 31. This position resembles the new (shifted) neutral axis of the beam, which will shift the strain in future cycles. This suggests that although a haversine *displacement* signal occurs, the *strains and stresses* in the beam will be pure sinusoidal (compression and tension). The amplitude of the sinusoidal strain signal will be equal (or even less) than half the original value of the haversine at the start of the test. In the new neutral position half of the beam material will be under compression, while the other half is subjected to tension.

Although the tension and compression are reversed every cycle, the compression might have a beneficial effect on the fatigue life. This means that there are two factors working against each other as far as fatigue and healing are concerned.

1. The reversed bending accelerates the fatigue failure because of the reversed stress in each cycle.
2. The compression during half of the cycle accelerates healing.

Depending on which factor has larger effect, the beam could experience either short or long fatigue life.

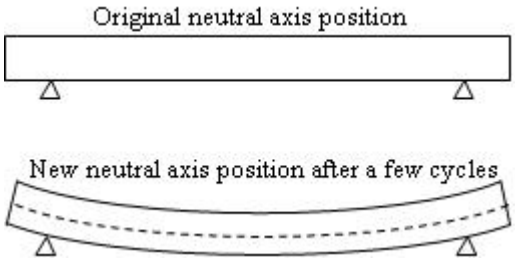

Figure 31. Viscous response will cause a shift of the neutral axis.

This phenomenon, however, does not occur in the case with rest period. In the strain-controlled haversine tests with rest period, the load pulses are remain close to haversine until the end of the test as shown in Figure 32. This happens because of the relaxation that occurs during the rest period even when the beam is subjected to creep. This implies that the bottom of the beam is mostly under tension, which may accelerate the fatigue failure. Again, two factors are working against each other in this case.

1. The continuous tension at the bottom of the beam accelerates the fatigue failure.
2. The rest period accelerates healing.

Depending on which factor has larger effect, the beam could experience either short or long fatigue life.

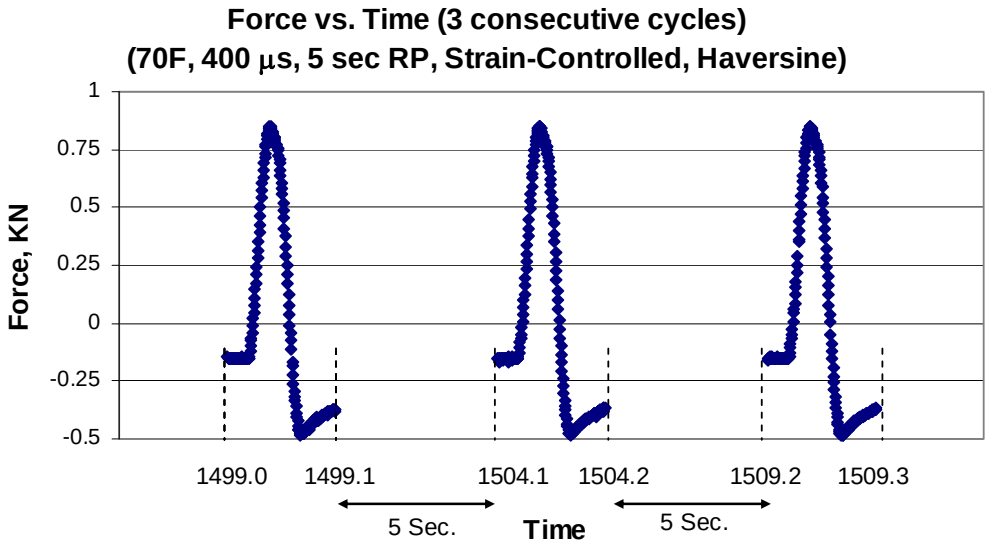

Figure 32. Force vs. time for a strain controlled test with haversine pulse with rest period.

In conclusion, the haversine test does not produce consistent results whether the test is run with or without rest period. The comparison in this case might produce erroneous results depending on the mix type, test temperature, strain level, and the duration of the rest period. In addition, the shift from haversine to sinusoidal in the stress and strain signals might induce additional variability, which makes it difficult to compare the results of tests under different conditions (26).

Sinusoidal Pulse Tests

Because of the inconsistency of the haversine test results, a number of sinusoidal strain- and stress-controlled tests were performed without and with rest period. Figure 33 and Figure 34 show the stiffness ratio versus number of loading cycles with and without rest periods using sinusoidal strain and stress-controlled tests, respectively. The two figures show that the test with a 5-second rest period resulted in a longer fatigue life than the test without rest period as expected.

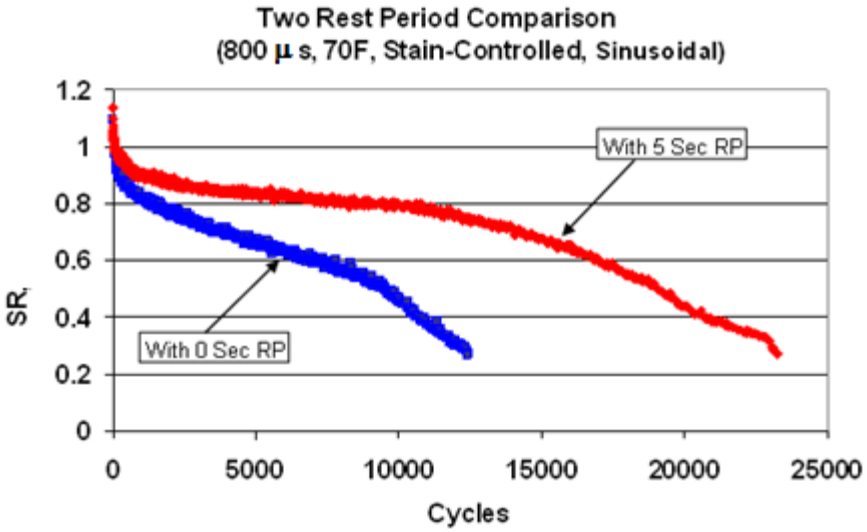

Figure 33. Stiffness ratio versus loading cycles with and without rest periods (sinusoidal strain-controlled, 70°F).

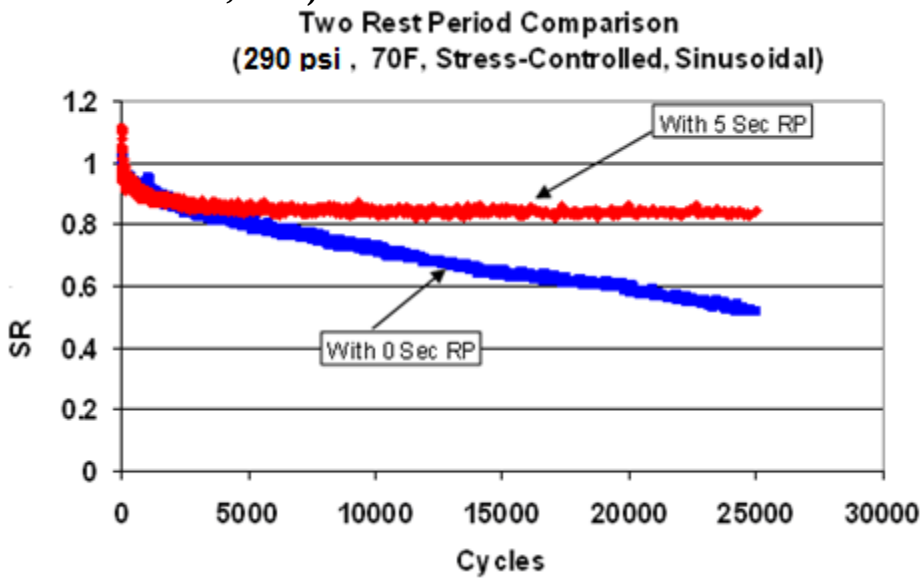

Figure 34. Stiffness ratio versus loading cycles with and without rest periods (sinusoidal stress-controlled, 290 psi, 70°F).

The force and displacement cycles were examined for the sinusoidal pulse tests at different conditions. Figure 35 and Figure 36 show the force and displacement versus time for the strain-controlled tests with sinusoidal pulses without and with rest period, respectively. Unlike the haversine tests, the figures show consistent sinusoidal force and displacement cycles throughout the test. Note that for this strain-controlled test (Figure 36), there is a small amount of force at the beginning of the rest period, but it dissipates at the end of the rest period.

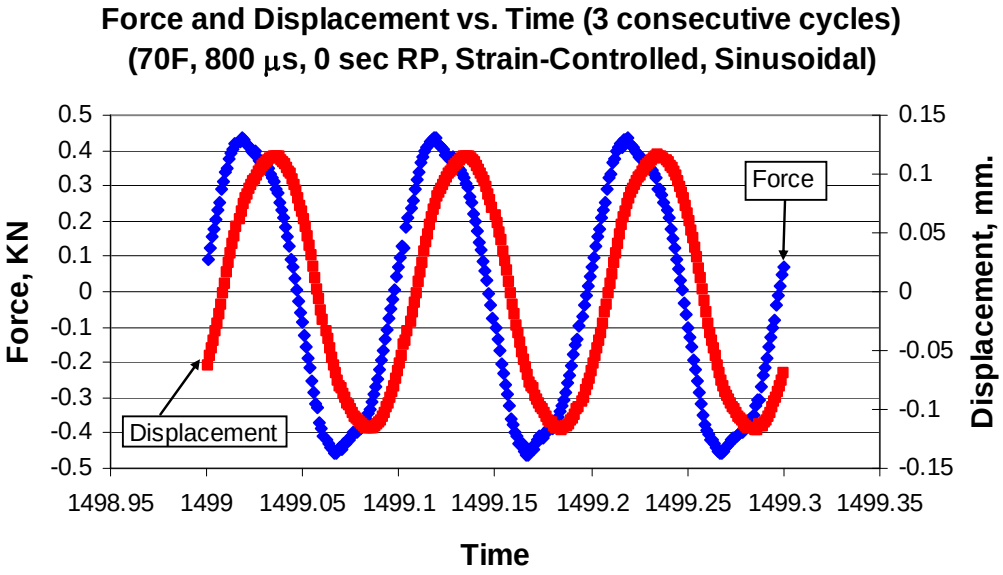

Figure 35. Force vs. time for a strain controlled test with sinusoidal pulse without rest period.

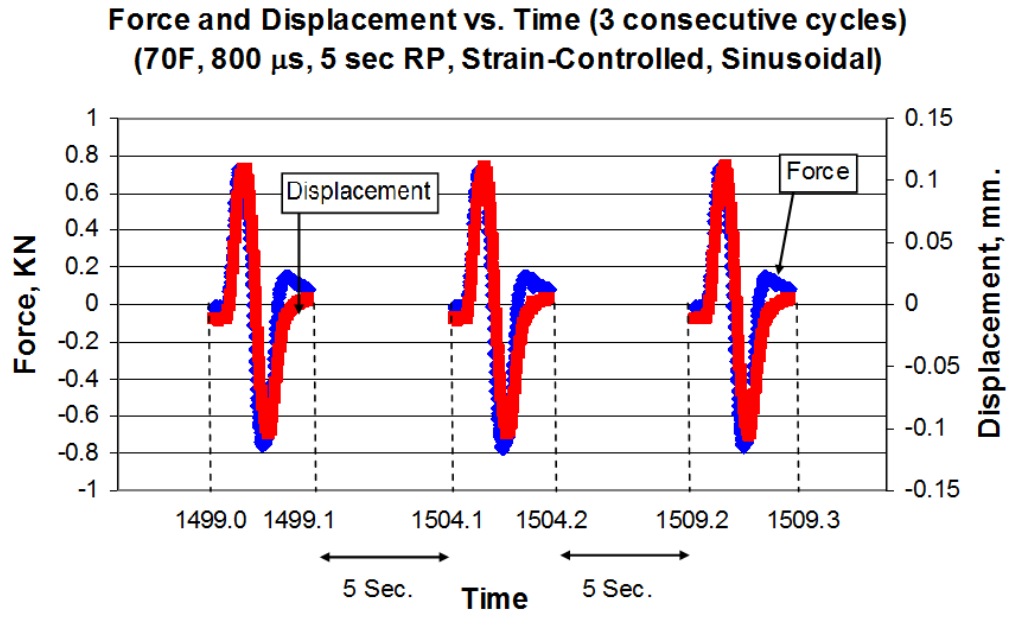

Figure 36. Force vs. time for a strain controlled test with sinusoidal pulse with rest period.

Figure 37 and Figure 38 show the force and displacement versus time for the stress-controlled tests with sinusoidal pulse without and with rest period, respectively. Again, the figures show consistent sinusoidal force and displacement cycles throughout the test.

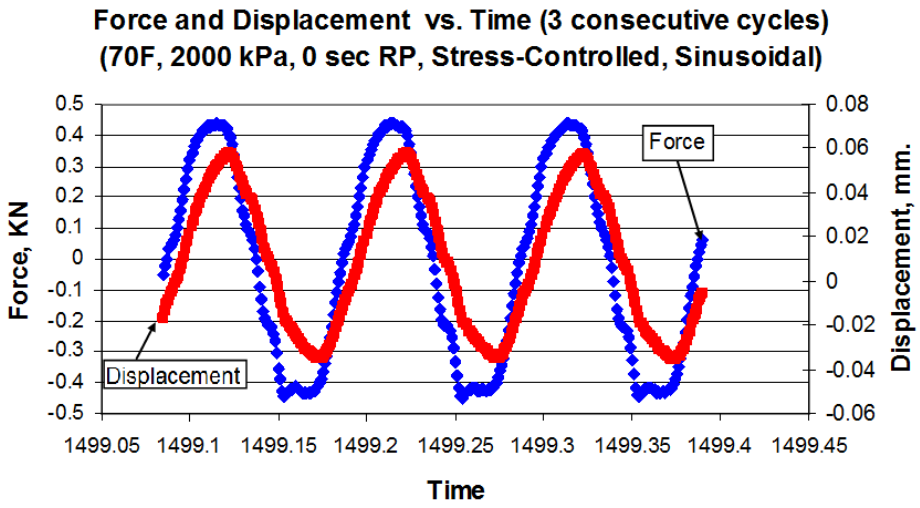

Figure 37. Force vs. time for a stress-controlled test with sinusoidal pulse without rest period.

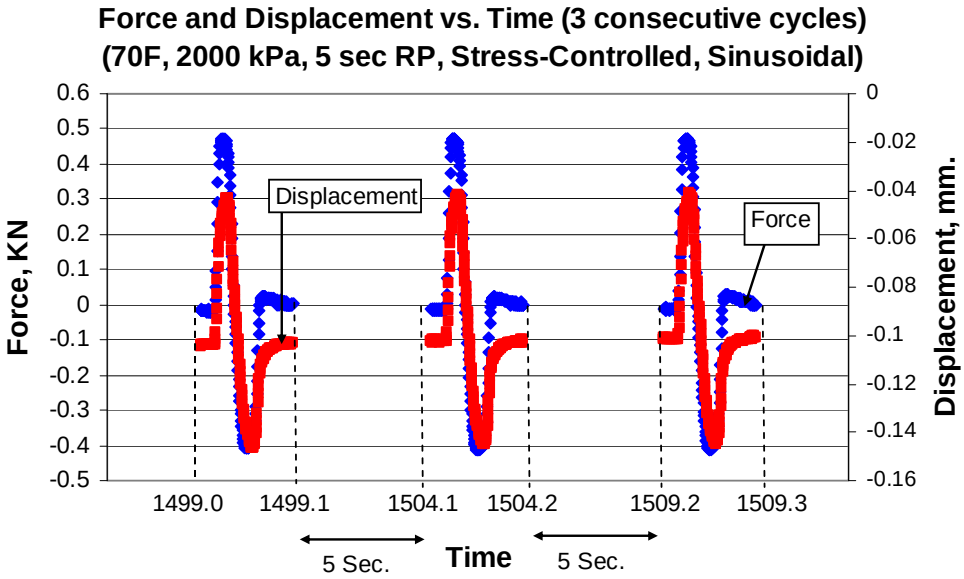

Figure 38. Force vs. time for a stress-controlled test with sinusoidal pulse with rest period.

Based on these results, sinusoidal pulse tests were selected instead of the haversine tests in the main experiment. Also, since there is not much difference between strain and stress controls, strain control was chosen to avoid the rapid accumulation of permanent deformation. Thus, it was decided to follow AASHTO T 321 to complete the project.

Simulation of Field Condition

At the bottom of the asphalt layer in the field strain signals look more like a haversine than sinusoidal when a wheel load is passing. Therefore, using haversine signals in lab tests would be more realistic. Based on the previous discussion, however, it is hard to simulate the field condition in the lab since the beam fatigue test with constant haversine deflections will

immediately change into tests with constant sinusoidal deflections. It is also important to note that only the surface layer is tested in the lab without consideration of the bottom layers (base, subbase or subgrade). Asphalt is a viscoelastic material and in contrast with the road there is no 'elastic' bottom layer in the lab fatigue test to 'push' the specimen back to its original position after the load is removed (109). Since neither the haversine wave nor the sinusoidal wave exactly simulates the field condition, it is important to use sinusoidal waves to obtain consistent results as discussed before.

Dissipated Energy Calculations

Calculation of the dissipated energy during the flexure fatigue test requires a time lag between stress and strain. For example, a linear elastic material will not have dissipated energy since the stress and strain are in-phase. For the beam fatigue test without rest period, the dissipated energy can be calculated since there is a phase lag between stress and strain as shown in Figure 35 and Figure 37. However, if the rest period is introduced, the HMA material relaxes during the rest period and stress and strain will be almost in-phase at the beginning of each cycle as shown in Figure 36 and Figure 38. Therefore, the dissipated energy calculated for the test with rest period is expected to be less accurate than the case without rest period. In this study, it was decided not to use the dissipated energy approach.

VERIFICATION OF EQUALITY AMONG MACHINES USING SINUSOIDAL WAVEFORM AND SYNTHETIC BEAMS WITH 5 SECOND REST PERIOD

After deciding to use the sinusoidal strain control test, an additional pilot study was conducted by running beam fatigue tests to verify the assumption of equality among beam fatigue testing machines using synthetic beams. It was also decided to use a 5 second rest period, which is the same rest period that to be used in the main experiment. Another purpose of this pilot study was to solve any testing problems that might be encountered before starting the main experiment.

Experimental Conditions

The following experimental conditions were used.

1. Two machines: IPC1 and IPC2.
2. Two synthetic beams with two levels of stiffness: low and high.
3. Sinusoidal load at a 10 Hz frequency with a rest time of 5 seconds between pulses for 2,500 cycles.
4. One strain level of 800 microstrain
5. One test temperature of 20°C.

A complete factorial experiment was conducted with a total of 12 tests (2 machines x 2 beams x 1 strain levels x 3 replicates).

Comparison of the IPC1 and IPC2 Machines

A statistical analysis similar to the previous analyses was performd following the same procedure. A comparison analysis of IPC1 and IPC2 machines were made. Table 24 summarizes the statistical results.

Table 24. Results of the Statistical Analysis of the Machine Type Comparisons.

	Sum of Squares	DF	Mean Square	F Value	Prob > F
IPC1 vs. IPC2	8.52E+09	1	8.52E+09	0.98	0.3485

The results showed that there are no significant differences among the results of the two machines. This shows that both machines can be used in the study interchangeably, which can improve the test production.

RECOMMENDATION FOR THE MAIN EXPERIMENT

- Strain-controlled sinusoidal tests will be performed in the main experiment according to AASHTO T 321 procedure.
- The dissipated energy approach is not suitable for the test with rest period. Instead, the stiffness-based method should be used.
- Use the IPC1 and IPC2 machines since there are no statistical differences between them.

CHAPTER 7

HMA ENDURANCE LIMIT AND HEALING

BACKGROUND

The main purpose of this chapter is to develop a mathematical procedure to determine an HMA endurance limit based on healing. The proposed mathematical procedure would relate the HMA healing phenomenon to the endurance limit, which makes this procedure unique compared to previous research projects that studied these concepts separately. Six factors that affect fatigue response of asphalt mixtures were evaluated, which are binder type, binder content, air voids, temperature, magnitude of the rest period applied after each loading cycle, and number of cycles to failure for the test without rest period (N_f). The procedure was implemented using test results from representative asphalt concrete mixtures.

As mentioned earlier in Chapter 4, the healing index (HI) can be defined as the difference between the SR for the tests with and without rest period at the number of cycles to failure for the test without rest period ($N_{f\ w/o\ RP}$) as shown in Figure 7 and Equation 15 in Chapter 3.

According to this HI definition, SR needs to be recorded for both tests with and without a rest period at $N_{f\ w/o\ RP}$ as shown in Figure 7. Also, extrapolation was used to predict the SR for the test with rest period at N_f w/o RP since it was decided to run all tests with rest period up to 20,000 cycles only. Figure 8 in Chapter 3 shows the extrapolation process to determine SR for the tests with a rest period at $N_{f\ w/o\ RP}$.

PROCEDURE FOR DETERMINING HEALING-BASED ENDURANCE LIMIT

Since a fractional factorial design of experiment was implemented as discussed in Chapter 3, it was expected that some test combinations would not be tested. Hence, in case where no test without a rest period was run under certain conditions to match a test with a rest period, there is a need to predict $N_{f\ w/o\ RP}$ in order to extend the test with rest period to that $N_{f\ w/o\ RP}$ so SR can be calculated. Therefore, a regression model based on all tests without rest period was developed to predict $N_{f\ w/o\ RP}$ at any required test combination; this regression model permits a decision on the degree of extrapolation needed for the tests with rest period. Four methods were attempted to develop a fatigue model. Three of these methods used the NCHRP MEPDG K_1, K_2, and K_3 format, while the fourth method used a linear regression procedure that directly correlates the binder content, air voids content, and the applied strain with the value of $N_{f\ w/o\ RP}$. Details of the model development are given in a succeeding section.

Once $N_{f\ w/o\ RP}$ is predicted, the required extrapolation for the test with rest period can be completed and SR can be determined for both tests with and without rest period. After determining the SR values, all data points were used to establish the general SR model. The following is the general form of the SR model based on the six factors:

$$SR = a_1 + a_2\,AC + a_3\,V_a + a_4\,(BT) + a_5\,(RP) + a_6\,(T) + a_7\,N_{f\ w/o\ RP} + \text{2-factor interactions} + \text{3-factor interactions} \quad (23)$$

where

- SR = Stiffness Ratio

- $a_1, a_2 \ldots a_n$ = Regression coefficients
- AC = Percent asphalt content
- V_a = Percent air voids
- BT = Binder type
- RP = Rest period (sec)
- T = Temperature (°F)
- $N_{f\ w/o\ RP}$ = Number of cycles to failure (test without rest period)

Once the SR model is developed, HI for any test combination can be computed with Equations 23 and 15. The next step is to correlate the computed healing index to the endurance limit. All HI data points can be plotted versus the strain levels that were used for each test at each temperature separately since it is expected that the endurance limit values will vary with test temperature. Figure 39 illustrates the general relationship between healing index and strain at each temperature.

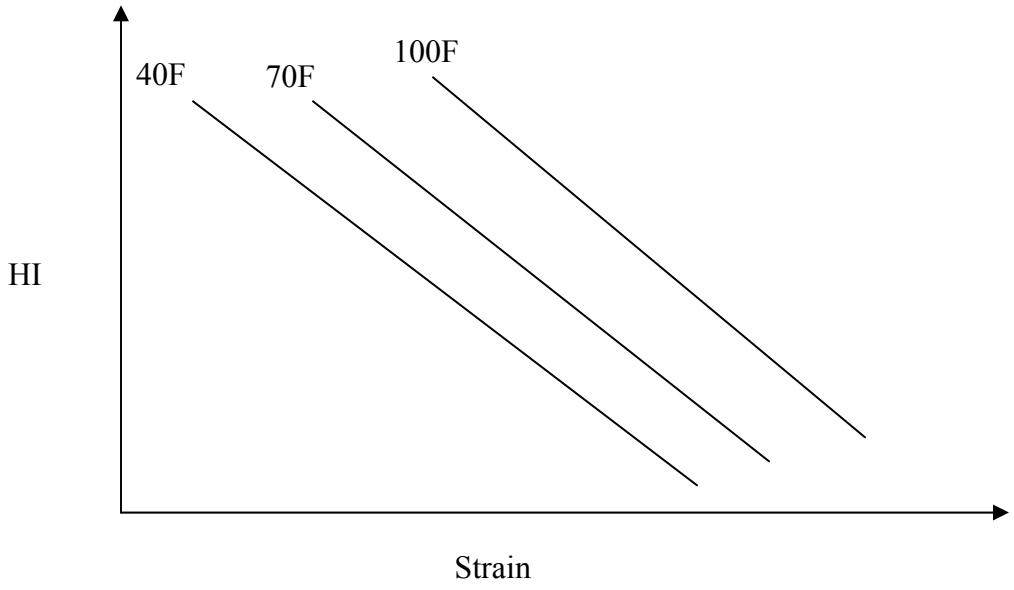

Figure 39. Healing index versus strain levels at 3 test temperatures.

Since it is hypothecated that the endurance limit occurs when no damage is incurred using the test with rest period, the endurance limit can be estimated at an HI of 0.5 where $SR_{w/o\ RP} = 0.5$ and $SR_{w/\ RP} = 1.0$ (no damage). Figure 40 shows a schematic of the estimated endurance limit at each temperature.

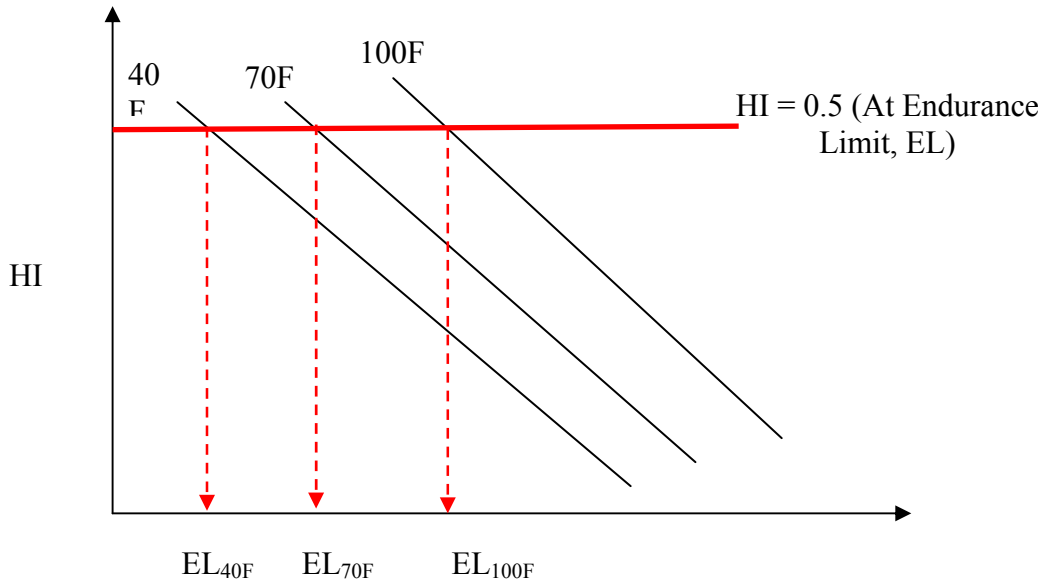

Figure 40. Endurance limit determination at each temperature based on HI.

FIRST GENERATION INTEGRATED STIFFNESS RATIO MODEL

The following discusses the first attempt to implement the proposed endurance limit procedure using test results from the three mixtures made with PG 58-28, PG 64-22 and PG 76-16 binders.

Developing an N_f Model

In order to determine the two levels of $N_{f\ w/o\ RP}$ to be used in the experiment, fatigue tests were performed at the optimum mix design conditions (4.5% asphalt content and 7% air voids) without rest period up to failure (50% stiffness ratio) at 40, 70 and 100°F as shown in Figure 41 to Figure 43 for the PG 58-28, PG 64-22, and PG 76-16, respectively. These figures were used to determine the recommended strain levels at each temperature. The criterion for selecting the two strain levels at each temperature was to reach an N_f value (for tests without rest period) of a reasonable number of cycles, viz., 30,000 and 100,000 cycles, at the high and low strain levels, respectively.

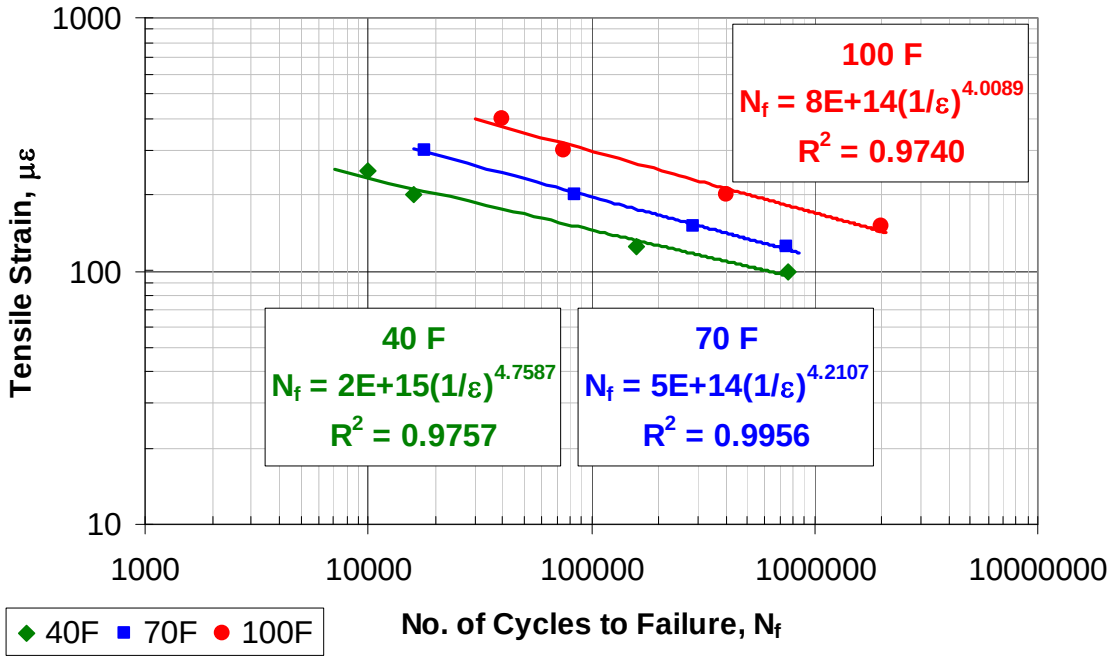

Figure 41. Tensile strain vs. number of cycles to failure for the PG 58-28 mixture.

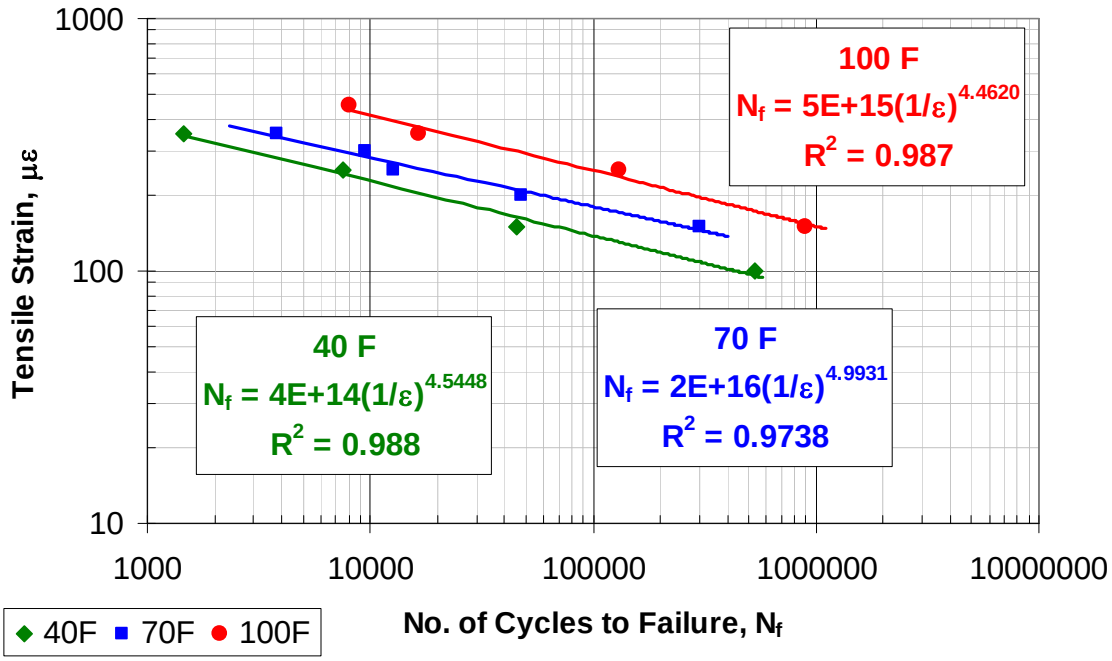

Figure 42. Tensile strain vs. number of cycles to failure for the PG 64-22 mixture.

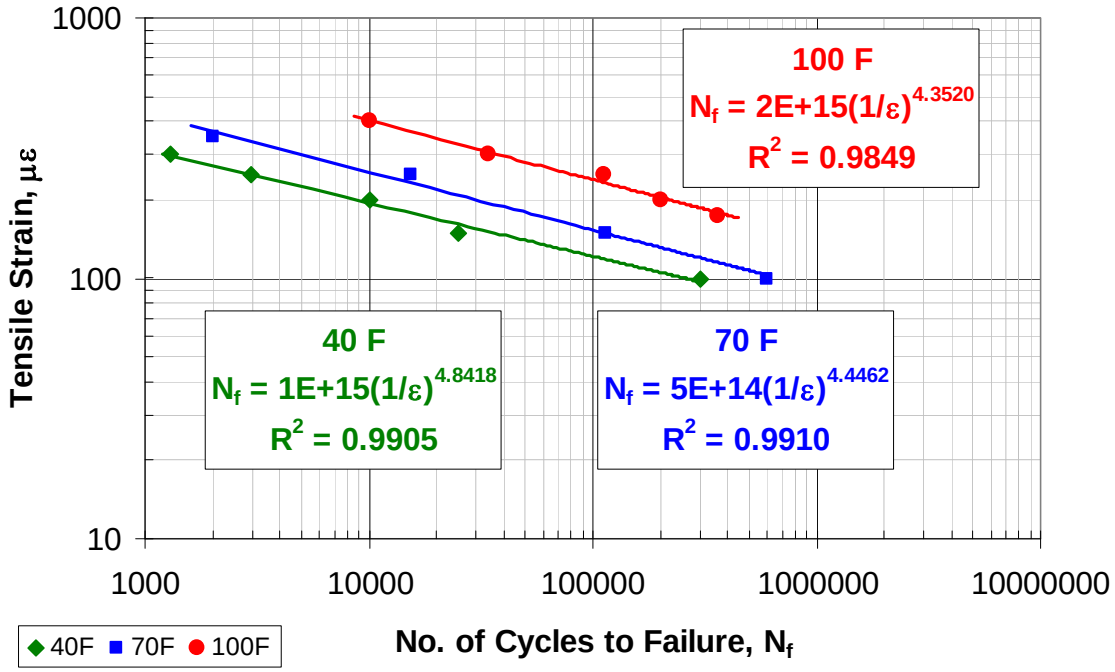

Figure 43. Tensile strain vs. number of cycles to failure for the PG 76-16 mixture.

Table 26 summarizes the strains for the three mixtures at the three test temperatures in order to complete the test within 30,000 and 100,000 cycles.

Table 26. Strains for the Three Mixtures at the Three Test Temperatures.

T, F	N_f, cycles	Strain, με		
		PG 58-28	PG 64-22	PG 76-16
40	100,000	145	100	138
	30,000	170	150	175
70	100,000	200	137.5	188
	30,000	263	200	238
100	100,000	295	313	238
	30,000	415	388	325

As mentioned above, four methods were attempted to predict $N_{f\ w/o\ RP}$ for the missing cells. The following sections discuss the methods used to calculate the K_1, K_2, and K_3 model coefficients. Data from the PG 64-22 mixture were used to check these different methods.

Method 1: One General K_1, K_2, K_3 for All Data Points

In this method, tests without rest period were used as one set to determine one general model with a single K_1, K_2, K_3 set similar to the NCHRP MEPDG procedure. The STATISTICA (128) software was used in the statistical analysis. The following is the model that was developed:

$$N_f=8.49227*(1/\varepsilon)^{2.7179}*(1/E_0)^{0.9252} \quad (24)$$
$R^2 = 0.4306$

where ε is the initial strain and E_0 is the initial stiffness.

Figure 44 shows the measured versus predicted N_f using this model. The model has a low prediction accuracy indicated by the low R^2 value (R^2=0.43). Developing one model for all the without-rest-period data points representing different binder contents and air voids is likely a major reason for the poor accuracy of the model.

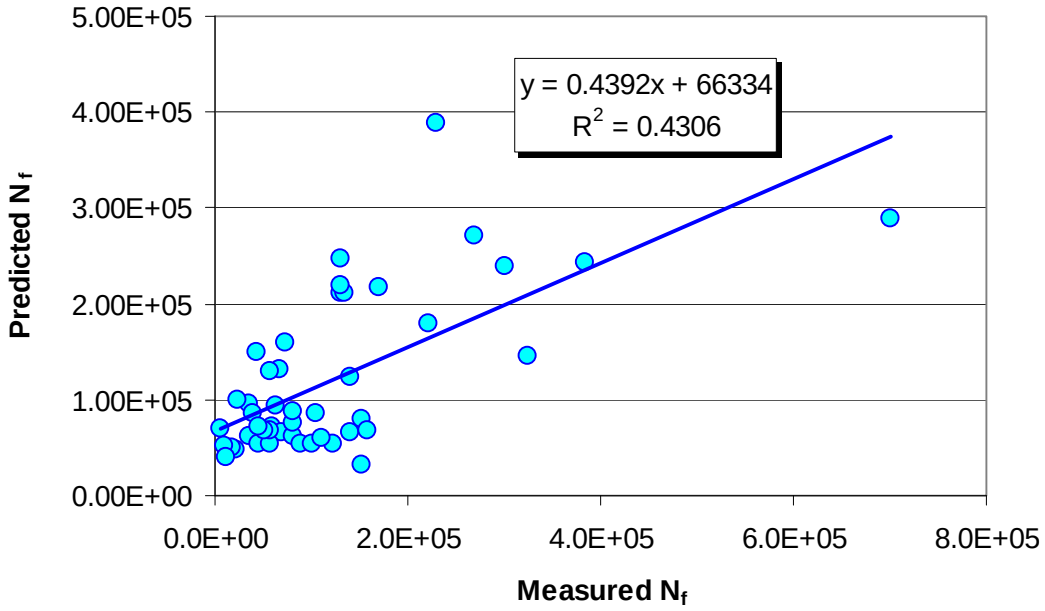

Figure 44. Measured versus predicted N_f (Method 1).

Method 2: Different K_1 for Each Binder Content and Air Void Combination and a Single Set of K_2 and K_3 Values

The main difference between this method and the previous one is that K_1 was calculated using the NCHRP MEPDG equation based on the binder content (AC) and air voids (V_a) data.

Since there were 4 different combinations of AC and V_a used, four values of K_1 were calculated. Using STATISTICA, a single K_2 and K_3 set was determined. The following are the models that were developed:

For 4.2 AC and 4.5 V_a:

$$N_f=0.000429*(1/\varepsilon)^{4.5564}*(1/E_0)^{1.2635} \quad (25)$$

For 4.2 AC and 9.5 V_a

$$N_f=0.0000602*(1/\varepsilon)^{4.5564}*(1/E_0)^{1.2635} \quad (26)$$

For 5.2 AC and 4.5 V_a

$$N_f=0.000777*(1/\varepsilon)^{4.5564}*(1/E_0)^{1.2635} \quad (27)$$

For 5.2 AC and 9.5 V_a

$$N_f=0.000102*(1/\varepsilon)^{4.5564}*(1/E_0)^{1.2635} \quad (28)$$

Overall $R^2=0.3504$

Figure 45 shows the measured versus predicted N_f values based on the second method. More reasonable values for the three coefficients were obtained using this method since it accounted for the different binder contents and air voids. However, a lower prediction accuracy was obtained, which indicates the need of having a specific coefficient set for each combination.

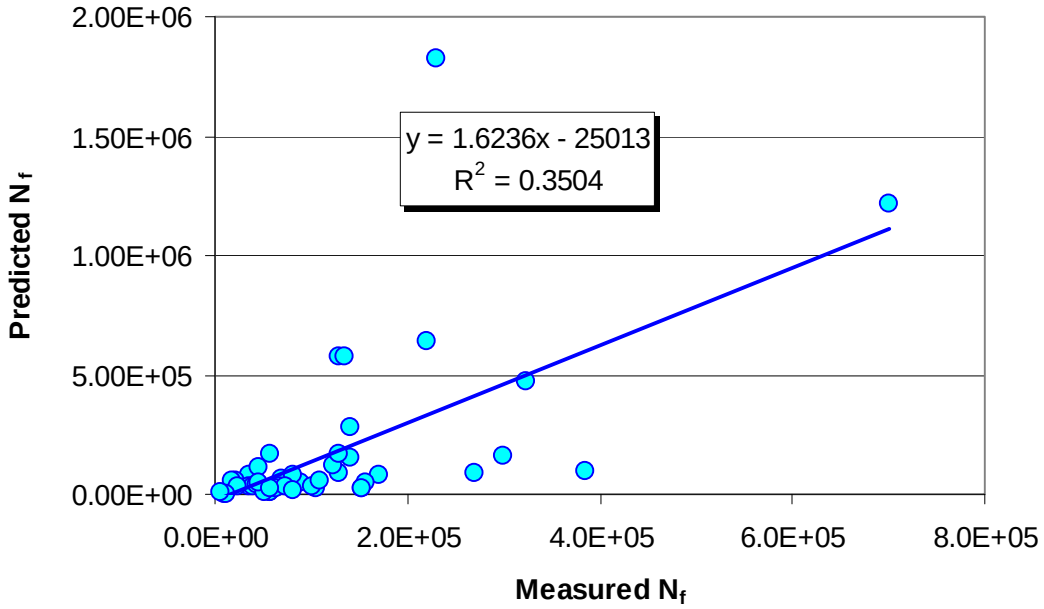

Figure 45. Predicted versus measured N_f (Method 2).

Method 3: Different K_1, K_2, and K_3 Sets for Each Ac-V_a Combination

In this case, the data points were separated into 4 groups according to their AC-V_A properties. Each one of the four groups had a different set of K_1, K_2, and K_3. The following are the models that were developed:

For 4.2 AC and 4.5 V_a:

$$N_f=2972.382*(1/\varepsilon)^{1.7978}*(1/E_0)^{0.8135} \quad (29)$$

For 4.2 AC and 9.5 V_a

$$N_f=1.15*10\text{^}-21*(1/\varepsilon)^{13.7971}*(1/E_0)^{4.06539} \quad (30)$$

For 5.2 AC and 4.5 V_a

$$N_f=42.21357*(1/\varepsilon)^{1.9939}*(1/E_0)^{0.56654} \quad (31)$$

For 5.2 AC and 9.5 V_a

$$N_f=0.84045*(1/\varepsilon)^{2.7715}*(1/E_0)^{0.8039} \quad (32)$$

Overall $R^2=0.6169$

Figure 46 shows the measured versus measured N_f values using the third method. It is noticed that by treating each AC-V_a combination as a different mix, the overall prediction accuracy increased to $R^2 = 0.62$.

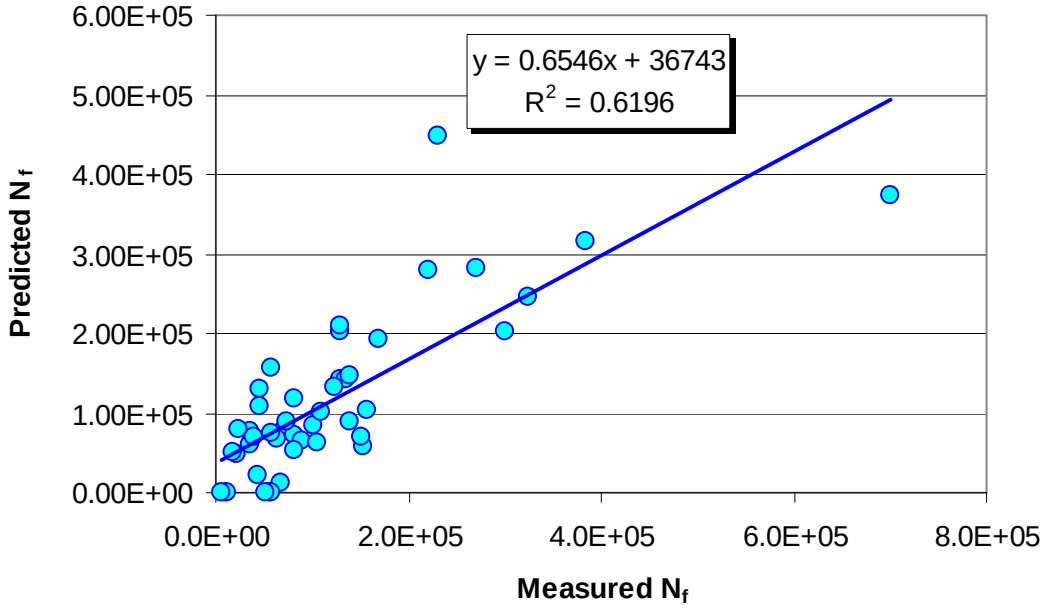

Figure 46. Measured versus predicted N_f (Method 3).

Method 4: Different N_f Model for Each Temperature

The values of the K_1, K_2, and K_3 coefficients obtained with Method 3 were out of the range considered reasonable, likely due to a lack of enough data points for model development because of the fractional factorial design. For example, at some temperatures only one strain level was used. This can lead the statistical program to produce unreasonable values of the coefficients. As a result, in Method 4 a linear regression model was developed for each temperature. These models had the mathematical form in Equation 33.

$$\text{Log}\,(N_{f\ w/o\ RP}) = a + b\,AC + c\,V_a + d\,\varepsilon \quad (33)$$

The three N_f models (3 mixtures x 3 temperatures) have R^2 values ranging from 0.624 to 0.964, which are much higher than those of the previous three methods. The analysis also showed that these models are more rational and accurate than the models obtained in the first three methods.

Figure 47 compares the three NCHRP MEPDG methods and Method 4. Based on these results, the fourth method was used in the rest of the study.

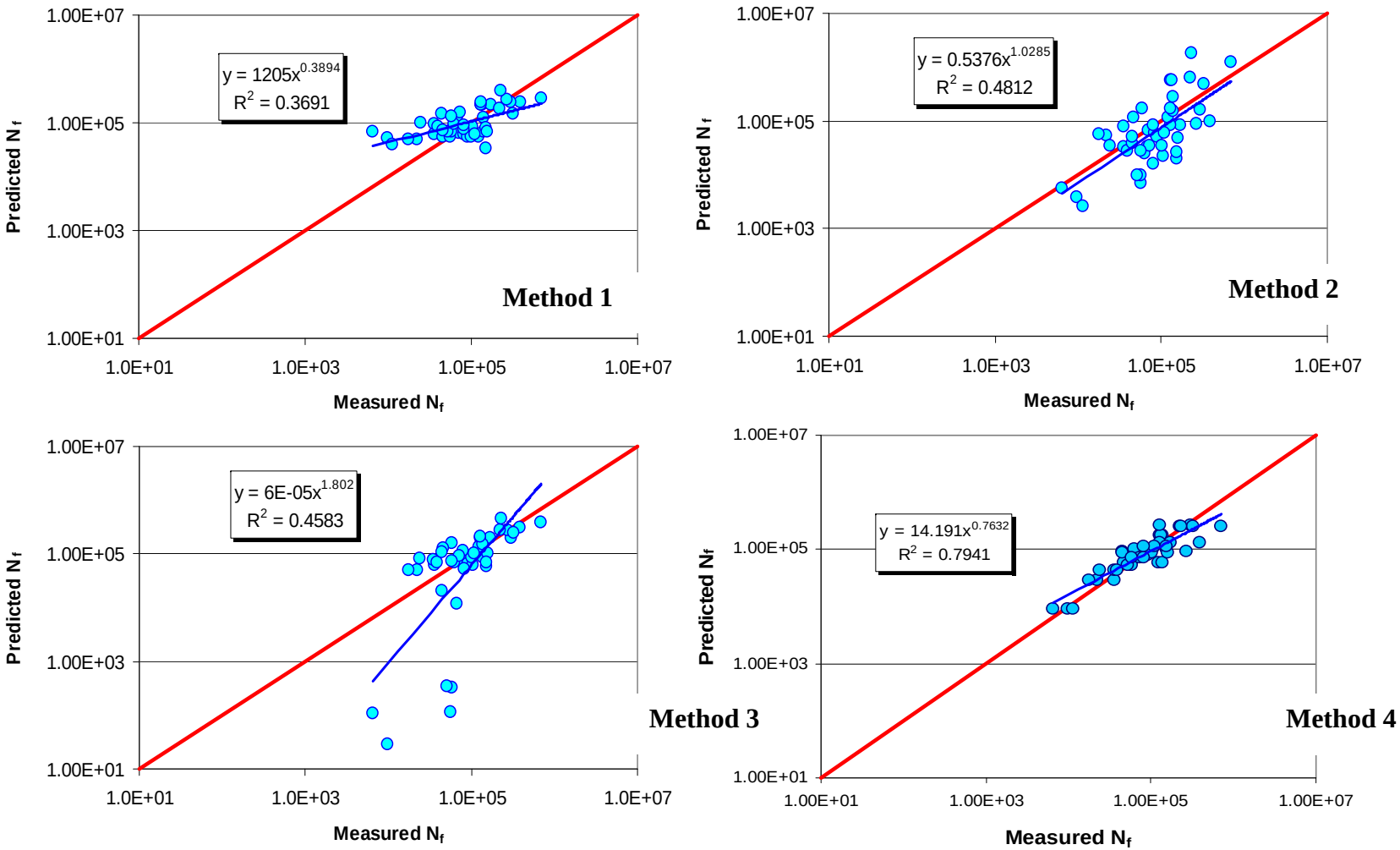

Figure 47. Measured versus predicted N_f using the 3 predicted AASHTO MEPDG models and the AC- V_a based model.

Developing a First Generation SR Model

The SR values were determined at the $N_{f\ w/o\ RP}$ values for all 288 data points and used to develop an integrated stiffness ratio model for the three mixtures. All data points are presented in Appendix A. The general form of the SR model based on the six factors is shown in Equation 34.

The JMP software (98) was used in developing the integrated model by trying different combinations of factors. The significant factors are selected if the individual p-values are less than the significant level of 0.05 (the yellow highlighted cells). Hierarchy was maintained in the model, which means that if there is a significant interaction between two factors, their individual effects were included in the model even if they are not significant. Table 25 shows the final results for the model after removing the insignificant factors.

Table 25. Results for the Selected Significant Factors for the First Generation SR Model.

Source	DF	F Ratio	Prob > F
Binder Type	2	166.5917	0.0298*
Binder Content(4.2,5.2)	1	36.3884	<.0001*
Air Voids(4.5,9.5)	1	27.6618	<.0001*
Nf(50000,150000)	1	126.4891	<.0001*
Rest Period(0,5)	1	10766.64	<.0001*
Temperature	2	32.9617	<.0001*
Binder Type*Binder Content	2	4.7033	0.0111*
Binder Type*Rest Period	2	118.8344	<.0001*
Binder Type*Temperature	4	17.5194	<.0001*
Binder Content*Rest Period	1	40.4089	<.0001*
Air Voids*Rest Period	1	34.3220	<.0001*
Air Voids*Temperature	2	8.3959	0.0003*
Nf*Rest Period	1	129.0273	<.0001*
Nf*Temperature	2	17.0101	<.0001*
Rest Period*Temperature	2	30.9743	<.0001*
Binder Type*Binder Content*Temperature	4	2.5896	0.0376*
Binder Type*Rest Period*Temperature	4	16.7807	<.0001*
Air Voids*Rest Period*Temperature	2	7.5962	0.0006*
Nf*Rest Period*Temperature	2	12.6873	<.0001*

*Significant factor

Summary of Fit

Parameter	Value
R-Squared	0.981223
Adjusted R-Squared	0.97827
Root Mean Square Error	0.024834
Mean of Response	0.673556
Observations	288

Three factors needed to be changed from categorical factors to numerical factors: N_f, temperatures, and binder type. Although the N_f values were estimated in advance using the optimum design conditions, the actual testing resulted in a relatively large range of N_f values. Because of the large variability of the N_f values, N_f was initially treated as a categorical variable (Low and High). However, treating N_f as categorical variable would prevent the use of specific N_f values other than those used in the study. To resolve this issue, an average "low" value and an average "high" value of N_f were calculated based on all data points for all three mixtures. The average low level of N_f was 50,000 cycles, whereas the average high level of N_f was 150,000 cycles.

In addition, temperature was also treated as a categorical variable in the preliminary stage of developing the model because of the inability of the fractional factorial statistical software to deal with three numerical levels of temperatures (40, 70, and 100°F) and two numerical levels of the other variables. As a result, the software produced a different coefficient for each of the three temperatures. To convert temperature from a categorical to a numerical variable, relationships between the three levels of temperature (40, 70, and 100°F) and the categorical coefficients were developed. While converting the binder type from categorical variable to numerical, it was decided to use the elastic modulus (stiffness) values obtained from the E* test at 70°F and 10 Hz at the optimum design condition (4.7% AC and 7% V_a) for each mix. The values that were used in the analysis were 785, 1017, and 1905 ksi for PG 58-28, PG 64-22, and PG 76-16 mixtures, respectively. Figure 48 shows the categorical coefficients versus temperatures.

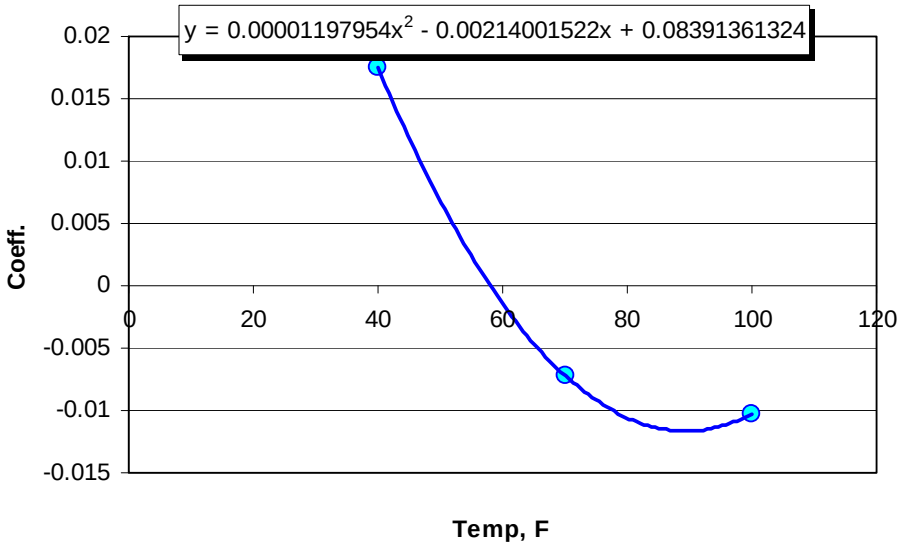

(a)

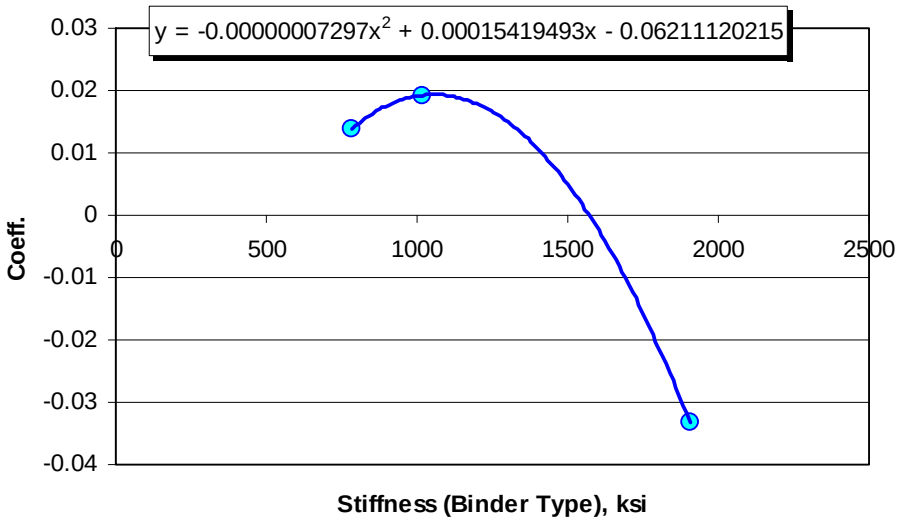

(b)

Figure 48. Categorical coefficients versus temperatures for the integrated model: (a) coefficient for Stiffness (Binder Type), (b) coefficient for Temperature, (c) coefficient for Binder Type*Binder Content, and (d) Temperature*Air Voids.

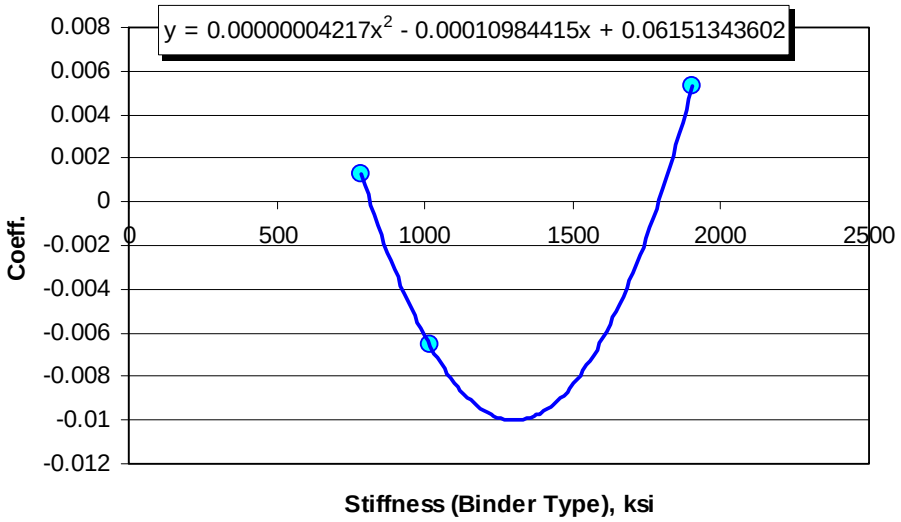

(c)

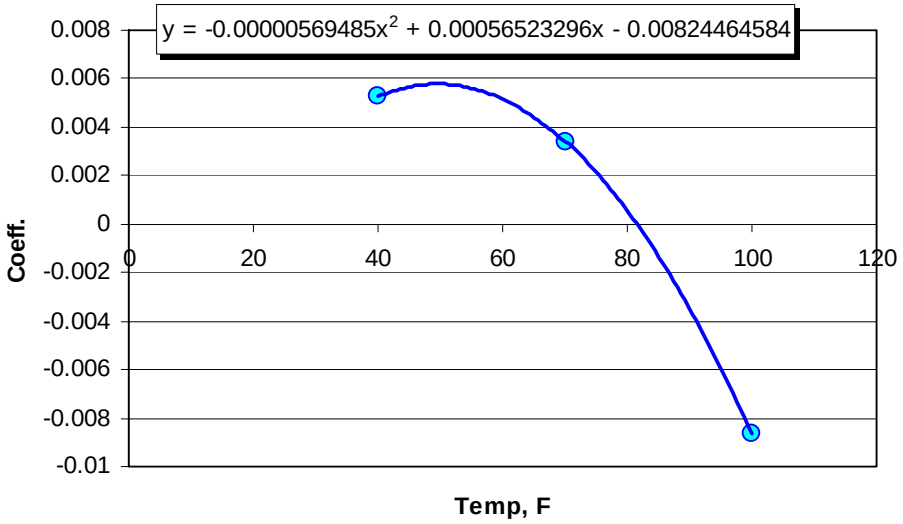

(d)

Figure 48. (Continued). Categorical coefficients versus temperatures for the integrated model: (a) coefficient for Stiffness (Binder Type), (b) coefficient for Temperature, (c) coefficient for Binder Type*Binder Content, and (d) Temperature*Air Voids.

The values of N_f, temperature, and binder type (stiffness) were replaced by the developed relationships, giving the final first generation integrated model shown below.

$$SR = 0.1564774 + (0.00079*BT) + (0.070059744*AC) + (0.00393*V_a) + (0.10095*RP) - (1.268*10^{-7}*N_f) - (0.0024676*T) - (0.0001677*BT*AC) + (3.29961x10^{-5}*BT*RP) + (3.488*10^{-6}*BT*T) + (0.00794848*AC*RP) - (0.0042225*V_a*RP) + (0.0006044*AC*T) - (0.0001035*V_a*T) - (2.889*10^{-8}*RP*N_f) + (2.9191*10^{-9}*N_f*T) - (0.0025*RP*T) - (3.97*10^{-7}*BT^2) - (1.20135*10^{-5}*T^2) + (8.434*10^{-8}*BT^2*AC) - (2.8756*10^{-8}*BT^2*RP) + (1.9558*10^{-6}*AC*T^2) + (6.6137*10^{-7}*V_a*T^2) - (1.582*10^{-11}*N_f*T^2) + (1.262x10^{-5}*RP*T^2) - (1.176*10^{-6}*V_a*RP*T^2) + (3.124*10^{-12}*N_f*RP*T^2) - (7.4*10^{-7}*BT*AC*T) + (3.92*10^{-7}*BT*RP*T) + (0.00013185*V_a*RP*T) + (2.19*10^{-9}*N_f*RP*T) \quad (34)$$

In Equation 34, SR is the stiffness ratio, BT is the binder type, AC is the asphalt content (%), V_a is the percent air voids, RP is the rest period (seconds), N_f is the number of cycles to failure, and T is the temperature (^oF).

Figure 49 shows the integrated model's adequacy using the residual versus predicted plot and the residual versus row plot. The fitting model meets the requirement of normal distribution with constant variance. Figure 50 demonstrates measured versus predicted SR values based on the integrated model. The R^2 value of the developed model was very high (0.980), which is a good indication that the model is accurate.

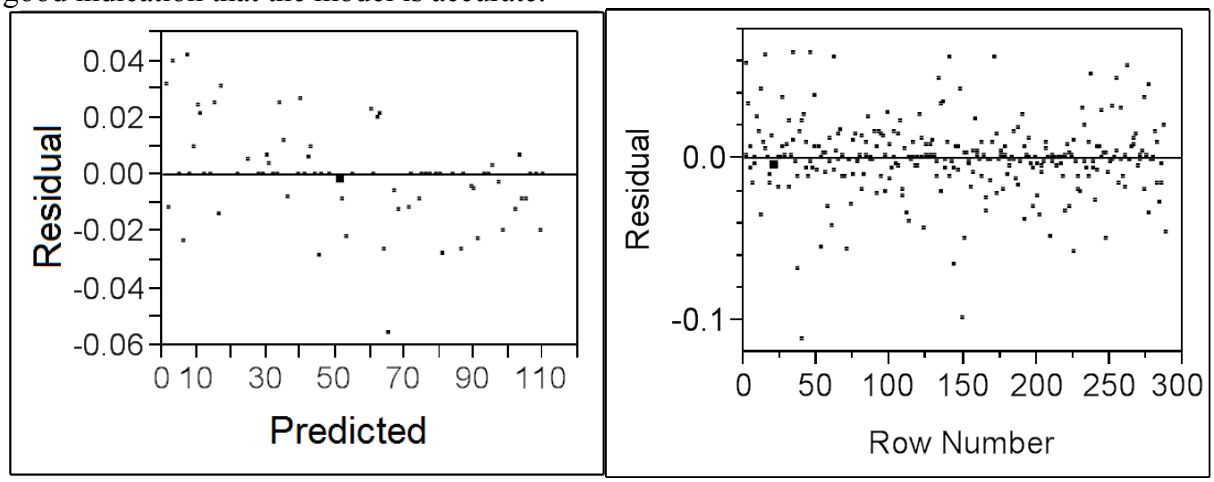

Figure 49. Residual vs. predicted and residual vs. row for the integrated model.

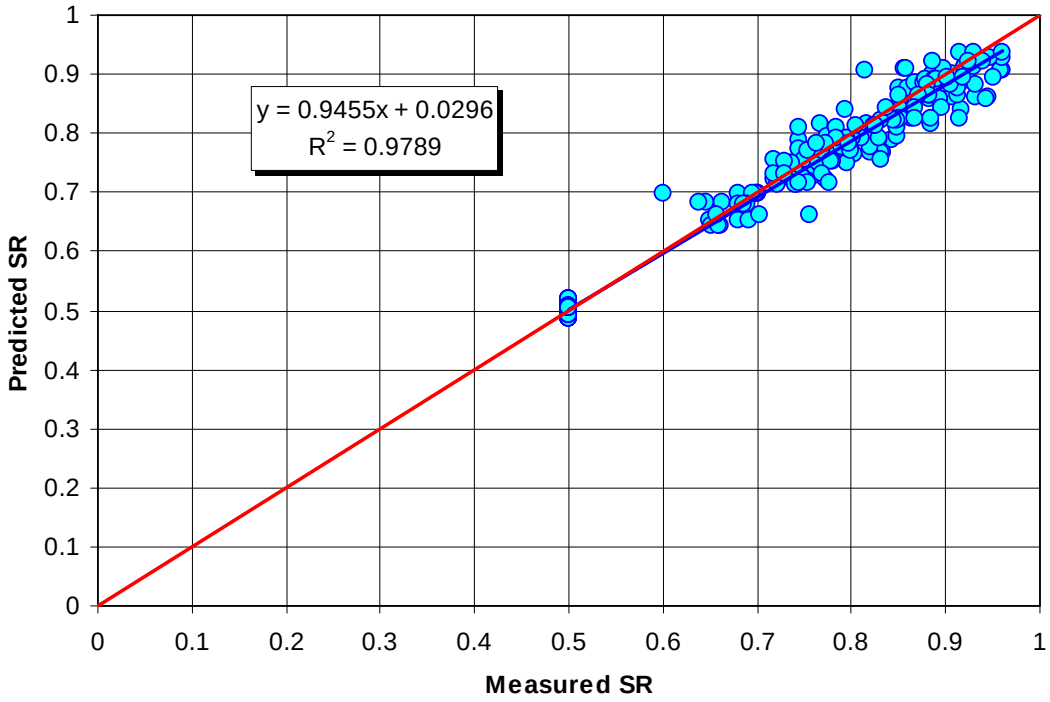

Figure 50. Measured versus predicted SR values based on the integrated SR model for all three mixtures.

Prediction of Healing Index and Endurance Limit

Using the form of the integrated SR model described above, the healing index values for all test combinations were computed. The next step was to relate the computed healing index to the endurance limit. The HI data points were plotted versus the strain used for each mixture at each temperature separately since different endurance limit values are expected for different mixtures and different temperatures. Figures 51-59 illustrate the relationship between healing index and strain level for each mixture at each temperature (3 mixtures x 3 temperatures). Note that there are two strain levels for each temperature. The relationship between the healing index and strain was assumed to be logarithmic.

As stated previously, it was proposed that the endurance limit will occur when complete healing is achieved during the rest period. This implies that the endurance limit can be estimated at a HI value of 0.5, which means $SR_{w/o\ RP}$ is equal to 0.5 and $SR_{w/\ RP}$ is equal to 1.0 (no damage). Referring to Figure 7, the fatigue curve for the test with rest period will be a horizontal line indicating that the value of the stiffness ratio will always be 1.0.

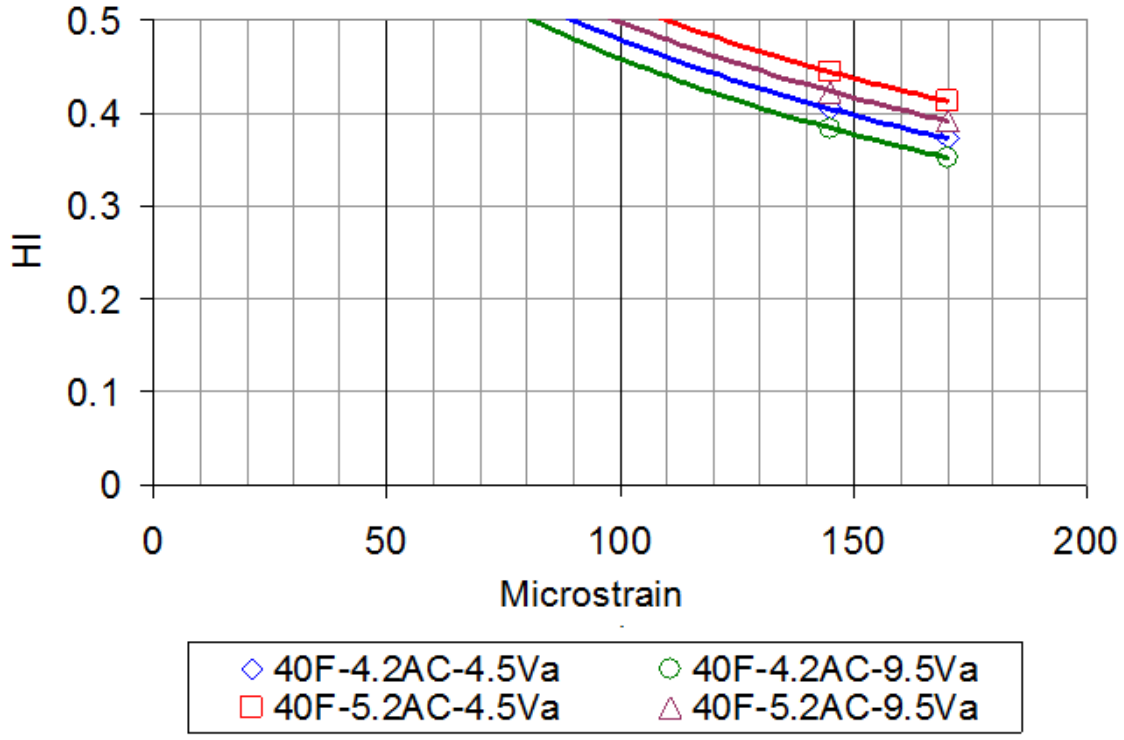

Figure 51. Healing Index versus strain levels for the PG 58-28 Mixture at 40 F.

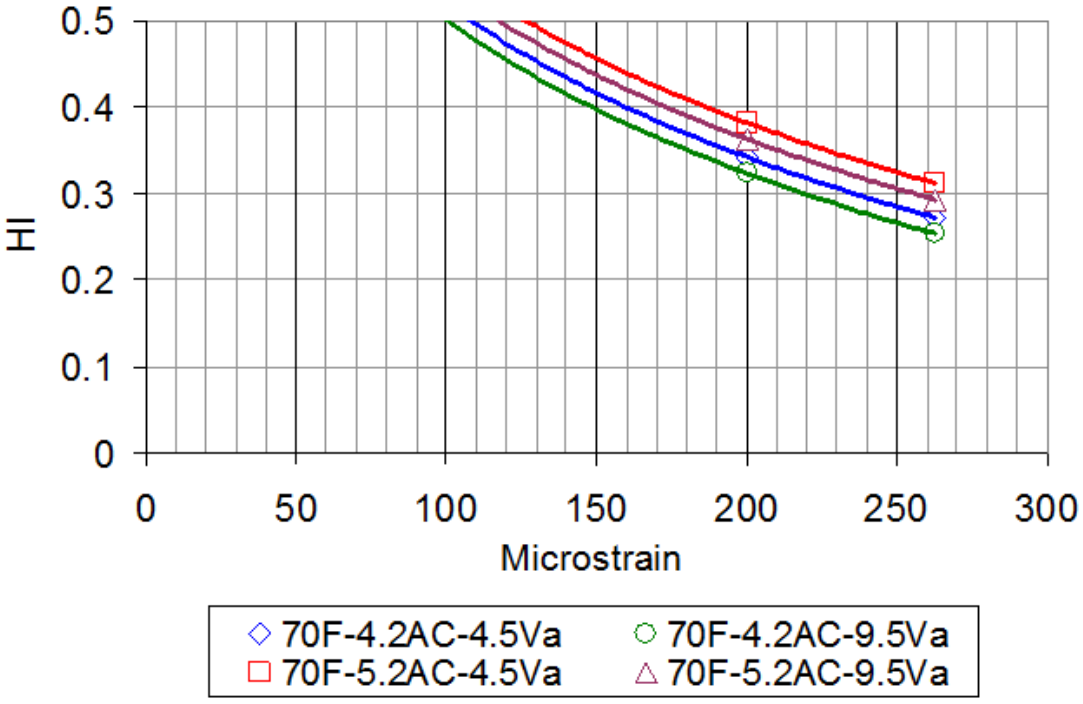

Figure 52. Healing Index versus strain levels for the PG 58-28 Mixture at 70 F.

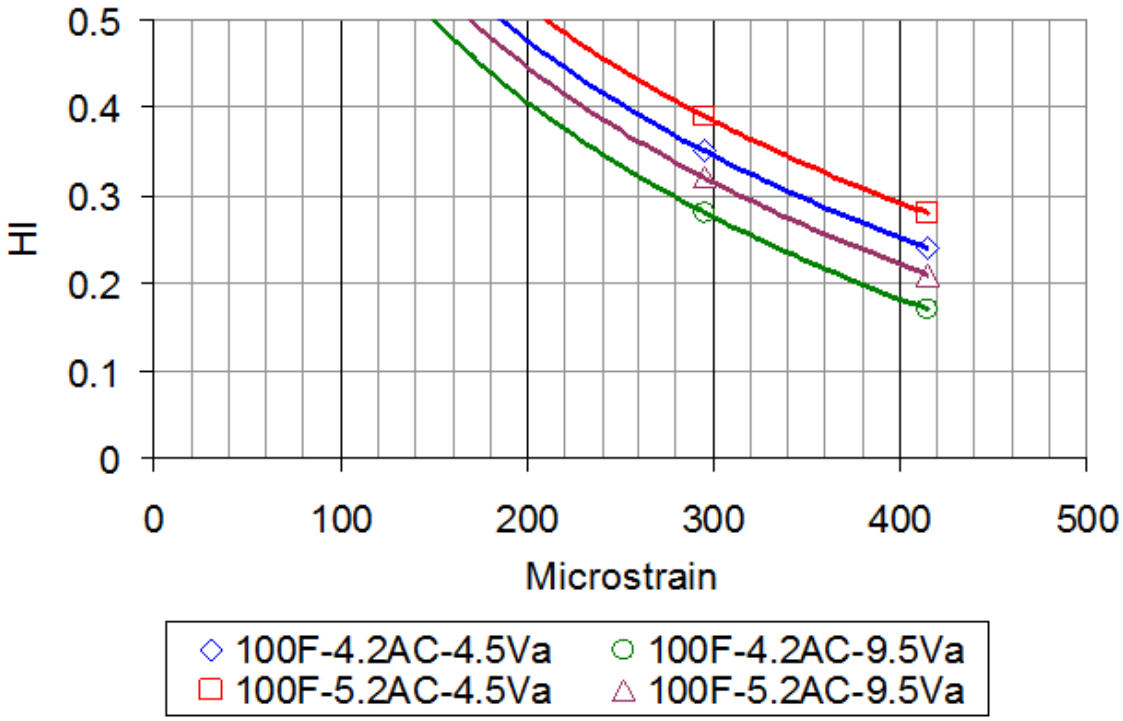

Figure 53. Healing Index versus strain levels for the PG 58-28 Mixture at 100 F.

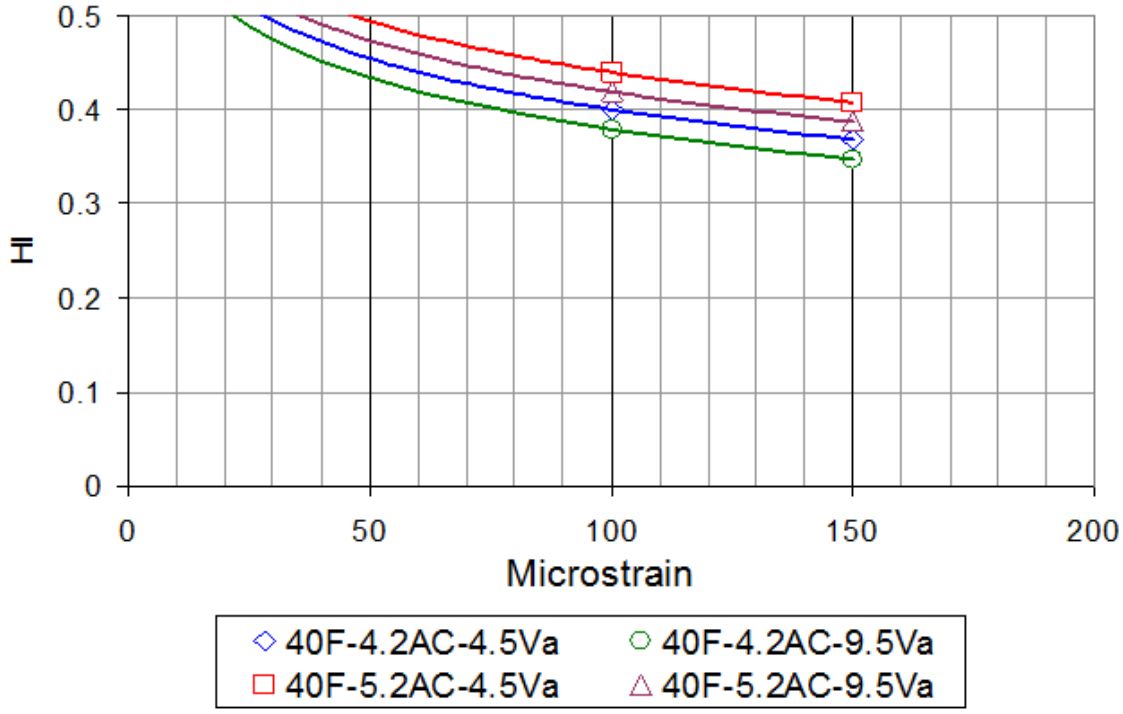

Figure 54. Healing Index versus strain levels for the PG 64-22 Mixture at 40 F.

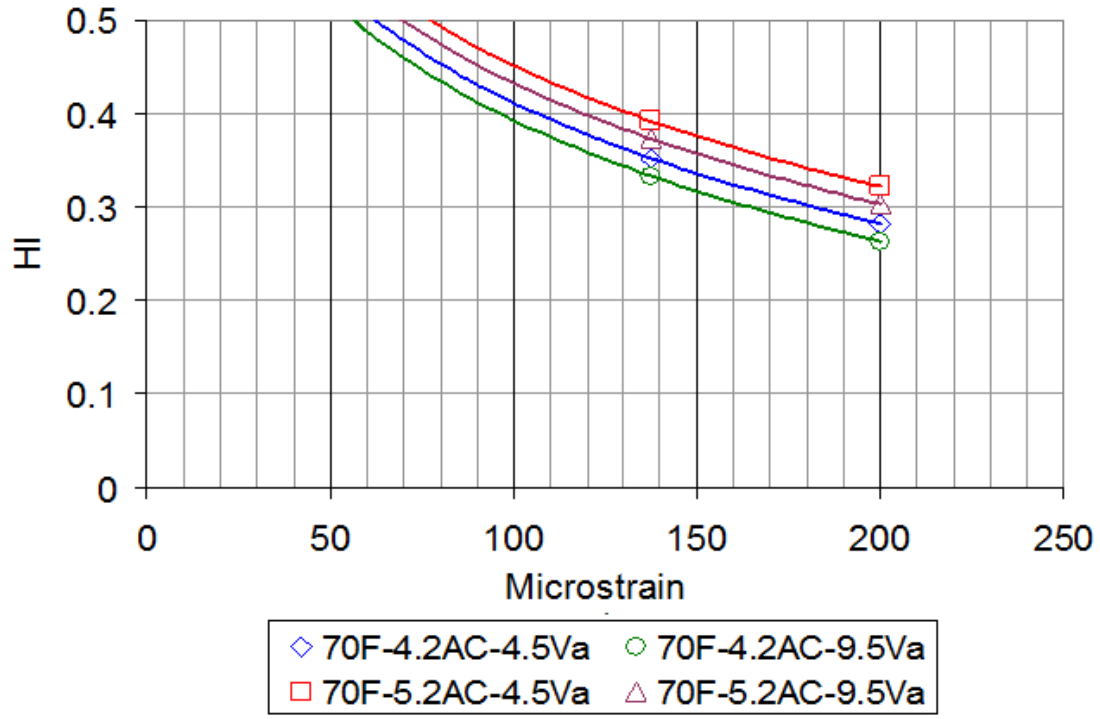

Figure 55. Healing Index versus strain levels for the PG 64-22 Mixture at 70 F.

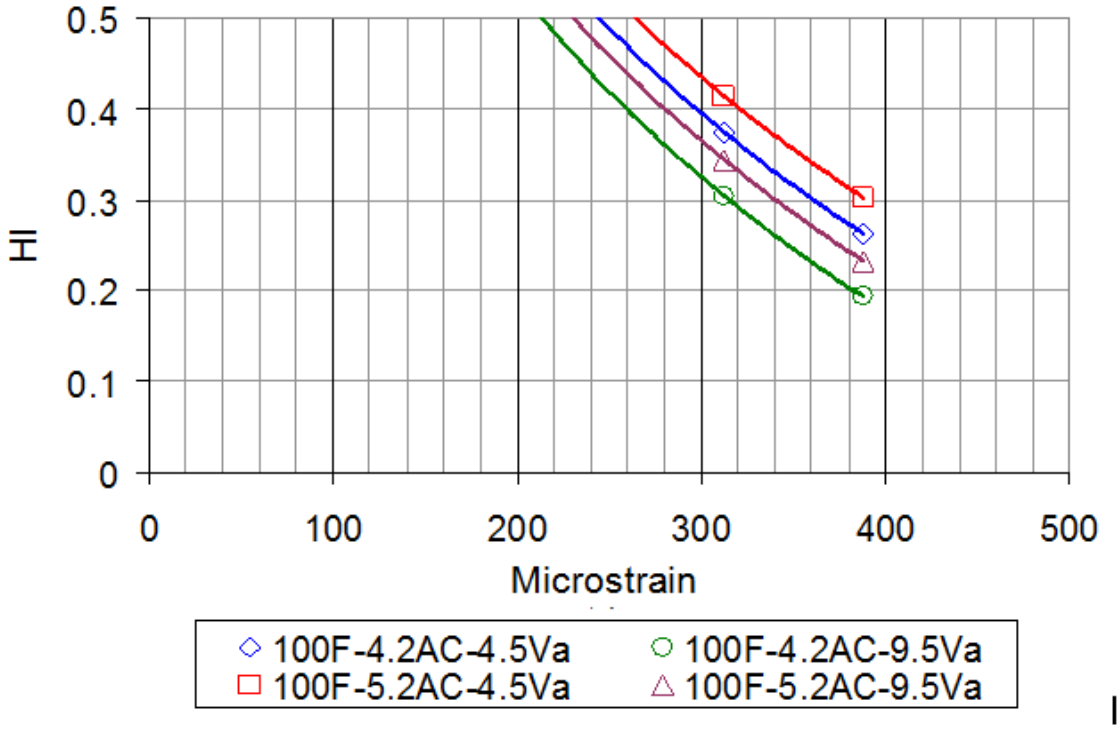

Figure 56. Healing Index versus strain levels for the PG 64-22 Mixture at 100 F.

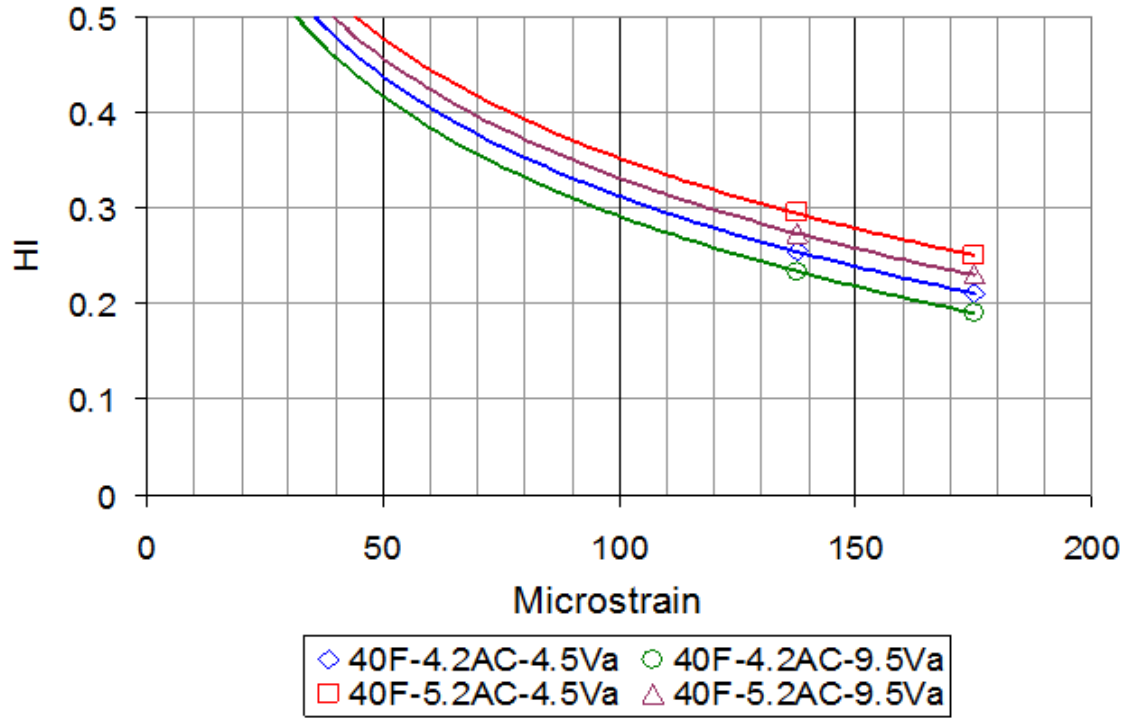

Figure 57. Healing Index versus strain levels for the PG 76-16 Mixture at 40 F.

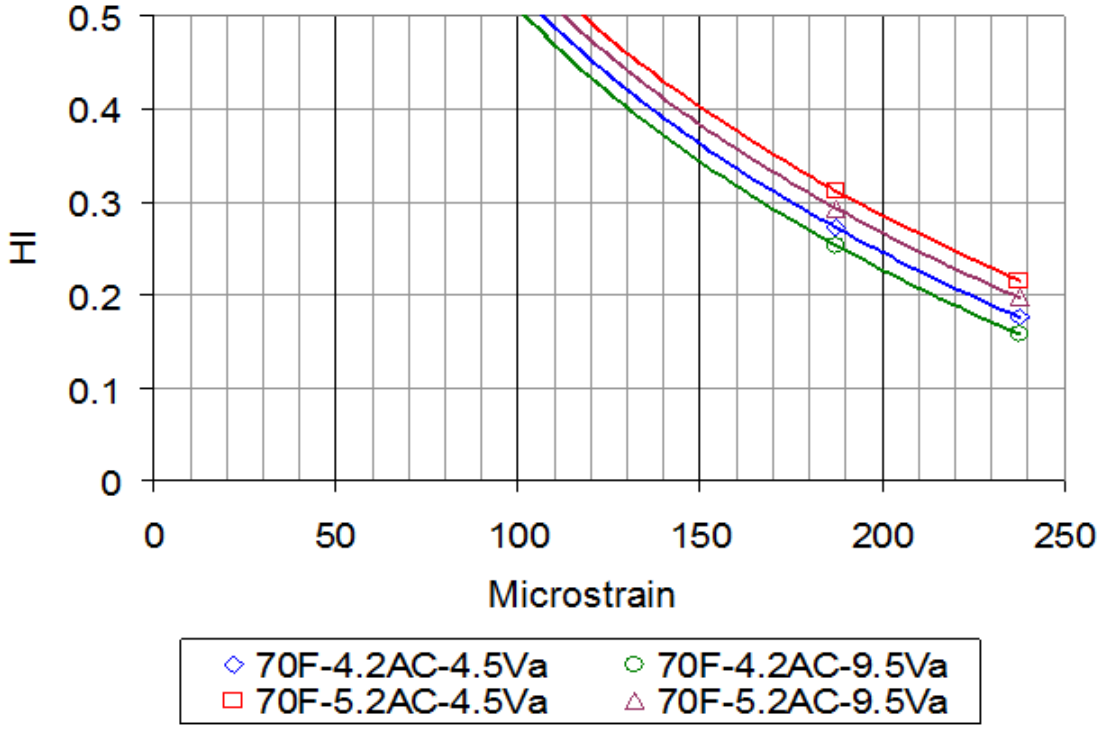

Figure 58. Healing Index versus strain levels for the PG 76-16 Mixture at 70 F.

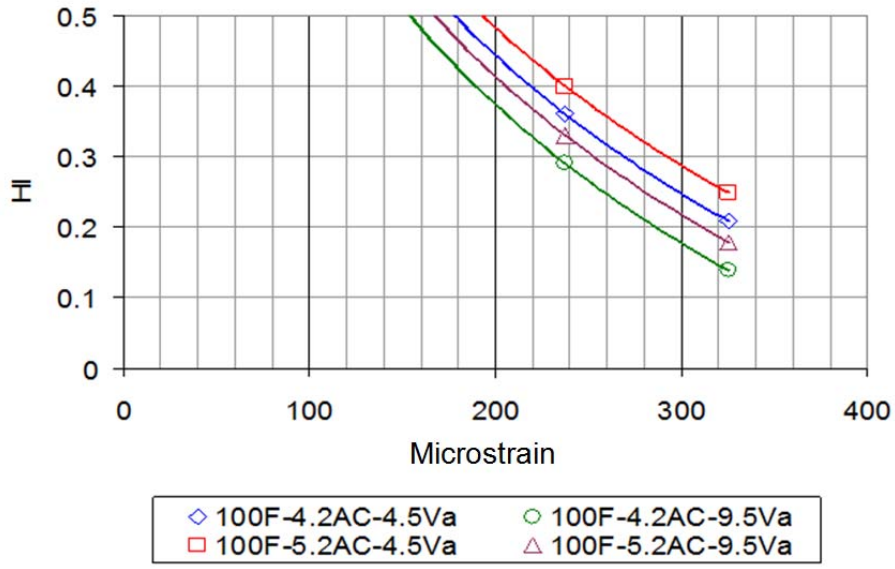

Figure 59. Healing index versus strain levels for the PG 76-16 Mixture at 100 F.

Figure 60 shows an example of the estimated endurance limits for all possible factor combinations based on the SR model at a 5-second rest period. The endurance limit ranged from 22 microstrain (με) (at 40°F) to 264 microstrain (at 100°F). As expected, increasing the binder content increased the endurance limit, while increasing the air voids decreased the endurance limit. It was also noted that the endurance limit increases with temperature.

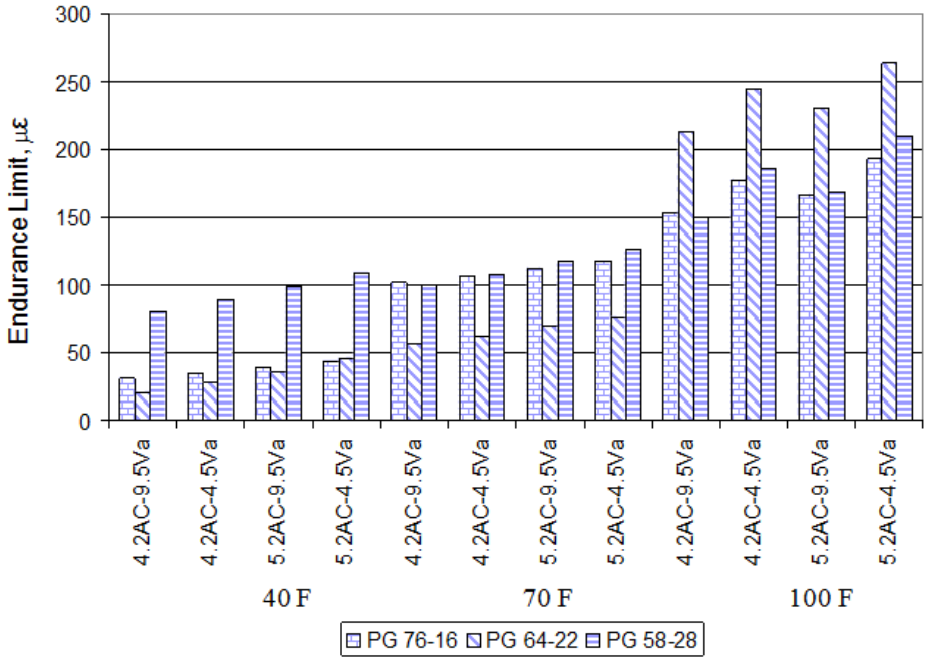

Figure 60. Endurance limits for different factor combinations for a 5-second rest period using the first generation SR model.

SECOND GENERATION INTEGRATED STIFFNESS RATIO MODEL

Model Simplification Using Initial Stiffness

Since the first generation integrated model developed in the previous section was complex and contained many factor interactions, there was a need to further simplify it. Since binder content, air voids, binder type, and temperature all affect stiffness, they were all replaced by the initial stiffness. Such an approach relates the endurance limit to a basic material property—stiffness—and the rest period that allows for healing.

Introducing Other Rest Periods and Strain Levels

Since the first generation SR model was based on two levels of rest period and two levels of strain, the mathematical relationship between endurance limit and these two factors cannot incorporate nonlinearity. In the previous section, a logarithmic function was arbitrarily used without good justification. If a linear relationship is assumed, increasing the rest period from 5 seconds to 10 seconds would double the endurance limit. This would contradict the results of previous studies as discussed in Chapter 2. Previous studies demonstrated that increasing the rest period above a certain optimum value would not yield a significant gain in the HMA healing, which means no improvement would occur to the endurance limit value. In order to check the nature of the relationship between endurance limit, rest period and, strain level, an additional study was performed in which two more rest periods levels and another strain level were introduced. Another objective of this additional study was to fill some of the missing cells in the main experiments that were not performed because of the use of a fractional factorial statistical design. This additional study gained more data points for developing the relationship between healing and endurance limit. It also allowed compilation of all the data to develop a regression model for the stiffness ratio that accounts for three strain levels and the four rest periods.

A design of experiment was used to randomly select the intended data points. The combined study considers the following factors:

- Binder type (3 levels: PG 58-28, PG 64-22, PG 76-16)
- Binder content (2 levels: optimum ± 0.5 %)
- Air void (2 levels: 4.5, 9.5 %)
- Strain level (3 levels: L, M, H)
- Temperature (3 levels: 40, 70, 100^{o}F)
- Rest period (4 levels: 0, 1, 5, 10 sec)

Table 27 shows the testing performed in this part of the study, which includes:

1. 47 test combinations for the additional study to introduce new levels for rest period and strain level.
2. 43 test combinations for 0 second rest period to complete the missing cells from the main experiment.

Table 27. Design of Experiment of the Additional Study*

Temp, F	Strain Level, με	Rest Period, sec	PG 76-16								PG 64-22								PG 58-28							
Binder Type																										
Binder Content, %			4.2				5.2				4.2				5.2				4.2				5.2			
Air Voids, %			4.5		9.5		4.5		9.5		4.5		9.5		4.5		9.5		4.5		9.5		4.5		9.5	
40	L	0																								
		1																								
		5																								
		10																								
	M	0																								
		1																								
		5																								
		10																								
	H	0																								
		1																								
		5																								
		10																								
70	L	0																								
		1																								
		5																								
		10																								
	M	0																								
		1																								
		5																								
		10																								
	H	0																								
		1																								
		5																								
		10																								
100	L	0																								
		1																								
		5																								
		10																								
	M	0																								
		1																								
		5																								
		10																								
	H	0																								
		1																								
		5																								
		10																								

* Highlighted cells show additional tests performed.

A key issue here was the large amount of required tests. The stiffness ratios of the mixture were analyzed using the following factors: temperature, binder content, air voids, rest period, and strain. A statistical analysis was used (99) to determine the minimum number of replicates to maintain the required accuracy. The results concluded that two replicates only for each test combination are needed to complete the additional study. Therefore, 180 tests (90 test combinations x 2 replicates) were conducted.

Developing the Second Generation SR Model

All the data from the main study (Section 7.3.2) and the additional study (Section 7.4.2) were combined in one master database that contained a total of 468 beam fatigue tests. The combined data were then used to build a simplified, second generation integrated stiffness ratio model that replaces four factors (binder type, binder content, air voids, and temperature) with the initial stiffness of the mixture, E_o. The model also accounts for the nonlinear effects of rest period and the applied strain on the healing and endurance limit of the material.

The regression models was built with two statistical software packages, STATISTICA and Excel. STATISTICA was used to determine the best initial values for the coefficients. An optimization process was performed using Excel to minimize the sum of squared error followed by setting the sum of error equal to zero.

Several trials were made to determine the best mathematical form to relate the three independent variables (rest period, strain level, and stiffness) with SR. It was found that there is a need for a logarithmic transformation for both strain and stiffness values. It was also concluded that the best mathematical form to relate SR with rest period was the tangent hyperbolic (tanh) function since it demonstrated no extra healing gained by applying 10 seconds rest period compared to 5 seconds observed during the laboratory tests as shown in Figure 61. This result is in agreement with the literature that showed an optimum rest period beyond which no more healing is gained (see Figure 61).

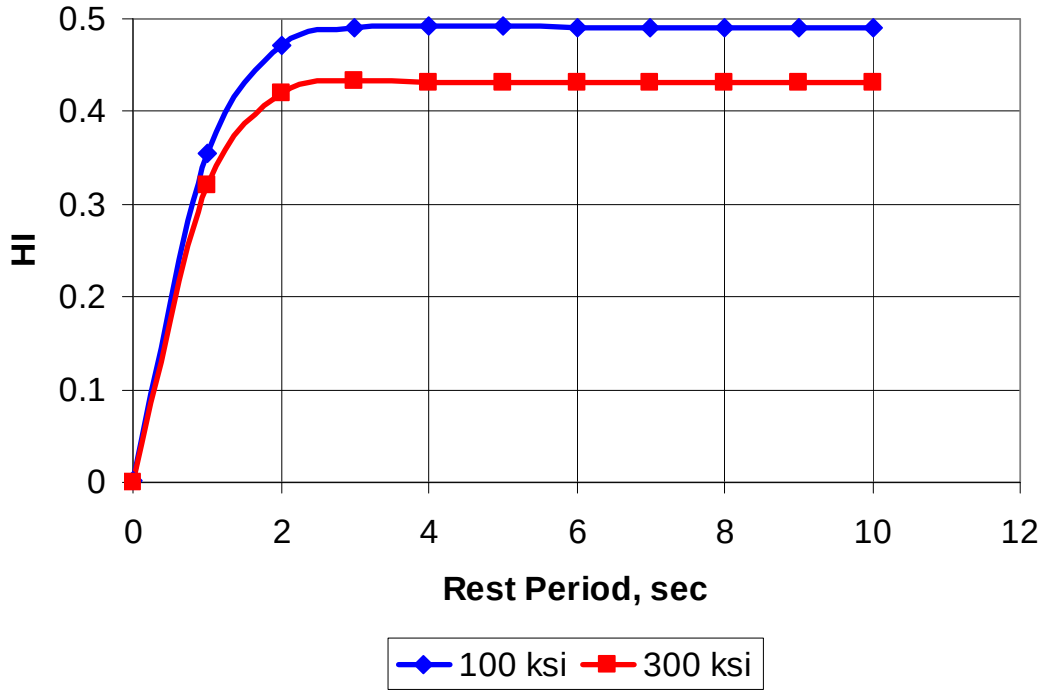

Figure 61. Healing index versus rest period at two stiffness levels.

Regression analysis was used to generate the second generation SR model that accounts for HMA stiffness and nonlinearity. The first trial was obtained with an R^2 value of 0.917. The model was further refined by removing ten outlier data points using the technique suggested by Montgomery (99).

The analysis was then repeated based on the remaining 458 data points and the following second generation model was obtained.

$$SR=0.6049-0.0457*\log(E_o)-0.0494*\log(\varepsilon)+ 2.0455*\tanh(0.7743*RP) +0.0204*\log(E_o)*\log(\varepsilon)-0.1287*\log(E_o)*\tanh(0.6644*RP)-0.5937*Log(\varepsilon)*\tanh(0.7445*RP) \quad (35)$$

In Equation 35, SR is the stiffness ratio, E_o is the initial flexural stiffness (ksi), ε is the applied strain (microstrain), and RP is the rest period (seconds).

Using this model, the R^2 improved to 0.921 and the skewness of the data was significantly reduced. Figure 62 shows predicted versus measured SR after removing the outliers.

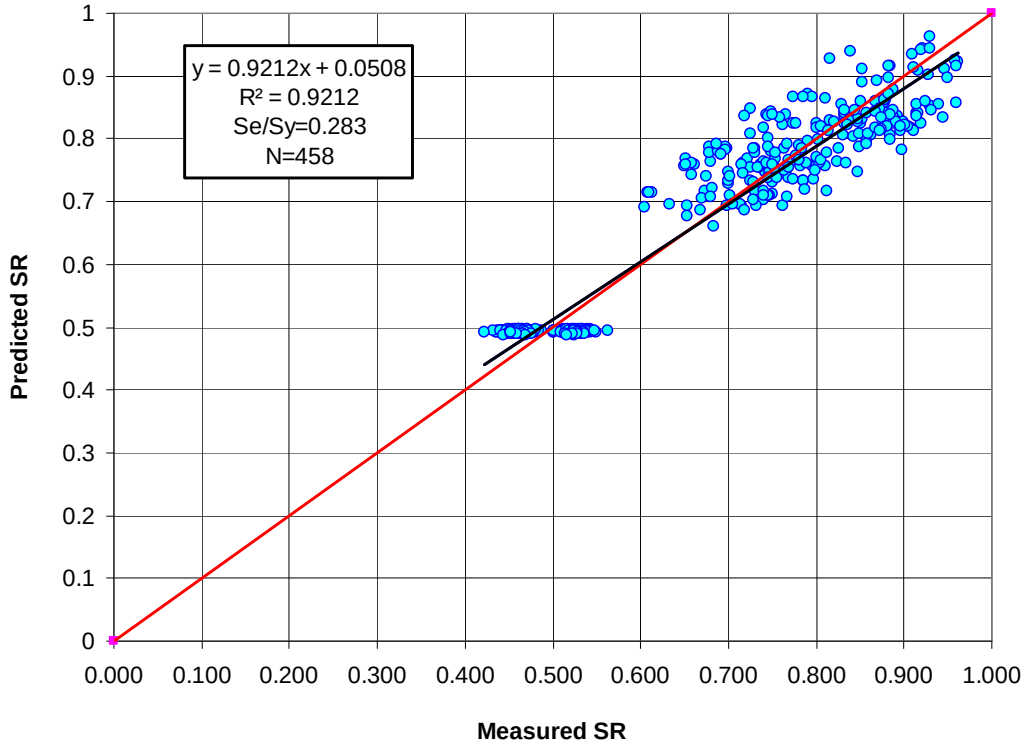

Figure 62. Measured versus predicted SR for the second generation model.

Figure 63 to Figure 67 demonstrate the SR versus strain at several rest periods. Similar to the first generation model discussed above, the endurance limit occurs when complete healing happens during the rest period at a stiffness ratio of 1.0.

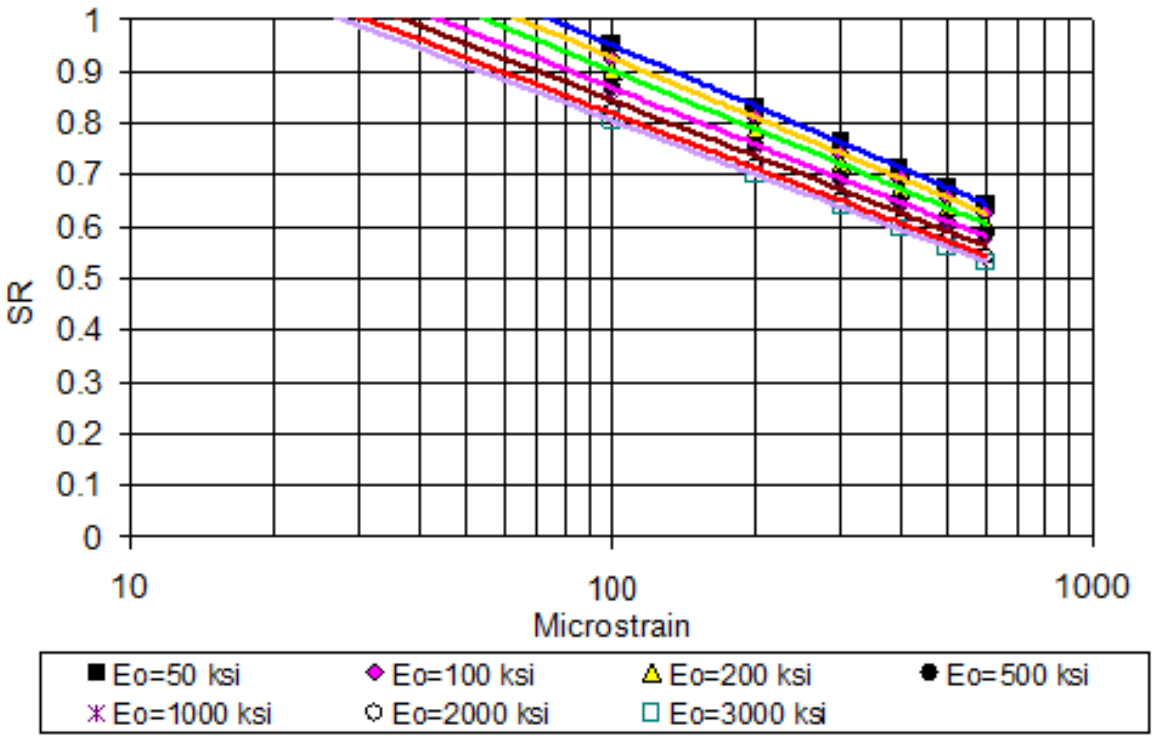

Figure 63. SR vs. strain for several initial stiffness values and 1 second rest period.

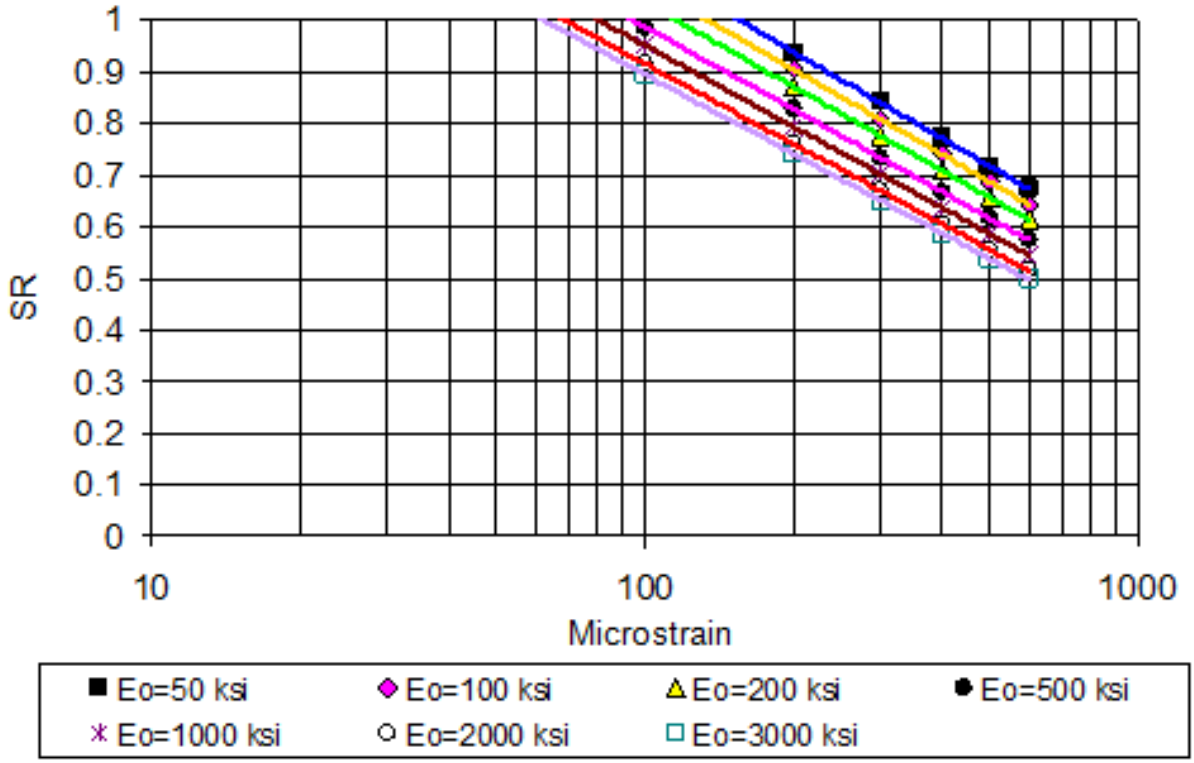

Figure 64. SR vs. strain for several initial stiffness values and 2 second rest period.

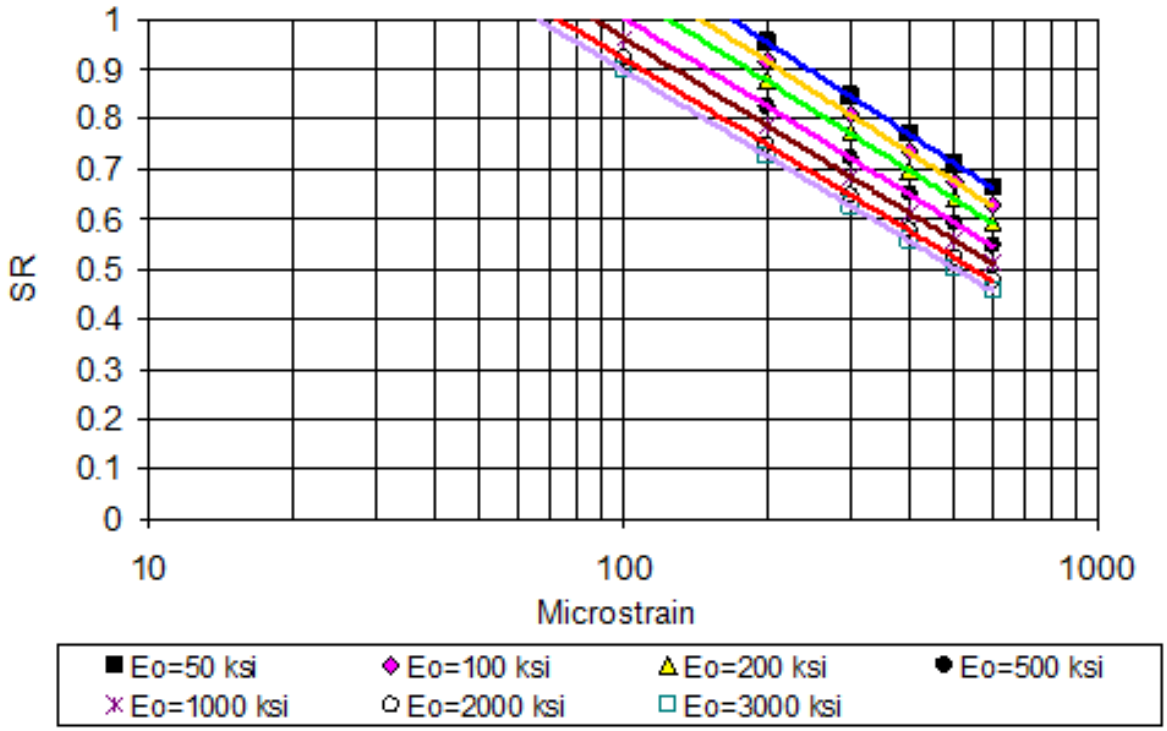

Figure 65. SR vs. strain for several initial stiffness values and 5 second rest period.

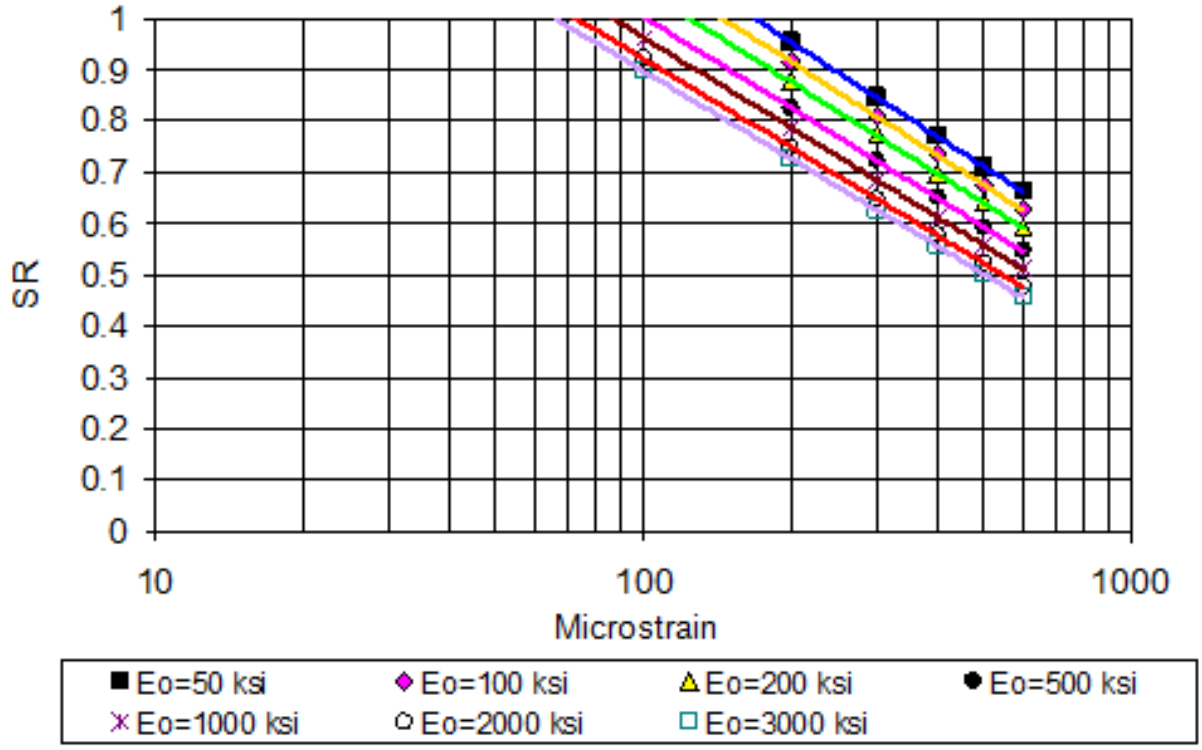

Figure 66. SR vs. strain for several initial stiffness values and 10 second rest period.

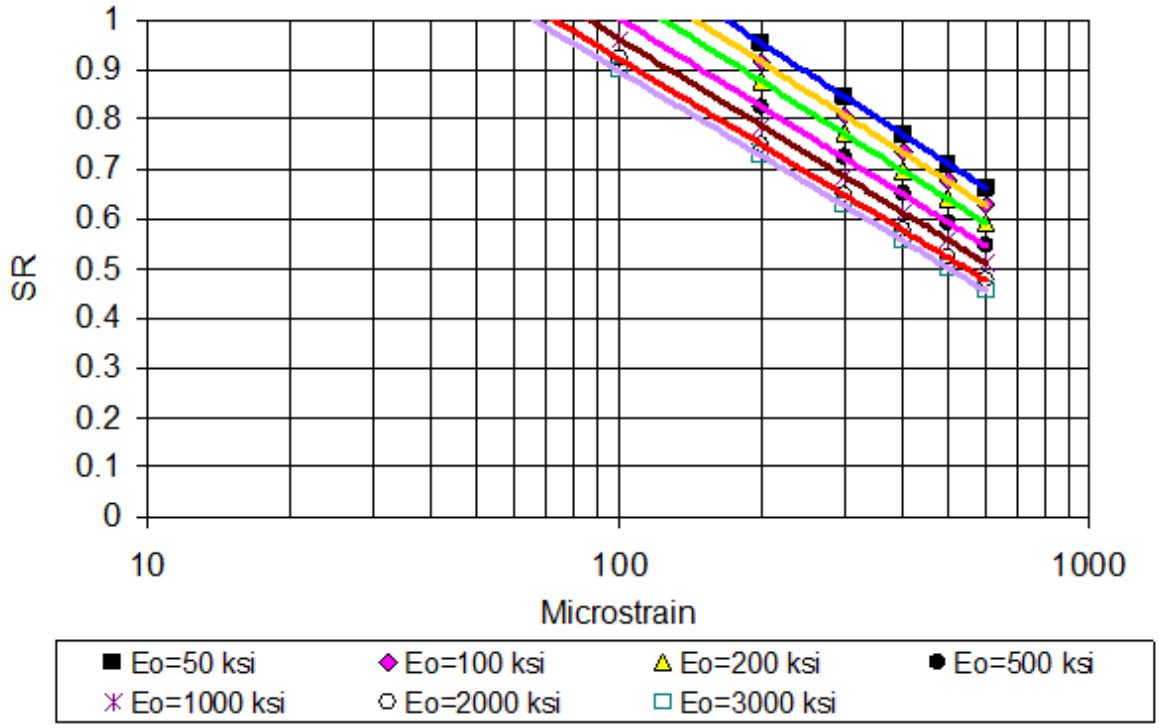

Figure 67. SR vs. strain for several initial stiffness values and 20 second rest period.

Figure 68 illustrates the summary of the endurance limit values for several rest periods and stiffness values. The endurance limit values ranged from 30 microstrain (1 seconds rest period and 3,000 ksi stiffness) to 170 microstrain (5 seconds and 50 ksi stiffness). Note that the endurance limit values at 5 seconds were the same as 10 and 20 seconds. This indicates that no more improvement of the endurance limit occurs beyond 5 seconds. In addition, the endurance limit increases as the stiffness of the mixture decreases. In other words, softer mixtures allow for larger strains to be applied without causing fatigue damage to the HMA layer. The value of the allowed strain that does not cause fatigue damage increases as the rest period between load applications increases up to 5 seconds.

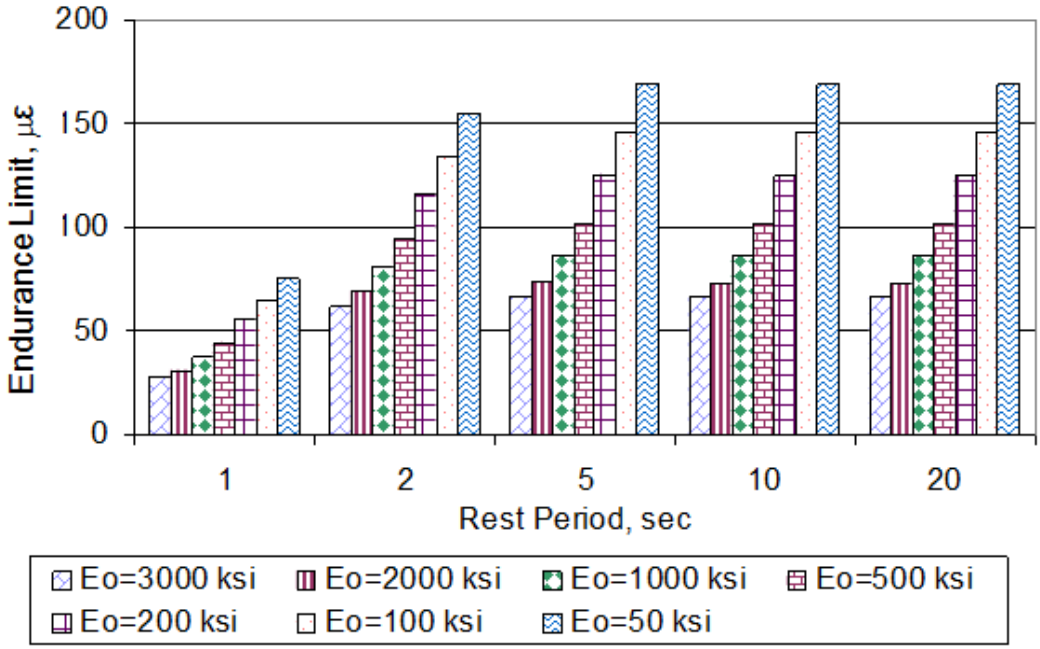

Figure 68. Summary of endurance limit values for several rest periods and stiffness values (based on second generation SR model).

THIRD GENERATION INTEGRATED STIFFNESS RATIO MODEL

The data points of the second generation SR model were collected at $N_{f\ w/o\ RP}$. Since the applied strain was pre-selected to reach failure for the test without a rest period at a certain value of number of cycles ($N_{f\ w/o\ RP}$), the strain and $N_{f\ w/o\ RP}$ were highly correlated. This issue resulted in removing either strain or $N_{f\ w/o\ RP}$ from the second generation model since these two factors are co-linear. In order to include N in the third generation model, SR data were collected at three different locations along the SR-N relationship for tests with rest period in order to remove the statistical co-linearity between strain and N. Figure 69 shows the typical SR-N relationships for the tests with and without rest period and the locations where data points were selected. For the test with rest period curve, two of the points were taken during the test, while the third point was taken at $N_{f\ w/o\ RP}$. Note that the test results with rest period are extrapolated to $N_{f\ w/o\ RP}$ as discussed in Chapter 7.

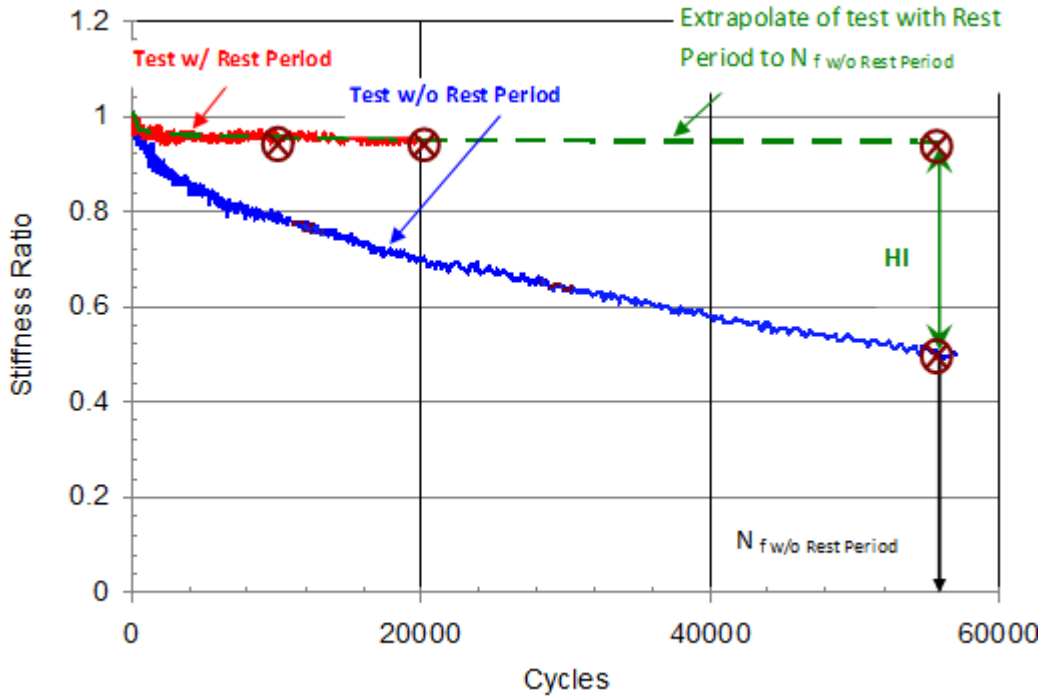

Figure 69. Selection of data point locations.

In this third generation model development, a total of 946 data points were used to build the model. The R^2 value of the model was 0.887. A statistical analysis (127) was then done to remove outliers in order to improve the accuracy of the model. Consequently, 12 data points were excluded from the analysis, which increased the R^2 value from 0.877 to 0.891. Figure 70 shows predicted versus measured SR after removing the outliers.

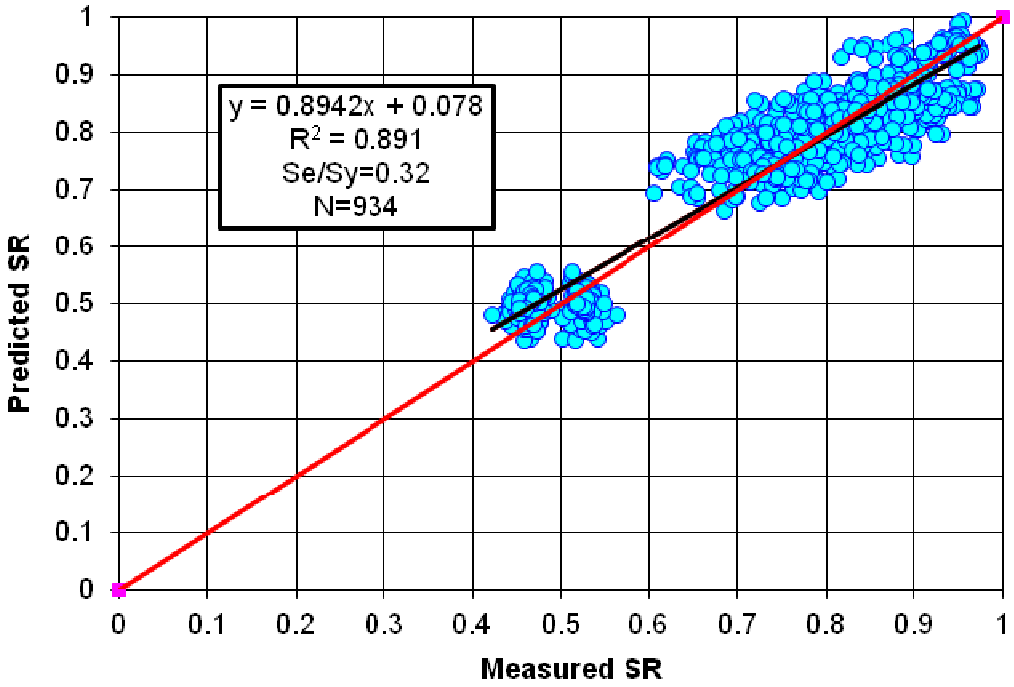

Figure 70. Measured versus predicted SR for the third generation SR Model after removing data outliers.

The third generation integrated stiffness ratio model after removing the outliers is shown below.

$$SR=2.0844-0.1386*\log(E_o)-0.4846*\log(\varepsilon)-0.2012*\log(N)+ 1.4103*\tanh(0.8471*RP)+0.0320*\log(E_o)*\log(\varepsilon)-0.0954*\log(E_o)*\tanh(0.7154*RP)- 0.4746*\log(\varepsilon)*\tanh(0.6574*RP)+0.0041*\log(N) *\log(E_o)+0.0557*\log(N)*\log(\varepsilon)+0.0689*\log(N)*\tanh(0.259*RP) \quad (36)$$

In Equation 36, SR is the stiffness ratio, E_o is the initial flexural stiffness (ksi), ε is the applied strain (microstrain), RP is the rest period (seconds), and N is the number of cycles.

By substituting the stiffness ratio with 1.0 (no damage condition), the endurance limit can be predicted for different values of E_o and rest period.

Effect of N on Endurance Limit

After N was included in the model, it was important to know the effect of changing the value of N on the endurance limit. A sensitivity analysis study was performed, where SR was plotted versus strain and rest period for different E_o values and three levels of N (20,000, 100,000, 200,000 cycles).

Based on Figures 71 and 72, the number of loading cycles has little of no effect on the SR value for tests with rest period, especially at large values of N. Since the endurance limit is obtained at a SR value of 1.0, the number of loading cycles also has little or no effect on the

endurance limit. As a result, the endurance limit was calculated at a conservative value of 200,000 cycles in the rest of the study.

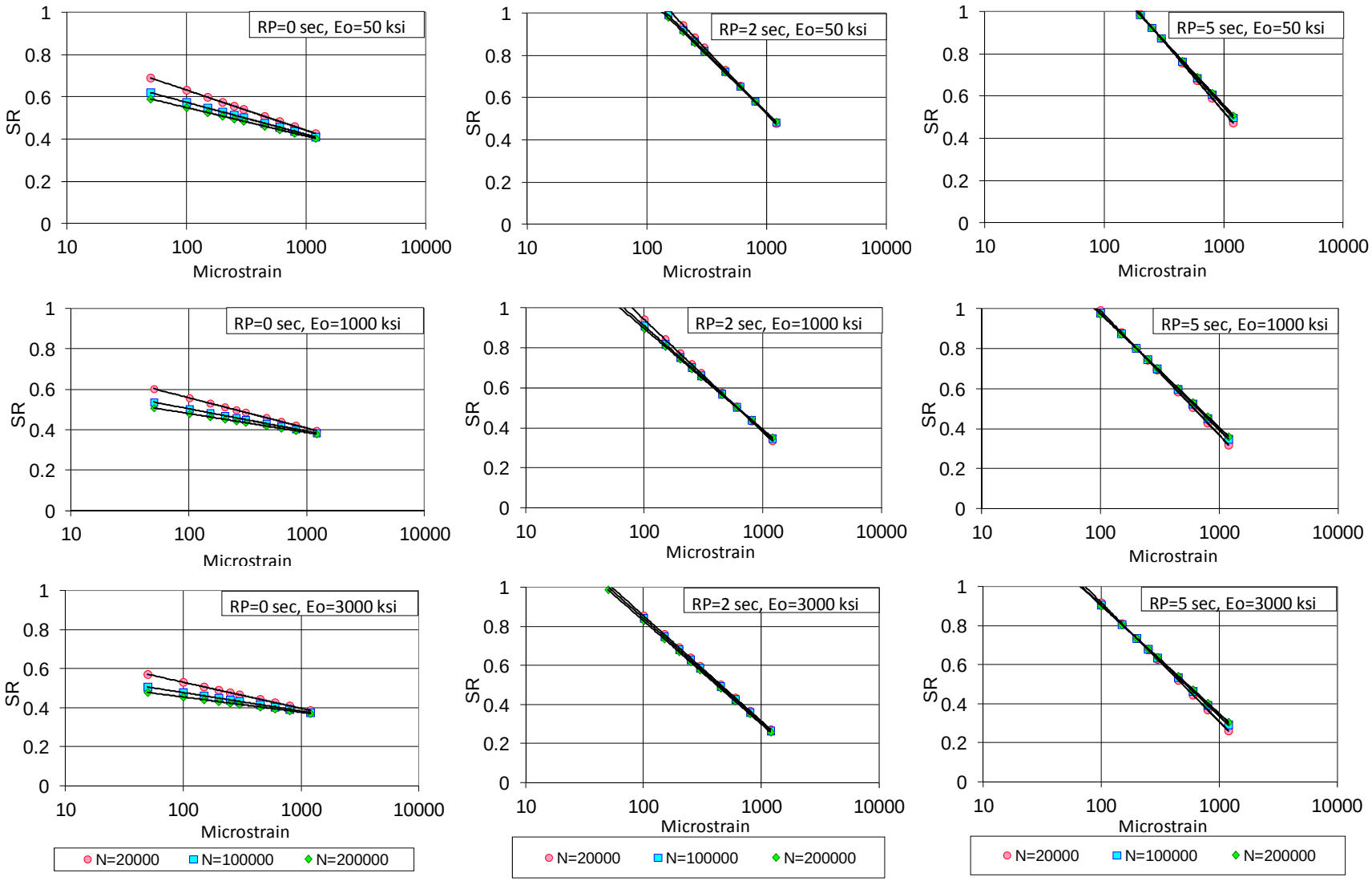

Figure 71. SR vs. ε at different values of rest period, stiffness and N.

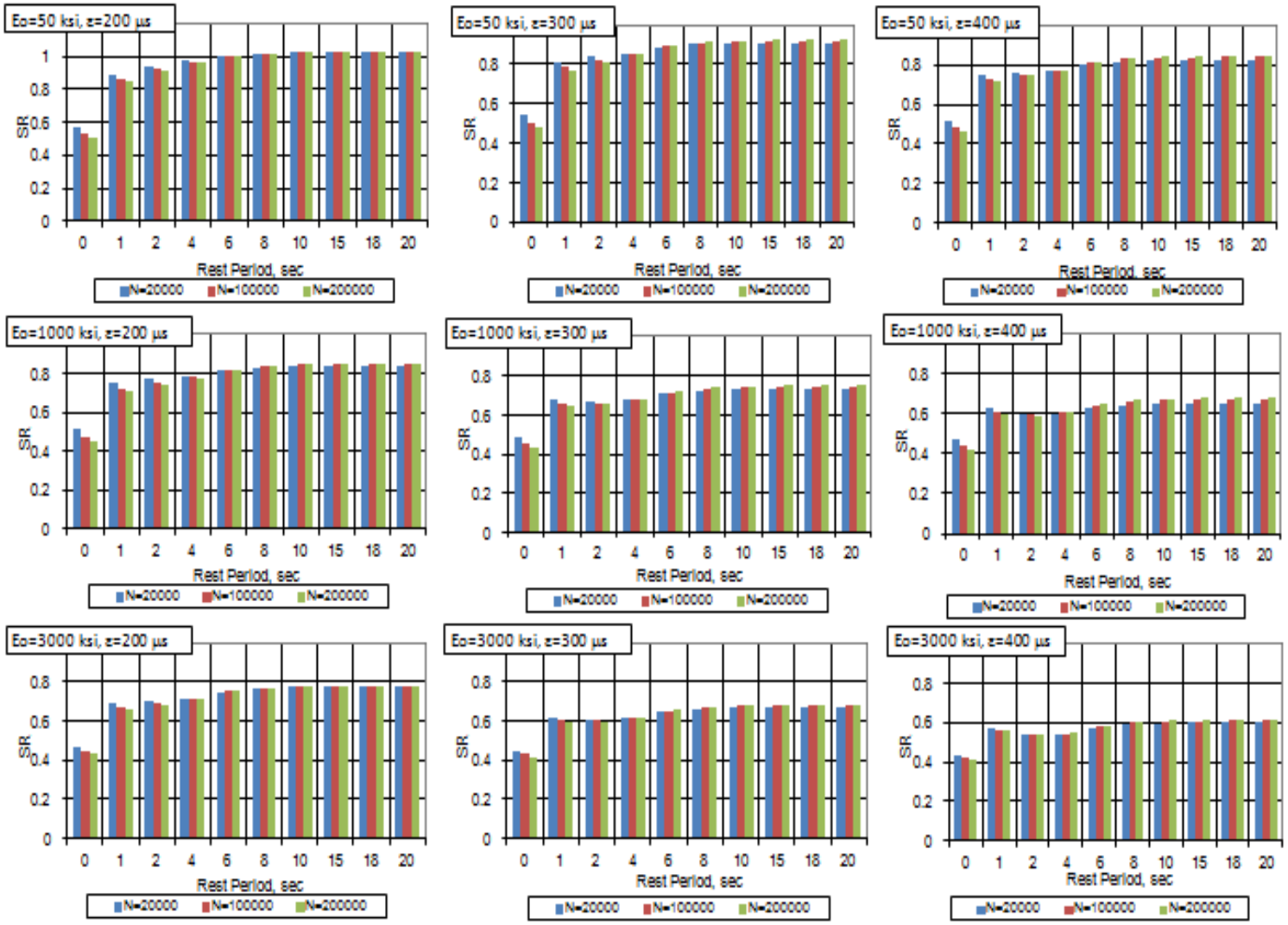

Figure 72. SR vs. rest period at different values of strain, stiffness and N.

Predicting Endurance Limit Using Third Generation SR Model

Figure 73 to Figure 77 demonstrate stiffness ratio versus strain level at several rest periods. The endurance limit occurs when complete healing happens during the rest period at an SR value of 1.0.

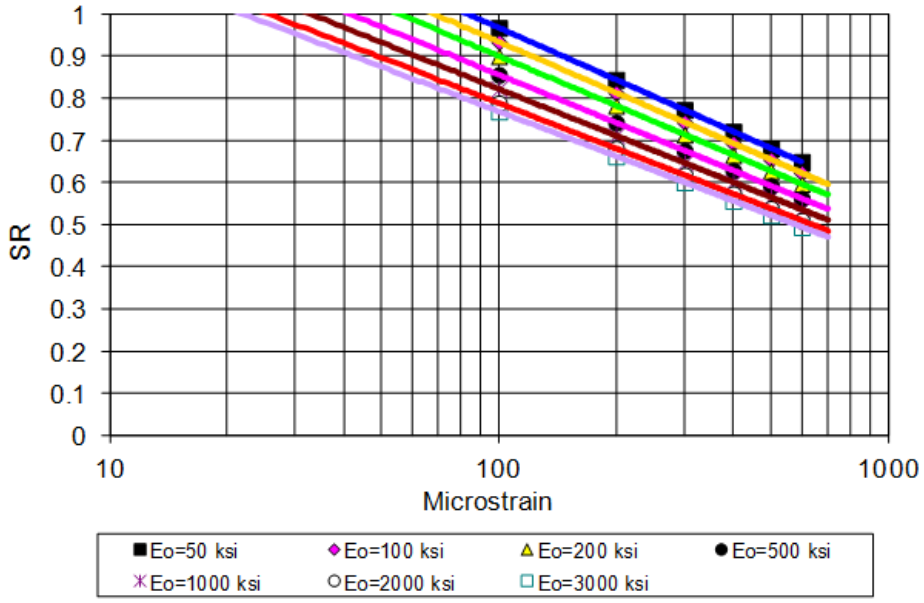

Figure 73. Strain versus SR for several initial stiffness values (RP = 1 sec, N=200,000 cycles).

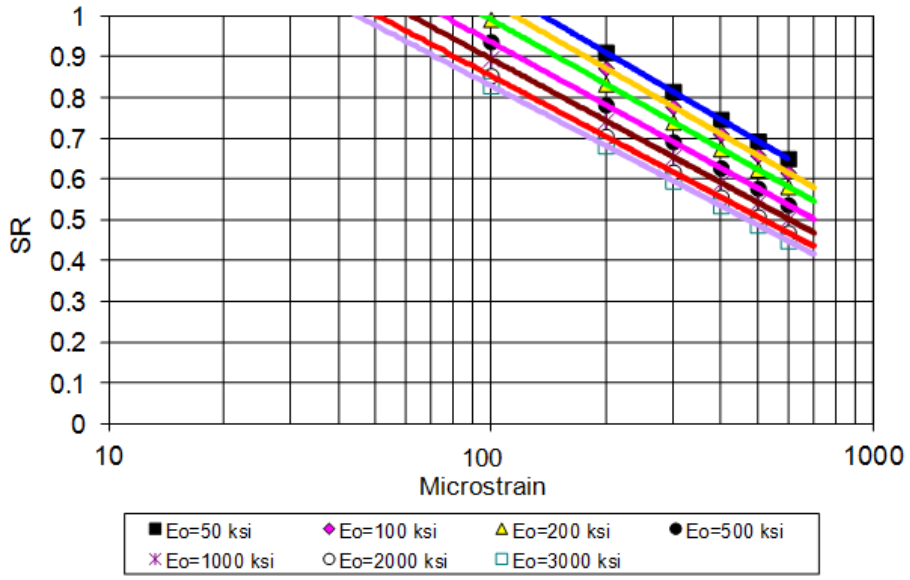

Figure 74. Strain versus SR for several initial stiffness values (RP = 2 sec, N=200,000 cycles).

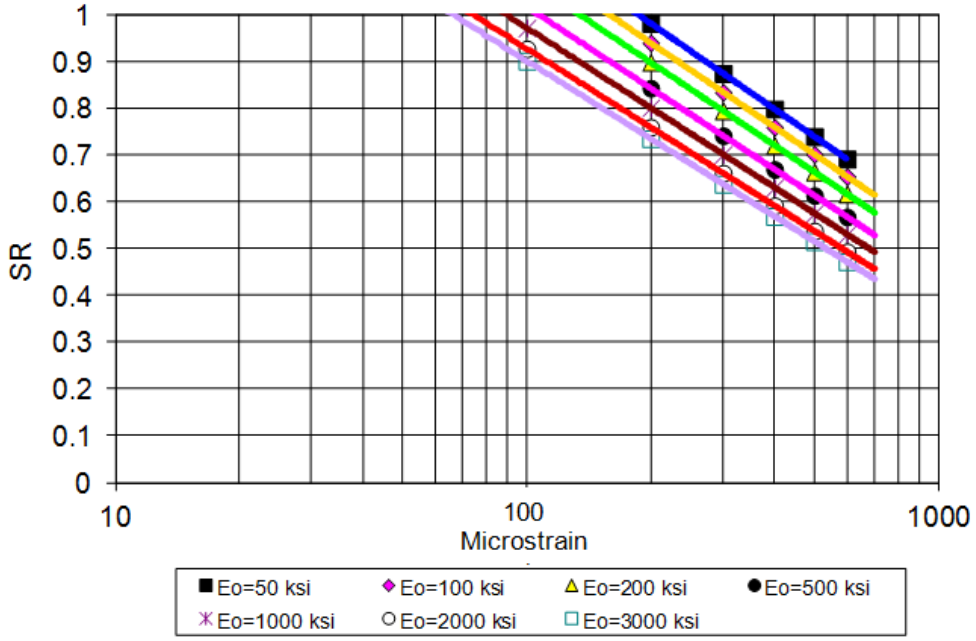

Figure 75. Strain versus SR for several initial stiffness values (RP = 5 sec, N=200,000 cycles).

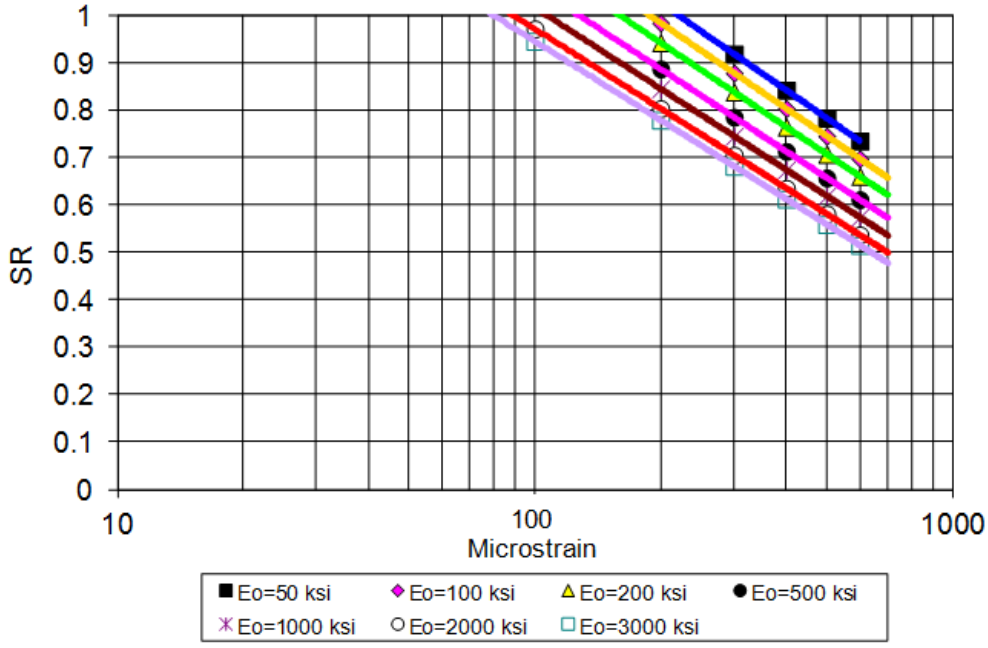

Figure 76. Strain versus SR for several initial stiffness values (RP = 10 sec, N=200,000 cycles).

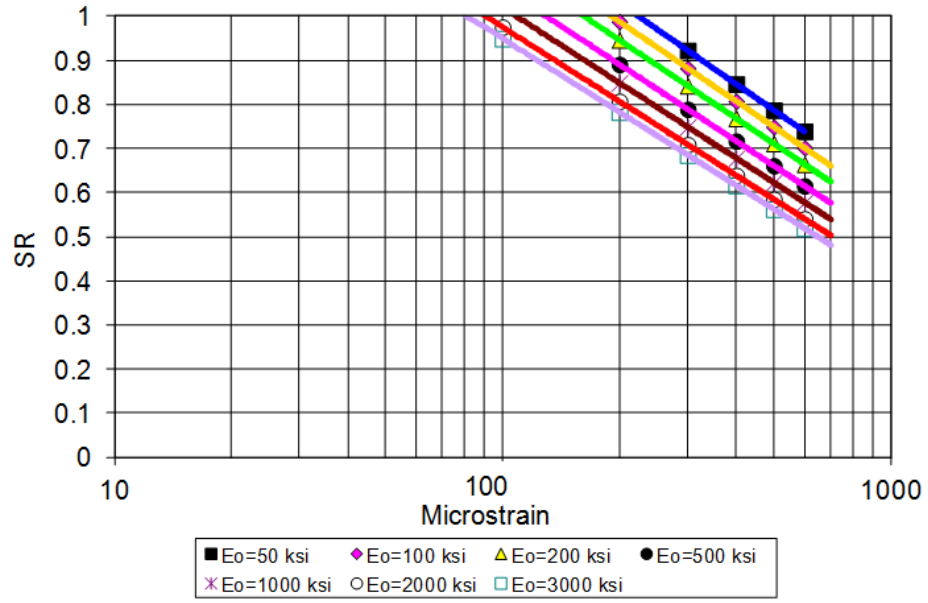

Figure 77. Strain versus SR for several initial stiffness values (RP = 20 sec, N=200,000 cycles).

Figure 78 illustrates the summary of the endurance limit values for several rest periods and stiffness levels. The endurance limit values ranged from 22 microstrain (1 seconds rest period and 3,000 ksi stiffness) to 223 microstrain (20 seconds and 50 ksi stiffness). It was noticed that the endurance limit values at rest periods of 10 and 20 seconds were the same. This indicates that no more improvement on endurance limit occurs beyond 10 seconds.

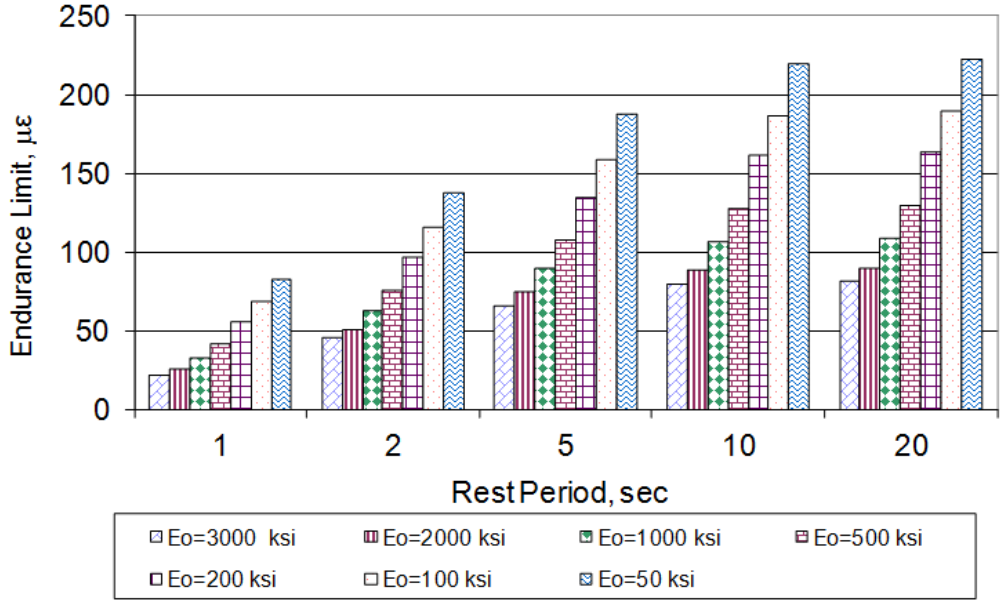

Figure 78. Summary of endurance limit values versus several rest periods and stiffness values (based on third generation SR model).

Comparison between Endurance Limits of Second and Third Generation Models

After developing the third generation model, it was important to compare the predicted endurance limit values between this model and the second generation model developed in Section 7.4.3 because of their similarities. Table 28 compares predicted endurance limit values from the two models at several values of rest period and stiffness. The table shows that the percent difference between the endurance limits of the second and third models ranges from -18% – 9%. It can be concluded that both models produce comparable endurance limit results.

Table 28. Predeicted Endurance Limit Values using the Second and Third Generation SR models.

Rest Period, Sec	Stiffness, ksi	Predicted EL, με		Percent Difference*
		Second Generation	Third Generation	
1	3,000	26	22	-18
1	2,000	30	26	-16
1	1,000	37	32	-14
1	500	46	41	-12
1	200	59	56	-6
1	100	71	69	-3
1	50	85	82	-3
2	3,000	47	45	-4
2	2,000	53	51	-5
2	1,000	64	62	-3
2	500	76	76	0
2	200	96	96	0
2	100	114	115	1
2	50	133	138	3
5	3,000	66	66	0
5	2,000	74	74	0
5	1,000	88	90	2
5	500	104	108	3
5	200	130	134	3
5	100	152	159	4
5	50	177	187	6
10	3,000	76	80	5
10	2,000	85	88	4
10	1,000	101	106	5
10	500	119	127	7
10	200	148	161	8
10	100	173	187	7
10	50	202	220	8
20	3,000	77	81	5
20	2,000	86	90	4
20	1,000	102	108	6
20	500	121	129	6
20	200	150	164	8
20	100	175	190	8
20	50	204	223	9

*Percent Difference = $100 * (EL_{3rd\ gen} - EL_{2nd\ gen}) / EL_{3rd\ gen}$

CHAPTER 8

INCORPORATING ENDURANCE LIMIT IN THE MEPDG

After developing the third generation stiffness ratio model (Equation 36), the predicted endurance limit values were incorporated in the strain-N_f fatigue relationships in the NCHRP MEPDG software.

INCORPORATING ENDURANCE LIMIT IN STRAIN-N_F FATIGUE RELATIONSHIPS

The third generation model developed in this project (Equation 36) has the following form:

$$SR = f(E_o, \varepsilon, N, RP) \quad (37)$$

where,

SR = Stiffness ratio = 1 – Damage Level
E_o = Initial flexural stiffness
ε = Applied strain
N = Number of loading cycles to reach a certain level of damage
PR = Rest period

In an effort to better understand the basic relationship between endurance limit and the conventional ε -N_f fatigue relation, all tests that were performed at zero second rest period were used to generate a general K_1, K_2, and K_3 fatigue equation. The K_1, K_2, and K_3 coefficients were 0.009076, 3.900307, and 1.123101, respectively. The strain-N_f relations associated with these coefficients are shown on the left side of Figures 79-81.

These developed K_1, K_2, K_3 coefficients were coupled with predicted endurance limit values from the third generation SR model as illustrated in the left side of Figures 79-81.

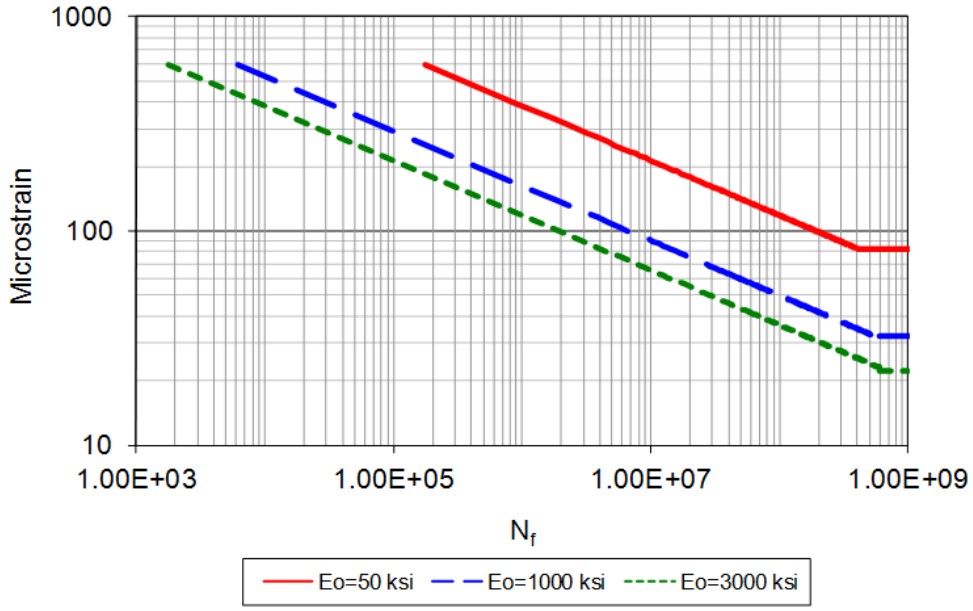

Figure 79. ε-N_f relationship for different stiffness values (Endurance Limit is calculated using the third generation model and 1 sec. rest period).

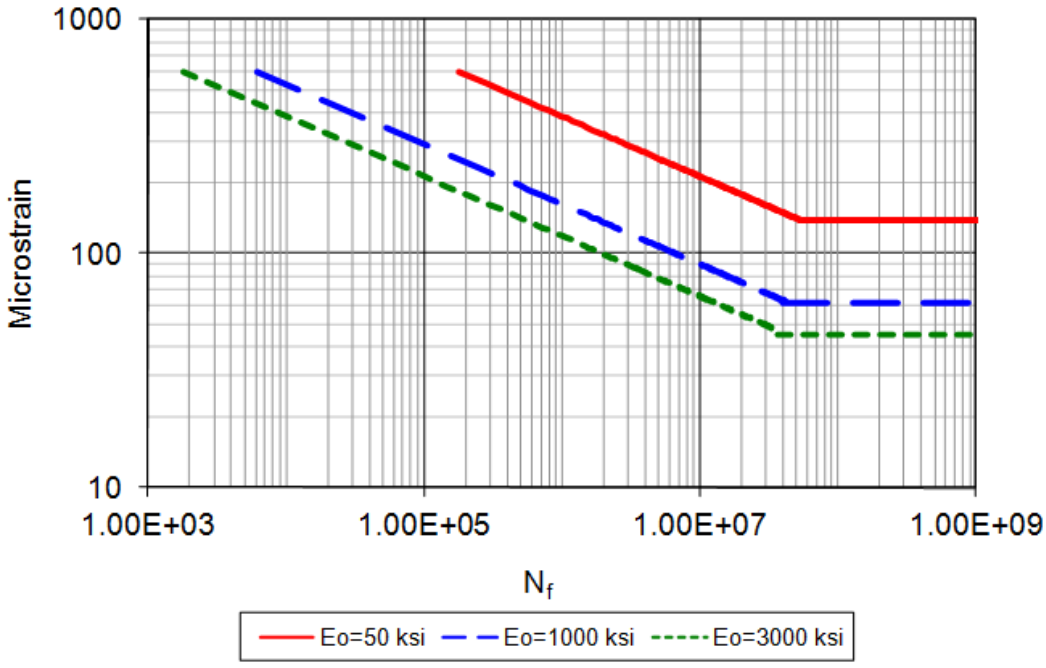

Figure 80. ε-N_f relationship for different stiffness values (Endurance Limit is calculated using the third generation model and 2 sec. rest period).

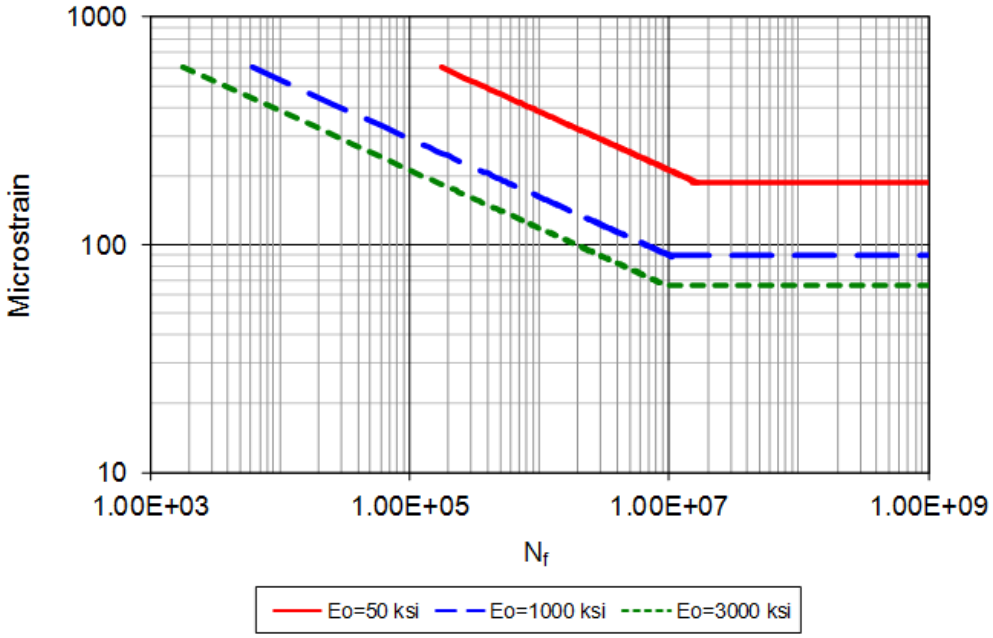

Figure 81. ε-Nf relationship for different stiffness values (Endurance Limit is calculated using the third generation model and 5 sec. rest period).

The third general model (Equation 36) was also used to determine the endurance limit, which is the strain at a combination of the following parameters:

1. Flexural stiffness.
2. A stiffness ratio of 1.0, indicating no damage.
3. Number of loading cycles. The discussion in Chapter 7 indicates that the endurance limit is not affected by the number of cycles, especially if the number of cycles is large.
4. Rest period.

The endurance limits obtained for different conditions were added to the ε-N_f relationships shown in Figures 79-81. This means that the ε-N_f curves cannot be extended to very low strain values, but need to stop once the endurance limit is reached. Thus, if the applied strain is below the endurance limit, no fatigue damage will occur. Figures 79-81 show that the endurance limit is between 22-82 microstrain for a 1 second rest period and increases to 45-138 microstrain at 2 second rest period and 66-187 microstrain at 5 second rest period. This means that increasing the spacing between trucks allows for more healing and, therefore, larger truck loads that can be accommodated without fatigue damage.

INCORPORATING ENDURANCE LIMIT IN THE MEPDG

The current MEPDG software (AASHTOWare™ Pavement ME Design™) requires the designer to input the following design parameters related to fatigue performance.

1. K_1, K_2, K_3 coefficients obtained from fatigue test results obtained from with 0 second rest period.

2. A single value of endurance limit.

In this NCHRP study, the rest period between loading cycles was introduced to match the behavior of real traffic loads in the field. The previous section shows that the endurance limit values vary depending on the rest period between loading cycles. In the MEPDG software, a simulation is performed every approximately one-fifth of a month during the pavement service life. Therefore, the incorporation of the endurance limit into the MEPDG software requires additional software to calculate endurance limit values for the rest period associated with each 2-hour MEPDG simulation and input them into the MEPDG software during the analysis process.

The parameters that are needed in the proposed software are discussed below.

Rest Period (RP)

The rest period is a function of the average annual daily truck traffic (AADTT) during the one-fifth of a month simulation period. The rest period between truck axles in seconds is calculated as an average value every simulation period. This requires calculation of the actual truck spectrum for each simulation period during each month as shown in Figure 82 and division of the month into 5 time increments.

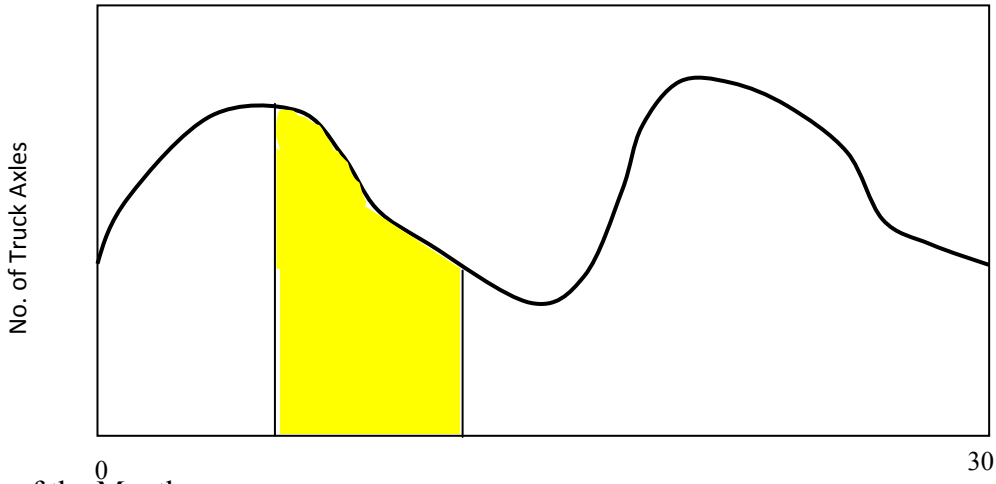

Figure 82. Example of truck axle distribution during the days of the month.

The RP value (in seconds) in this case can be calculated as follows:

$$RP = 3{,}600 \times 2 / \sum(N_T * N_A) \quad (38)$$

where,

N_T = Number of trucks in the 2-hour increment considered in the analysis

N_A = Average number of axles in each truck

K_1, K_2, K_3 Coefficients

There are two options to obtain the K_1, K_2, K_3 coefficients:

1. Use the national fatigue model coefficients available in the NCHRP MEPDG software. This can be treated as Level 3 fatigue data.
2. Perform regular fatigue tests with zero second rest period for at least two different temperatures. The strain versus N_f data points can then be input to a statistical package (for example STATISTICA) for a nonlinear estimation of the K_1, K_2, K_3 coefficients, which are specific for each mixture. This is considered the most accurate method to determine fatigue coefficients (Level 1).
3.

Endurance Limit

Similarly, the endurance limit can be obtained for every 2-hour MEPDG simulation using the third general model (Equation 36) for a stiffness ratio of 1.0 (no fatigue damage) and a large value of N such as 200,000 cycles.

Calculating Fatigue Damage

The fatigue damage is then calculated at every time increment during the MEPDG simulation. The model used for the calculation of the fatigue damage in the MEPDG is as follows:

$$N_f = C \times K_1 (1/\varepsilon_t)^{K_2} (1/E_o)^{K_3} \quad (39)$$

where:

N_f = Number of repetitions to reach fatigue failure
ε_t = Strain at the critical location
E_o = Flexure stiffness of the HMA
K_1, K_2, K_3 = Laboratory fatigue coefficients
C = Laboratory to field adjustment factor

The MEPDG software divides the HMA layer into sublayers. The JULEA program then calculates the critical tensile strain for every time increment. The estimation of the fatigue damage in the MEPDG software is based on Miner's law given by the following equation.

$$D_{i=1-T} = \Sigma (n_i / N_i) \quad (40)$$

where:

$D_{i=1-T}$ = Cumulative damage for periods 1 through T
T = Total number of periods
n_i = Actual traffic for period i

N_i = Traffic allowed under conditions prevailing in period i

The endurance limit is calculated for every time increment as discussed before. At the same time, the critical strain value of the HMA layer (or sublayer) for each truck axle for this period is calculated using the JULEA program. If the critical strain calculated from the JULEA program is less than the fatigue endurance limit, the axle should not be counted in the analysis for this period, which means that there is no fatigue damage caused by this axle. However, if the critical strain is greater than the fatigue endurance limit, the axle is counted as causing fatigue damage during this period.

CHAPTER 9

SUMMARY, FINDINGS, AND RECOMMENDATIONS FOR FUTURE RESEARCH

SUMMARY

Building perpetual pavements has been a goal of the highway community for many years. The concept of perpetual pavement requires a knowledge of the endurance limit of HMA. The main purpose of this study was to validate the endurance limit for HMA using laboratory beam fatigue tests with rest periods between loading cycles. A comprehensive study was performed to estimate the endurance limit of typical HMA due to healing that occurs during the rest periods. Six main factors were selected for evaluation: binder type, binder content, air voids, test temperature, duration of the rest period between loading cycles, and strain level. A 6-factor fractional factorial statistical design was used in order to reduce the number of tests and still obtain reliable results.

The binder and aggregate used in this study were characterized by a local commercial laboratory followed by a Superpave mix design. Before testing, the two beam fatigue machines were calibrated and several QA studies were performed to insure comparable test results and to verify the proper testing conditions. Both beam fatigue machines produced statistically the same results.

Extensive laboratory displacement-controlled flexure fatigue tests were performed according to AASHTO T3 21-03 test procedure. HMA was used with three unmodified binder types, two binder contents, two levels of air void, three levels of applied strain, three test temperatures and four values of rest periods between loading cycles. The stiffness ratio was obtained for different conditions and the healing index was determined. The results were statistically analyzed and the endurance limits were obtained at a stiffness ratio value of 1.0. The study assumes that the endurance limit is related to healing that occurs during the rest period between loading cycles. Three rational predictive model generations were developed that can predict the stiffness ratio at various test conditions which can be related to the healing gained during the rest period. The strain level that allows for complete healing was obtained to estimate the endurance limit below which a very large number of load repetitions can be applied to the pavement without fatigue damage.

After developing the third generation stiffness ratio model, the predicted endurance limit values were integrated in the strain-N_f fatigue relationships as a step toward incorporating the endurance limit in the MEPDG software.

FINDINGS

The following are the key findings of this research.

1. HMA exhibits an endurance limit that varies with mixture properties and pavement design conditions. There is no single value of the endurance limit for all conditions. The endurance limit varies depending on the applied strain, binder type, binder content, air voids, temperature, and the frequency of the load application.

2. The endurance limit ranged from 22 microstrain to 264 microstrain.
3. Softer binder mixtures exhibit higher endurance limit values than stiffer binder mixtures.
4. High binder contents and low air voids produced the highest endurance limit values compared to low binder contents and high air voids, which showed the lowest endurance limit.
5. Endurance limit values were higher at high temperatures, which correspond to soft mixtures compared to low temperatures that correspond to stiff mixtures.
6. HMA stiffness can represent the combined effect of four pavement mixture variables: binder type, binder content, air voids, and temperature.
7. The true relationship between the rest period and healing index is a tangent hyperbolic (tanh) function, which indicates that there is no additional healing gained after reaching a certain rest period. Based on the results of this study, the rest period that ensures complete healing ranges from 5 to 10 seconds based on pavement design conditions.
8. Number of loading cycles has little effect on endurance limit for tests with a rest period. This finding suggests that the endurance limit can be determined based on a relatively low number of load cycles since damage will be always healed at the end of each loading cycle.
9. The relationship between strain and number of cycles to failure for tests with rest period can be predicted for any rest period-stiffness combination by setting the stiffness ratio at 50 percent in the model.
10. The predicted endurance limit values based on second and third generation models were comparable. Therefore, either model can be used to obtain the endurance limit of typical HMAs.

Using the results of this study with the developed methodology to incorporate endurance limit in the MEPDG will enable the design of perpetual pavements that can sustain a large number of truck loads. If traffic volumes and vehicle weights are controlled, a very large number of vehicle repetitions can be applied without causing fatigue damage to the HMA layer.

RECOMMENDATIONS FOR FUTURE RESEARCH

This research effort resulted in development of a simplified integrated prediction model to predict healing and endurance limit for conventional HMA mixtures. In order to gain more understanding of the endurance limit for asphalt mixtures, the following items are recommended:

- Field validation studies are a prudent step in implementing the integrated prediction model. This might be achieved by monitoring perpetual pavements designed using the integrated prediction models developed in this study.
- A validation database may be developed to confirm that the relationship between pavement mixture parameters and endurance limit is adequate and appropriate.
- The validity of the healing-based endurance limit method to determine the endurance limit should be verified for other mix types such as warm mix asphalt, asphalt rubber, and polymer modified mixtures.

REFERENCES

1. Monismith, C. L., J. A. Epps, and F. N. Finn. “Improved Asphalt Design.” Proceedings, Journal of the Association of Asphalt Paving Technologists Vol. 54, 1985.
2. Monismith, C. L. and D. B. McLean, “Technology of Thick Lift Construction: Structural Design Considerations” Proceedings, Association of Asphalt Paving Technologists, Vol. 41, pp. 258-304, 1972.
3. Carpenter S. H. K. Ghuzlan, and S. Shen, “Fatigue Endurance Limit for Highway and Airport Pavements,” Transportation Research Record: Journal of the Transportation Research Board, No. 1832, TRB, National Research Council, Washington, D.C., pp. 131-138, 2003
4. Advanced Pavement Laboratory, National Cooperative Highway Research Program Project NCHRP 9-44, Research Plan, Washington, DC, Nov. 2008.
5. Marshall R. Thompson, Samuel H. Carpenter, “Considering Hot-Mix-Asphalt Fatigue Endurance Limit in Full-Depth Mechanistic-Empirical Pavement Design”, International conference on perpetual pavement, Ohio 2006.
6. Carpenter, S. H., and S. Shen, “A Dissipated Energy Approach to Study HMA Healing in Fatigue,” Journal of the Transportation Research Board, 2006.
7. Prowell, B. et al., “Endurance Limit of Hot Mix Asphalt Mixtures to Prevent Fatigue Cracking in Flexible Pavements,” NCHRP 9-38, Updated Draft Final Report, NCHRP, May 2008.
8. Abojaradeh, M., “Effective Fatigue Models for Arizona Asphalt Concrete Mixtures,” Ph.D. Dissertation, Arizona State University, Tempe, AZ. December 2003.
9. Long-Term Pavement Performance Program, “Distress Identification Manual for the Long-Term Pavement Performance Project,” Report No. SHRP-P-338, Strategic Highway Research Program, National Research Council, Washington, DC, 1993.
10. SHRP, A-404. "Fatigue Response of Asphalt-Aggregate Mixes". Strategic Highway Research Program, National Research Council, 1994.
11. Finn, F. N., C. L. Saraf, R. Kulkarni, K. Nair, W. Smith, and A. Abdullah. “The Use of Distress Prediction Subsystem for the Design of Pavement Structure.” Proceedings, Fourth International Conference on the Structural Design of Asphalt Pavements, University of Michigan, Ann Arbor, 1977.
12. Shell, “Shell Pavement Design Manual Asphalt Pavements and Overlays for Road Traffic,” Shell International Petroleum, London, 1978.
13. Asphalt Institute. “Research and Development of the Asphalt Institute’s Thickness Design Manual (MS-1),” Ninth Edition. Research Report No. 82-2 RR-82-2 College Park, MD Aug. 1982.
14. Chomton, J. S., and P. J. Valayer. “Applied Rheology of Asphalt Mixes, Practical Applications.” Proceedings, Third International Conference on the Structural Design of Asphalt Pavements, London, Vol. I., 1972.
15. Van Dijk, W., “Practical Fatigue Characterization of Bituminous Mixes.” Proceedings Journal of the Association of Asphalt Paving Technologists. Phoenix, Arizona, Vol. 44. , p.38, 1975.

16. Van Dijk, W., and W. Visser. "The Energy Approach to Fatigue for Pavement Design." Proceedings Journal of the Association of Asphalt Paving Technologists Vol. 46. pp. 1-40, 1977.
17. Pronk, A.C., and P.C. Hopman, "Energy Dissipation: The Leading Factor of Fatigue". Highway Research: Sharing the Benefits. Proceedings of the Conference the United States Strategic Highway Research Program. London, 1990.
18. Tayebali, A. A., J. A. Deacon, and C. L. Monismith. "Development and Evaluation of Surrogate Fatigue Models for SHRP A-003A Abridged Mix Design Procedure." Journal of the Association of Asphalt Paving Technologists Vol. 64, pp. 340-366, 1995.
19. Tayebali, A.A., John A. Deacon, John S. Coplantz, and Carl L. Monismith. "Modeling Fatigue Response of Asphalt-Aggregate Mixtures". Asphalt Paving Technology, Vol. 62, 1993.
20. NCHRP. 2004. "Guide for Mechanistic-Empirical Design of New and Rehabilitated Pavement Structures, Project 37-1A". Washington DC: National Cooperative Highway Research Program, Transportation Research Board, National Research Council.
21. Bazin, P., and J.B. Saunier. Deformability, "Fatigue and Healing Properties of Asphalt Mixes". Proceedings, Second International Conference on the Structural design of Asphalt Pavements. University of Michigan, 1967.
22. Pell, P.S. and K.E. Cooper, "The Effect of Testing and Mix Variables on the Fatigue Performance of Bituminous Materials". Proceedings, Asphalt Paving Technology, Vol. 44, 1975.
23. Tayebali, A.A., G.M. Rowe and J.B. Sousa, "Fatigue Response of Asphalt-Aggregate Mixtures". Proceedings, Asphalt Paving Technology, Vol. 61, pp. 333-360, 1992.
24. Rowe, G.M., "Performance of Asphalt Mixtures in the Trapezoidal Fatigue Test". Proceedings, Asphalt Paving Technology, Vol. 62, 1993.
25. Tangella, SCSR, et al., "Summary Report on Fatigue Response of Asphalt Mixtures," Report No. SHRP-A-312, Strategic Highway Research Program, Washington, D.C., Feb. 1990.
26. Pronk, A.C., "Comparison of 2 and 4 point fatigue tests and healing in 4 point dynamic bending test based on the dissipated energy concept". Proceedings of the eighth international conference on asphalt pavements, Seattle, Washington, pp. 987-994, 1997.
27. NCHRP Project 9-44A. Validating an Endurance Limit for HMA Pavements: Laboratory Experiment and Algorithm Development, Quarterly Progress Report, Arizona State University, Tempe, Arizona, June, 2010.
28. Tsai, B.-W., V.N. Kannekanti, and J.T. Harvey, "The Application of Genetic Algorithm in Asphalt Pavement Design," Accepted for publication by Transportation Research Record: Journal of the Transportation Research Record Board, TRB, National Research Council, Annual Meeting CD-Rom, Washington, D.C., 2004.
29. Tsai, B.-W., J.T. Harvey, and Monismith, C. L., "The Application of Weibull Theory in Asphalt Concrete Fatigue Performance Prediction," Transportation Research Record: Journal of the Transportation Research Record Board, TRB, National Research Council, Annual Meeting CD-Rom, Washington, D.C., 2003.
30. Tsai, B.-W., J.T. Harvey, and Monismith, C. L., "Characterization of Mix Fatigue Damage Process Using Three-Stage Weibull Equation and Tree-Based Model," Transportation

Research Record: Journal of the Transportation Research Record Board, TRB, National Research Council, Annual Meeting CD-Rom, Washington, D.C., 2005.
31. Biligiri, K., Kaloush, K., Mamlouk, M., Witczak, M., "Rational Modeling of Tertiary Flow for Asphalt Mixtures". Journal of the Transportation Research Board, No. 2001, pp 63-72. Washington, D.C., 2007.
32. Harvey, J., Bor-Wen Tsai. "Effect of Asphalt Content and Air Void Content on Mix Fatigue and Stiffness." Transportation Research Record No: 1543, Washington, D.C. pp. 38-45, 1996.
33. Tayebali, A. A., G.M. Rowe, and J.B. Sousa. "Fatigue Response of Asphalt Aggregate Mixtures." Journal of the Association of Asphalt Paving Technologists Vol: 61. pp. 333-360, 1994.
34. Sousa, J.B., Pais, J.C., Prates, M.,Barros, R., langlios, P., and Leclerc, AM. "Effect of Aggregate Gradation on Fatigue Life of Asphalt Concrete Mixes." Transportation Research Record No: 1630, Washington, D.C., 1998.
35. Button, J.W. and Lytton, R.L. "Evaluation of Fabrics, Fibers and Grids in Overlays". Sixth International Conference on the Structural Design of Asphalt Pavements. Ann Arbor, Michigan, 1987.
36. Pell, P.S. "Characteristics of Fatigue behavior" Highway Research Special Report No. 140, National Research Council, Washington D.C., pp. 49-64, 1973.
37. Monismith, C.L. and J.A. Deacon. "Fatigue of asphalt paving mixtures". Journal of Transportation Engineering, 95(2): pp. 317-345, 1969.
38. Monismith, C L, Secor, K E and Blackmer, W., "Asphalt mixture behaviour in repeated flexure", Proceedings of Association of Asphalt Paving Technologists, Vol. 30, pp.188-222, 1961.
39. Raithby, K.D. and A.B. Sterling "The effect of rest periods on the fatigue performance of a hot-rolled asphalt under repeated loading". Journal of the Association of Asphalt Paving Technologists, 39: 134-152, 1970.
40. McElvane, J., and Pell, P. S. "Fatigue Damage of Asphalt, Effect of Rest Periods." Highways and Road Construction, 1973.
41. Verstraeten, J., J. E. Romain, and V. Veverka, "The Belgian Road Research Center's Overall Approach Structural Design", Fourth International Conference on The Structural Design of Asphalt Pavements, Vol. 1, Proc., Ann Arbor, MI, Aug 1977.
42. Francken, L., "Fatigue Performance of Bituminous Road Mix under Realistic Conditions" Transportation Research Record 712. Washington D.C., pp.30-37, 1979.
43. Hsu, T. W. and K. H. Tseng, "Effect of Rest Periods on Fatigue Response of Asphalt Concrete Mixtures." Journal of Transportation Engineering, ASCE. Vol. 122, No. 4, 1996.
44. Breysse, D.; C. De La Roche, V. Domec and J.J. Chauvin. "Influence of rest time on recovery and damage during fatigue testes on bituminous composites". In Materials and Structures, Vol. 36, pp. 648-651, 2003.
45. Castro, M. and Sanchez, J.A. Fatigue and Healing of Asphalt Mixtures: Discriminate Analysis of Fatigue Curves, Journal of Transportation Engineering, ASCE, Vol. 132, No. 2, pp. 168-174, 2006.

46. Raithby, K. D. and Sterling, A. B. “Some Effects of Loading History on the Performance of Rolled Asphalt”, TRRL-LR 496, Crowthorne, England, 1972.
47. Bonnaure, F., Huibbers, A.H.J.J., and Booders, A. "A Laboratory Investigation of the Influence of Rest Periods on Fatigue Characteristics of Bituminous Mixes." Proceedings, the Association of Asphalt Paving Technologists, Vol. 51, 104, 1982.
48. Harvey, J., "University of California - Berkeley SHRP A-003A Asphalt Concrete Specimen Preparation Manual, Version 3.0," SHRP Technical Memorandum No. TMUCB- A-003A-91-2, Berkeley, 1991.
49. Pell, P. S. and Hanson, J. M. "Behavior of Bituminous Road Base Materials under Repeated Loading," Proceedings, Association of Asphalt Paving Technologists, 201, 229, 1973.
50. Bonnot, J. "Asphalt Aggregate Mixtures." Transportation Research Record1096, Transportation Research Board, Washington, D. C., pp. 42-50, 1986.
51. Majidzadeh, K., Kauffmann, E. M., and Ramsamooj, D. V. “Application of fracture mechanics in the analysis of pavement fatigue.” Proc., Association of Asphalt Paving Technologists, Association of Asphalt Paving Technologists, White Bear Lake, Minn., 40, 227–246, 1971.
52. Barksdale, R.D. and Miller, J. H., III. “Development of Equipment and Techniques for Evaluating Fatigue and Rutting Characteristics of Asphalt Concrete Mixes”. Report SCEGIT-77-147. School of Civil Engineering, Georgia Institute of Technology, Atlanta, 1977.
53. Sousa, J.B. “Dynamic Properties of Pavement Materials.” Ph.D. thesis, University of California, Berkeley, 1986.
54. Raithby, K. D. and Ramshaw, J. T. “Effect of Secondary Compaction on the Fatigue Performance of a Hot-Rolled Asphalt, TRRL-LR 471, Crowthorne, England, 1972.
55. Kunst, P.A.J.C. “Surface Cracking on Asphalt Layers, Working Committee B12, Hoevelaken, Holland, 1989.
56. Kennedy, T. W. "Characterization of Asphalt Pavement Materials Using the Indirect Tensile Test," Proceedings, The Association of Asphalt Paving Technologists, Vol. 56, 1977.
57. Moore, R. K. and T. W. Kennedy. “Tensile Behavior of Subbase Materials under Repetitive Loading.” Research Report 98-12, Center for Highway Research, University of Texas at Austin, Austin, TX, 1971.
58. Navarro, D. and T, W. Kennedy. "Fatigue and Repeated-Load Elastic Characteristics of In-service Asphalt-Treated Pavement.” Research Report No.183-2, Center for Highway Research, the University of Texas at Austin, 1975.
59. Cowher, K. “Cumulative Damage of Asphalt Materials under Repeated-Load Indirect Tension.” Research Report Number 183-3. Center for Highway Research – University of Texas at Austin, 1975.
60. Suresh, S., “Fatigue of Materials” 2nd Edition. Cambridge University Press, USA, pp 1-679, 1998.
61. Phillips, M.C. Multi-Step Models for Fatigue and Healing, and Binder Properties Involved in Healing. Proceedings, Eurobitume Workshop on Performance Related Properties for Bituminous Binders, Luxembourg, Paper No. 115, 1998.

62. Jacobs, M.M.J. “Crack Growth in Asphaltic Mixes,” PhD. Thesis, Delft University of Technology, Netherlands, 1995.
63. Lytton, R. L. “Characterizing Asphalt Pavements for Performance” Transportation Research Record, 1767, Transportation Research Board, Washington, D. C., pp. 5-16, 2000.
64. S. Pager and M. Tirrell, J. Chem. Phys., 5194-5198, 1981.
65. Peterson J.C., “Chemical Composition of Asphalt Related to Asphalt Durability: State of the Art”, Transportation Research Record, Vol #999, 1984.
66. Ensley, Keith E. "A Kinetic Investigation of Association in Asphalt," Colloid Interface Sci., vol. 53, pp. 452-460, 1975.
67. Kim, Y.R., D.N. Little, and F.C. Benson “Chemical And Mechanical Evaluation On Healing Mechanism Of Asphalt Concrete”. Journal of the Association of Asphalt Paving Technologists (AAPT), Vol. 59. pp. 241-276, 1990.
68. Bazin, P., and Saunier, J.B. "Deformability, fatigue and healing properties of asphalt mixes." Proceedings of the Second International Conference on the Structural Design of Asphalt Pavements, Ann Arbor, Michigan, USA, pp. 553-569. 1967.
69. Kim, Y, R. and Little, D, N. “Evaluation of Healing in asphalt concrete by means of the theory of nonlinear viscoelasticity”, Journal of Transportation Research Record: Transportation Research Board, No. 1228, pp. 198-210, 1989.
70. Kim, Y., Little, D. N. and Lytton, R. L. “Effect of Moisture Damage on Material Properties and Fatigue Resistance of Asphalt Mixtures.” In Transportation Research Record 1832, TRB, National Research Council, Washington, D.C., pp. 48-54, 2004.
71. Kim, Y. and Y.R. Kim, "Evaluation of Microcrack Damage Growth and Healing of Asphalt Concrete Pavements Using Stress Wave Method," Proceedings of the 11th ASCE Engineering Mechanics Specialty Conference, pp. 612-615, 1996.
72. Schapery R. A. Correspondence Principles and a Generalized J-Integral for Large Deformation and Fracture Analysis of Viscoelastic Media, International Journal of Fracture Mechanics, Vol. 25, No. 3, pp. 195-223, 1984.
73. Schapery, R. A. ‘‘On the mechanics of crack closing and bonding in linear viscoelastic media.’’ International Journal of Fracture, 39, pp. 163–183, 1989.
74. Wöhler, A. "Versuche uber die Festigkeit der Eisenbahnwagenachsen"; English summary (1867). Engineering, 4, 160-161, 1860.
75. Prot, E. M. "Rev Metallurgie." translated by Ward, E.J. WADC Tech Rep, pp. 52-148, 1948.
76. Lagace, P. A., and Allen, M. W. "Evaluation of the Alternative Manufacturing Methods for Bonding Graphite/epoxy composites." 30th National SAMPE Symposium, 1985.
77. Monismith, C. L., and D. B. McLean, “Structural Design Considerations”, Proceedings of the Association of Asphalt Paving Technologists, Vol. 41, 1972.
78. Maupin, G. W., Jr. and J. R. Freeman, Jr. “Simple Procedure for Fatigue Characterization of Bituminous Concrete” Final Report No. FHWA-RD-76-102, Federal Highway Administration, Washington, DC 1976.
79. Nunn, M. “Long-life Flexible Roads”. Proceedings of the 8th International Conference on Asphalt Pavements, Vol. 1. University of Washington, Seattle, WA, Pp. 3-16, August 1997.

80. Nishizawa, T., S. Shimeno, and M. Sekiguchi. “Fatigue Analysis of Asphalt Pavements with Thick Asphalt Mixture Layer”, Proceedings of the 8th International Conference on Asphalt Pavements, Vol. 2. University of Washington, Seattle, WA,. Pp. 969-976, August 1997.
81. Wu, Z., Z. Q. Siddique, and A. J. Gisi. “Kansas Turnpike – An Example of Long Lasting Asphalt Pavement”. Proceedings International Symposium on Design and Construction of Long Lasting Asphalt Pavements. National Center for Asphalt Technology, Auburn, Pp. 857-876, AL 2004.
82. Mahoney, J. P., “Study of Long-Lasting Pavements in Washington State, Transportation Research Circular No. 503”, Perpetual Bituminous Pavements, Transportation Research Board, pp 88-95, Washington, DC 2001.
83. Newcomb, D. Perpetual Pavements: A Synthesis. APA 101, Asphalt Pavement Alliance, Lanham, MD 2002.
84. Monismith, C. L., J. A. Epps, et al., "Asphalt Mixture Behavior in Repeated Flexure." Report No. TE 70-5, Institute of Transportation and Traffic Engineering, University of California, Berkley, 303 pp., 1970.
85. Monismith, C. L., and Long, F., "Overlay Design for Cracked and Seated Portland Cement Concrete (PCC) Pavement—Interstate Route 710." Technical Memorandum TM UCB PRC99-3, Pavement Research Center, Institute for Transportation Studies, University of California, Berkeley, 1999.
86. Von Quintus, Harold L., J.A. Scherocman, C.S. Hughes, and T.W. Kennedy, Asphalt-Aggregate Mixture Analysis System: AAMAS, NCHRP Report No. 338, National Cooperative Highway Research Program, National Research Council, Washington, DC, March 1991.
87. Von Quintus, Harold L. “Application of the Endurance Limit Premise in Mechanistic-Empirical Based Pavement Design Procedures”, July 2006.
88. Carpenter, S.H. “Fatigue Performance of IDOT Mixtures, Civil Engineering Studies”, Illinois Center for Transportation Series No 07.-007, University of Illinois at Urbana-Champaign, July, 2006.
89. Newcomb, D.E., Buncher, M., and Huddleston, I.J., “Concepts of Perpetual Pavements,” Transportation Research Circular Number 503, Perpetual Bituminous Pavements, Transportation Research Board, Washington, D.C., December, 2001.
90. Advanced Asphalt Technologies, LLC, “Hot Mix Asphalt Endurance Limit Workshop: Executive Summary,” National Cooperative Highway Research Program Project 9-44, November, 2007.
91. Kim, B. and Roque, R., “Evaluation of Healing Property of Asphalt Mixtures,” Transportation Research Record No. 1970, Transportation Research Board, Washington, D.C., 2006.
92. Romanoschi, S., Gisi, A., Portillo, M., and Dumitru, C., “First Findings from the Kansas Perpetual Pavements Experiment” Transportation Research Record: Journal of the Transportation Research Board, No. 2068, Washington, D.C., 2008, pp. 41–48.
93. Bhattacharjee, S., Swamy, A., and Daniel, J., “Application of Elastic–Viscoelastic Correspondence Principle to Determine Fatigue Endurance Limit of Hot-Mix Asphalt”.

Transportation Research Record: Journal of the Transportation Research Board, No. 2126, Washington, D.C., 2009, pp. 12–18.
94. Nunn, M. and Ferne, B.W., "Design and Assessment of Long-Life Flexible Pavements," Transportation Research Circular Number 503, Perpetual Bituminous Pavements, Transportation Research Board, Washington, D.C., December, 2001.
95. Brown, S.R., Thom, N.H., and Hakim, B.A., "Performance and Rehabilitation of Heavy-duty Pavements in the UK: Some Case Studies," Proceedings, International Symposium of Design and Construction of Long Lasting Asphalt Pavements, National Center for Asphalt Technology, Auburn, AL, 2004.
96. Uhlmeyer, J.S., Willoughby, K., Pierce, L.M., and Mahoney, J.P., "Top-Down Cracking in Washington State Asphalt Concrete Wearing Courses," Transportation Research Record No. 1730, Transportation Research Board, Washington, D.C., 2000.
97. R.L. Plackett and J.P. Burman, "The Design of Optimum Multifactorial Experiments", Biometrika 33 (4), pp. 305-25, June 1946.
98. JMP software, SAS Institute Inc, http://www.jmp.com/.
99. Montgomery, Douglas C., Design and Analysis of Experiments, Wiley, 2008.
100. Uniform Standard Specifications for Public Works Construction Sponsored and Distributed By the Maricopa Association of Governments, 2011, AZ.
101. AASHTO Designation: T321-03. Determining the Fatigue Life of Compacted Hot-Mix Asphalt (HMA) Subjected to Repeated Flexural Bending.
102. SHRP Designation: M-009. Standard Method of Test for Determining the Fatigue Life of Compacted Bituminous Mixtures Subjected to Repeated Flexural Bending.
103. Harvey, J., et al., "Evaluation of Fatigue and Permanent Deformation Properties of Several Asphalt-Aggregate Field Mixes Using Strategic Highway Research Program A-003A Equipment," Record 1454, Transportation Research Board, Washington, D.C., 1994.
104. American Association of State Highway and Transportation Officials. "Mixture Conditioning of Hot Mix Asphalt (HMA)" Standard Practice AASHTO R 30, Washington D.C.
105. American Association of State Highway and Transportation Officials. "Theoretical Maximum Specific Gravity And Density Of Bituminous Paving Mixtures" Test Method AASHTO T 209, Washington D.C.,
106. American Association of State Highway and Transportation Officials. Bulk Specific Gravity of Bituminous Mixtures Using Saturated Surface Dry Specimens, Test Method AASHTO T 166 – 00, Standard Specifications for Transportation Materials and Methods of Sampling and Testing, Part II – Tests, Twentieth Edition, 2000.
107. Montgomery, D. C., Design and Analysis of Experiments, Wiley, 2008.
108. ASTM, "Standard Test Method for Determining Fatigue Failure of Compacted Asphalt Concrete Subjected to Repeated Flexural Bending," Test method ASTM D7460, ASTM International, 100 Barr Harbor Drive, West Conshohocken, Pennsylvania, USA.
109. Pronk A.C., "Haversine Fatigue Testing in Controlled Deflection Mode: Is It Possible?" Presented at the Transportation Research Board meeting, 2010.
110. Pronk A.C. and S.M.J.G Erkens., "A note on fatigue bending tests using a haversine loading", International Journal on Road Design, Vol. 2, Issue 4, 2001.

111. Shen, S. and S. H. Carpenter, “Application of Dissipated Energy Concept in Fatigue Endurance Limit Testing,” Transportation Research Record, Journal of Transportation Research Board, No. 1929, pp. 165 – 173, 2005.
112. AASHTO Provisional Standards, "Standard Test Method for Determination the Fatigue Life of Compacted Hot Mix Asphalt (HMA) Subjected to Repeated Flexural Bending". TP8-94, September 1994.
113. Ghuzlan, K., S.H. Carpenter, “Energy-Derived, Damage-Based Failure Criterion for Fatigue Testing”. Transportation Research Record No: 1723, Washington, D.C., pp. 141-149, 2001.
114. Pronk, A. C., and P. C. Hopman. “Energy Dissipation: The Leading Factor of Fatigue.” Proceedings, United State Strategic Highway Research Program – Sharing the Benefits, October 29-31 London, 1990.
115. Asphalt Institute. “Thickness Design Asphalt Pavements for Highways and Streets.” Manual Series No.1, MS-1. Lexington, KY. 1991.
116. Huang, Y.H. “Pavement Analysis and Design,” Prentice Hall, Englewood Cliffs, N.J. 1993.
117. Van Dijk, W., and W. Visser. “The Energy Approach to Fatigue for Pavement Design.” Proceedings Journal of the Association of Asphalt Paving Technologists Vol. 46. pp. 1-40, 1977.
118. Rowe, G. M., and M. G. Bouldin. “Improved Techniques to Evaluate the Fatigue Resistance of Asphalt Mixtures”. EUROBITUME Conference Barcelona, Spain, September 2000.
119. Epps, J.A. and C.L. Monismith. “Influence of mixture variables on the flexural fatigue properties of asphalt concrete”. Journal of the Association of Asphalt Paving Technologists, 38: 423-464, 1969.
120. Monismith, C. L. “Asphalt Mixture Behavior in Repeated Flexure, Report No. TE 66-66, ITIE”, to California Division of Highways, University of California, 1966.
121. Said, S.F., “Variable in Roadbase Layer Properties Conducting Indirect Tensile Test”, Eight International Conference on The Structural Design of Asphalt Pavements, Vol. 2 Proc., Seattle, Washington, August 1997.
122. Verstraeten, J., “Influence des caractéristiques du bitume sur les propriétés en fatigue des mélanges bitumineux”. RILEM, 1976.
123. W. N. Houston, M. W. Mirza, C. E. Zapata, and S. Raghavendra “Simulating The Effects Of Hot Mix Asphalt Aging For Performance Testing And Pavement Structural Design” NCHR Research Results Digest 324, October 2007.
124. NCHRP Project 944-A. Validating an Endurance Limit for HMA Pavements: Laboratory Experiment and Algorithm Development, Quarterly Progress Report, Arizona State University, Tempe, Arizona, June, 2010.
125. Stat-Ease, Inc. http://www.statease.com/
126. Box, G. E. P., Cox, D. R., “An Analysis of Transformations”, Journal of the Royal Statistical Society, Series B 26(2), pp.211-252, 1964.
127. Montgomery, D. C., Peck, E. A., and Vining, G. G., Introduction to Linear Regression Analysis, Wiley, 2001.

128. STATISTICA software, StateSoft, http://www.statsoft.com/#.
129. Minitabe software, http://www.minitab.com/en-US/default.aspx

APPENDIX A
SUMMARY OF BEAM FATIGUE TEST RESULTS

Table A1 is a summary of results obtained from the beam fatigue experiment. The following is a description of the different columns used in the table.

- Serial Number.
- Specimen ID: Actual ID marked on each specimen for identification.
- Machine Used: IPC-1 and IPC-2.
- Temperature: Three test temperatures of 40, 70, and 100 F were used.
- PG Binder Grade: PG 76-16, PG 64-22, and PG 58-22.
- AC%: Two binder contents of 4.2 and 5.2 % were used.
- Target V_a%: 4.5 and 9.5%.
- Measured V_a%: Actual air void of each specimen.
- Applied Strain: A constant-strain sinusoidal loading was applied at a frequency of 10 Hz according to the AASHTO T-321 procedure. The values shown in the table are half of the peak-to-peak values.
- Initial Stress: The tensile stress calculated at the 50^{th} cycle of each test.
- Initial Stiffness: The initial flexural stiffness calculated at the 50^{th} cycle of each test. The relationships between strain, stress and flexural stiffness are shown in Equations A-1, A-2 and A-3.

$$\varepsilon_t = 12\,\delta\,h / (3\,L^2 - 4\,a^2) \quad \text{(A-1)}$$

$$\sigma_t = 3\,a\,P / b\,h^2 \quad \text{(A-2)}$$

$$S_o = \sigma_t / \varepsilon_t \quad \text{(A-3)}$$

where,

ε_t = Applied strain
σ_t = Initial stress
S_o = Initial flexural stiffness
P = Load
b = Average specimen width
h = Average specimen height
δ = deflection at the center of the beam
a = Space between inside clamps
L = Length of beam between outside clamps

- Rest Period: 0, 1, 5, and 10 seconds.
- N_f (at SR=0.5): All tests without rest period were conducted until failure (stiffness ratio of 0.5). Values shown in this column are for tests without rest period only.
- Cycle Number: Three points were selected on the SR-N relationship for each test, at which the stiffness ratios were used in the analysis. Two of these points were taken

during the test, while the third point was taken at $N_{f\ w/o\ RP}$. Note that the results of the tests with rest period were extrapolated to $N_{f\ w/o\ RP}$ as discussed in Chapter 7.

- Stiffness Ratio at Cycle Number: The stiffness ratios at the corresponding cycle numbers are recorded in the table and used in the analysis.

Table A1. Beam Fatigue Test Results

Serial Number	Specimen ID	Machine Used	Temperature, F	PG Binder Grade	AC %	Target V_a %	Measured V_a %	Applied Strain, με	Initial Stress, psi	Initial Stiffness, ksi	Rest Period, Sec	N_f (at SR=0.5)	Cycles Number			Stiffness Ratio at Cycle Number		
													N_1	N_2	N_3	SR_{N1}	SR_{N2}	SR_{N3}
1	21	IPC-1	40	76-16	4.2	4.5	5.541	175	294.5	1682.8	0	27676	24405			0.527		
2	24	IPC-1	40	76-16	4.2	4.5		175	339.6	1940.7	0	32190	24405			0.531		
3	17	IPC-2	40	76-16	4.2	4.5	5.227	175	391.8	2238.9	0	13350	24405			0.464		
4	7	IPC-1	40	76-16	4.2	9.5	10.31	137.5	185.1	1346.3	0	286070	231971			0.531		
5	16	IPC-2	40	76-16	4.2	9.5	10.3	137.5	206.1	1499.2	0	219610	231971			0.472		
6	20	IPC-2	40	76-16	4.2	9.5	8.918	137.5	172.5	1254.7	0	190232	231971			0.454		
7	22	IPC-2	40	76-16	5.2	4.5	4.339	137.5	223.8	1627.7	0	342760	341261			0.500		
8	6	IPC-1	40	76-16	5.2	4.5	5.55	137.5	226.8	1649.1	0	320000	341261			0.464		
9	2	IPC-1	40	76-16	5.2	4.5	4.327	137.5	245.9	1788.5	0	361023	341261			0.540		
10	20	IPC-2	40	76-16	5.2	9.5	6.201	175	233.7	1335.3	0	22790	18000			0.542		
11	23	IPC-2	40	76-16	5.2	9.5	4.859	175	194.7	1112.8	0	19590	18000			0.515		
12	9	IPC-1	40	76-16	5.2	9.5	8.797	175	263.7	1506.9	0	11620	18000			0.480		
13	20	IPC-1	70	76-16	4.2	4.5	5.256	237.5	173.6	731.03	0	14640	15757			0.462		
14	11	IPC-2	70	76-16	4.2	4.5	5.434	237.5	172.9	728.12	0	9020	15757			0.455		
15	12	IPC-2	70	76-16	4.2	4.5	5.259	237.5	203.9	858.55	0	23612	15757			0.539		
16	12	IPC-1	70	76-16	4.2	9.5	9.261	187.5	128.0	682.58	0	75470	80410			0.471		
17	24	IPC-1	70	76-16	4.2	9.5	10.2	187.5	112.3	598.79	0	94520	80410			0.531		
18	11	IPC-2	70	76-16	4.2	9.5	9.442	187.5	136.7	728.84	0	71239	80410			0.459		
19	3	IPC-1	70	76-16	5.2	4.5	4.612	187.5	152.8	814.8	0	162180	163845			0.509		
20	14	IPC-2	70	76-16	5.2	4.5	4.001	187.5	126.6	675.1	0	152896	163845			0.475		

21	16	IPC-2	70	76-16	5.2	4.5	5.023	187.5	109.7	584.88	0	176459	163845			0.527		
22	23	IPC-1	70	76-16	5.2	4.5	4.859	237.5	200.4	843.84	0	67950	50076			0.542		
23	17	IPC-2	70	76-16	5.2	4.5	4.629	237.5	122.9	517.27	0	56707	50076			0.522		
24	28	IPC-1	70	76-16	5.2	4.5	5.705	237.5	111.8	470.81	0	25570	50076			0.450		
25	7	IPC-1	70	76-16	5.2	9.5	10.84	237.5	151.3	637.19	0	15434	17388			0.479		
26	11	IPC-2	70	76-16	5.2	9.5	9.209	237.5	127.1	534.96	0	20520	17388			0.528		
27	14	IPC-2	70	76-16	5.2	9.5		237.5	115.4	485.96	0	16210	17388			0.477		
28	19	IPC-1	100	76-16	4.2	4.5	5.558	237.5	43.2	182	0	82320	132241			0.438		
29	23	IPC-2	100	76-16	4.2	4.5		237.5	47.8	201.47	0	189080	132241			0.541		
30	26	IPC-1	100	76-16	4.2	4.5	5.775	237.5	50.4	212.34	0	125324	132241			0.473		
31	17	IPC-1	100	76-16	4.2	9.5	8.606	325	53.5	164.71	0	12140	24314			0.441		
32	22	IPC-2	100	76-16	4.2	9.5	9.716	325	26.1	80.292	0	35390	24314			0.543		
33	4	IPC-2	100	76-16	4.2	9.5	8.596	325	35.5	109.14	0	25413	24314			0.467		
34	24	IPC-2	100	76-16	5.2	4.5	5.602	325	51.7	159.17	0	124920	125898			0.475		
35	19	IPC-1	100	76-16	5.2	4.5	6.008	325	38.2	117.46	0	132093	125898			0.518		
36	20	IPC-1	100	76-16	5.2	4.5	6.201	325	62.4	192.08	0	120680	125898			0.451		
37	22	IPC-1	100	76-16	5.2	9.5	10.31	237.5	23.0	97.007	0	191270	165576			0.531		
38	10	IPC-1	100	76-16	5.2	9.5	9.845	237.5	22.3	94.045	0	121150	165576			0.463		
39	31	IPC-2	100	76-16	5.2	9.5		237.5	25.6	107.87	0	184309	165576			0.524		
40	24	IPC-1	100	76-16	5.2	9.5	9.009	325	40.2	123.81	0	101540	105003			0.460		
41	8	IPC-1	100	76-16	5.2	9.5	9.933	325	30.4	93.668	0	115250	105003			0.527		
42	13	IPC-2	100	76-16	5.2	9.5		325	29.9	91.939	0	98220	105003			0.438		
43	9	IPC-1	40	76-16	4.2	4.5	4.925	137.5	306.7	2230.2	5		320471	10000	20000	0.743	0.829	0.811
44	10	IPC-1	40	76-16	4.2	4.5	5.63	137.5	262.4	1908	5		320471	10000	20000	0.726	0.818	0.799
45	14	IPC-2	40	76-16	4.2	4.5	5.695	137.5	280.7	2041.1	5		320471	10000	20000	0.749	0.833	0.816
46	1	IPC-2	40	76-16	4.2	4.5	5.015	175	350.0	2000	5		22819	10000	20000	0.699	0.731	0.704
47	4	IPC-2	40	76-16	4.2	4.5	5.775	175	339.1	1937.9	5		22819	10000	20000	0.679	0.713	0.685

48	6	IPC-1	40	76-16	4.2	4.5	5.185	175	335.7	1918.2	5		22819	10000	20000	0.696	0.729	0.701
49	8	IPC-1	40	76-16	4.2	9.5	9.39	175	213.4	1219.4	5		5000			0.717		
50	21	IPC-2	40	76-16	4.2	9.5	9.198	175	248.9	1422	5		5000			0.703		
51	15	IPC-2	40	76-16	4.2	9.5	10.25	175	263.6	1506.5	5		5000			0.695		
52	10	IPC-1	40	76-16	5.2	4.5	4.257	175	276.7	1581.4	5		24263	10000	20000	0.790	0.814	0.796
53	13	IPC-1	40	76-16	5.2	4.5	4.947	175	325.9	1862.1	5		24263	10000	20000	0.781	0.806	0.786
54	18	IPC-2	40	76-16	5.2	4.5	5.017	175	266.9	1525	5		24263	10000	20000	0.803	0.825	0.808
55	2	IPC-2	40	76-16	5.2	9.5	9.494	137.5	186.3	1354.7	5		243051	10000	20000	0.774	0.845	0.830
56	4	IPC-2	40	76-16	5.2	9.5	9.447	137.5	173.0	1258.2	5		243051	10000	20000	0.790	0.856	0.842
57	12	IPC-1	40	76-16	5.2	9.5		137.5	197.0	1432.8	5		243051	10000	20000	0.811	0.871	0.858
58	8	IPC-1	70	76-16	4.2	4.5	6.103	187.5	180.7	963.55	5		105252	10000	20000	0.726	0.796	0.775
59	5	IPC-2	70	76-16	4.2	4.5	4.478	187.5	151.3	806.97	5		105252	10000	20000	0.741	0.807	0.787
60	13	IPC-2	70	76-16	4.2	4.5	5.31	187.5	136.8	729.78	5		105252	10000	20000	0.762	0.822	0.805
61	13	IPC-1	70	76-16	4.2	9.5		237.5	173.1	728.93	5		11104	3000	5000	0.680	0.740	0.717
62	1	IPC-2	70	76-16	4.2	9.5	10.07	237.5	139.0	585.37	5		11104	3000	5000	0.692	0.750	0.727
63	6	IPC-2	70	76-16	4.2	9.5	9.633	237.5	198.9	837.52	5		11104	3000	5000	0.650	0.715	0.690
64	1	IPC-1	70	76-16	5.2	4.5	4.621	187.5	152.0	810.7	5		195502	10000	20000	0.811	0.869	0.856
65	5	IPC-2	70	76-16	5.2	4.5	5.305	187.5	134.5	717.47	5		195502	10000	20000	0.801	0.861	0.847
66	9	IPC-2	70	76-16	5.2	4.5	5.744	187.5	149.0	794.4	5		195502	10000	20000	0.801	0.861	0.847
67	4	IPC-1	70	76-16	5.2	4.5	5.514	237.5	185.8	782.5	5		32445	10000	20000	0.737	0.776	0.753
68	8	IPC-1	70	76-16	5.2	4.5	5.824	237.5	181.5	764.32	5		32445	10000	20000	0.717	0.758	0.734
69	21	IPC-2	70	76-16	5.2	4.5	5.352	237.5	175.5	738.95	5		32445	10000	20000	0.773	0.807	0.787
70	19	IPC-1	70	76-16	5.2	9.5	9.335	187.5	105.7	563.63	5		124280	10000	20000	0.766	0.828	0.811
71	15	IPC-1	70	76-16	5.2	9.5	9.277	187.5	107.4	572.85	5		124280	10000	20000	0.745	0.814	0.795
72	18	IPC-2	70	76-16	5.2	9.5	8.357	187.5	113.1	603.42	5		124280	10000	20000	0.759	0.823	0.805
73	2	IPC-1	100	76-16	4.2	4.5	4.746	237.5	57.5	241.93	5		108407	10000	20000	0.851	0.890	0.878
74	3	IPC-1	100	76-16	4.2	4.5	5.519	237.5	80.6	339.53	5		108407	10000	20000	0.863	0.899	0.888

75	7	IPC-2	100	76-16	4.2	4.5	6.33	237.5	49.5	208.41	5		108407	10000	20000	0.853	0.891	0.880
76	16	IPC-1	100	76-16	4.2	4.5	6.628	325	47.5	146.28	5		46138	10000	20000	0.722	0.772	0.749
77	18	IPC-1	100	76-16	4.2	4.5	5.455	325	72.9	224.23	5		46138	10000	20000	0.742	0.789	0.767
78	22	IPC-2	100	76-16	4.2	4.5	5.233	325	53.8	165.41	5		46138	10000	20000	0.741	0.788	0.767
79	18	IPC-1	100	76-16	4.2	9.5	9.932	237.5	45.6	192.07	5		59581	10000	20000	0.718	0.776	0.754
80	28	IPC-1	100	76-16	4.2	9.5	7.822	237.5	43.3	182.29	5		59581	10000	20000	0.750	0.801	0.781
81	23	IPC-2	100	76-16	4.2	9.5	9.727	237.5	45.0	189.34	5		59581	10000	20000	0.832	0.867	0.853
82	14	IPC-1	100	76-16	4.2	9.5	9.528	325	49.0	150.64	5		25357	10000	20000	0.652	0.693	0.662
83	5	IPC-2	100	76-16	4.2	9.5	9.283	325	58.3	179.34	5		25357	10000	20000	0.661	0.702	0.672
84	10	IPC-2	100	76-16	4.2	9.5	9.147	325	55.1	169.65	5		25357	10000	20000	0.659	0.700	0.669
85	15	IPC-1	100	76-16	5.2	4.5		237.5	44.6	187.87	5		337869	10000	20000	0.893	0.929	0.922
86	12	IPC-2	100	76-16	5.2	4.5	5.376	237.5	46.7	196.68	5		337869	10000	20000	0.944	0.963	0.959
87	7	IPC-2	100	76-16	5.2	4.5	5.008	237.5	54.3	228.53	5		337869	10000	20000	0.894	0.929	0.922
88	29	IPC-1	100	76-16	5.2	4.5	6.558	325	61.4	188.93	5		143797	10000	20000	0.796	0.853	0.838
89	31	IPC-2	100	76-16	5.2	4.5	4.745	325	63.9	196.59	5		143797	10000	20000	0.766	0.832	0.815
90	32	IPC-2	100	76-16	5.2	4.5	5.551	325	62.2	191.52	5		143797	10000	20000	0.736	0.809	0.790
91	33	IPC-1	100	76-16	5.2	9.5	9.02	237.5	32.8	137.93	5		185694	10000	20000	0.829	0.880	0.868
92	16	IPC-2	100	76-16	5.2	9.5	9.15	237.5	26.2	110.19	5		185694	10000	20000	0.796	0.856	0.842
93	17	IPC-2	100	76-16	5.2	9.5	9.59	237.5	25.8	108.79	5		185694	10000	20000	0.785	0.849	0.834
94	5	IPC-1	100	76-16	5.2	9.5	10.04	325	40.4	124.27	5		79031	10000	20000	0.679	0.753	0.728
95	6	IPC-1	100	76-16	5.2	9.5	10.08	325	38.3	117.77	5		79031	10000	20000	0.689	0.760	0.736
96	25	IPC-2	100	76-16	5.2	9.5	8.956	325	31.8	97.799	5		79031	10000	20000	0.686	0.758	0.734
97	36	IPC-2	40	76-16	4.2	4.5	5.856	137.5	314.3	2286.1	0	294160	305580			0.457		
98	40	IPC-1	40	76-16	4.2	4.5	5.894	137.5	306.6	2229.7	0	317000	305580			0.514		
99	34	IPC-1	40	76-16	4.2	4.5	5.554	195	355.1	1820.9	0	5830	5405			0.510		
100	27	IPC-2	40	76-16	4.2	4.5	6.24	195	313.0	1604.9	0	4980	5405			0.480		
101	3	IPC-2	40	76-16	4.2	9.5	8.641	175	214.7	1226.8	0	18200	19165			0.478		

102	2	IPC-2	40	76-16	4.2	9.5	8.306	175	259.4	1482	0	20130	19165			0.511		
103	39	IPC-1	40	76-16	5.2	4.5	5.571	175	352.5	2014.2	0	28640	30415			0.478		
104	36	IPC-1	40	76-16	5.2	4.5	5.504	175	342.1	1954.6	0	32190	30415			0.518		
105	38	IPC-1	40	76-16	5.2	4.5	5.33	195	261.7	1341.9	0	8650	7625			0.529		
106	37	IPC-1	40	76-16	5.2	4.5	5.44	195	265.9	1363.6	0	6600	7625			0.451		
107	43	IPC-2	40	76-16	5.2	9.5	9.686	137.5	205.2	1492.1	0	211050	220845			0.457		
108	34	IPC-2	40	76-16	5.2	9.5	10.07	137.5	211.2	1536.2	0	230640	220845			0.521		
109	35	IPC-2	40	76-16	5.2	9.5	9.058	195	228.2	1170.2	0	4445	4965			0.458		
110	39	IPC-2	40	76-16	5.2	9.5	9.831	195	227.0	1164	0	5485	4965			0.511		
111	29	IPC-1	70	76-16	4.2	4.5	5.124	187.5	137.4	732.96	0	82920	108690			0.443		
112	33	IPC-1	70	76-16	4.2	4.5	6.178	187.5	159.6	851.01	0	134460	108690			0.542		
113	37	IPC-1	70	76-16	4.2	9.5	9.366	237.5	166.3	700.09	0	13780	12213			0.522		
114	9	IPC-1	70	76-16	4.2	9.5	10.25	237.5	161.5	679.98	0	10645	12213			0.465		
115	19	IPC-1	70	76-16	4.2	9.5	9.472	262.5	150.6	573.59	0	4980	4380			0.517		
116	25	IPC-1	70	76-16	4.2	9.5	7.983	262.5	181.1	689.83	0	3780	4380			0.466		
117	30	IPC-1	70	76-16	5.2	9.5	9.135	187.5	115.5	615.84	0	137600	126160			0.531		
118	29	IPC-2	70	76-16	5.2	9.5	9.813	187.5	109.9	586.17	0	114720	126160			0.475		
119	36	IPC-1	70	76-16	5.2	9.5	9.822	262.5	145.4	554.04	0	9405	8780			0.532		
120	32	IPC-1	70	76-16	5.2	9.5		262.5	141.3	538.14	0	8155	8780			0.451		
121	32	IPC-2	100	76-16	4.2	4.5	6.325	325	64.7	198.95	0	55660	52290			0.529		
122	28	IPC-2	100	76-16	4.2	4.5	5.405	325	60.0	184.62	0	48920	52290			0.470		
123	31	IPC-1	100	76-16	4.2	9.5	10.48	237.5	33.3	140.03	0	59155	61942			0.477		
124	38	IPC-2	100	76-16	4.2	9.5	9.913	237.5	33.8	142.26	0	64729	61942			0.515		
125	33	IPC-2	100	76-16	5.2	4.5	5.717	237.5	42.9	180.61	0	372847	342101			0.541		
126	35	IPC-2	100	76-16	5.2	4.5	5.597	237.5	41.9	176.32	0	311355	342101			0.443		
127	34	IPC-2	100	76-16	5.2	4.5	5.187	415	57.0	137.36	0	63280	59960			0.513		
128	30	IPC-2	100	76-16	5.2	4.5	5.204	415	60.8	146.48	0	56640	59960			0.469		

129	25	IPC-2	40	76-16	4.2	4.5	5.41	195	396.8	2034.9	10		5405	2000	3000	0.782	0.817	0.803
130	31	IPC-2	40	76-16	4.2	4.5	5.263	195	393.1	2015.8	10		5405	2000	3000	0.811	0.841	0.829
131	40	IPC-1	40	76-16	5.2	9.5	9.714	137.5	181.3	1318.3	1		220845	10000	20000	0.730	0.814	0.795
132	38	IPC-2	40	76-16	5.2	9.5	8.814	137.5	183.0	1330.6	1		220845	10000	20000	0.763	0.836	0.820
133	42	IPC-1	40	76-16	5.2	9.5	9.084	137.5	212.7	1546.7	10		220845	10000	20000	0.878	0.916	0.907
134	21	IPC-2	40	76-16	5.2	9.5	9.156	137.5	203.7	1481.7	10		220845	10000	20000	0.880	0.917	0.909
135	37	IPC-1	40	76-16	5.2	9.5	9.218	195	267.6	1372.3	5		4965	1000	2500	0.731	0.801	0.761
136	41	IPC-2	40	76-16	5.2	9.5	8.826	195	249.3	1278.6	5		4965	1000	2500	0.696	0.774	0.729
137	15	IPC-1	70	76-16	4.2	4.5	4.671	237.5	190.0	800.17	1		15757	5000	10000	0.673	0.724	0.693
138	30	IPC-2	70	76-16	4.2	4.5	6.174	237.5	204.1	859.2	1		15757	5000	10000	0.613	0.673	0.637
139	26	IPC-1	70	76-16	4.2	9.5	7.58	187.5	138.5	738.45	1		80410	10000	20000	0.619	0.707	0.678
140	27	IPC-1	70	76-16	4.2	9.5	7.557	187.5	124.1	662.11	1		80410	10000	20000	0.651	0.732	0.705
141	29	IPC-2	70	76-16	4.2	9.5		237.5	200.8	845.29	10		12213	5000	10000	0.726	0.760	0.733
142	27	IPC-1	70	76-16	5.2	9.5	9.545	237.5	128.9	542.9	5		17388	5000	10000	0.748	0.790	0.766
143	26	IPC-2	70	76-16	5.2	9.5	9.177	237.5	140.5	591.46	5		17388	5000	10000	0.692	0.743	0.715
144	28	IPC-1	70	76-16	5.2	9.5	9.071	262.5	182.3	694.4	10		8780	2000	4000	0.675	0.746	0.712
145	3	IPC-2	70	76-16	5.2	9.5	9.877	262.5	159.8	608.76	10		8780	2000	4000	0.700	0.765	0.734
146	35	IPC-2	100	76-16	4.2	9.5	8.903	325	51.7	159.05	1		24314	10000	20000	0.608	0.653	0.618
147	36	IPC-2	100	76-16	4.2	9.5	8.903	325	53.9	165.91	1		24314	10000	20000	0.609	0.653	0.618
148	27	IPC-1	100	76-16	5.2	4.5	5.116	325	62.6	192.73	10		125897	10000	20000	0.733	0.804	0.785
149	26	IPC-2	100	76-16	5.2	4.5	5.641	325	59.4	182.73	10		125897	10000	20000	0.801	0.854	0.840
150	11	IPC-2	100	76-16	5.2	4.5		415	58.7	141.42	1		59960	10000	20000	0.654	0.725	0.697
151	25	IPC-1	100	76-16	5.2	4.5	5.078	415	105.2	253.5	1		59960	10000	20000	0.684	0.749	0.724
152	7	IPC-1	40	64-22	4.2	4.5	5.978	100	231.0	2310.3	0	140000	135000			0.518		
153	3	IPC-1	40	64-22	4.2	4.5	6.684	150	222.5	1483.2	0	36000	25263			0.531		
154	2	IPC-2	40	64-22	4.2	4.5	7.695	150	294.9	1966.2	0	22150	25263			0.465		
155	14	IPC-1	40	64-22	4.2	4.5	5.642	100	130.1	1300.5	0	130000	135000			0.480		

156	15	IPC-1	40	64-22	4.2	4.5	4.971	150	283.6	1890.7	0	17640	25263			0.451		
157	19	IPC-2	40	64-22	4.2	4.5	5.673	100	129.8	1297.5	0	135000	135000			0.500		
158	2	IPC-1	40	64-22	4.2	9.5	10.48	100	126.7	1267.1	0	385000	228333			0.549		
159	4	IPC-2	40	64-22	4.2	9.5	8.406	100	126.7	1267.1	0	170000	228333			0.435		
160	14	IPC-2	40	64-22	4.2	9.5	11.34	100	125.3	1253.1	0	130000	228333			0.476		
161	13	IPC-1	40	64-22	5.2	4.5	5.277	150	189.0	1260.2	0	58430	91801			0.432		
162	30	IPC-2	40	64-22	5.2	4.5	5.528	150	256.4	1709.1	0	122543	91801			0.528		
163	27	IPC-2	40	64-22	5.2	4.5	4.102	150	207.5	1383.2	0	140000	91801			0.534		
164	1	IPC-2	40	64-22	5.2	4.5	5.862	150	261.0	1740.3	0	46230	91801			0.535		
165	1	IPC-1	40	64-22	5.2	9.5	9.564	100	113.9	1139.3	0	300000	215000			0.453		
166	7	IPC-2	40	64-22	5.2	9.5	9.16	100	110.1	1100.9	0	130000	215000			0.528		
167	11	IPC-1	40	64-22	5.2	9.5	8.028	150	172.0	1146.6	0	35480	33077			0.516		
168	16	IPC-2	40	64-22	5.2	9.5	10.29	150	156.8	1045	0	39400	33077			0.524		
169	15	IPC-1	40	64-22	5.2	9.5	9.726	150	135.0	899.85	0	24350	33077			0.446		
170	9	IPC-1	70	64-22	4.2	4.5	5.764	200	120.2	601.04	0	70000	80667			0.446		
171	4	IPC-2	70	64-22	4.2	4.5	5.289	200	130.1	650.65	0	82000	80667			0.510		
172	24	IPC-1	70	64-22	4.2	4.5	6.786	200	146.9	734.45	0	90000	80667			0.530		
173	8	IPC-1	70	64-22	4.2	9.5	9.361	137.5	102.0	742.12	0	44490	127417			0.466		
174	11	IPC-1	70	64-22	4.2	9.5	9.771	200	150.6	752.84	0	56660	55433			0.500		
175	16	IPC-1	70	64-22	4.2	9.5	9.276	137.5	117.9	857.73	0	67760	127417			0.533		
176	17	IPC-1	70	64-22	4.2	9.5	9.815	200	116.1	580.49	0	57830	55433			0.511		
177	7	IPC-2	70	64-22	4.2	9.5	8.981	137.5	53.8	391.25	0	270000	127417			0.528		
178	20	IPC-2	70	64-22	4.2	9.5	9.071	200	115.1	575.28	0	51810	55433			0.441		
179	25	IPC-1	70	64-22	5.2	4.5	4.08	137.5	83.9	610.21	0	221300	415210			0.460		
180	18	IPC-2	70	64-22	5.2	4.5	5.296	137.5	50.3	365.71	0	700000	415210			0.509		
181	26	IPC-1	70	64-22	5.2	4.5	4.304	137.5	105.8	769.23	0	324330	415210			0.533		
182	10	IPC-1	70	64-22	5.2	9.5	9.625	200	90.8	453.8	0	104710	106773			0.478		

183	21	IPC-1	70	64-22	5.2	9.5	9.572	200	81.7	408.49	0	63090	106773			0.441		
184	20	IPC-2	70	64-22	5.2	9.5	8.993	200	97.1	485.71	0	152520	106773			0.539		
185	12	IPC-1	100	64-22	4.2	4.5	6.621	312.5	48.3	154.68	0	157680	101233			0.562		
186	17	IPC-1	100	64-22	4.2	4.5	5.43	312.5	45.9	146.91	0	45000	101233			0.422		
187	8	IPC-2	100	64-22	4.2	4.5	5.248	312.5	61.8	197.88	0	101020	101233			0.500		
188	6	IPC-2	100	64-22	4.2	9.5	7.958	387.5	43.2	111.51	0	9680	9180			0.515		
189	26	IPC-1	100	64-22	4.2	9.5	10.02	387.5	57.6	148.75	0	11410	9180			0.521		
190	9	IPC-2	100	64-22	4.2	9.5	9.101	387.5	31.4	81.124	0	6450	9180			0.451		
191	17	IPC-1	100	64-22	5.2	4.5	5.325	387.5	37.1	95.735	0	110060	114283			0.461		
192	20	IPC-1	100	64-22	5.2	4.5	4.64	387.5	28.8	74.409	0	80860	114283			0.455		
193	22	IPC-1	100	64-22	5.2	4.5	3.9	387.5	70.8	182.81	0	151930	114283			0.532		
194	2	IPC-2	100	64-22	5.2	9.5	5.43	312.5	19.5	62.416	0	72720	70550			0.516		
195	6	IPC-1	100	64-22	5.2	9.5	4.49	312.5	24.1	77.213	0	57960	70550			0.461		
196	5	IPC-2	100	64-22	5.2	9.5	4.115	312.5	37.1	118.76	0	80970	70550			0.532		
197	10	IPC-1	40	64-22	4.2	4.5	5.415	100	190.0	1900.3	5		179804	10000	20000	0.815	0.869	0.856
198	21	IPC-2	40	64-22	4.2	4.5	4.981	100	201.7	2016.9	5		179804	10000	20000	0.961	0.972	0.970
199	22	IPC-2	40	64-22	4.2	4.5	5.737	100	193.6	1935.7	5		179804	10000	20000	0.958	0.970	0.967
200	12	IPC-2	40	64-22	4.2	9.5	10.1	150	317.9	2119	5		21419	10000	20000	0.805	0.825	0.807
201	21	IPC-2	40	64-22	4.2	9.5	8.878	150	214.0	1426.7	5		21419	10000	20000	0.857	0.872	0.859
202	23	IPC-2	40	64-22	4.2	9.5	8.914	150	214.9	1432.9	5		21419	10000	20000	0.832	0.849	0.834
203	2	IPC-1	40	64-22	5.2	4.5	5.413	100	229.6	2296	5		362911	10000	20000	0.960	0.974	0.971
204	5	IPC-1	40	64-22	5.2	4.5	4.115	100	249.8	2498.3	5		362911	10000	20000	0.947	0.966	0.962
205	15	IPC-1	40	64-22	5.2	4.5	5.78	100	102.1	1020.5	5		362911	10000	20000	0.930	0.954	0.949
206	10	IPC-1	40	64-22	5.2	4.5	4.72	150	232.2	1547.9	5		59402	10000	20000	0.887	0.910	0.901
207	12	IPC-1	40	64-22	5.2	4.5	5.499	150	219.5	1463.4	5		59402	10000	20000	0.914	0.932	0.925
208	23	IPC-2	40	64-22	5.2	4.5	3.805	150	333.2	2221.1	5		59402	10000	20000	0.908	0.927	0.919
209	9	IPC-1	40	64-22	5.2	9.5	9.057	100	144.4	1443.6	5		264119	10000	20000	0.921	0.946	0.941

210	4	IPC-2	40	64-22	5.2	9.5	9.808	100	150.1	1500.8	5		264119	10000	20000	0.920	0.945	0.940
211	18	IPC-1	40	64-22	5.2	9.5	9.387	100	143.2	1431.7	5		264119	10000	20000	0.929	0.952	0.947
212	12	IPC-1	40	64-22	5.2	9.5	9.506	150	215.1	1434.2	5		43231	10000	20000	0.917	0.932	0.925
213	13	IPC-1	40	64-22	5.2	9.5	10.69	150	215.1	1434.2	5		43231	10000	20000	0.880	0.901	0.891
214	25	IPC-2	40	64-22	5.2	9.5	9.7	150	217.7	1451.6	5		43231	10000	20000	0.880	0.901	0.891
215	5	IPC-1	70	64-22	4.2	4.5	5.512	137.5	110.4	802.64	5		136082	10000	20000	0.883	0.915	0.906
216	23	IPC-1	70	64-22	4.2	4.5	6.309	137.5	123.7	899.79	5		136082	10000	20000	0.853	0.894	0.883
217	13	IPC-2	70	64-22	4.2	4.5	5.794	137.5	118.1	858.94	5		136082	10000	20000	0.869	0.905	0.895
218	11	IPC-1	70	64-22	4.2	4.5	5.713	200	159.7	798.26	5		79442	10000	20000	0.745	0.804	0.784
219	29	IPC-2	70	64-22	4.2	4.5	4.813	200	155.7	778.39	5		79442	10000	20000	0.843	0.879	0.867
220	20	IPC-1	70	64-22	4.2	4.5	5.511	200	146.0	730.13	5		79442	10000	20000	0.830	0.870	0.856
221	15	IPC-1	70	64-22	4.2	9.5	11.02	137.5	87.2	634.51	5		92534	10000	20000	0.916	0.936	0.930
222	22	IPC-1	70	64-22	4.2	9.5	9.031	137.5	84.8	616.73	5		92534	10000	20000	0.853	0.889	0.878
223	1	IPC-2	70	64-22	4.2	9.5	10.77	137.5	66.5	483.89	5		10000	20000		0.843	0.827	
224	4	IPC-1	70	64-22	5.2	4.5	4.879	200	195.0	974.77	5		145898	10000	20000	0.767	0.832	0.815
225	24	IPC-1	70	64-22	5.2	4.5	3.893	200	151.5	757.71	5		145898	10000	20000	0.884	0.916	0.908
226	19	IPC-2	70	64-22	5.2	4.5	6.64	200	97.0	485.07	5		145898	10000	20000	0.816	0.867	0.854
227	14	IPC-1	70	64-22	5.2	9.5	9.265	137.5	80.6	586.21	5		169942	10000	20000	0.912	0.938	0.932
228	22	IPC-2	70	64-22	5.2	9.5	9.654	137.5	77.0	560.18	5		169942	10000	20000	0.885	0.919	0.910
229	23	IPC-2	70	64-22	5.2	9.5	9.433	137.5	79.4	577.1	5		169942	10000	20000	0.883	0.917	0.909
230	8	IPC-1	70	64-22	5.2	9.5	9.256	200	107.8	538.99	5		99209	10000	20000	0.774	0.830	0.813
231	19	IPC-1	70	64-22	5.2	9.5	11.46	200	102.0	509.96	5		99209	10000	20000	0.820	0.864	0.851
232	17	IPC-2	70	64-22	5.2	9.5	9.17	200	103.5	517.69	5		99209	10000	20000	0.848	0.886	0.875
233	28	IPC-1	100	64-22	4.2	4.5	6.116	387.5	70.5	181.82	5		35592	10000	20000	0.751	0.789	0.768
234	27	IPC-1	100	64-22	4.2	4.5	6.755	387.5	83.5	215.39	5		35592	10000	20000	0.741	0.781	0.759
235	6	IPC-2	100	64-22	4.2	4.5	5.254	387.5	63.5	163.8	5		35592	10000	20000	0.730	0.772	0.749
236	13	IPC-1	100	64-22	4.2	9.5	10.16	312.5	40.5	129.59	5		22483	10000	20000	0.849	0.864	0.851

237	10	IPC-2	100	64-22	4.2	9.5	9.764	312.5	40.4	129.39	5		22483	10000	20000	0.745	0.772	0.749
238	19	IPC-1	100	64-22	4.2	9.5	9.517	312.5	40.7	130.2	5		22483	10000	20000	0.784	0.807	0.787
239	3	IPC-1	100	64-22	4.2	9.5	8.81	387.5	50.9	131.28	5		8940	2000	4000	0.700	0.766	0.736
240	24	IPC-1	100	64-22	4.2	9.5	10.49	387.5	50.8	131.03	5		2000	4000		0.688	0.647	
241	5	IPC-2	100	64-22	4.2	9.5	8.485	387.5	48.3	124.7	5		8940	2000	4000	0.700	0.766	0.736
242	16	IPC-1	100	64-22	5.2	4.5	5.48	312.5	43.5	139.29	5		278516	10000	20000	0.898	0.931	0.924
243	11	IPC-2	100	64-22	5.2	4.5	5.199	312.5	33.5	107.19	5		278516	10000	20000	0.857	0.903	0.894
244	9	IPC-2	100	64-22	5.2	4.5	4.694	312.5	37.0	118.52	5		278516	10000	20000	0.858	0.904	0.894
245	26	IPC-1	100	64-22	5.2	9.5	8.409	387.5	49.0	126.41	5		27820	10000	20000	0.750	0.782	0.761
246	3	IPC-2	100	64-22	5.2	9.5	7.111	387.5	37.3	96.236	5		27820	10000	20000	0.762	0.793	0.772
247	24	IPC-2	100	64-22	5.2	9.5	10.3	387.5	35.7	92.163	5		27820	10000	20000	0.747	0.780	0.758
248	35	IPC-1	40	64-22	4.2	9.5	10.32	150	205.8	1371.9	0	14930	21535			0.481		
249	43	IPC-2	40	64-22	4.2	9.5		150	196.5	1309.8	0	28140	21535			0.514		
250	39	IPC-1	40	64-22	4.2	9.5	9.568	215	262.7	1221.8	0	2820	2615			0.512		
251	40	IPC-2	40	64-22	4.2	9.5	10.07	215	255.7	1189.1	0	2410	2615			0.471		
252	40	IPC-1	40	64-22	5.2	4.5	4.15	100	150.2	1502	0	357470	338245			0.525		
253	42	IPC-2	40	64-22	5.2	4.5	4.488	100	155.6	1556	0	319020	338245			0.472		
254	41	IPC-2	40	64-22	5.2	4.5	4.973	215	299.6	1393.7	0	4450	5380			0.451		
255	44	IPC-2	40	64-22	5.2	4.5	4.61	215	310.5	1444.1	0	6310	5380			0.530		
256	38	IPC-1	70	64-22	4.2	4.5	5.61	137.5	88.1	640.5	0	130000	145000			0.461		
257	45	IPC-1	70	64-22	4.2	4.5		137.5	99.4	723.16	0	160000	145000			0.535		
258	44	IPC-1	70	64-22	4.2	9.5		280	170.3	608.25	0	14260	25130			0.461		
259	42	IPC-1	70	64-22	4.2	9.5	10.44	280	179.8	642.2	0	36000	25130			0.535		
260	35	IPC-1	70	64-22	5.2	4.5	4.424	200	117.2	585.98	0	129930	139015			0.454		
261	36	IPC-2	70	64-22	5.2	4.5	4.705	200	126.8	634.16	0	148100	139015			0.522		
262	8	IPC-1	70	64-22	5.2	4.5	4.894	280	158.8	566.98	0	55300	64000			0.450		
263	39	IPC-1	70	64-22	5.2	4.5	4.892	280	167.0	596.31	0	72700	64000			0.532		

264	31	IPC-2	70	64-22	5.2	9.5	9.078	137.5	66.7	485.1	0	176050	167725			0.545		
265	32	IPC-2	70	64-22	5.2	9.5	10.07	137.5	60.5	440.29	0	159400	167725			0.466		
266	42	IPC-1	100	64-22	4.2	4.5		387.5	63.5	163.9	0	31296	34983			0.469		
267	16	IPC-1	100	64-22	4.2	4.5	4.968	387.5	65.1	168.02	0	38670	34983			0.523		
268	40	IPC-2	100	64-22	4.2	4.5		420	54.7	130.34	0	23470	25610			0.471		
269	41	IPC-1	100	64-22	4.2	4.5		420	55.8	132.78	0	27750	25610			0.521		
270	48	IPC-1	100	64-22	4.2	9.5	8.626	312.5	48.3	154.52	0	23888	26802			0.469		
271	46	IPC-2	100	64-22	4.2	9.5	9.976	312.5	33.9	108.43	0	29716	26802			0.534		
272	58	IPC-1	100	64-22	4.2	9.5		420	47.0	111.99	0	5773	6249			0.474		
273	45	IPC-2	100	64-22	4.2	9.5	9.84	420	37.7	89.842	0	6725	6249			0.528		
274	46	IPC-2	100	64-22	5.2	4.5	4.777	312.5	38.9	124.52	0	278840	266425			0.535		
275	43	IPC-2	100	64-22	5.2	4.5	5.049	312.5	36.5	116.84	0	254010	266425			0.460		
276	29	IPC-2	100	64-22	5.2	9.5	9.291	387.5	35.3	91	0	30755	27320			0.526		
277	30	IPC-2	100	64-22	5.2	9.5	9.233	387.5	36.5	94.138	0	23885	27320			0.478		
278	33	IPC-2	100	64-22	5.2	9.5	9.413	420	34.7	82.714	0	19271	18461			0.522		
279	37	IPC-1	100	64-22	5.2	9.5	10.14	420	35.9	85.486	0	17650	18461			0.455		
280	34	IPC-2	40	64-22	4.2	4.5	5.456	150	293.7	1958.3	5		25263	10000	20000	0.778	0.805	0.785
281	36	IPC-1	40	64-22	4.2	4.5	5.323	150	276.5	1843.3	5		25263	10000	20000	0.900	0.912	0.903
282	38	IPC-2	40	64-22	4.2	9.5	10.26	100	164.3	1643.2	5		228333	10000	20000	0.909	0.937	0.931
283	30	IPC-2	40	64-22	4.2	9.5	9.125	100	151.2	1512.4	5		228333	10000	20000	0.839	0.890	0.878
284	36	IPC-1	40	64-22	4.2	9.5	10.27	215	353.6	1644.7	1		2615	600	1000	0.747	0.814	0.790
285	37	IPC-1	40	64-22	4.2	9.5	9.053	215	335.3	1559.5	1		2615	600	1000	0.702	0.781	0.754
286	6	IPC-2	40	64-22	5.2	4.5	4.48	150	275.1	1834.1	1		106991	10000	20000	0.804	0.854	0.840
287	37	IPC-1	40	64-22	5.2	4.5	4.481	150	265.3	1768.7	1		106991	10000	20000	0.789	0.843	0.828
288	47	IPC-1	40	64-22	5.2	4.5	5.066	215	479.1	2228.2	10		5380	2500		0.882	0.896	
289	3	IPC-2	40	64-22	5.2	4.5	5.093	215	347.1	1614.6	10		5380	1500	2500	0.872	0.898	0.887
290	28	IPC-2	70	64-22	4.2	9.5	9.128	280	150.5	537.59	5		25130	10000	20000	0.745	0.775	0.752

291	18	IPC-2	70	64-22	4.2	9.5	8.511	280	163.8	585.17	5		25130	10000	20000	0.726	0.758	0.734
292	31	IPC-2	70	64-22	5.2	4.5	5.156	137.5	100.0	727.25	10		272815	10000	20000	0.928	0.952	0.947
293	7	IPC-2	70	64-22	5.2	4.5	4.563	137.5	105.9	770.11	10		272815	10000	20000	0.950	0.966	0.963
294	29	IPC-1	70	64-22	5.2	4.5	5.653	280	201.2	718.57	1		64000	10000	20000	0.732	0.789	0.767
295	38	IPC-2	70	64-22	5.2	4.5	4.966	280	194.2	693.53	1		64000	10000	20000	0.698	0.762	0.738
296	38	IPC-2	70	64-22	5.2	9.5	9.19	200	100.6	502.87	1		106773	10000	20000	0.716	0.789	0.767
297	28	IPC-1	70	64-22	5.2	9.5	9.412	200	105.8	529.16	1		106773	10000	20000	0.752	0.816	0.797
298	43	IPC-1	100	64-22	4.2	4.5		312.5	58.0	185.51	1		101233	10000	20000	0.812	0.859	0.845
299	44	IPC-2	100	64-22	4.2	4.5		312.5	50.8	162.53	1		101233	10000	20000	0.682	0.762	0.738
300	35	IPC-2	100	64-22	4.2	4.5	5.053	420	75.0	178.48	5		25610	10000	20000	0.762	0.791	0.770
301	39	IPC-2	100	64-22	4.2	4.5	5.509	420	68.8	163.81	5		25610	10000	20000	0.634	0.678	0.646
302	29	IPC-1	100	64-22	4.2	9.5	9.313	420	56.8	135.28	10		6249	2000	4000	0.670	0.728	0.693
303	31	IPC-1	100	64-22	4.2	9.5	9.254	420	54.2	129.08	10		6249	2000	4000	0.680	0.737	0.702
304	27	IPC-1	100	64-22	5.2	9.5	8.953	312.5	33.0	105.56	1		70550	10000	20000	0.786	0.834	0.817
305	35	IPC-1	100	64-22	5.2	9.5	9.651	312.5	32.1	102.74	1		70550	10000	20000	0.785	0.832	0.815
306	20	IPC-1	40	58-28	4.2	4.5	5.063	145	191.1	1317.6	0	71250	75423			0.459		
307	24	IPC-1	40	58-28	4.2	4.5	5.203	145	221.6	1528.5	0	85000	75423			0.529		
308	19	IPC-2	40	58-28	4.2	4.5	5.149	145	194.6	1342	0	70020	75423			0.461		
309	4	IPC-1	40	58-28	4.2	9.5	10.09	170	204.9	1205.3	0	30760	33393			0.455		
310	20	IPC-1	40	58-28	4.2	9.5	8.729	170	179.7	1056.9	0	22610	33393			0.458		
311	18	IPC-2	40	58-28	4.2	9.5	9.225	170	250.7	1474.7	0	46810	33393			0.537		
312	5	IPC-1	40	58-28	5.2	4.5	6.985	170	199.9	1176	0	36160	43530			0.466		
313	7	IPC-1	40	58-28	5.2	4.5	4.888	170	207.8	1222.1	0	53970	43530			0.538		
314	9	IPC-1	40	58-28	5.2	4.5	6.154	170	205.3	1207.4	0	40460	43530			0.461		
315	2	IPC-1	40	58-28	5.2	9.5	9.545	145	153.4	1058	0	79000	81487			0.487		
316	19	IPC-2	40	58-28	5.2	9.5	10.2	145	152.8	1054	0	88900	81487			0.526		
317	21	IPC-2	40	58-28	5.2	9.5	9.718	145	163.8	1129.7	0	76560	81487			0.478		

318	6	IPC-1	70	58-28	4.2	4.5	5.382	200	82.4	411.94	0	38210	40860			0.483		
319	1	IPC-2	70	58-28	4.2	4.5	4.714	200	72.8	364.06	0	39350	40860			0.467		
320	11	IPC-2	70	58-28	4.2	4.5	4.895	200	110.7	553.27	0	45020	40860			0.528		
321	2	IPC-1	70	58-28	4.2	9.5	9.683	262.5	97.2	370.27	0	23760	25480			0.458		
322	22	IPC-1	70	58-28	4.2	9.5	9.658	262.5	73.0	277.93	0	27760	25480			0.534		
323	37	IPC-2	70	58-28	4.2	9.5	10.67	262.5	112.1	427	0	24920	25480			0.462		
324	3	IPC-1	70	58-28	5.2	4.5	5.188	262.5	118.1	449.81	0	54230	53827			0.511		
325	12	IPC-1	70	58-28	5.2	4.5	4.994	262.5	109.9	418.65	0	58540	53827			0.529		
326	20	IPC-2	70	58-28	5.2	4.5	5.93	262.5	96.4	367.3	0	48710	53827			0.448		
327	17	IPC-1	70	58-28	5.2	9.5	9.601	200	41.0	204.83	0	79640	80480			0.473		
328	4	IPC-2	70	58-28	5.2	9.5	10.76	200	52.6	262.77	0	85659	80480			0.528		
329	12	IPC-2	70	58-28	5.2	9.5	9.374	200	67.3	336.28	0	76140	80480			0.452		
330	18	IPC-1	70	58-28	5.2	9.5	9.464	262.5	74.4	283.51	0	25310	26833			0.479		
331	20	IPC-1	70	58-28	5.2	9.5	9.202	262.5	60.8	231.46	0	30080	26833			0.525		
332	11	IPC-2	70	58-28	5.2	9.5	9.432	262.5	71.2	271.12	0	25110	26833			0.476		
333	22	IPC-1	100	58-28	4.2	4.5	5.545	415	29.3	70.682	0	20673	23488			0.450		
334	3	IPC-2	100	58-28	4.2	4.5	4.666	415	28.8	69.44	0	22550	23488			0.462		
335	10	IPC-2	100	58-28	4.2	4.5	5.089	415	28.0	67.415	0	27240	23488			0.532		
336	26	IPC-1	100	58-28	4.2	9.5	10.54	295	19.3	65.312	0	100000	89187			0.534		
337	16	IPC-2	100	58-28	4.2	9.5	8.602	295	21.1	71.434	0	93430	89187			0.511		
338	17	IPC-2	100	58-28	4.2	9.5	8.575	295	17.2	58.327	0	74130	89187			0.465		
339	22	IPC-1	100	58-28	5.2	4.5	5.595	295	15.4	52.25	0	185000	182797			0.509		
340	16	IPC-2	100	58-28	5.2	4.5	6	295	15.1	51.297	0	203390	182797			0.534		
341	24	IPC-1	100	58-28	5.2	4.5	6.185	295	15.0	50.798	0	160000	89187			0.463		
342	11	IPC-1	100	58-28	5.2	4.5	5.981	415	24.1	57.996	0	43000	182797			0.467		
343	1	IPC-2	100	58-28	5.2	4.5	5.015	415	24.2	58.2	0	38000	182797			0.469		
344	23	IPC-1	100	58-28	5.2	4.5	6.168	415	25.3	60.958	0	58000	182797			0.536		

345	15	IPC-1	100	58-28	5.2	9.5	9.002	415	19.4	46.753	0	43000	46333			0.514		
346	7	IPC-2	100	58-28	5.2	9.5	9.128	415	17.9	43.241	0	47000	46333			0.524		
347	5	IPC-2	100	58-28	5.2	9.5	10.51	415	14.1	34.051	0	33000	46333			0.443		
348	41	IPC-1	40	58-28	4.2	4.5	5.395	170	237.2	1395	5		41000	10000	20000	0.912	0.925	0.918
349	5	IPC-2	40	58-28	4.2	4.5	4.875	170	251.7	1480.7	5		41000	10000	20000	0.850	0.874	0.861
350	7	IPC-2	40	58-28	4.2	4.5	5.239	170	249.6	1468.3	5		41000	5000	15000	0.860	0.882	0.870
351	1	IPC-1	40	58-28	4.2	9.5	8.489	145	222.6	1534.9	5		35661	10000	20000	0.888	0.912	0.903
352	7	IPC-2	40	58-28	4.2	9.5	9.341	145	176.4	1216.7	5		35661	10000	20000	0.868	0.896	0.886
353	3	IPC-2	40	58-28	4.2	9.5	9.366	145	169.1	1166.3	5		35661	10000	20000	0.877	0.904	0.894
354	6	IPC-1	40	58-28	5.2	4.5	6.645	145	189.8	1308.8	5		67569	10000	20000	0.915	0.936	0.929
355	18	IPC-1	40	58-28	5.2	4.5	5.847	145	183.2	1263.3	5		67569	10000	20000	0.960	0.970	0.967
356	15	IPC-2	40	58-28	5.2	4.5	6.043	145	195.6	1349.2	5		67569	10000	20000	0.930	0.947	0.941
357	3	IPC-1	40	58-28	5.2	9.5	9.146	145	190.0	1310.6	5		90784	10000	20000	0.940	0.954	0.949
358	10	IPC-2	40	58-28	5.2	9.5	9.744	145	173.2	1194.6	5		90784	10000	20000	0.925	0.943	0.937
359	29	IPC-1	40	58-28	5.2	9.5	8.946	145	127.9	882.32	5		90784	10000	20000	0.887	0.914	0.905
360	8	IPC-1	40	58-28	5.2	9.5	9.601	170	186.9	1099.7	5		81482	10000	20000	0.879	0.898	0.888
361	16	IPC-2	40	58-28	5.2	9.5	9.289	170	191.4	1126.1	5		81482	10000	20000	0.888	0.906	0.897
362	28	IPC-2	40	58-28	5.2	9.5	9.227	170	179.9	1058.1	5		81482	10000	20000	0.891	0.909	0.900
363	8	IPC-1	70	58-28	4.2	4.5	4.795	262.5	115.5	440.04	5		38598	10000	20000	0.768	0.797	0.777
364	2	IPC-2	70	58-28	4.2	4.5	4.782	262.5	105.1	400.24	5		38598	10000	20000	0.800	0.825	0.807
365	39	IPC-2	70	58-28	4.2	4.5	5.36	262.5	145.5	554.11	5		38598	10000	20000	0.753	0.784	0.762
366	8	IPC-1	70	58-28	4.2	9.5	9.589	200	93.3	466.41	5		26210	10000	20000	0.848	0.873	0.860
367	5	IPC-1	70	58-28	4.2	9.5	10.08	200	73.6	367.77	5		26210	10000	20000	0.845	0.870	0.857
368	24	IPC-2	70	58-28	4.2	9.5	9.733	200	71.6	358.16	5		26210	10000	20000	0.832	0.860	0.846
369	27	IPC-1	70	58-28	4.2	9.5	9.014	262.5	114.7	437.09	5		39288	10000	20000	0.781	0.803	0.783
370	21	IPC-2	70	58-28	4.2	9.5	9.9	262.5	108.5	413.45	5		39288	10000	20000	0.779	0.801	0.781
371	23	IPC-2	70	58-28	4.2	9.5	10.23	262.5	79.1	301.49	5		39288	10000	20000	0.729	0.755	0.731

372	10	IPC-1	70	58-28	5.2	4.5	5.699	200	71.6	357.77	5		21466	10000	20000	0.931	0.948	0.942
373	45	IPC-1	70	58-28	5.2	4.5	5.918	200	113.6	568.08	5		21466	10000	20000	0.905	0.927	0.919
374	46	IPC-2	70	58-28	5.2	4.5	5.245	200	115.0	575.03	5		21466	10000	20000	0.881	0.909	0.900
375	2	IPC-1	70	58-28	5.2	4.5	5.502	262.5	112.8	429.67	5		82935	10000	20000	0.805	0.840	0.824
376	13	IPC-1	70	58-28	5.2	4.5	4.853	262.5	116.6	444	5		82935	10000	20000	0.824	0.856	0.841
377	44	IPC-2	70	58-28	5.2	4.5	5.665	262.5	79.9	304.44	5		82935	10000	20000	0.826	0.857	0.843
378	22	IPC-1	70	58-28	5.2	9.5		200	44.4	221.96	5		45315	10000	20000	0.883	0.909	0.900
379	23	IPC-1	70	58-28	5.2	9.5		200	55.8	278.97	5		45315	10000	20000	0.851	0.883	0.872
380	14	IPC-2	70	58-28	5.2	9.5	8.883	200	70.4	351.93	5		45315	10000	20000	0.872	0.900	0.890
381	21	IPC-1	100	58-28	4.2	4.5	5.619	295	22.5	76.134	5		67926	10000	20000	0.837	0.878	0.866
382	12	IPC-2	100	58-28	4.2	4.5	5.501	295	30.9	104.85	5		67926	10000	20000	0.896	0.921	0.913
383	13	IPC-2	100	58-28	4.2	4.5	4.938	295	27.6	93.614	5		67926	10000	20000	0.868	0.900	0.890
384	23	IPC-1	100	58-28	4.2	4.5	4.91	415	32.8	78.967	5		96110	10000	20000	0.769	0.795	0.774
385	4	IPC-2	100	58-28	4.2	4.5	5.005	415	29.0	69.917	5		96110	10000	20000	0.718	0.748	0.723
386	42	IPC-2	100	58-28	4.2	4.5	5.276	415	37.0	89.088	5		96110	10000	20000	0.729	0.763	0.738
387	6	IPC-1	100	58-28	4.2	9.5	9.366	415	33.6	80.906	5		23484	10000	20000	0.756	0.780	0.758
388	15	IPC-2	100	58-28	4.2	9.5	8.338	415	29.9	71.988	5		23484	10000	20000	0.658	0.692	0.661
389	13	IPC-1	100	58-28	4.2	9.5	9.843	415	31.3	75.472	5		23484	10000	20000	0.702	0.732	0.705
390	14	IPC-1	100	58-28	5.2	4.5	5.102	295	24.2	82.184	5		21415	10000	20000	0.950	0.965	0.961
391	8	IPC-2	100	58-28	5.2	4.5	5.841	295	24.4	82.602	5		21415	10000	20000	0.919	0.943	0.938
392	19	IPC-2	100	58-28	5.2	4.5	5.575	295	25.6	86.945	5		21415	10000	20000	0.901	0.930	0.923
393	17	IPC-1	100	58-28	5.2	4.5	6.662	415	34.7	83.513	5		183209	10000	20000	0.798	0.834	0.818
394	21	IPC-1	100	58-28	5.2	4.5	5.862	415	34.9	84.041	5		183209	10000	20000	0.773	0.813	0.795
395	4	IPC-2	100	58-28	5.2	4.5	5.386	415	26.2	63.205	5		183209	10000	20000	0.764	0.807	0.787
396	1	IPC-1	100	58-28	5.2	9.5	9.551	295	19.8	67.126	5		44766	10000	20000	0.914	0.938	0.932
397	6	IPC-2	100	58-28	5.2	9.5	8.159	295	18.8	63.861	5		44766	10000	20000	0.884	0.918	0.910
398	9	IPC-2	100	58-28	5.2	9.5	9.063	295	17.6	59.507	5		44706	10000	20000	0.868	0.906	0.897

399	27	IPC-1	100	58-28	5.2	9.5	9.67	415	16.6	39.906	5		167069	10000	20000	0.777	0.815	0.796
400	26	IPC-1	100	58-28	5.2	9.5	9.034	415	18.1	43.541	5		167069	10000	20000	0.753	0.795	0.774
401	13	IPC-2	100	58-28	5.2	9.5	9.098	415	21.1	50.798	5		167069	10000	20000	0.744	0.787	0.766
402	32	IPC-1	40	58-28	4.2	4.5	4.966	170	266.6	1568.2	0	34905	36171			0.461		
403	33	IPC-1	40	58-28	4.2	4.5	5.65	170	240.5	1414.6	0	37436	36171			0.470		
404	26	IPC-1	40	58-28	4.2	4.5	5.613	220	302.5	1375	0	8940	8325			0.516		
405	40	IPC-1	40	58-28	4.2	4.5	4.936	220	288.1	1309.6	0	7710	8325			0.458		
406	28	IPC-1	40	58-28	4.2	9.5	9.554	145	182.6	1259.2	0	62180	64065			0.519		
407	31	IPC-1	40	58-28	4.2	9.5	10.43	145	180.5	1244.8	0	65950	64065			0.518		
408	25	IPC-1	40	58-28	4.2	9.5	11.1	220	256.9	1167.7	0	6600	7200			0.480		
409	30	IPC-1	40	58-28	4.2	9.5	9.502	220	280.5	1275	0	7800	7200			0.466		
410	43	IPC-1	40	58-28	5.2	4.5	6.565	145	177.0	1220.4	0	98590	95845			0.527		
411	31	IPC-1	40	58-28	5.2	4.5	5.731	145	171.6	1183.2	0	93100	95845			0.452		
412	39	IPC-1	40	58-28	5.2	9.5	8.809	170	193.6	1138.9	0	36000	40390			0.452		
413	30	IPC-2	40	58-28	5.2	9.5	8.755	170	187.0	1100	0	44780	40390			0.548		
414	34	IPC-1	40	58-28	5.2	9.5	9.447	220	228.0	1036.3	0	7910	9265			0.460		
415	31	IPC-1	40	58-28	5.2	9.5	10.19	220	225.7	1025.8	0	10620	9265			0.471		
416	43	IPC-2	70	58-28	4.2	4.5		262.5	107.6	410.06	0	27630	24560			0.525		
417	25	IPC-2	70	58-28	4.2	4.5	5.797	262.5	147.1	560.27	0	21490	24560			0.524		
418	27	IPC-2	70	58-28	4.2	4.5	5.628	330	143.1	433.56	0	14040	12360			0.462		
419	28	IPC-2	70	58-28	4.2	4.5	4.835	330	141.7	429.53	0	10680	12360			0.526		
420	39	IPC-2	70	58-28	4.2	9.5	10.19	200	59.9	299.57	0	39300	41750			0.465		
421	29	IPC-2	70	58-28	4.2	9.5	9.907	200	80.6	403	0	44200	41750			0.467		
422	33	IPC-1	70	58-28	5.2	4.5	4.803	200	80.2	400.82	0	72570	89935			0.525		
423	32	IPC-2	70	58-28	5.2	4.5	5.546	200	93.2	466.13	0	107300	89935			0.472		
424	42	IPC-1	70	58-28	5.2	4.5	5.566	330	134.8	408.55	0	33160	29650			0.528		
425	37	IPC-2	70	58-28	5.2	4.5	5.107	330	111.5	337.82	0	26140	29650			0.525		

426	30	IPC-1	100	58-28	4.2	4.5	4.895	295	18.0	61.032	0	105510	96535			0.468		
427	31	IPC-2	100	58-28	4.2	4.5	5.37	295	25.1	85.158	0	87560	96535			0.528		
428	35	IPC-2	100	58-28	4.2	4.5	5.801	500	33.4	66.762	0	12300	11185			0.451		
429	34	IPC-2	100	58-28	4.2	4.5	4.653	500	33.7	67.486	0	10070	11185			0.515		
430	9	IPC-2	100	58-28	4.2	9.5	9.884	415	30.0	72.248	0	23500	26760			0.475		
431	11	IPC-2	100	58-28	4.2	9.5	9.6	415	26.2	63.196	0	30020	26760			0.466		
432	33	IPC-1	100	58-28	4.2	9.5	10.32	500	31.8	63.517	0	8040	9255			0.527		
433	32	IPC-2	100	58-28	4.2	9.5	8.903	500	30.8	61.622	0	10470	9255			0.468		
434	35	IPC-1	100	58-28	5.2	4.5	5.225	500	34.9	69.713	0	21420	19575			0.523		
435	25	IPC-1	100	58-28	5.2	4.5	5.73	500	23.2	46.352	0	17730	19575			0.516		
436	32	IPC-1	100	58-28	5.2	9.5	10.26	295	12.3	41.738	0	158740	167565			0.460		
437	24	IPC-2	100	58-28	5.2	9.5	9.517	295	13.8	46.937	0	176390	167565			0.451		
438	37	IPC-2	40	58-28	4.2	4.5		170	224.8	1322.2	10		36171	10000	20000	0.874	0.894	0.883
439	38	IPC-1	40	58-28	4.2	4.5	5.763	170	290.7	1710.2	10		8325	2000	4000	0.884	0.902	0.892
440	17	IPC-2	40	58-28	4.2	4.5	5.787	220	306.9	1395.1	1		8325	2000	4000	0.746	0.800	0.773
441	36	IPC-1	40	58-28	4.2	4.5		220	308.9	1404	1		64065	10000	20000	0.745	0.795	0.769
442	38	IPC-2	40	58-28	4.2	9.5	8.237	145	188.1	1297.1	1		64065	10000	20000	0.813	0.853	0.838
443	12	IPC-1	40	58-28	4.2	9.5	9.347	145	183.7	1266.6	1		33393	10000	20000	0.754	0.806	0.786
444	36	IPC-1	40	58-28	4.2	9.5	9.785	170	229.2	1348.4	5		33393	10000	20000	0.814	0.842	0.826
445	35	IPC-2	40	58-28	4.2	9.5	10.64	170	230.7	1357.2	5		7200	2000	3500	0.872	0.891	0.880
446	10	IPC-2	40	58-28	4.2	9.5	9.668	220	299.4	1360.7	10		7200	2000	3500	0.848	0.878	0.865
447	14	IPC-1	40	58-28	4.2	9.5	9.618	220	292.1	1327.5	10		9265	2500	5000	0.799	0.838	0.821
448	35	IPC-1	40	58-28	5.2	9.5	10.1	220	236.5	1074.8	1		9265	2500	5000	0.787	0.828	0.806
449	25	IPC-1	40	58-28	5.2	9.5	8.448	220	242.0	1099.9	1		40860	10000	20000	0.740	0.790	0.764
450	14	IPC-1	70	58-28	4.2	4.5	5.347	200	88.1	440.25	5		40860	10000	20000	0.875	0.896	0.886
451	16	IPC-2	70	58-28	4.2	4.5	5.845	200	107.9	539.37	5		12360	3000	6000	0.832	0.860	0.846
452	9	IPC-2	70	58-28	4.2	4.5	4.653	330	154.3	467.67	10		12360	3000	6000	0.728	0.782	0.756

453	18	IPC-1	70	58-28	4.2	4.5	5.141	330	182.6	553.34	10		89935	10000	20000	0.715	0.772	0.744
454	30	IPC-2	70	58-28	5.2	4.5	5.734	200	88.0	439.75	1		89935	10000	20000	0.835	0.875	0.862
455	38	IPC-1	70	58-28	5.2	4.5	5.2	200	79.7	398.31	1		29650	10000	20000	0.780	0.833	0.816
456	28	IPC-2	70	58-28	5.2	4.5	5.19	330	140.3	425.09	5		29650	10000	20000	0.768	0.800	0.780
457	29	IPC-1	70	58-28	5.2	4.5	5.675	330	137.4	416.38	5		29650	10000	20000	0.741	0.776	0.754
458	15	IPC-1	100	58-28	4.2	4.5	5.325	295	26.2	88.792	10		96535	10000	20000	0.896	0.922	0.914
459	29	IPC-2	100	58-28	4.2	4.5	5.265	295	25.3	85.81	10		96535	10000	20000	0.836	0.876	0.864
460	34	IPC-1	100	58-28	4.2	9.5	8.368	500	37.4	74.73	5		9255	2000	4500	0.605	0.694	0.647
461	42	IPC-2	100	58-28	4.2	9.5	10.22	500	37.0	74.072	5		9255	2000	4000	0.654	0.731	0.696
462	39	IPC-1	100	58-28	5.2	4.5	6.023	415	32.7	78.738	1		46333	10000	20000	0.713	0.765	0.742
463	36	IPC-2	100	58-28	5.2	4.5	5.874	415	31.1	74.928	1		46333	10000	20000	0.706	0.760	0.736
464	41	IPC-2	100	58-28	5.2	4.5	5.271	500	41.7	83.494	10		19575	10000	15000	0.668	0.697	0.680
465	49	IPC-1	100	58-28	5.2	4.5	5.956	500	40.4	80.876	10		19575	10000	15000	0.718	0.743	0.728
466	33	IPC-2	100	58-28	5.2	9.5	10.04	415	21.8	52.603	10		41000	10000	20000	0.751	0.794	0.773
467	52	IPC-1	100	58-28	5.2	9.5		415	23.5	56.731	10		41000	10000	20000	0.769	0.808	0.789

APPENDIX B
SUMMARY OF QUALITY ASSURANCE RESULTS

Two IPC (IPC-1 and IPC-2) beam fatigue devices were used in this study. It was important to insure that both devices measure statistically identical responses during the experimental testing program. In order to accomplish this goal, statistical ANOVA experiments were designed and implemented to verify this hypothesis.

Table B1 to B6 show a summary of results obtained from the comparative studies that were performed between the two IPC beam fatigue machines to insure that there is no statistical difference between the two machines results. The following is a description of the different tables shown in this appendix.

- Table B1 shows the flexural stiffness of the synthetic beams under different test conditions.
- Table B2 shows the analysis of variance on the IPC1 and IPC2 data using synthetic beams.

Because of the significant difference results obtained in the first experiment, it was necessary to re-calibrate the machines and carefully tune them.

- Table B3 shows the flexural stiffness of the synthetic beams under different test conditions after recalibration.
- Table B4 shows the analysis of variance on the IPC1 and IPC2 data using synthetic beams after recalibration.
- Table B5 shows the flexural stiffness of the HMA beams under different test conditions.
- Table B6 shows the analysis of variance on the IPC1 and IPC2 data using HMA beams.

Table B1. Stiffness of Synthetic Beams (in psi) for first experiment.

Machine Type	Beam Stiffness					
	Low		Medium		High	
	Low Strain Level	High Strain Level	Low Strain Level	High Strain Level	Low Strain Level	High Strain Level
IPC 1	99946	96794	166500	163808	356391	350240
	93030	93330	168694	165120	361653	358960
Average	96488.0	95062.0	167597.0	164464.0	359022.0	354600.0
Standard Deviation	4890.4	2449.4	1551.4	927.7	3720.8	6166.0
Coefficient of variation, %	5.1	2.6	0.9	0.6	1.0	1.7
IPC 2	99957	93709	173738	166747	368045	368929
	102855	95107	174970	169706	381828	377047
Average	101406.0	94408.0	174354.0	168226.5	374936.5	372988.0
Standard Deviation	2049.2	988.5	871.2	2092.3	9746.1	5740.3
Coefficient of variation, %	2.0	1.0	0.5	1.2	2.6	1.5

Table B2. Analysis of Variance for the Logarithm Transformed IPC1 and IPC2 Data Using Synthetic Beams.

Source	Sum of Squares	DF	Mean Square	F Value	Prob > F
Model	1.34	4	0.34	3769.02	< 0.0001 significant
Machine Type	1.25E-03	1	1.25E-03	14.01	0.0014
Beam Type	1.34	2	0.67	7526.64	< 0.0001
Strain Level	7.85E-04	1	7.85E-04	8.8	0.0079
Residual	1.70E-03	19	8.92E-05		
Lack of Fit	6.81E-04	7	9.73E-05	1.15	0.395 not significant
Pure Error	1.01E-03	12	8.45E-05		
Correlation Total	1.35	23			
Std. Dev.	9.45E-03		R-Squared	0.9987	
Mean	5.26		Adj R-Squared	0.9985	
C.V.	0.18		Pred R-Squared	0.998	

Table B3. Stiffness Results (in psi) of the Repeated Experiment After Recalibration Using Synthetic Beams.

Machine Type	Beam Stiffness					
	Low		Medium		High	
	Low Strain Level	High Strain Level	Low Strain Level	High Strain Level	Low Strain Level	High Strain Level
IPC 1	99946	96794	166500	163808	356391	350240
	93030	93330	168694	165120	361653	358960
Average	96488.0	95062.0	167597.0	164464.0	359022.0	354600.0
Standard Deviation	4890.4	2449.4	1551.4	927.7	3720.8	6166.0
Coefficient of variation, %	5.1	2.6	0.9	0.6	1.0	1.7
IPC 2	99391	98190	168211	164207	357373	354662
	101535	95032	173583	163663	360103	361799
Average	100463.0	96611.0	170897.0	163935.0	358738.0	358230.5
Standard Deviation	1516.0	2233.0	3798.6	384.7	1930.4	5046.6
Coefficient of variation, %	1.5	2.3	2.2	0.2	0.5	1.4

Table B4. Analysis of Variance for The IPC1 and IPC2 Data After Recalibration Using Synthetic Beams.

Source	Sum of Squares	DF	Mean Square	F Value	Prob > F
Model	2.91E+11	4	7.28E+10	8408.07	< 0.0001 significant
Machine Type	2.26E+07	1	2.26E+07	2.61	0.1227
Beam Type	2.91E+11	2	1.46E+11	16810.9	< 0.0001
Strain Level	6.87E+07	1	6.87E+07	7.94	0.011
Residual	1.65E+08	19	8.66E+06		
Lack of Fit	2.84E+07	7	4.05E+06	0.36	0.9102 not significant
Pure Error	1.36E+08	12	1.13E+07		
Cor Total	2.91E+11	23			
Std. Dev.	2942.26		R-Squared	0.9994	
Mean	2.07E+05		Adj R-Squared	0.9993	

Table B5. Stiffness of HMA Beams (in psi).

Machine Type	Test Temperature					
	40 F		70 F		100 F	
	Low Strain Level	High Strain Level	Low Strain Level	High Strain Level	Low Strain Level	High Strain Level
IPC 1	1713850	1685934	603145	647078	154210	188782
	1496119	1319385	637156	776303	158065	156016
Average	1604984	1502660	620151	711691	156138	172399
Standard Deviation	153959	259189	24049	91376	2726.03	23168.8
Coefficient of variation, %	9.59	17.25	3.88	12.84	1.75	13.44
IPC 2	1529680	1561575	599774	718700	152757	173428
	1672471	1375957	800803	573901	158557	155748
Average	1601076	1468766	700289	646301	155657	164588
Standard Deviation	100969	131252	142149	102388	4100.69	12501.5
Coefficient of variation, %	6.31	8.94	20.30	15.84	2.63	7.60

Table B6. Analysis of Variance betwwen IPC1 and IPC2 using HMA specimens.

Source	Sum of Squares	DF	Mean Square	F Value	Prob > F
Temperature	8.22556E+12	2	4.11278E+12	443.08	< 0.0001 significant
Strain Level	261102663	1	261102663	0.03	0.869 not significant
Machine	1698938055	1	1698938055	0.18	0.674 not significant
Error	1.76364E+11	19	9282340905		
Correlation Total	1.76364E+11	23			
R-Squared	0.9790				
Adj R-Squared	0.9746				